Universidade do Minho
Escola de Ciências da Saúde

Maria do Carmo Pereira da Costa

Study of the homologue of the Machado-Joseph disease gene in *Mus musculus*

Abril de 2008

Universidade do Minho
Escola de Ciências da Saúde

Maria do Carmo Pereira da Costa

Study of the homologue of the Machado-Joseph disease gene in *Mus musculus*

Tese de Doutoramento em Ciências da Saúde
Especialização em Ciências Biológicas e Biomédicas

Trabalho efectuado sob a orientação da:

Prof. Doutora Patrícia Espinheira de Sá Maciel
Professora Auxiliar da Escola de Ciências da Saúde
Universidade do Minho

Trabalho efectuado sob a co-orientação de:

Prof. Doutora Manuela Morgadinho Faustino Monteiro dos Santos
Professora Associada da Faculdade de Medicina
Université de Montréal

Professor Doutor António Jorge dos Santos Pereira de Sequeiros
Professor Catedrático do Instituto de Ciências Biomédicas Abel Salazar
Universidade do Porto

Abril de 2008

Aos meus Pais e Irmão

AGRADECIMENTOS / ACKNOWLEDGEMENTS

Gostaria de agradecer em primeiro lugar à minha orientadora Prof. Doutora Patrícia Maciel por estes nove anos e meio de verdadeiro crescimento científico que me proporcionou. Obrigada Patrícia por ter acreditado na minha capacidade de trabalho desde o início, por todos os desafios que me propôs, pelo dinamismo e pelas inúmeras discussões científicas. A afirmação “Está quase...” durante a escrita desta tese foi sempre de grande motivação para mim! Muitos momentos foram vividos ao longo destes anos que eu jamais esquecerei, uns bons, outros menos bons, mas o importante é que sempre sobrevivemos neste mundo difícil da Ciência em Portugal! Agora continuo a dizer o mesmo que dizia em Outubro de 1998, quando comecei: quero fazer Ciência!

Ao Professor Jorge Sequeiros, meu co-orientador, por me ter aceite na UnIGENe onde comecei este percurso científico. Queria agradecer-lhe tudo o que aprendi sobre genética humana e sobre aconselhamento genético de doenças raras e incuráveis, entre as quais a doença de Machado-Joseph. Obrigada por me ter consciencializado para a aplicabilidade da investigação na melhoria da qualidade de vida dos doentes, quer a nível da terapêutica quer a nível do aconselhamento genético.

À Prof. Doutora Manuela Santos, minha co-orientadora, por me ter recebido na sua equipa no CHUM, em Montréal, onde “cresci” bastante a nível pessoal e científico. Obrigada Manuela por tudo o que aprendi consigo e por todo o apoio extra laboratorial que me deu! I would like to thank to Manuela’s lab group by their sympathy and cooperation, in particular to Carlos Miranda, Mark Tessaro, Laura Montermini, Ricardo and Hortence.

À Prof. Doutora Elsa Logarinho pelo apoio nos estudos de y2h, RNAi e muito mais… Obrigada Elsa pelos grandes momentos de entusiasmo científico que vivemos!

À Doutora Fernanda Bajanca pela excelente colaboração no estudo do desenvolvimento. A colaboração certa no momento certo! Obrigada pela força, entusiasmo, amizade e todos os bons momentos que partilhamos!

À Doutora Sandra Macedo Ribeiro pela sua colaboração desde o início deste trabalho e por me ter recebido no seu laboratório, em particular no último ano. A toda a sua equipa e em especial ao Ricardo Tomé por me terem recebido da melhor forma!

Aos membros do Concelho Científico da Escola de Ciências da Saúde da Universidade do Minho por terem acreditado nas minhas capacidades e me terem concedido a bolsa de Doutoramento da FCT, sem a qual a realização deste trabalho não teria sido possível.

A todas as pessoas que trabalham no ICVS por todo o apoio que me deram ao longo destes últimos quatro anos. É muito bom trabalhar num sítio onde se vêem sorrisos nos corredores e caras bem dispostas, atrás de uma porta, prontas a resolverem os problemas! Queria agradecer em especial o apoio técnico da Goreti, Luís, Magda e funcionários.

Ao Dr. Rui Fernandes da ATAF (IBMC) pelo apoio técnico prestado na microscopia electrónica e por toda a sua simpatia e bons momentos passados no laboratório e no microscópio. Queria agradecer também ao Professor Roberto Salema pelo apoio na compreensão da ultrastrutura celular. Gostaria também de agradecer o apoio técnico da Doutora Paula Sampaio (IBMC) nos meus primeiros passos na microscopia confocal. Ainda do IBMC, queria agradecer à Doutora Margarida Duarte pelo seu apoio desde o início do trabalho.

Aos investigadores principais do domínio de Neurociências – Patrícia Maciel, Joana Palha, Nuno Sousa e Armando Almeida – por terem formado um grupo de trabalho dinâmico que tenho a certeza que irá ser muito competitivo, a nível nacional e internacional, no futuro. Queria agradecer a todos os elementos deste domínio por tudo o que aprendi nas nossas reuniões semanais e pela partilha de conhecimentos e de meios no laboratório.

Aos colegas da UnIGENe, onde comecei este trabalho, pelos bons momentos que passamos juntos: Cláudia, Anabela Ferro, Paula, Carlos Melo, Isabel Alonso, Isabel Silveira, Fátima, Andreia Perdigão, Maria José, Vítor, Teresa, Joana, Pedro Seada, Tiago, Milena, Carolina, Ana e muitos outros que por lá passaram…

À Doutora Laura Guimarães por tudo o que me ensinou sobre estatística e pelas óptimas conversas que tivemos nos dias que passamos no ICBAS.

À Prof. Doutora Alda Sousa pelo que aprendi sobre genética populacional e suas aplicabilidades e pela óptima colaboração que tivemos.

Aos meus colegas do ID2, Dina Ruano, Fernanda Marques e João Sousa, pelo óptimo convívio no laboratório! Obrigada Fernanda pelos momentos de boa disposição!

Às minhas colegas de grupo que me aturaram todos estes anos, pois a vivência do dia-a-dia, de inúmeras horas, é sempre a que mais exige de nós como pessoas! Vivemos muitos momentos de variadas emoções! Obrigada pelo apoio! Desejo-vos a todas – Ana João, Anabela Fernandes, Anabela Ferro, Andreia Castro, Cláudia Santos e Mónica Santos – o melhor futuro possível!

Às minhas amigas Mónica Gonçalves, Sandra e Daniela pela sua amizade que, apesar das minhas muitas ausências, continua sempre a mesma!

À minha amiga Dina Ruano por todo o seu apoio, conselhos e pela sua energia contagiante!

Aos meus amigos Rodrigo e Lira por todos os bons momentos que passamos juntos! Foram as viagens Porto-Braga-Porto, os serões no "Firmeza Palace" e muitas outras situações de companheirismo que me fizeram perceber o quanto a vossa amizade é importante para mim!

Ao meu amigo João Sousa, já do tempo da faculdade, quero agradecer todas as conversas em que me ouve com paciência, todos os conselhos recheados de bom senso e toda a sua disponibilidade para me apoiar mesmo quando lhe falta o tempo!

À minha amiga Mónica Santos pelo companheirismo, pelo apoio incondicional sobretudo durante a fase de escrita da tese, pelas "chamadas de atenção" nos momentos certos… enfim, por ter estado sempre presente!

À minha amiga Cláudia Santos pela sua presença constante, carinho, força, conselhos e por me "chamar à Terra" sempre que é preciso! Cláudia, a tua amizade é preciosa para mim.

Às minhas "velhas" amigas Luísa e Elsa simplesmente pelos grandes laços de amizade que nos unem e fazem com que eu nunca me sinta só!

Aos meus grandes amigos Gustavo, Diogo, Miguel, Xico, Rui e Filipa por todos estes longos anos de aventuras e desventuras da nossa juventude, que tornaram a nossa amizade num bem essencial! Obrigada por me terem ajudado a ver a vida de uma outra forma e por todo o apoio, amizade e carinho que sempre me deram!

Ao Pedro Jaime por todos os anos que nos uniram e nos fizeram crescer como pessoas. Obrigada pelas inúmeras horas que passaste à minha espera, pela tua amizade… e por tudo! Tudo de bom e de mau foi importante!

À minha família pelo apoio constante que sempre me deram. Gostaria de agradecer em particular aos meus tios, Francisca e Manuel, que são para mim os meus "segundos pais", assim como às minhas primas Manuela e Cristina, como minhas irmãs, pelo convívio que sempre nos uniu e por todo o carinho e apoio que me deram. A doçura e afecto das pequeninas, Beatriz e Maria, foram muito importantes durante estes últimos anos. Ao Artur, o meu "irmão mais velho", pelo nosso entendimento. À memória dos meus avós Joaquim e Alzira por todo o carinho que me deram. À minha avó Ana por todo o amor que me dá e por ser, desde sempre para mim, um exemplo de uma grande mulher independente e forte!

Ao meu irmão Diogo, que tanto amo, por ser um exemplo de sobrevivência e de luta pela vida e por ser a alegria da nossa casa! Pelos muitos momentos em que os 20 anos, que nos separam na idade, se invertem e me dá colo, carinho e até conselhos, e por todos os outros momentos de cumplicidade que nos unem.

Aos meus Pais por todo o amor que me dão, por estarem sempre presentes, do meu lado, mesmo quando não tomo as decisões certas, por me terem ensinado que é com o nosso trabalho que lutamos por aquilo que queremos e por todo o esforço que têm feito para que eu chegasse aqui. Fizeram tudo por mim! Esta tese é nossa!

Este trabalho foi co-financiado pela Fundação para a Ciência e a Tecnologia (FCT) (POCI 2010 e FSE) através de uma bolsa de Doutoramento (SFRH/BD/9759/2003) e dos projectos (Proj.33759/99 e POCI/SAU-MMO/60412/2004); pela Fundação Luso-Americana para o Desenvolvimento (Proc.3.L./A.II/P.582/99); e pela National Ataxia Foundation.

Study of the homologue of the Machado-Joseph disease gene in *Mus musculus*

ABSTRACT

Polyglutamine-associated (polyQ) diseases are the most common class of inherited neurodegenerative disorders. These yet untreatable disorders (nine at this moment) are characterised by a selective neuronal death, specific of each disease, and caused by the expansion of a polyQ tract in the corresponding proteins. The pathogenic mechanism underlying these disorders remains to be disclosed. Although a toxic gain-of-function of the expanded polyQ proteins has been proposed as a potential model of pathogenesis, recently another model emerged, proposing a combination of a gain-of-function of the mutant protein with a partial loss-of-function of the normal protein. Thus, the knowledge of the normal function of these proteins, and not only the cellular effect of the expanded polyQ proteins, may be important for the development of therapeutic strategies for polyQ disorders. Among these polyQ proteins, the physiological function is only known for four of them. Ataxin-3 (ATX3) is a polyQ protein that, when expanded, leads to Machado-Joseph disease (MJD), which is the most frequent spinocerebellar ataxia worldwide.

Even though, *in vitro*, deubiquitinating (DUB) and deneddylase enzymatic activities have been attributed to ATX3, suggesting a potential role in the ubiquitin-proteasome system (UPS), the physiological role of this protein remains unknown. Our main goal was to get insight into the function of ATX3 using the mouse as a model.

During this work, we have performed an extensive exploratory study of both the mouse homologue gene (*Mjd*) and of its encoded protein, mATX3. We have cloned the *Mjd* gene, characterised its genomic structure, and performed bioinformatic and functional studies of its 5' flanking region. The gene structure was shown to be highly similar to its human counterpart in both the number and size of exons and introns. Promoter studies revealed that the *Mjd* gene is highly activated in P19 muscle-differentiated cells, which was in conformity with the binding of the muscle-specific transcription factor MyoD, verified here, by EMSA. As the human, mATX3 was shown to have a ubiquitous expression pattern being highly expressed in muscle, ciliated cells, and in the spermatozoid flagella. We have also verified that this protein is expressed since the early embryonic developmental stages (E9.5). We have demonstrated that mATX3 displays *in vitro* activities of: (1) DUB, towards K48 and K63-linked polyubiquitin chains, and towards a monoubiquitinated fluorogenic substrate; and (2) deneddylase of a neddylated fluorogenic substrate. These activities suggest possible roles of mATX3 in protein degradation through the UPS, but also in the regulation of other cellular processes, such as regulation of the subcellular localisation of proteins, endocytosis, protein trafficking, and DNA repair. Using the yeast two-

hybrid system (y2h) we have identified 81 putative protein interactors of mATX3, presenting different subcellular localisations, in agreement with the widely distributed subcellular pattern of mATX3 here described in skeletal muscle, pontine nuclei and seminiferous tubules, using immunoelectron microscopy. Among these interactors, we have cloned and confirmed the interaction of 18 new proteins with mATX3, using additional/complementary y2h assays. These novel mATX3 interactions pointed to possible roles of mATX3 in transcription regulation, protein synthesis and degradation, cell cycle, cellular proliferation, differentiation and motility.

Several data obtained in these descriptive studies led us to explore some hypotheses for the potential physiological role(s) of mATX3, particularly in the skeletal muscle. We have found that the *Mjd* gene, potentially regulated by Foxo transcription factors, is a stress-response gene being upregulated in the skeletal muscle of starved or cold-exposed mice. These results might suggest a potential role of mATX3 in the regulation of protein synthesis and/or degradation in the stress-response, which should be further confirmed in the future.

Interestingly, we have also found here that mATX3 might be regulating the activity of the SCF complex, an E3 ubiquitin ligase involved in the UPS, through the interaction with Cul1 and Nedd8. Structural sarcomeric components, such as myosin and actin are degraded through the UPS. In fact, we have demonstrated, using y2h assays, that mATX3 interacts with four sarcomeric proteins (Tnni1, Tnni2, Acta1, and Myh2), which, in turn, might be possible substrates of the enzymatic activities of mATX3 leading to the regulation of these protein amount, stability, and assembly (in the particular case of myosin). These preliminary results indicate a putative physiological role of mATX3 in muscle structure maintenance that must be further explored.

Finally, we have demonstrated that mATX3 is important for muscle differentiation using siRNA assays in C2C12 cells, thus showing the first ever described phenotype of cells lacking mATX3. These cells revealed to be misaligned, continue to proliferate, and present a delay in myogenic differentiation, which seem to be due to a deregulation of the integrin signaling pathway, namely through the down-regulation of α5 and α7 integrin subunits. In particular, we have shown that the α5 integrin subunit, degraded by the UPS, might be a substrate of mATX3 DUB activity in its rescue from proteasomal degradation, given that these two proteins interact in GST pull-down assays. Additionally, proteomic studies of these C2C12 cells revealed that absence of mATX3 might be affecting the following integrin signaling transduction-associated processes: cytoskeleton assembly, transcription repression, protein synthesis/degradation, and cell cycle.

Data obtained with this work should contribute to an advance in the knowledge of the normal function of ATX3, which might be disrupted in the MJD context, and might also be important in the unveiling of the function of other basal cellular mechanisms.

Estudo do gene homólogo ao gene da doença de Machado-Joseph em *Mus musculus*

RESUMO

As doenças de poliglutaminas (poliQ) constituem o grupo mais comum de doenças neurodegenerativas hereditárias. Estas doenças incuráveis (actualmente nove) são caracterizadas por perda neuronal selectiva, específica de cada doença, e causadas por uma expansão de um segmento poliQ nas proteínas correspondentes. O mecanismo patogénico destas doenças continua desconhecido. Apesar de ter sido proposto como modelo de patogénese um ganho de função tóxica das proteínas expandidas, recentemente surgiu outro modelo, propondo uma combinação do ganho de função das proteínas mutadas com uma perda de função das proteínas normais. Deste modo, o conhecimento da função normal destas proteínas, e não só do efeito celular das proteínas poliQ expandidas, pode ser importante para o desenvolvimento de estratégias terapêuticas para as doenças de poliQ. Entre estas proteínas, a função fisiológica só é conhecida para quatro delas. A ataxina-3 (ATX3) é uma proteína poliQ que, quando expandida, leva à doença de Machado-Joseph (MJD), que é a ataxia espinocerebelosa mais frequente em todo o mundo.

Apesar de terem sido atribuídas à ATX3, *in vitro*, as actividades enzimáticas de desubiquitinase (DUB) e desnedilase sugerindo uma possível função no sistema ubiquitina-proteassoma (UPS), a função fisiológica desta proteína continua desconhecida. O nosso objectivo principal foi contribuir para o conhecimento da função da ATX3 usando o ratinho como modelo.

Neste trabalho, realizamos um extenso estudo exploratório do gene homólogo em ratinho (*Mjd*) e da sua codificada proteína, mATX3. Nós clonamos o gene *Mjd*, caracterizamos a sua estrutura genómica e efectuamos estudos bioinformáticos e funcionais da sua região 5' flanqueante. A estrutura do gene é muito semelhante à do seu correspondente humano tanto no número como no tamanho de exões e intrões. Os estudos do promotor mostraram que o gene Mjd era altamente activado em células P19 diferenciadas em músculo, o que está de acordo com a verificação, por EMSA, da ligação do factor de transcrição específico de músculo MyoD. Tal como a ATX3 humana, a mATX3 revelou um padrão de expressão ubíquo sendo altamente expressa no músculo, células ciliadas e nos flagelos dos espermatozóides. Verificamos também que esta proteína é expressa desde os primeiros estádios de desenvolvimento embrionário (E9.5). Demonstramos que a mATX3 apresenta actividades *in vitro* de: (1) DUB, de cadeias poliubiquitinadas K48 e K63-ligadas, e de um substrato fluorogénico monoubiquitinado; e (2) desnedilase, de um substrato fluorogénico nedilado. Estas actividades sugerem possíveis papéis da mATX3 na degradação proteica através do UPS mas também na regulação de outros processos celulares tais como, a regulação da localização subcelular de proteínas, endocitose, tráfego proteico, e reparação de DNA. Usando o sistema de yeast two-hybrid (y2h), identificámos

81 prováveis interactores proteicos da mATX3, apresentando diferentes localizações subcelulares, de acordo com o padrão de distribuição subcelular da mATX3, aqui descrito, no músculo esquelético, núcleos pônticos e tubos seminíforos, usando imunomicroscopia electrónica. Entre estes interactores, clonamos e confirmamos a interacção de 18 novas proteínas com a mATX3, usando ensaios adicionais/ complementares de y2h. Estas novas interacções apontam para possíveis funções da mATX3 na regulação da transcrição, síntese e degradação proteica, ciclo celular, e proliferação, diferenciação e motilidade celular.

Os resultados obtidos nestes estudos descritivos levaram-nos a explorar algumas hipóteses para as potenciais funções fisiológicas da mATX3, em particular no músculo esquelético. Verificamos que o gene *Mjd*, provavelmente regulado pelos factores de transcrição Foxo, é um gene de resposta ao stress estando aumentado no músculo esquelético de ratinhos em jejum ou expostos ao frio. Estes resultados poderão sugerir uma possível função da mATX3 na regulação da síntese e/ou degradação proteica na resposta ao stress, que deverá ser explorada em detalhe no futuro.

Neste trabalho, demonstramos que a mATX3 pode estar a regular a actividade do complexo SCF, uma E3 ubiquitina ligase envolvida no UPS, através da sua interacção com a Cul1 e Nedd8. Componentes sarcoméricos estruturais, como a miosina e a actina, são degradados através do UPS. De facto, demonstramos, usando ensaios de y2h, que a mATX3 interactua com quatro proteínas sarcoméricas (Tnni1, Tnni2, Acta1, e Myh2), que, por sua vez, poderão ser possíveis substratos das actividades enzimáticas da mATX3 levando à regulação da quantidade, estabilidade, e organização (em particular da miosina) destas proteínas. Estes resultados preliminares indicam uma potencial função fisiológica da mATX3 na manutenção estrutural do músculo esquelético que deverá ser confirmada no futuro.

Finalmente, verificamos que a mATX3 é importante para a diferenciação muscular usando ensaios de siRNA em células C2C12, mostrando o primeiro fenótipo observado para células sem mATX3. Estas células mostraram-se desalinhadas, continuando a proliferar e apresentando um atraso na diferenciação miogénica, o que parece ser a uma desregulação da via de sinalização das integrinas, nomeadamente pelo decréscimo das subunidades α5 e α7 das integrinas. Em particular, demonstrámos que a subunidade α5 da integrina, degradada pelo UPS, poderá ser um substrato da actividade de DUB da mATX3 no impedimento da sua degradação proteassomal, dado que estas duas proteínas interactuam em ensaios de GST pull-down. Adicionalmente, estudos de proteómica destas células sem mATX3 mostraram que a ausência desta proteína poderá estar a afectar os seguintes processos celulares associados com a via de transdução das integrinas: organização do citosqueleto, repressão da transcrição, síntese/degradação proteica e ciclo celular.

Os resultados obtidos neste trabalho contribuirão para o avanço do conhecimento da função normal da ATX3, que poderá estar afectada no contexto da MJD, e pode também ser importante para a descoberta de outros mecanismos celulares basais.

CONTENTS

ABBREVIATIONS

aa, amino acid

Akt, acute transforming retrovirus thymoma

3-AT, 3-amino-1,2,4-triazole

AlzD, Alzheimer's disease

ALS, amyotrophic lateral sclerosis

ATX3, ataxin-3

bHLH, basic helix-loop-helix

bp, base pair

BSA, bovine serum albumin

cAMP,

CREB, cAMP response element binding protein

CREBBP, CREB binding protein

CRLs, cullin-RING ligases

DAPI, 4',6-Diamidino-2-phenylindole dihydrochloride

DBE, daf-16 family member binding element

DMSO, dimethylsulfoxide

DNA, deoxyribonucleic acid

DTT, dithiotreithol

DUB, deubiquitinating enzyme

E, embryonic day

ECM, extracellular matrix

EDTA,

EMSA, electrophoretic mobility-shift assay

FoxO, forkhead box "Other"

GAL, galactosidase

X-Gal, 5-bromo-4-chloro-3indolyl-β-D-galactopyranoside

HDAC3, histone deacetylase 3

Hepes,

IPTG, isopropyl-β-D-thiogalactopyranoside

Kb, kilo bases

mATX3, mouse ataxin-3

β**-ME**,β-mercaptoethanol

MJD, Machado-Joseph disease

min, minute

MMP2, metalloproteinase-2

MMR, mismatch repair

MMTS, methyl methane thiosulfonate

MPCs, muscle precursor cells

MRFs, myogenic regulatory factors

mRNA, messenger ribonucleic acid

MSC, muscle satellite cell

MTJ, myotendinous junction

NEDD8, neural precursor cell expressed developmentally down-regulated gene 8

NER, nucleotide excision repair

NMJ, neuromuscular junction

OD, optical density

PBS, phosphate-buffered saline

PCAF, p300/CREBBP associated factor

PCR, polymerase chain reaction

PD, Parkinson's disease

PMSF, phenylmethylsulphonyl fluoride

polyQ, polyglutamine

polyUb, polyubiquitin

RA, retinoic acid

RNA, ribonucleic acid

RT-PCR, reverse transcriptase polymerase chain reaction

SELS, selenoprotein S

SMA, spinal muscular atrophy

SNAREs, soluble *N*-ethylmaleimide-sensitive fusion attachment protein receptors

SNP, single nucleotide polymorphism

α-syn, α-synuclein

SYVN1, synoviolin

TFA, trifluoroacetic acid

TNR, trinucleotide repeat

U snRNP, uridin-rich small nuclear ribonucleoprotein

UAS, upstream activating sequence

Ub, ubiquitin

UBL, ubiquitin-like protein

UIM, ubiquitin interacting motif

UPS, ubiquitin proteasome system

y2h, yeast two-hybrid

Chapter 1

General Introduction

1.1. Neurodegenerative diseases

Trough human evolution we have been observing an extension of the life expectancy. Therefore, and in particular in developed countries, human populations are increasingly tending to become aging societies, where neurodegenerative disorders are, together with cancer, one of the most feared group of diseases. Among all diseases, neurodegenerative disorders represent 2%, and in many cases, they have a genetic cause. Since the middle of the last century, many efforts have been made to identify the *loci* responsible for each disease in order to: (1) offer molecular diagnosis, presymptomatic and pre-natal testing to the affected families; (2) understand the pathogenic mechanism underlying each mutated gene; and (3) create cellular and/or animal models of study, allowing the assessment of potential therapies.

Neurodegenerative disorders are usually progressive, of late onset, and involve selective loss of neuronal cell bodies, axons, dendrites and/ or synapses. In our days, even with the existence of models of study for a number of diseases, it remains difficult to determine the spatiotemporal relationships between these cellular events. However, it is essential to define the first causal event, in order to understand the pathogenic mechanism, and to develop therapeutic strategies (Conforti et al. 2007).

Alzheimer's disease (AD) is the most common form of progressive dementia in the elderly, affecting ~5% of persons over 65 years of age. AD is characterized by the presence of amyloid plaques in brain, neurofibrillary tangles and dystrophic neuritis that could have different origins (Coleman and Yao 2003). Familial AD cases (rare) result from mutations in genes involved in the processing of the amyloid precursor protein (APP), namely *APP* itself, presenilin 1 (*PS1*) and presenilin 2 (*PS2*) (Rogaeva 2002). Studies in both cortical biopsies and animal models showed that the most frequent early features in AD are synaptic loss and neuritic dystrophy (Tsai et al. 2004; Jacobsen et al. 2006), but their causes and consequences for the cell bodies are still unknown.

Parkinson's disease (PD) is the second most common neurodegenerative disorder after AD, affecting approximately 1% of the population over age 50 (Polymeropoulos et al. 1996). The main clinical features of classical PD are the characteristic postural abnormalities, resting tremor, muscular rigidity, bradykinesia, and dementia. Pathological hallmarks of PD are the extensive neuronal loss in the pars compacta of substantia nigra, and the presence of Lewy bodies, intraneuronal inclusions containing α-synuclein (α-syn), one of the proteins mutated in some familial PD cases (Polymeropoulos et al. 1997). Mutations in other genes namely *parkin*, *DJ-1*, *PINK1*, and *LRRK2* were also identified in PD families. α-synuclein regulates the folding of soluble *N*-ethylmaleimide-sensitive fusion attachment protein

receptors (SNAREs), essential for neurotransmitter release and synapse survival (Chandra et al. 2005). The early degenerative signs in PD patients and mutant α-synuclein transgenic mouse models seem to appear in synapses, axons and dendritic trees (Braak et al. 2006; Martin et al. 2006). Nevertheless, some acute PD models show that cell bodies degenerate independently of axon dysfunction (Sajadi et al. 2004). Thus, the subcellular site for the first degenerative steps in PD remains unclear.

In amyotrophic lateral sclerosis (ALS), the neurons affected are the upper and lower motor neurons leading to paralysis and death in 2-5 years after diagnosis (Kunst 2004). This is also a disease with various causes, but some rare familial cases are explained by missense mutations in the Cu^{2+}-Zn^{2+} superoxide dismutase 1 (SOD1). Disease neurons show oxidative damage, protein aggregation, vacuolar pathology, retardation of axonal transport, neurofilament accumulation, and glutamate excitotoxicity (Boillee et al 2006). The existence of different mouse models that mimic some clinical features of ALS have been essential to reveal that the first neurodegenerative steps in this disease seem to be synapse and axon dysfunction (Kieran et al. 2005).

Another neurodegenerative disorder is spinal muscular atrophy (SMA), which is characterized by the degeneration of motor neurons in the spinal cord, causing progressive weakness of the limbs and trunk, followed by muscle atrophy (Wirth 2000). It is caused by mutations in the survival motor neuron 1 (*SMN1*) (Wirth 2000). The SMN protein is ubiquitous, highly expressed in the nucleus where it is important for the uridin-rich small nuclear ribonucleoprotein (U snRNP) complex assembly (Eggert et al 2006), but is also present in axons, being associated with microtubules and growth cones (Zhang et al 2003). Even though studies of mouse and zebrafish SMA models indicate that the initial site of degeneration is the axon, other nuclear processes might also contribute to cell death (Cifuentes-Diaz et al 2002; McWhorter et al 2003).

Polyglutamine (polyQ) diseases (Table 1.1) are dominant disorders characterized by an expansion of a polyQ segment in several unrelated proteins. In each disease, there is a specific subgroup of neurons that are affected, and one characteristic feature in some of these disorders is the presence of intracellular inclusions. PolyQ diseases are a subclass of the unstable repeat disorders caused by an expansion of a CAG triplet repeat located in the coding region of the genes, giving rise to a stretch of glutamine residues in the corresponding proteins. These disorders are individually rare, although as a group they represent the most common class form of inherited neurodegenerative disorders. At the moment, this class of diseases comprises nine diseases: the spinocerebellar ataxias SCA1, SCA2, Machado-Joseph disease/ SCA3, SCA6, SCA7, and SCA17, dentatorubral-pallydoluysian atrophy (DRPLA), SBMA, and Huntington disease (HD) (Table 1.1). All these disorders are autosomal dominantly inherited, with the exception of SBMA that is X-linked. The polyQ

diseases are, in general, characterised by neuronal dysfunction, resulting in selective neurodegeneration of specific regions of the brain for each disorder (Cummings and Zoghbi 2000). The proteins involved in polyQ disorders have so different functions and localisations that it becomes difficult to define a common pathway for the neuronal death. Synapses and axons have been proposed to be the earliest sites of degeneration in Huntington disease (HD) (the most studied among the polyQ diseases) (Murphy et al 2000; Li et al 2001), although nuclear events could also be important (Conforti et al. 2007).

In summary, the sites of the earliest molecular events leading to neurodegeneration remain controversial although, in many cases, the first sites to degenerate seem to be the synapses and the axons. Synapse loss could be reverted by other nerve terminals, but the consequent loss of retrogradely transported survival factors might induce cell and axon death. Therefore, the molecular pathogenesis could involve several cellular compartments. Since molecular events involved in neurodegeneration, at least seem to be in part, specific for each disease, it is of great importance to create models of study for each disease that will be fundamental to unveil each pathogenic mechanism and to test new therapies. Moreover, the study of the normal function of the causative proteins may also contribute to define the cellular and molecular target mechanisms, in these (so far) untreatable diseases.

1.2. Pathogenic mechanisms of polyglutamine disorders

Among the nine proteins implicated in the polyQ diseases (Table 1.1), the physiological function is known only for four of them: the androgen receptor (mutated in SBMA), the voltage-gated α1A subunit of calcium channel ($CACNA1_A$) (SCA6), the transcription activator atrophin-1 (DRPLA), and the TATA-box binding protein (TBP) (SCA17).

In fact, polyQ proteins do not show any sequence similarities between each other, except for the polyQ segment itself. The creation of transgenic mouse models for HD and MJD expressing a truncated fragment of the corresponding expanded polyQ protein, and showing some of the disease phenotypes, namely repeat instability, demonstrated that the polyQ segment itself seems to confer a toxic gain-of-function to the protein (Ikeda et al. 1996; Mangiarini et al. 1996). However, distinctive selective neuronal loss only occurs in transgenic mice expressing the expanded polyQ, in the context of the full-length protein (Reddy et al. 1998). This might be due to specific interactions established by the polyQ-flanking regions. Nevertheless, some evidences support the hypothesis that a loss of normal function of the proteins may also be important in the pathogenesis or its selectivity (Leavitt et al. 2006).

Table 1.1. Polyglutamine diseases

Disease		Gene				Protein	
cause	symbol	name	repeat unit			name	repeat tract
			type	normal length	pathogenic length		
altered protein function	**SCA1**	*ATXN1*	(CAG)n	6-39	40-82	ataxin-1	**polyQ**
	SCA2	*ATXN2*	(CAG)n	15-24	32-200	ataxin-2	
	MJD (SCA3)	*ATXN3*	(CAG)n	12-44	51-87	ataxin-3	
	SCA6	*CACNA1A*	(CAG)n	4-20	20-29	$CACNA1_A$	
	SCA7	*ATXN7*	(CAG)n	4-35	37-306	ataxin-7	
	SCA17	*TBP*	(CAG)n	25-42	43-63	TBP	
	DRPLA	*ATN1*	(CAG)n	7-34	49-88	atrophin-1	
	SBMA	*AR*	(CAG)n	9-36	38-62	androgen receptor	
	HD	*HD*	(CAG)n	6-35	36-121	huntingtin	

DRPLA, dentatorubral-pallidoluysian atrophy; HD, Huntington disease; MJD, Machado-Joseph disease; SBMA, spinal and bulbar muscular atrophy; SCA, spinocerebellar ataxia;

Indeed, in this year, emerged a new model proposing a combination of a gain-of-function of the expanded polyQ proteins, and a loss-of-function of the normal proteins (Lim et al. 2008).

Although the normal functions and pathological effects of the mutated proteins are not clear, there seem to be common pathogenic pathways. There are two main potential pathogenic mechanisms underlying polyQ diseases: (1) protein misfolding and aggregation, and (2) transcription deregulation.

1.2.1. Protein misfolding and aggregation

Aggregation of the mutated protein is a common feature of al polyglutamine diseases (Orr and Zoghbi 2007). There are some evidences that the expanded polyQ segment confers a new three-dimensional conformation to the proteins (Orr and Zoghbi 2007).

One hypothesis, the “polar zipper” theory, is based on the possibility that expanded units of polyQ proteins establish strong hydrogen bonds with each other, leading to insoluble parallel β-sheet structures (Perutz et al. 1994).

Another possibility underlying the aggregation process is the fact that transglutaminases are able to cross-link with polyQ proteins (Kahlem et al. 1996; Karpuj et al. 1999).

In addition, mutated proteins in their misfolded state may acquire a toxic function through aberrant protein interactions, which can lead to the formation of aggregates and the further recruitment of molecules, such as other polyQ proteins, including transcription factors and transactivators (Cummings and Zoghbi 2000; Chai et al. 2001).

An additional explanation for the occurrence of protein aggregates in these disorders is based on the above mentioned evidence that the polyQ tract itself, or protein fragments containing the expanded polyQ stretch, can be toxic. Indeed, poly Q proteins such as huntingtin, androgen receptor, atrophin-1 and ataxin-3 (ATX3) can be cleaved *in vitro* by caspases (Goldberg et al. 1996; Kobayashi et al. 1998; Wellington et al. 1998; Berke et al. 2004). In addition it was recently shown that ATX3 is cleaved by calcium-dependent calpain proteases (Haacke et al. 2007). These protein fragments, carrying the expanded polyQ, might be functioning as "seeds" for the formation of aggregates. Particularly, in the case of MJD, this hypothesis has proved to have biological relevance, given the finding of a cytotoxic protein segment in both MJD transgenic mice and MJD patients (Goti et al. 2004). Additionally, results from our group using MJD transgenic worms suggested that the C-terminal fragments of human ATX3 act as nucleators for the formation of aggregates, in an age-dependent manner (Teixeira-Castro 2007).

The presence of polyQ-containing aggregates in patients' brains is a fact. However, their role in the cell still remains a mistery: are they toxic or protective?

These cytoplasmic and/or nuclear neuronal aggregates, present in polyQ disease patient's brains, contain ubiquitin, ubiquitin-like proteins, proteasome subunits, chaperones, and polyQ proteins (Paulson et al. 1997b; Chai et al. 1999a; Chai et al. 1999b; Takahashi et al. 2001; Chai et al. 2004; Mori et al. 2005). This led to the proposal that depletion of these factors could explain the toxicity of aggregates in the cellular context.

The involvement of the protein quality control machinery, and the additional evidence that over-expression of chaperones in animal or cellular models of these diseases ameliorated the polyQ toxicity (Warrick et al. 1998; Warrick et al. 1999; Kobayashi et al. 2000), suggested that polyQ proteins ubiquitin-conjugated are probably targeted to proteasomal degradation, in an attempt to re-establish the cellular homeostasis. In fact, proteasome inhibition in cells expressing mutant ATX3 led to increased aggregation, suggesting an important role of the proteasome in aggregate clearance (Chai et al. 1999b). When the cellular capacity to process the mutant proteins is exceeded, the proteins become clustered into insoluble proteinaceous aggregates. The recruitment of proteasomal subunits into aggregates raises the possibility of proteasome impairment in polyQ disorders. It was shown that aggregates can be trapped in the proteasome, and irreversibly sequester it (Holmberg et al. 2004).

However, several other evidences suggest that aggregates can function as a protective cellular mechanism for stacking the toxic mutant proteins. Indeed, aggregates are natural occurring species, given that Marinesco bodies are found in the substantia nigra as a result of the metabolism of normal aging neurons (Fujigasaki et al. 2001). Additional evidence against their toxic role is the fact that neuronal aggregates are not exclusively found in the cells of the regions presenting neuronal loss (Rolfs et al. 2003). Furthermore, the induction of conditions leading to a reduction of aggregate formation gave rise to enhanced toxicity of a fragment of mutant huntingtin in neuronal cultures (Saudou et al. 1998).

The solution for this dilemma about the toxic or protective role of aggregates in polyQ diseases will continue to interest the research community, in order to find in which way aggregates can be a target for the development of therapeutic strategies for these disorders.

1.2.2. Transcription deregulation

In several polyQ disorders, early alterations in transcription are verified, which might be a response to perturbed cellular metabolism. Mutant polyQ proteins have been shown to interact with proteins involved in the transcription machinery, namely the CREB-binding protein (CREBBP), p300/CREBBP associated factor (PCAF), TAFII130, and SP1 (Li et al. 2002; Okazawa 2003). Overexpression of these transcription regulators was shown to overcome polyQ toxicity, both *in vitro* in cellular models for MJD, SBMA, and HD (McCampbell et al. 2000; Dunah et al. 2002), as well as *in vivo* in a polyQ model in *Drosophila* (Taylor et al. 2003). This indicates a transcription deregulation in polyQ pathogenesis.

Several polyQ-protein interactors have acetyltransferase activity. Acetylation of histones relaxes the DNA structure promoting transcription, whereas hypoacetylation represses gene activity (Grewal and Moazed 2003). The equilibrium of histone acetylation/ deacetylation is controlled by histone acetyltransferases and deacetyltransferases (HDACs). Thus, polyQ proteins may be toxic by their direct inhibition of the acetyltransferase activity of transcription regulators, leading to diminished gene expression. In fact, treatment of *Drosophila* and mouse models of HD with HDAC inhibitors has been shown to ameliorate the disease phenotype and to decrease cell degeneration, with the increase of histone acetylation and consequent transcription activation (Steffan et al. 2001; Ferrante et al. 2003; Hockly et al. 2003).

1.3. Machado-Joseph disease (MJD)

The history of the description of this disorder is a good example of the difficulty to define a disease as a single entity, in the context of variable symptomatology.

MJD was first described in Northern American families but of Azorean ancestry. In 1972, Nakano and co-authors reported a family descendent from William Machado, a native from São Miguel in Azores, presenting progressive hereditary ataxia. They nominated this disorder as "Machado disease" (Nakano et al. 1972). In the same year, Woods and Schaumburg observed another family of Azorean ancestry, the Thomas family, which although showing similar clinical features of Machado disease, presented some particular clinical and pathological signs that led them to define this disorder as a novel clinical entity – "nigro-spino-dentatal degeneration" (Woods and Schaumburg 1972). Four years later, Rosenberg and collaborators described the "Joseph family", again another Azorean-ancestry family (from Flores) presenting a "new" hereditary ataxia, different from the former two (Rosenberg et al. 1976). A fourth Azorean family was reported to carry the "Azorean disease of the nervous system" in 1977 (Romanul et al. 1977). The clinical heterogeneity that is presently known to characterise this disease led those authors to diagnose the families for distinct ataxias.

Finally, in 1975, the Portuguese clinicians and researchers, Paula Coutinho and Corino Andrade studied the first 15 families from the Azorean Islands and proposed that the above mentioned diseases were indeed variations of the same clinical disease (Coutinho and Andrade 1978). They defined this as "Machado-Joseph disease", a single disorder characterised by a high clinical variability, proposing the clinical classification of patients into three subtypes that accommodate all this variability.

In our days, Machado-Joseph disease (MJD), now also called spinocerebellar ataxia type 3 (SCA3), is known to be the most common dominantly inherited ataxia worldwide (15-45% of all forms in different countries and ethnic populations) (Margolis 2002; Schols et al. 2004; Paulson 2007).

1.3.1. Clinical definition

MJD patients suffer from a progressive neurodegenerative disorder appearing more frequently between the ages of 20 and 50 years, in which the intellect is preserved (Coutinho and Andrade 1978; Coutinho 1992). The preservation of cognitive function is a key feature of MJD in its differential diagnosis among the vast group of spinocerebellar ataxias (Coutinho 1992). The common features of MJD are cerebellar ataxia, progressive external

ophtalmoplegia, pyramidal signs, dystonia, rigidity, and distal muscle atrophies (Coutinho and Andrade 1978; Lima and Coutinho 1980).

As mentioned above, the highly variable clinical presentation led to a definition of four clinical sub-phenotypes: **type I**, characterised by the dominance of pyramidal and extrapyramidal anomalies, in addition to ataxia and other signs, with an early age-at-onset and fast progression; **type II**, with typical cerebellar ataxia, progressive external ophtalmoplegia and pyramidal signs appearing at an intermediate age; **type III**, with late onset and slow progression of peripheral signs, such as muscle atrophies; and **type IV**, the rarest, characterised by the presence of Parkinsonic signs, associated to the core clinical features (Coutinho and Andrade 1978; Lima and Coutinho 1980; Coutinho 1992; Rosenberg 1992).

1.3.2. Anatomopathological features

The main neuropathological hallmarks of MJD patients are the neuronal degeneration and loss in the following regions: dentate nucleus in the cerebellum, substantia nigra (pars compacta and reticulata), spinocerebellar tracts, pontine nucleus, anterior horn cells of the medulla, motor cranial nuclei, and the striatum (Woods and Schaumburg 1972; Coutinho and Sequeiros 1981; Coutinho 1992; Ross 1995). More recently, it was shown that all the precerebellar nuclei and the thalamus were also affected in MJD patients (Rüb et al. 2003; Rüb et al. 2005).

In addition, although intracytoplasmic inclusions were observed to a lesser extent than intranuclear ones, both types of ATX3-containing inclusions are found in the above mentioned regions of MJD patients (Yamada et al. 2004), constituting another hallmark in the pathological characterisation of MJD.

1.3.3. Genetics

Since the first description of MJD as “Machado disease”, that this disorder was described in all reports as being of autosomal dominant inheritance, which means that the presence of the mutation in one single allele is sufficient to cause the disease. In addition, the observation of the MJD families showed that affected offspring usually manifested the disease earlier, with fast progression, and with more severe symptoms (Coutinho and Sequeiros 1981; Sequeiros and Coutinho 1993). This phenomenon of anticipation, characteristic in MJD families, is a common feature of dynamic diseases.

Eleven years after the first disease description, its causative gene was mapped to chromosome 14q32.1 (Takiyama et al. 1993). Later, this gene localisation was further confirmed in the Azorean families (Sequeiros et al. 1994), and the *MJD1* gene was finally cloned by positional cloning (Kawaguchi et al. 1994). The mutated gene in MJD (now designated *ATXN3*), was shown to comprise a trinucleotide CAG repeat in the coding region that was expanded in MJD patients (Kawaguchi et al. 1994).

This knowledge allowed the establishment of the molecular diagnosis of MJD, based on the determination of the CAG repeat length, and the consequent confirmation of the disease in families of different origins (Maciel et al. 1995; Higgins et al. 1996; Lindblad et al. 1996; Lopes-Cendes et al. 1996b; Gaspar et al. 2001). This CAG repeat is highly polymorphic, ranging from 12-41 trinucleotide units in normal alleles, and 55-86 in the expanded alleles present in MJD patients (Maciel et al. 2001). The presence of several single nucleotide polymorphisms (SNPs) surrounding the CAG repeats (Maciel et al. 1999; Costa et al. 2002), in addition to other molecular techniques, allowed us to improve the MJD molecular diagnosis (Maciel et al. 2001).

In addition, the determination of the CAG repeat size in MJD families allowed researchers to verify the existence of intergenerational instability, meaning that the repeat tracts may present different lengths in progenitors and offspring. The paternal mutant alleles were found to be more unstable then the maternal ones, thus more prone to expand or contract in the offspring (Maciel et al. 1995; Maruyama et al. 1995; Igarashi et al. 1996). This dynamic mutation causing MJD may explain the phenomenon of anticipation observed in the families, since there is an inverse correlation between the $(CAG)_n$ length and the age at onset of disease (Maciel et al. 1995; Maciel et al. 1999). Moreover, the CAG repeat was also found to be somatically unstable, i.e. presenting different lengths in cells from the same tissue (Lopes-Cendes et al. 1996a). This phenomenon was not preferentially associated to the MJD affected brain regions (Lopes-Cendes et al. 1996a).

The genomic structure of the *ATXN3* gene, and the subsequent knowledge of the number and size of exons and introns was only established in 2001 (Ichikawa et al. 2001). The gene spans 48,240 bp, comprising 11 exons, being the CAG repeat localised in exon 10. In the same report, it was shown that the *ATXN3* is ubiquitously expressed and encodes four different transcripts of 1.4, 1.8, 4.5, and 7.5 Kb, thought to result from alternative splicing (occurring in exons 2, 10, and 11), and from different polyadenylation signals (Ichikawa et al. 2001). At the moment, five *ATXN3* cDNA variants were described: MJD1a, MJD 2-1, MJD1-1, MJD5-1, and H2 (Kawaguchi et al. 1994; Goto et al. 1997; Ichikawa et al. 2001). The MJD1-1 and MJD5-1 variants only differ in the size of their 3' UTR.

1.3.4. Ataxin-3 protein(s)

The *ATXN3* gene encodes ataxin-3 (ATX3), a protein with a molecular weight of 42 KDa, possessing a polyQ tract in the C-terminal (Kawaguchi et al. 1994; Goto et al. 1997).

The expression pattern of ATX3 is controversial. ATX3 was shown to be ubiquitously expressed, being mainly cytoplasmatic, in peripheral tissues, throughout the brain, and in lymphoblastoid cell lines (Paulson et al. 1997a; Wang et al. 1997). Mutant ATX3 was shown to accumulate in the nucleus, as ubiquitylated inclusions, only in neurons from regions affected in MJD (Paulson et al. 1997b). However, other researchers showed both ATX3 cytoplasmic and nuclear localisation in MJD patient's brains (Wang et al. 1997). Further contradiction findings were reported, as in MJD brains and HeLa cell lines ATX3 was found to be cytosolic, while being nuclear and mitochondrial after sub-cellular fractionation (Trottier et al. 1998). Studies in mammalian cells demonstrated that ATX3 though not exclusively, was mostly found in the nucleus, being associated to the inner nuclear membrane (Tait et al. 1998). The additional finding of a nuclear localisation signal (NLS) in ATX3 strengthened the evidence for a nuclear localisation, being normal ATX3 indeed translocated to the nucleus and independently of the polyQ tract size (Tait et al. 1998).

These contradicting observations could be due, in part, to the use of different antibodies, which might be recognising potential protein isoforms or protein cleavage products with different subcellular localisation.

ATX3 comprises a Josephin domain, at its N-terminal, followed by two or three ubiquitin interacting motif (UIM) domains (depending on the potential isoform), and the polyQ segment (Figure 1.1).

The UIM domain is a highly conserved sequence that was initially found in the proteasome S5a subunit, and afterwards found in several proteins participating in the ubiquitination processes and in endocytosis (Young et al. 1998; Miller et al. 2007). The UIMs can act either to bind ubiquitin or ubiquitinated proteins, or to promote ubiquitination (Miller et al. 2004).

So far, no specific studies about the ATX3 protein isoforms were reported. However, since different cDNA variants were cloned, we can speculate about the existence of the correspondent four protein isoforms (Figure 1.1). These proteins were designated in 2003 (Albrecht et al. 2003): **ATX3-v1**, constituted by 361 amino acids (aa), is encoded by the MJD1-1 and MJD5-1 cDNAs, carries three UIMs and possesses an hydrophilic C-terminal (Goto et al. 1997); **ATX3-v2** is the longest variant (364 aa), the corresponding protein of MJD2-1, contains two UIMs before the polyQ tract and an hydrophobic C-terminal (Goto et al. 1997); **ATX3-v3** (348 aa) is the protein encoded by the cDNA variant cloned for the first time, MJD1a, corresponding to a truncated variant of ATX3-v2 in 16 aa due to a premature

stop codon that is the result of the TA<u>A</u>^{1118}/TA<u>C</u>^{1118} SNP (Kawaguchi et al. 1994); and **ATX3-v4** (306 aa) is 55 aa shorter then ATX3-v1 due to the absence of the residues encoded by exon 2 in the H2 cDNA variant, carrying an incomplete Josephin domain which lacks the catalytic cysteine 14 (C14) (Ichikawa et al. 2001) (Figure 1.1).

In 2003, using bioinformatic analyses, it was shown for the first time that the Josephin domain, comprising the first 198 aa of ATX3, was a highly evolutionarily conserved domain that possessed the predictive catalytic triad (C14-H119-N134) typical of ubiquitin C-terminal hydrolases (UCHs), and thus, might have a role as a ubiquitin-specific cysteine protease (USP) (Scheel et al. 2003). In the same year and also using bioinformatic approaches it was suggested that ATX3 could be an ubiquitin-interacting protein, localising to polyQ aggregates in a UIM-dependent manner, and partially modulating the Josephin domain (Donaldson et al. 2003).

In fact, these potential observations were confirmed *in vitro*, by the binding of ATX3 to K^{48}-linked ubiquitin (Ub) chains, hydrolysing preferentially protein chains containing more than four Ub (Burnett et al. 2003; Chai et al. 2004). This deubiquitinating (DUB) activity of ATX3 was shown to be dependent on the conserved cysteine 14 (C14) *in vitro* (Burnett et al. 2003; Chai et al. 2004), and *in vivo* as overexpression of C14A-mutated protein in neuronal

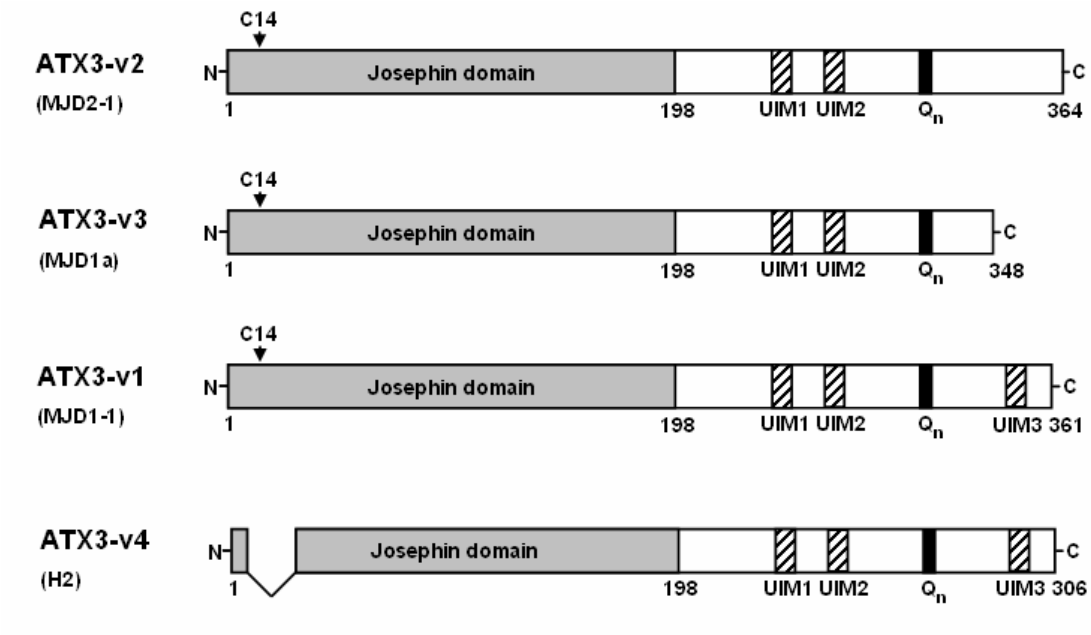

Figure 1.1. Schematic representation of the ATX3 protein variants. ATX3 may exist as four different protein variants. The accession numbers of the proteins are the following: for ATX3-v1, Q96TC4; ATX3-v2, Q96TC3; ATX3-v3, AAB33571.1; and ATX3-v4, BAB18798. The corresponding cDNA variants are indicated in parenthesis.

cells led to an accumulation of ubiquitylated proteins (Berke and Paulson 2003). More recently, it was shown that ATX3 catalytic activity is able to regulate its own cellular turnover exerting its (Todi et al. 2007). ATX3 is also able to bind ubiquitylated proteins in a manner that is regulated by its UIM domains (Berke et al. 2005), and interestingly the ATX3 UIMs are capable of inhibiting the aggregation of expanded huntingtin (Miller et al. 2007).

A three-dimensional structure is still unavailable for the entire ATX3. However, the first studies, using limited proteolysis and NMR assays, revealed the existence of a region resistant to proteolysis, and a flexible C-terminal region, comprising the polyQ tract (Masino et al. 2003). Later, using NMR analysis of the Josephin domain alone, it was possible to observe that this domain, rich in α-helices, adopts an open semi-elongated L-structure, in agreement with its cysteine-mediated activity (Nicastro et al. 2005).

1.3.5. Ataxin-3 homologues

ATX3 is an evolutionarily conserved protein. Alignment of the ATX3 protein sequence with others in databases showed a long list of homologue proteins in other species. As examples, ATX3 homologous proteins were found in the ***Rattus norvegicus*** (NP-067734) (Schmidtt et al. 1997), ***Mus musculus*** (NP_083981) (Costa et al. 2004), ***Gallus gallus*** (NP_989688.1) (Linhartová et al. 1999), ***Xenopus tropicalis*** (NP_001016389.1), ***Danio rerio*** (AAY28605.1), ***Caenorhabditis elegans*** (NP_506873.1) (Rodrigues et al. 2007), and ***Arabidopsis thaliana*** (NP_190981.1) species, sharing 84, 84, 75, 72, 68, 37, and 36% of identity with ATX3-v1, respectively (Figure 1.2).

In relation to the ATX3 rat homologue, only the cDNA sequence is known; it is very similar to the human, and there are two transcripts, one with 6 Kb, ubiquitously expressed, and another one with 1.3 Kb specifically expressed in the testis (Schmidtt et al. 1997).

The study of the mouse *Mjd* homologue gene and of its encoded protein is the main theme of this thesis and will be discussed in the following chapters. Very recently, the first knockout mouse for the *Mjd* gene was reported, showing to be apparently normal at the phenotypic level, but revealing an accumulation of ubiquitinated proteins, reinforcing the idea that this protein is regulating protein ubiquitination (Schmitt et al. 2007).

Recently, we reported an extensive study of the ATX3 homologue in *Caenorhabditis elegans* (Rodrigues et al. 2007). In this study, the genomic structure of the *atx-3* gene was determined, and the gene was shown to be expressed throughout development, but mainly in the adult stages. The worm homologue protein presents DUB activity, *in vitro*, as its human counterpart, and localises both in the cytoplasm and the nucleus. The transcriptomic analysis of knockout *atx-3* animals, also with no apparent phenotype, revealed that this

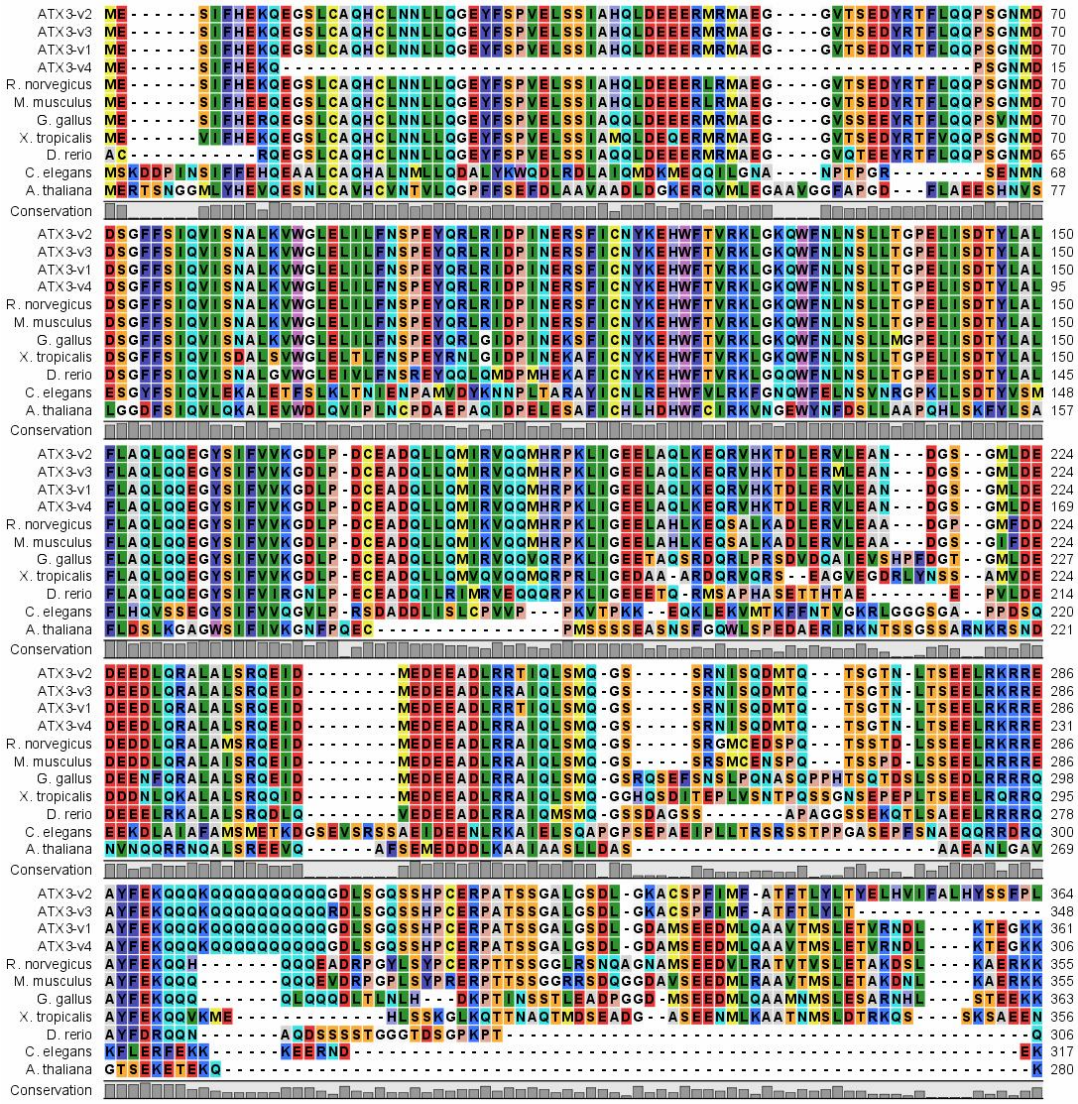

Figure 1.2. Multiple sequence alignment of the human ATX3 variants (v1, v2, v3, and v4) with the homologues in *Rattus norvegicus*, *Mus musculus*, *Gallus gallus*, *Xenopus tropicalis*, *Danio rerio*, *Caenorhabditis elegans*, and *Arabidopsis thaliana*. The alignment was performed using the CLC Workbench 3.5.1 program.

protein might be involved in the ubiquitin-proteasome system (UPS), structure/motility and signal transduction (Rodrigues et al. 2007).

1.3.6. Ataxin-3 interactors and potential function(s)

As described, there are already two genetically modified organisms available that are null for the expression of the *ATXN3* homologue genes. Both the *C. elegans* (Rodrigues et al. 2007) and mouse (Schmitt et al. 2007) knockout models do not present an obvious phenotype, which suggests that ATX3 is not essential for cell survival. Since there is not a

specific pathway obviously disrupted by the absence of ATX3 expression, the knowledge of the ATX3 molecular partners is of great importance in order to define the molecular mechanisms in which this protein is involved and, subsequently, to obtain some insight into its physiological role.

Several efforts have been made during the past seven years to identify the protein interactors of ATX3. At this moment, about 27 molecular partners of ATX3 are known (Table 1.2). These ATX3 interactions pointed out for its involvement in four principal pathways: cellular DNA damage response, transcription regulation, protein surveillance mechanism, and aggresome formation.

The interactors that support a possible function of ATX3 in the cellular DNA damage response were the first ones to be reported, in 2000 (Wang et al. 2000). These were the two

Table 1.2. Known protein interactors of ATX3

Protein		
Name	**Description**	**Reference**
ACCN2	amiloride-sensitive cation channel 2, neuronal	Shen et al. 2006
ARHGDIA	Rho GDP dissociation inhibitor (GDI) alpha	Shen et al. 2006
CHIP	STIP1 homology and U-box containing protein 1	Jana et al. 2005
CREBBP	CREB binding protein	Li et al. 2002
Derlin-1	Der1-like domain family, member 1	Wang et al. 2006
Dynein	dynein, cytoplasmic 2, heavy chain 1	Burnett et al 2005
FOXO4	forkhead box Other 4	Araujo et al. 2007
HDAC3	histone deacetylase 3	Evert et al. 2006
HDAC6	histone deacetylase 6	Burnett et al 2005
HHR23A	RAD23 homolog A (*S. cerevisiae*)	Wang et al. 2000
HHR23B	RAD23 homolog B (*S. cerevisiae*)	Wang et al. 2000
NCOR1	nuclear receptor co-repressor 1	Evert et al. 2006
NEDD8	neural precursor cell expressed, developmentally down-regulated 8	Ferro et al. 2007
PARK2	parkin	Tsai et al. 2003
PCAF	p300/CREBBP-associated factor	Li et al. 2002
PLIC-1	protein linking IAP to the cytoskeleton	Heir et al. 2006
p300	E1A binding protein p300	Li et al. 2002
p45	proteasome (prosome, macropain) 26S subunit, ATPase, 5	Wang et al. 2007
SELS	selenoprotein S	Wang et al. 2006
SUMO1	SMT3 suppressor of mif two 3 homolog 1 (S. cerevisiae)	Shen et al. 2006
SYVN1	synovial apoptosis inhibitor 1, synoviolin	Wang et al. 2006
TBP	TATA box binding protein	Araujo et al. 2007
TUBB	tubulin, beta	Zhong et al. 2006
UBB	ubiquitin B	Ferro et al. 2007
UBE4B	ubiquitination factor E4B (UFD2 homolog, yeast)	Matsumoto et al. 2004
VCP	valosin-containing protein	Dai et al. 2000
WT1	Wilms tumor 1	Araujo et al. 2007

human homologues of the yeast DNA repair protein RAD23 (HHR23A and HHR23B), which play important roles in the UPS, and in the general DNA damage-repair mechanism, the nucleotide excision repair (NER) (Li et al. 1997; Sugasawa et al. 1997; Hsieh et al. 2005).

However, a high number of ATX3 partners identified to the date also indicate that this protein is involved in the transcription regulation mechanism. One of the possible roles of ATX3, in this specific mechanism, is to act as a transcriptional repressor either by interacting with the cAMP-response element binding (CREB)- binding protein (CREBBP), p300, and p300/CREBBP associated factor (PCAF), inhibiting the CREB-mediated transcription pathway; or by directly binding to histone acetylation sites (Li F et al. 2002). Additional evidence supported a potential function as a transcriptional repressor, since ATX3 promotes the deacetylation of histones, namely by its binding to specific chromatin regions of the metalloproteinase-2 (*MMP2*) gene promoter, recruiting the histone deacetylase 3 (HDAC3) and the nuclear receptor co-repressor 1 (NCOR1) to these regions (Evert et al. 2006). Another putative function of ATX3 in the transcriptional regulation of gene expression might be the modulation of transcription factor activity, as suggested by its direct interaction with several transcription factors, such as the forkhead box Other 4 (FOXO4), Wilm's tumor 1 (WT1) and TFIID (TBP) (Araujo et al. 2007). These transcription factors came out from the ATX3 interacting transcription factor profiling recently reported (Araujo et al. 2007). However, the functional studies revealing the effect of ATX3 interaction with these transcription factors are still being performed.

Another series of ATX3 interactors indicate that ATX3 is playing a role in the protein surveillance machinery. The first evidence supporting this hypothesis appeared in 2001, with the discovery of an interaction between ATX3 and valosin-containing protein (VCP) (Hirabayashi et al. 2001). This molecular chaperone was shown to act in combination with ATX3 and HHR23B in the retro-translocation of polyubiquitinated substrates from the endoplasmic reticulum to the 26S proteasome (Hirabayashi et al. 2001; Kobayashi et al. 2002; Doss-Pepe et al. 2003; Boeddrich et al. 2006; Zhong and Pittman 2006). Recently, it was reported that this transient association of ATX3 with the endoplasmic reticulum membrane is mediated by its interaction with VCP and components of the Derlin-VIMP complex, namely derlin-1, synoviolin (SYVN1), and selenoprotein S (SELS) (Wang et al. 2006). Furthermore, ATX3 interacts with several ubiquitin-protein ligases (E3) and multiubiquitination enzymes (E4), such as parkin (Tsai et al. 2003), CHIP (Jana et al. 2005), p300 (Li et al. 2002), PCAF (Li et al. 2002), and ubiquitination factor E4B (UBE4B) (Matsumoto et al. 2004).

One of the most important findings was that ATX3 is a deubiquitinating enzyme (DUB), hydrolysing polyubiquitin (polyUb) chains *in vitro*, preferably K48-linked polyUb

chains containing four or more ubiquitin molecules (Burnett et al. 2003; Donaldson et al. 2003). This DUB activity seems to be conserved throughout evolution, given that the *C. elegans* ATX3 homologue also presents this activity *in vitro*, suggesting that it might be of functional relevance (Rodrigues et al. 2007). Additionally, it was recently shown that ATX3 interacts, although weakly, with monomeric ubiquitin, and of great importance, that ATX3 also interacts with neural precursor cell expressed developmentally down-regulated 8 (NEDD8), as well as it presents deneddylase activity (Ferro et al. 2007). NEDD8 is essential for the activity of SCF-like complexes, which are cullin-organised E3 ubiquitin ligases that determine the degradation of several substrates by the UPS. The deneddylase activity of ATX3 may be one of its potential roles in the modulation of the UPS (Ferro et al. 2007).

There are also some ATX3 interactors described that pinpoint a role for this protein in aggresome formation. In 2005, it was shown that ATX3 is essential for the formation of perinuclear aggresomes, namely by its interaction with histone deacetylase 6 (HDAC6) and dynein, which are proteins required for the aggresome arrangement and transport of misfolded proteins (Burnett and Pittman 2005). PLIC-1 (protein linking IAP to the cytoskeleton), a ubiquitin-like protein that binds to the ubiquitin-interacting motif (UIM) of some proteins, also interacts with ATX3 (Heir et al. 2006). This interaction occurs preferably in conditions of high aggregation, namely in expanded polyQ protein context, both ATX3 and PLIC-1 being proteins shuttled to the perinuclear aggresomes (Heir et al. 2006). However, the specific role of ATX3 in aggresome formation is still unknown.

Several other ATX3 interactors were found, that were directly related to its degradation or to the pathogenic effect of the mutated ATX3. Ataxin-3 seems to interact with itself *in vitro*, through its Josephin domain (Gales et al. 2005), and consequently to be a substrate of itself (Berke et al. 2005). Very recently, it was shown that the DUB catalytic activity of ATX3 regulates its cellular turnover, ubiquitination, and subcellular distribution (Todi et al. 2007). Also, it was shown that p45, an ATPase subunit of the 19S proteasome, interacts with ATX3 and stimulates its degradation *in vitro* (Wang et al. 2007), corroborating previous data which demonstrated that the expanded ATX3 is polyubiquitinated and degraded by the proteasome, being this process mediated by the ubiquitination factor E4B (UBE4B), an ubiquitin chain assembly factor homologue of yeast UFD2a (Matsumoto et al. 2004).

Interestingly, and possibly related to the ATX3 subcellular localisation, is the fact that ATX3 also interacts with the small ubiquitin-like modifier-1 (SUMO-1), a protein involved in the sumoylation post-transcriptional modification process (Shen et al. 2006; Miller et al. 2007). We could speculate that ATX3 may be a target of sumoylation, which might be affecting its subcellular localisation. SUMO-1 was identified as an interactor of ATX3 in a yeast two-hybrid screening of a human cDNA library in conjunction with two other interactors,

rhodopsin (Rho) guanosine diphosphate (GDP) dissociation inhibitor (GDI) alpha (ARHGDIA), and neuronal amiloride-sensitive cation channel 2 (ACCN2) (Shen et al. 2006).

1.4. The ubiquitin-proteasome system (UPS)

The regulation of specific protein levels is crucial for many cellular processes. Both protein synthesis and protein degradation must be tightly regulated for cell survival. Eukaryotic cells have two main mechanisms for protein degradation: lysosomes and proteasomes. While the lysosomes degrade the majority of endocytosed (membrane) proteins, the proteasome degrades most long and short-lived normal and abnormal proteins within the cell (Goldberg 2003). The 26S proteasomes, localised in the cytoplasm and in the nucleus (von Mikecz 2006), are housekeeping multisubunit proteolytic machines, ATP-driven, that preferentially degrade proteins tagged with polyubiquitin chains (Elsasser and Finley 2005). This large structure of 2000 KDa is constituted by the central 20S proteasome, in which the proteins are cleaved, and two 19S complexes, which provide substrate specificity and regulation (Elsasser and Finley 2005).

1.4.1. Ubiquitin and polyubiquitin chains

Ubiquitin (Ub) is a small 76 amino acid protein, highly evolutionarily conserved in all eukaryotes (Glickman and Ciechanover 2002).

Polyubiquitin chains are assembled via an isopeptide linkage between the lysine residue of the previous ubiquitin and the C-terminal glycine residue of the subsequent ubiquitin. Due to the presence of seven lysine residues in the ubiquitin molecule (K6, K11, K27, K29, K33, K48, and K63), different multiubiquitin chains can be formed *in vivo*, although the biological relevance of some types of polyUb conjugations remains unknown (Woelk et al. 2007). Proteins conjugated with a K48-linked polyUb chain are, in general, sent to the proteasome for degradation. Monoubiquitination or polyubiquitination using other lysines, such as K63, are involved in the regulation of subcellular localisation, vesicular trafficking, endocytosis, DNA repair, and translation (Glickman and Ciechanover 2002; Woelk et al. 2007).

1.4.2. Protein ubiquitination

Ubiquitin is covalently linked to proteins in a process mediated by a multienzyme

cascade involving in general three types of enzymes: E1 (Ub-activating enzyme), E2 (Ub-conjugating enzyme) and E3 (Ub-protein ligase) (Figure 1.3). The process of ubiquitination is balanced by the reverse process of deubiquitination catalysed by deubiquitinating (DUB) enzymes (see section 1.5).

E1 activates ubiquitin in an ATP-dependent manner through the formation of a thiol esther between a reactive cysteine in E1 and the C-terminal of ubiquitin. Ubiquitin is then transferred from E1 first to a catalytic cysteine within the ubiquitin-conjugating (UBC) domain of E2, and then to E3 (Hershko 1983). E3s catalyse the last step, that is the formation of a stable isopeptide linkage between the carboxyl-terminal glycine of ubiquitin and the ε-amino

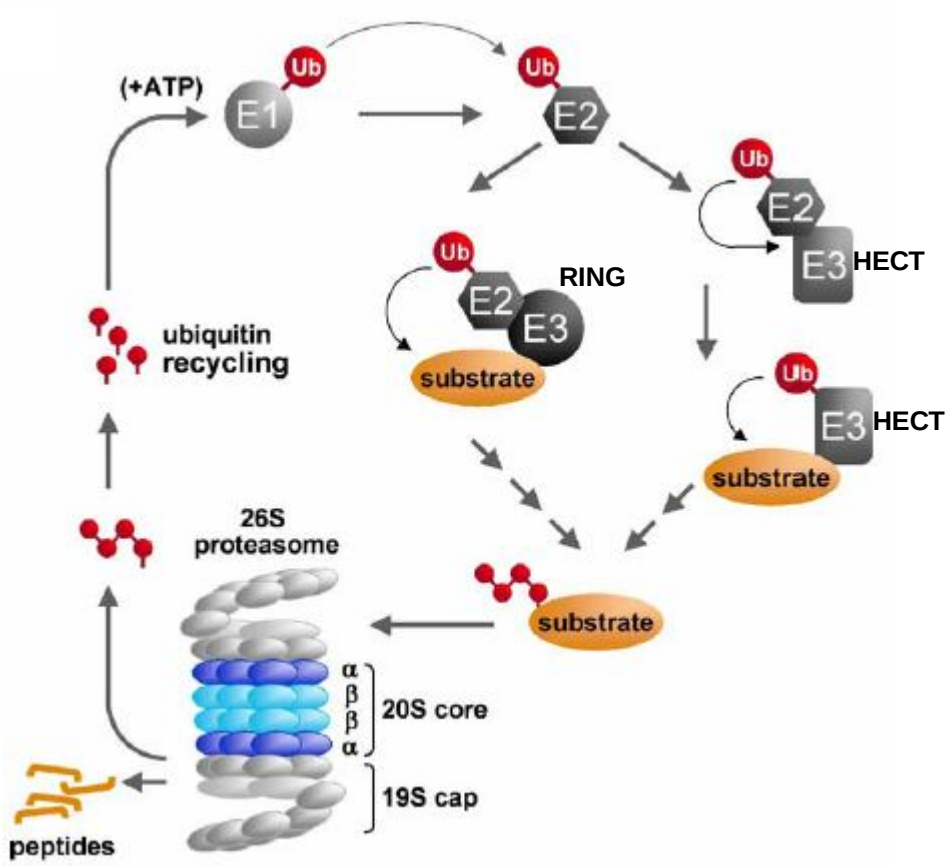

Figure 1.3. The conjugation of ubiquitin (Ub) to substrates usually involves three steps: an initial activation step, catalyzed by E1; an intermediate step, in which the ubiquitin is covalently linked to a conjugating enzyme, E2; and a final step, in which the ubiquitin reaches its ultimate destination of the substrate amino group. The last step is facilitated by the E3 ligase enzyme family. Some types of E3s facilitate ubiquitin conjugation to the substrate directly from E2 by acting as a bridging factor (RING-type). Another type of E3 forms an ubiquitin-thiol-ester intermediate, before the ubiquitin is transferred to the substrate (HECT-type). After linkage of a polyubiquitin chain onto the protein that is to be degraded, its recognition occurs at the 19S cap of the 26S proteasome (a*dapted from Zolk et al. 2006*).

group of a lysine residue in the target protein. However, in some cases, multiubiquitination requires the additional activity of certain ubiquitin-chain elongation factors, denominated as E4 enzymes, which catalyse polyubiquitin-chain assembly in collaboration with E1, E2, and E3 enzymes (Hoppe 2005).

Eukaryotic cells contain one E1, but multiple E2s and E3s. The substrate specificity depends mainly on the identity of the E3 ligases.

There are two main families of E3 Ub-protein ligases known, the HECT (homologous to E6-associated protein C terminus) and the RING (really interesting new gene)-finger (Pickart 2001). The HECT domain E3 enzymes function themselves as ubiquitin carriers, i.e., the HECT catalytic domain forms a thioester intermediate with ubiquitin before transferring it to the bound substrate (Scheffner et al. 1993) (Figure 1.4). Conversely, the RING domain class E3 does not have catalytic activity by itself, but uses the Zn-binding RING structural motif to recruit and direct an E2 enzyme towards specific substrates, which are mostly recognised by associated substrate recruitment subunits (Jackson et al. 2000) (Figure 1.4).

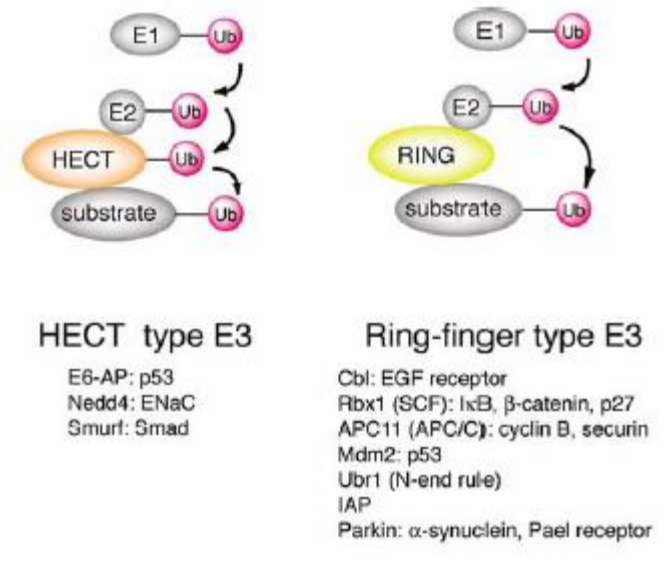

Figure 1.4. Two families of ubiquitin-protein ligases (E3s). HECT type and RING-finger type E3s have been identified at the molecular level. Unlike HECT type E3s, RING-finger E3s do not form thiol-ester intermediates with ubiquitin. Examples of each E3 family and their target proteins are indicated (*adapted from Hatakeyama and Nakayama 2003*).

The definition of E4s as a novel class of enzymes (Hoppe 2005), participating in the protein ubiquitination machinery, is a controversial theme since other researchers proposed this class as a new family of E3 enzymes, the U-box E3s (Hatakeyama and Nakayama 2003).

The prototype of a U-box protein is the yeast ubiquitin fusion degradation 2 (Ufd2) that was first identified as an Ub-chain assembly factor and denominated as E4 (Koegl et al. 1999). Hatakeyama and colleagues have demonstrated *in vitro* that some mammalian U-box proteins, including UFD2a (the mouse homologue of Ufd2), possess E3 activity (Hatakeyama et al. 2001). In contrast, UFD2a-dependent multiubiquitination of ATX3 requires additional E3 activity, and thus in this situation UFD2a functions as an E4, and not an E3 enzyme (Matsumoto M et al. 2004).

E4 enzymes might regulate the inactivation of certain proteins that have acquired a different function by monoubiquitination, acting on the switch from the mono to the

multiubiquitinated state of these proteins (Hoppe 2005). The E4 enzymes can be of two types: U-box type, including Ufd2, UFD2a, UFD2b, and CHIP; and the non-U-box type such as p300, and BUL1 (binds to ubiquitin ligase)- BUL2 (Hoppe 2005).

1.4.3. Ubiquitin-like proteins

As mentioned above, the modification of proteins by ubiquitination is not strictly to send them for proteasomal degradation. Through the protein tagging with ubiquitin and ubiquitin-like (UBL) proteins, the cell provides a diverse family of modified proteins that can be identified by downstream protein receptors/interactors and used to control many cellular regulatory pathways (Welchman et al. 2005).

Proteins of the ubiquitin family have been defined by their structural similarity with ubiquitin and can be divided into two classes (Walters et al. 2004): type I UBLs are similar to ubiquitin, and can either freely or covalently attached to other proteins via an enzymatic cascade; type II proteins comprise ubiquitin-like domains, and/or ubiquitin-associated (UBA) domains within the context of a large protein. These type II proteins are able to bind to proteasome subunits, through the UBL domain, and to Ub or polyUb chains, by the UBA domain (Welchman et al. 2005). Several UBL proteins are listed in Table 1.3.

1.4.4. The roles of UPS

The UPS is thought to mediate selectively the degradation of “normal” proteins, the levels of which are crucial for several basal processes, such as cell cycle progression, differentiation, proliferation, the response to stress, antigen processing, signal transduction, transcriptional regulation, DNA repair, apoptosis, and organelle biogenesis (Glickman and Ciechanover 2002).

However, one other function of the UPS is to protect the cell from misfolded and damaged proteins. The folding of newly synthesised proteins into their proper conformation might be often unsuccessful, and they may then undergo degradation in a few minutes after their synthesis (Schubert et al. 2000). Once synthesised and properly folded, proteins are also constantly exposed to highly reactive molecules and to conditions that favour denaturation, in a process called “protein aging”. The UPS constitutes the cell quality control system, which monitors proteins for signs of misfolding, postsynthetic denaturation or chemical damage (Glickman and Ciechanover 2002).

Recently, UPS-mediated proteolysis has been implicated in the control of cellular processes affected in several disease conditions: cachexia, cardiac dysfunction, cancer, cataract formation, viral infections, autoimmune/ rheumatoid diseases, and

Table 1.3. Proteins of the ubiquitin-like family

Ubiquitin-like proteins		
Type	**Acronyn**	**Full name/description**
Type I	**NEDD8**	neural precursor cell expressed, developmentally down-regulated 8
	SUMO1	small ubiquitin-related modifier1
	SUMO2	small ubiquitin-related modifier2
	SUMO3	small ubiquitin-related modifier3
	ISG15/ UCRP	interferon-stimulated gene-15
	FAT10	F-adjacent transcript-10
	FUB1	fau ubiquitin-like protein
	UBL5	ubiquitin-like protein-5
	URM1	ubiquitin-related modifier-1
	ATG8	autophagy 8
	ATG12	autophagy 12
	UFM1	ubiquitin-fold modifier-1
Type II	**PLIC-1**	protein linking IAP to the cytoskeleton 1
	PLIC-2	protein linking IAP to the cytoskeleton 2
	HHR23A	RAD23 homolog A (*S. cerevisiae*)
	HHR23A	RAD23 homolog B (*S. cerevisiae*)
	NUB1	NEDD8 ultimate buster-1
	PARK2	parkin
	A1Up	ataxin-1 ubiquitin-like interacting protein
	BAG1	BCL-2 binding athanogene-1 protein
	UBQLN3	ubiquilin3
	Elongin-B	transcription elongation factor B (SIII), polypeptide 2
	U713	ubiquitin conjugating enzyme 7 interacting protein 3
	S3A1	splicing factor 3 subunit 1
	BAT3	HLA-B-associated transcript
	UCH14	ubiquitin carboxyl-terminal hydrolase 14

neurodegenerative diseases (Dahlmann 2007). Although this idea is still controversial, the UPS has been suggested to be impaired in some polyQ disorders, as is the case of MJD, thus constituting a putative therapeutical target (Davies et al. 2007).

1.5. Deubiquitinating enzymes

As described above, proteins can be modified by ubiquitin, and also by ubiquitin-like (UBL) molecules. These post-translational modifications are critical regulatory processes in many aspects of cell biology. More than twelve different Ub and UBL modifications have

been described (Welchman et al. 2005). The removal of Ub molecules from polypeptides is performed by deubiquitinating enzymes (DUBs). These enzymes, although playing key regulatory roles in multiple processes, are poorly understood in relation to their mode of regulation and substrate specificity. However, it is very unlikely that all the predicted DUBs are truly specific for Ub, instead they might display additional or exclusive activity toward UBL molecules (Nijman et al. 2005).

1.5.1. DUB classes

Although the majority of DUBs belong to the class of cysteine proteases, there are some metalloproteases.

The enzymatic activity of cysteine proteases relies on a catalytic triad localised in the active site: deprotonation of the thiol group of a cysteine is assisted by an adjacent histidine, which in turn is polarised by an aspartate residue. During catalysis (1) the cysteine performs a nucleophilic attack to the carbonyl group of the peptide bond (in DUBs is between the target and Ub); (2) the intermediate, containing a oxyanion is stabilised in the oxyanion hole (provided by the main chain of the cysteine and a glutamine, glutamate, or asparagine residue); (3) the result of the reaction is the release of the target protein and formation of a covalent intermediate with the Ub molecule; (4) the reaction of this intermediate results in the release of the free enzyme and Ub (Nijman et al. 2005).

In metalloproteases, a Zn^{2+} ion is stabilised by an aspartate and two histidine residues, and the intermediate with the substrate is released upon reaction with a water molecule.

Cysteine protease DUBs can be organised into four subclasses based on their Ub-protease domains: ubiquitin-specific protease (USP), ubiquitin C-terminal hydrolase (UCH), Otubain protease (OTU), and Machado-Joseph disease protein (MJD) (Nijman et al. 2005). All metalloprotease DUBs contain an Ub protease domain called JAMM (JAB1/MPN/Mov34 metalloenzyme). Three-dimensional structures of DUB catalytic domains from all these subclasses revealed the similarities and differences between cysteine proteases (Figure 1.5).

The UCH subclass, comprising four proteins, was suggested to preferentially cleave relatively small protein substrates (up to 20-30 aa) from Ub (Amerik and Hochstrasser 2004). However, another study demonstrated that larger substrates can be accommodated in their catalytic site (Misaghi et al. 2005). UCHs are thought to mainly act: (1) in the recycling of Ub when it is inappropriately conjugated to intracellular nucleophiles; or (2) in the processing of newly synthesised Ub, which is translated either as a polyubiquitin precursor or fused to ribosomal protein precursors (Nijman et al. 2005).

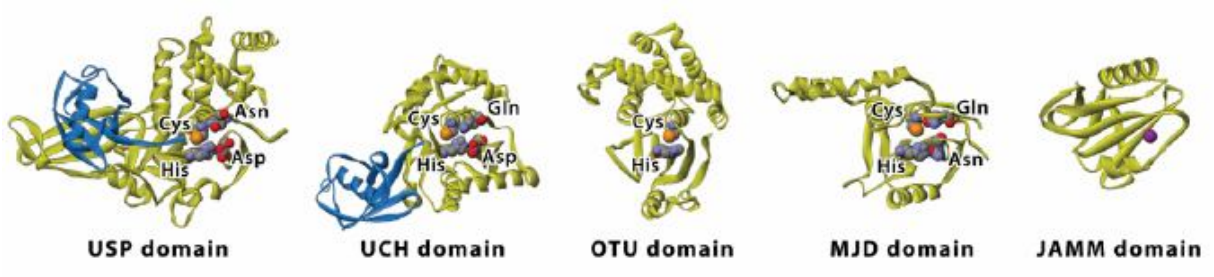

Figure 1.5. Structures of the catalytic domains of the five subclasses of Ub-specific proteases (yellow). Structures show the remarkable variability in secondary structure between the DUB classes. Catalytic centers are shown as Van der Waals spheres (carbon, gray; nitrogen, blue; oxygen, red; sulfur, orange; zinc, purple), and have been aligned for easy comparison. Ub is shown in blue in the two first structures. (*adapted from Nijman et al. 2005*)

The USP subclass, given its high diversity, is comparable to the class of E3 Ub-ligases in size. However, little is known about the function of these USPs.

The role of most of the OTU proteases also remains unknown. Nevertheless, the *otu* gene is involved in the development of the *Drosophila melanogaster* ovary, and the Otu protein was shown to cooperate with two heterogeneous nuclear ribonucleoproteins (hnRNPs) Hrb27c and Sqd (Squid), in the regulation of the localisation and translation of the gurken (grk) mRNA (Goodrich et al. 2004). However, the physiological role of the OTU proteases remains to be investigated.

The JAMM domain metalloproteases might have adopted new protease functions during evolution, and data indicates that some human JAMMs may be involved in more than Ub (or Ubl) processing (Nijman et al. 2005). In fact, the *Mycobacterium tuberculosis* gene *mec*$^{+}$ encodes a JAMM domain peptidase, involved in cysteine biosynthesis by cleaving cysteine from a peptide intermediate (Burns et al. 2005). Furthermore, the sequence alignment of the JAMM-domain proteins revealed that half of them have at least one amino acid variation in the conserved Zn^{2+} ion-stabilising residues, indicating that they might not be functional proteases (Nijman et al. 2005).

In evolutionary terms, MJD DUBs, the human variants of ataxin-3, seem to represent a relatively late addition to the Ub system, since no homologues were found in yeast (Nijman et al. 2005). Targets of these DUBs remain unknown.

1.5.2. DUB specificity

In the case of DUBs, specificity can be referred to the Ub or UBL moiety itself (substrate specificity) or the target protein to which the moiety is conjugated (target

specificity). However, the most probable way to determine overall DUB specificity might be a combinatorial mechanism relying on recognition of both target and the attached moiety.

1.5.2.1. Substrate specificity

In relation to substrates, DUBs may selectively act in specific polyubiquitin branches. The presence of other Ub binding domains, such as UIMs (as in the case of ataxin-3), may contribute to Ub chain selection (Raasi et al. 2005).

Although the majority of putative DUBs tested do display Ub protease activity *in vitro*, some of these may also be active toward UBL molecules. USP21, UCH-L3, CSN5 and human ATX3 are able to cleave both Ub and the UBL molecule NEDD8 (Burnett et al. 2003; Donaldson KM et al. 2003; Groisman et al. 2003; Nijman et al. 2005; Ferro A et al. 2007).

On another hand, there are UBL molecules that are exclusively processed by specific proteases. This is the case of SUMO molecules, which are thought to be cleaved from target proteins specifically by the SENP family of proteases.

1.5.2.2. Target specificity

Target recognition by DUBs may be directed by other motifs outside the catalytic core. Nonetheless, like most enzyme/substrate interactions, DUB/target interactions are expected to be weak and transient in the natural context, which complicates the identification of *in vivo* targets. A more stable DUB/target complex may occur in the case of proteins linked improperly to K48-polyUb chains, because these proteins must be continuously deubiquitinated to protect them from degradation, leading to a longer DUB/target interaction.

Auto-ubiquitination of E3 Ub-ligases is a common phenomenon, which may be reverted by a DUB/E3 interaction, leading to a stabilisation of the E3s (Wu et al. 2004). However, DUB/E3 interactions could also imply double regulation of both the target and its DUB by the E3 ligase (Li et al. 2005). A third possibility for DUB/E3 interactions is that the DUB recognition of the substrate might be dependent of the E3 ligase (Kee et al. 2005; Li et al. 2005).

1.5.3. Cellular and physiological role(s) of DUBs

An important remark is that gene deletion studies in yeast indicated that none of the USPs is required for cell growth and viability (Amerik et al. 2000). In conformity, the *ATXN3* homologue knockouts in mouse and *C. elegans* were viable, and did not present any obvious

phenotype (Rodrigues et al. 2007; Schmitt et al. 2007). So far, the main known functions of DUBs are in the ubiquitin-proteasome pathway, in endocytosis, and in the regulation of chromatin structure.

1.5.3.1. DUBs and the UPS

As described in section 1.4, proteins that need to be degraded are usually targeted to the proteasome by K48-linked polyubiquitin chains. DUBs are key regulators in the UPS and could play four different roles: (1) processing of ubiquitin precursors; (2) editing or rescue of ubiquitin conjugates, which are generally protein adducts but can also be ligated to abundant small nucleophiles such as glutathione; (3) recycling of ubiquitin or ubiquitin oligomers from ubiquitin–protein conjugates targeted for degradation; and (4) disassembly of unanchored ubiquitin oligomers (Figure 1.6).

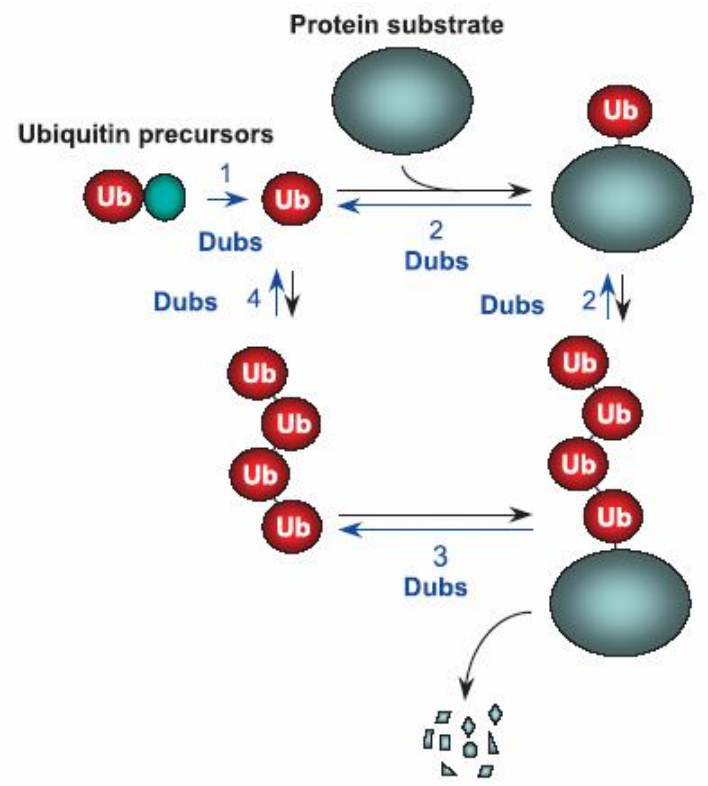

Figure 1.6. Functions of DUBs in the UPS. (1) Processing of ubiquitin precursors. (2) Editing or rescue of ubiquitin conjugates. (3) Recycling of ubiquitin or ubiquitin oligomers from ubiquitin–protein conjugates targeted for degradation. (4) Disassembly of unanchored ubiquitin oligomers. (*adapted from Amerik and Hochstrasser 2004*)

1.5.3.2. DUBs and endocytosis

Monoubiquitination and the attachment of K63-linked Ub dimer play an important role in endocytosis of receptors and protein sorting. After binding to ligands, receptor tyrosine kinases (RTKs) and adaptor proteins are monoubiquitinated at multiple sites, thereby being internalised. The E3 ligase for many RTKs is Cbl, which can also target proteins to degradation (Duan et al. 2004). Repeated ubiquitination or reduced deubiquitination may be the trigger for targeting into the lysosome though this process is unclear. Thus, DUBs are implicated in endocytosis at several levels, and also play important roles in other types of intracellular traffic.

1.5.3.3. DUBs and chromatin structure

Dynamic histone ubiquitination showed to be crucial in the regulation of transcription, as well as in double-strand-break formation during meiosis (Yamashita et al. 2004). Although most histones can be ubiquitinated, the dynamics of H2B monoubiquitination is better understood; both the ubiquitination and deubiquitination of H2B are necessary for optimal transcription, indicating a requirement for dynamic H2B modification by Ub (Henry et al. 2003).

1.6. Aims of the study

Mammalian species exhibit high homology at molecular, cellular, histological and physiological levels. For a long time, given their similarities to humans, rodents have been used as models of study in Biology. Studies in the rodent species have been of crucial importance to the knowledge of the physiological systems, functioning both in health and disease conditions. Among rodents, the mouse is the species of choice, given that our genetic knowledge of this species is quite developed, and a series of technologies are now available to manipulate its genome.

When we started this work, little was known about the function of ATX3. For this thesis, our main goal was to get insight into the function of ATX3, using the mouse as a model. But at the beginning, the mouse genome had not yet been sequenced, and nothing was known about the mouse homologue of the Machado-Joseph disease gene or its encoded protein. In general, our aims were thus the following:

- Characterisation of the mouse *Mjd* gene: cloning, determination of its genomic structure, and functional study of the promoter (Chapter 2);

- Characterisation of the mouse ATX3 (mATX3) protein: determination of its expression pattern in adulthood and during embryonic development, subcellular localisation, and biochemical activities (Chapter 2 and Chapter 4.2);

- Determination of the molecular partners of mATX3 and exploration of some hypotheses concerning its molecular function (Chapter 4);

- Assessment of potential physiological role of mATX3, focussing on the role of this protein (i) in the response to stress (Chapter 3); and (ii) in muscle development (Chapter 5).

Chapter 2

Characterisation of the mouse *Mjd* gene and of its encoded protein ataxin-3

Chapter partially based on the publication (Appendix 2):

Costa MC, Gomes-da-Silva J, Miranda CJ, Sequeiros J, Santos MM, Maciel P (2004) *Genomic structure, promoter activity, and developmental expression of the mouse homologue gene of the Machado-Joseph disease (MJD) gene*. Genomics 84:361-373

2.1. SUMMARY

MJD, a neurodegenerative disorder, is caused by the expansion of the $(CAG)_n$ tract in the *ATXN3* gene. This gene encodes the protein ataxin-3, a deubiquitinating enzyme (DUB), which is highly conserved through evolution. However, until now, the physiological role of this DUB activity was not clarified, and no other function(s) were attributed to ataxin-3 either in its normal state or when mutated in disease conditions. Given the high conservation of the protein, it is of great importance to use models of study in other species that could allow a better knowledge of both the function of this protein and its pathogenic mechanisms in the case of disease.

Here, and in order to characterise the mouse *ATXN3* homologue gene (*Mjd*), we cloned and determined the genomic structure of the mouse *Mjd* gene, that showed a similar structure to its human counterpart. We contributed to the functional characterisation of the *Mjd* TATA-less promoter. The *Mjd* gene 5'-flanking region contains conserved putative binding regions for transcription factors Sp1, USF, Arnt, Max, E47 and MyoD. We showed that the proximal -238 bp region its sufficient to direct maximal activity of the *Mjd* promoter in the P19 cellular system, and that upon differentiation of these P19 cells, the *Mjd* gene promoter is preferentially activated in endodermal and mesodermal derivatives, including cardiac and skeletal myocytes; and less so in neuronal precursors. Indeed, we have confirmed the *in vitro* binding of MyoD to the *Mjd* 1173 bp upstream region.

To confirm the orthology of the mouse *Mjd* gene, we have confirmed that mouse ataxin-3 (mATX3) conserves the DUB activity *in vitro* using both K^{48} and K^{63}-linked polyubiquitinated chains, and fluorimetric Ub-AMC assays. In this chapter, we were also able to show that mATX3 is ubiquitously expressed during embryonic development since E11.5 (the first studied stage), and in the adult. The expression was strong in regions of the CNS affected in MJD, and, interestingly, it was particularly abundant in all types of muscle and in ciliated epithelial cells, suggesting that this protein may be associated with the cytoskeleton, and may have an important function in cell structure and/or motility. Furthermore, we verified that, at the subcellular level, mATX3 localisation was not restricted to a specific organelle in all the tissues analysed (skeletal muscle, testis, pontine and dentate nuclei), which suggest that this protein may play roles in different cellular pathways.

2.2. INTRODUCTION

The MJD causative gene was mapped to chromosome 14q32.1 in 1993 (Takiyama et al. 1993) and cloned in 1994 (Kawaguchi et al. 1994), but its structure was only elucidated in

2001 (Ichikawa et al. 2001). Alternative splicing of the *ATXN3* gene results in the production of different isoforms of ATX3 (Goto et al. 1997), which are expressed in various tissues, and have been detected in the nucleus, in the inner nuclear membrane, in cytoplasm, and also in mitochondria (Paulson et al. 1997; Tait et al. 1998; Trottier et al. 1998; Ichikawa et al. 2001; Su et al. 2002).

Ataxin-3 is a recently discovered DUB that, in conjunction with other homologue proteins, and given their different predicted 3D structure in relation to the previous classes of DUBs, gave rise, to a new subclass of DUBs - MJDs (Nijman et al. 2005). DUB activity is conferred by its N-terminal Josephin domain, a globular structure containing the four essential residues Q9, C14, H119 and N134 responsible for its cysteine protease activity (Chow et al. 2004; Mao et al. 2005; Nicastro et al. 2005). ATX3 contains a polyglutamine (polyQ) tract in its C-terminal that is surrounded by two or three ubiquitin interacting motifs (UIMs) (Berke et al. 2005), depending on the protein isoform.

Several evidences suggest that ATX3 may have a role in the UPS, since this protein: (1) binds and hydrolyses K^{48}- linked multiubiquitin chains *in vitro* (Burnett et al. 2003; Doss-Pepe et al. 2003; Chai et al. 2004; Berke et al. 2005); (2) interacts with ubiquitin (Ub) and with neural precursor cell expressed developmentally down-regulated gene 8 (NEDD8), which is a ubiquitin-like (UBL) protein that regulates activity of E3 ligases (Ferro et al. 2007); and (3) associates with the proteasome interacting with p45 (an ATPase subunit of the 19S proteasome subunit) (Wang et al. 2007), and with VCP/p97 (an AAA ATPase important for the shuttling of many polyubiquitinated proteins to the proteasome) (Wang et al. 2006; Zhong and Pittman 2006).

Several protein sequences highly homologous to human ATX3 have been described in rat (Schmidtt et al. 1997) and chicken (Linhartová et al. 1999), and found in databases for mouse, *Fugu*, *Drosophila*, *C. elegans* and *A. thaliana* (Albrecht et al. 2003), suggesting that this protein is highly conserved during evolution and has functional relevance.

To gain insight into the function of ATX3, we isolated and characterised the mouse *Mjd* gene. We cloned the mouse *Mjd* gene, determined its genomic structure (∗), characterised (spatially and functionally) the promoter region using the P19 cellular model, expressed the recombinant mouse ATX3 (mATX3) protein, and analysed the expression pattern of mATX3 during mouse embryonic development and in the adult, as well as its subcellular localisation in some tissues of high mATX3 expression. Our results indicate that mATX3 conserves the deubiquitinating enzyme activity, was ubiquitously expressed and developmentally regulated, with high expression in muscle and ciliated epithelial cells, as well as in regions of the central nervous system (CNS) affected in MJD. In all the tissues analysed its localisation was not restricted to a specific cellular compartment.

 (∗) this study was performed before the mouse genome sequencing

2.3. MATERIALS AND METHODS

Computational methods

We applied the BLAST program (Altschul et al. 1990) to search for the homologue cDNA sequence in mouse with the accession number AK008675. All protein sequences were taken from the TrEMBL database. The accession numbers of human variants ATX3-v1, ATX3-v2/v3 as denoted in (Albrecht M et al. 2003), ATX3-v4 corresponding to H2 in (Ichikawa et al. 2001), rat ataxin-3 (rATX3) and mouse ataxin-3 (mATX3) are Q96TC4, Q96TC3, Q96TC3, BAB18798, O35815 and Q9CVD2, respectively. Multiple sequence alignment was constructed by means of CLUSTAL W (Thompson et al. 1994). Comparison of *ATXN3* sequence to the homologous 5' upstream region in the mouse *Mjd* gene was performed to uncover evolutionary conserved regions using TRES/TRANSFAC with a score of 95% (Wingender et al. 2000). Conserved regions in the *Mjd* gene were then scanned for the presence of potential transcription factors binding regions using TESS (Schug and Overton 1997).

Cloning of the full-length *Mjd* and *MyoD* cDNAs by RT-PCR

Total RNA was isolated from adult C57Bl/6 mouse brain and skeletal muscle, using Trizol reagent (Invitrogen). Five micrograms of total RNA were used to perform reverse transcription using the SuperScript™ First-Strand Synthesis System for RT-PCR (Invitrogen) with an oligo(dT) primer. In order to amplify the *Mjd* cDNA (1100 bp), PCR was performed using the Expand High Fidelity System (Roche), the primers mmMJD1 and mmMJD2 (Appendix 1, Table A.1), and 1.5 μL of total cDNA from mouse brain as template. To amplify the *Myod1* cDNA, PCR was carried out using the same system, the primers attB1Myod1 and attB2Myod2 (Appendix 1, Table A.2), and 1.5 μL of total cDNA from mouse skeletal muscle as template (1018 bp). The PCR conditions consisted of one cycle of 2 min at 94°C, followed by 32 cycles of one min at 94°C, one min at 62°C and one min at 72°C, and ending with 5 min at 72°C. The RT-PCR products corresponding to *Mjd* and to *Myod1* cDNAs were purified using GFX™ PCR DNA and Gel Band Purification Kit (GE Healthcare) and cloned in the pGEM-T Easy vector (Promega) (pMjd1) and in the pDONR207 vector using the Gateway system (Invitrogen Life Technologies) (pDON207Myod1), respectively, using the manufacturer instructions.

PCR

The probe (400 bp) used for screening the BAC library was amplified by PCR, using the *Mjd* cDNA (pMjd1) as template, with primers mmMJD1 and mmMJD3 (Appendix 1, Table A.1), and performed with the same cyclic parameters used for RT-PCR. The insertion of the restriction enzyme sites for the CAT reporter plasmids construction was performed using the reverse primer PMjd-1BglIIR in conjugation with one of the forward primers: PMjd-237KpnIF, PMjd-358KpnIF, PMjd-559KpnIF, PMjd-928KpnIF or PMjd-1173KpnIF (Appendix 1, Table A.3), giving rise to PCR products of 237 bp, 358 bp, 559 bp, 928 bp, and 1173 bp, respectively. The attB-flanked cDNA fragments encoding the full-length mouse ATX3 protein (mATX3, 1-355 aa), the Josephin domain (jos, 1-215 aa) and the C-terminal (UIMs, 215-355aa) were amplified by PCR, from the pMjd1 plasmid using, respectively, the primer pairs including the 5' and 3' attB site-specific recombination sequences (Gateway Cloning System): attB1Mjd/ attB2Mjd, attB1Mjd/ attB2Mjd:Jos, and attB1Mjd:UIMs/ attB2Mjd (Appendix 1, Table A.2). PCRs were all performed using the Expand High Fidelity System (Roche), under the following conditions: one cycle of 5 min at 95°C, followed by 35 cycles of one min at 95°C, one min at 55°C, one min at 72°C, and ending with 5 min at 72°C.

Isolation of a genomic BAC clone

The genomic BAC clone was obtained from Incyte Genomics, Inc.. Briefly, a BAC Mouse II library was screened by direct hybridisation, using a probe of 400 bp, constructed by PCR, using primers mmMJD1 and mmMJD3. These primers were designed on the basis of the cloned *Mjd* cDNA sequence. The positive BAC clone was grown overnight, at 37°C, in 2XYT medium containing the appropriate antibiotic (25 μg/mL of chloramphenicol). BAC DNA was isolated using the Qiagen Large-Construct Kit (Qiagen), and the manufacturer instructions.

Constructs and mutagenesis

To obtain different lengths of the 5'-flanking region of the *Mjd* gene, PCRs were performed, using the BAC clone 27521 as the template. For the CAT reporter plasmids construction we used the primer PMjd-1BglIIR to insert the 3' restriction enzyme site for BglII (at the position –1 bp) in all fragments, in conjugation with one of the primers PMjd-237KpnIF, PMjd-358KpnIF, PMjd-559KpnIF, PMjd-928KpnIF or PMjd-1173KpnIF, to insert the 5' restriction enzyme site for KpnI, at the respective lengths of the 5'-region -237, -358, -

559, -928 or –1173 bp. These PCR products were digested with BglII and KpnI and subcloned into digested BglII-KpnI pCAT3-Basic vector (Promega). The resultant constructs were p-237MjdCAT, p-358MjdCAT, p-559MjdCAT, p-928MjdCAT and p-1173MjdCAT.

The attB-PCR products corresponding to the cDNA fragments encoding the full-length mouse ATX3 protein (mATX3, 1-355 aa), the Josephin domain (jos, 1-215 aa) and the C-terminal (UIMs, 216-355 aa) were cloned into the pDONR207 vector using the Gateway Cloning System (Invitrogen) giving rise to the plasmids: pDONR207Mjd, pDONR207Mjd:jos and pDONR207Mjd:UIMs.

To obtain the pDONR207Mjd:C14A and pDONR207Mjd:jos:C14A plasmids a point mutation was introduced, corresponding to the alteration of the cysteine for an alanine residue at position 14, into the pDONR207Mjd and the pDONR207Mjd:jos plasmids using the mutagenesis primer Mjd-mutC14A (Appendix 1, Table A.4), the Pfu Turbo enzyme (Stratagene) and the DpnI endonuclease enzyme according to the published conditions (Makarova et al. 2000).

The recombinant His-tag protein expression plasmids pDEST17Myod1, pDEST17Mjd, pDEST17Mjd:jos, pDEST17Mjd:UIMs, pDEST17Mjd:C14A, and pDEST17Mjd:jos:C14A were obtained by recombination of the corresponding pDONR207 plasmids with the pDEST17 vector using the Gateway Cloning System (Invitrogen).

Expression and purification of recombinant His-tagged proteins

The recombinant hexahistidine-tagged Myod1, mATX3, mATX3:C14A, mATX3:jos, mATX3:jos:C14A, and mATX3:UIMs proteins were expressed in *Escherichia coli* BL21SI cells (Invitrogen). Cells were grown at 37ºC in LB/ON (without NaCl) medium containing 100 mg/l of ampicillin and 0.2% (w/v) of glucose until a cell density of 0.6 at 600 nm, the moment when the recombinant protein expression was induced by the addition of NaCl to a final concentration of 0.3 M and culture was further grown for 3 hours at 30ºC. Cells were harvested, ressuspended in buffer L (20 mM sodium phosphate (pH 7.5), 500 mM NaCl) (Gales et al. 2005), 10 mM imidazole, 50 mg/L lysozime and stored at -20ºC. Phenylmethylsulphonyl fluoride (PMSF) was added to the protein extract to a final concentration of 1mM, and after centrifugation the supernatant was collected and the recombinant protein was purified using the HiTrap Kit (GE Healthcare) being eluted in three fractions of buffer L containing 50 mM, 100 mM or 500 mM imidazole.

The fractions of the proteins mATX3, mATX3:C14A, mATX3:jos, and mATX3:jos:C14A, considered appropriate for further purification, were selected by SDS-PAGE analysis, applied to a HiPrep 26/60 Sephacryl S-200 high resolution column (GE Healthcare) equilibrated in buffer A (20 mM HEPES (pH7.5), 50 mM NaCl, 5% glycerol, 1

mM EDTA, 1 mM DTT), and protein was eluted with a flow rate of 0,5 mL/min, at 4 ºC, being monitored at 280 nm. After SDS-PAGE analysis, the fractions containing only protein monomers were pooled and concentrated in on Millipore Amicon Ultra-15 concentrators (cut-off 10 KDa, Millipore) to 1-2 mg/mL. Purified monomeric proteins were diluted into a 20 μM working solution and maintained in ice for enzymatic assays and then stored at -80 ºC.

Electrophoretic mobility-shift assay (EMSA)

The –928 bp fragment of the Mjd gene promoter, generated by KpnI/BglII restriction of the p-928MjdCAT, was used for EMSA. For the competition assay, single-stranded sense and antisense Myod1 oligonucleotides were synthesized based on both the sequence in the 5' region of the *Mjd* gene and on the binding matrix for Myod1 with the accession number M00184 (TRANSFAC database). The oligonucleotides Myod1-sense (5' AGCAGCTGTC) and Myod1-antisense (5'GACAGCTGCT) were annealed by incubation at 30ºC for 1 minute and by slow cooling to room temperature. DNA-protein binding assays were performed at room temperature for 30 minutes, using always the same amount of DNA (300 ng of the -928 bp fragment) and different quantities of recombinant mouse Myod1 protein in a final volume of 60 μL of TE. In the competition assay, the double-stranded oligonucleotides (200 ng) were incubated with the recombinant protein for 30 minutes before the incubation with the DNA. The mixtures were loaded in a 1% Nusieve 3:1 Agarose (FMC BioProducts) gel and electrophoresed at room temperature.

Cell culture and differentiation

The P19 clone was obtained from the American Type Collection. Cells were cultured (plating 10^6 cells in 75 cm^3 tissue culture flasks, every two days) in Dulbecco's modified Eagle's medium (DMEM), supplemented with 10% fetal bovine serum (FBS), in a 5% CO_2 humidified chamber at 37°C. To promote cellular differentiation, cells were cultured as aggregates, in bacterial Petri dishes, in medium supplemented with 1 μM all-trans retinoic acid (RA) (Sigma) for neuronal differentiation, or with 1% DMSO for cardiac/skeletal myocytes differentiation. Cells ($1x10^5$/ mL culture) were plated into bacterial Petri dishes (day 0), and incubated with medium (no-treatment) or with RA- or DMSO-supplemented medium, for two days. After two days, floating aggregates were collected and washed with medium, and replated into bacterial Petri dishes for one additional day. At day 3, the aggregates were harvested, dissociated by treatment with 0.25% trypsin, 1 mM EDTA (Gibco BRL), and then

plated in DMEM, 10% FBS in 60-mm diameter tissue culture-grade dishes. At day 4, cells were transfected with constructs p-237MjdCAT and p-1173MjdCAT.

Mouse C2C12 myoblasts were cultured in growth medium (GM) corresponding to Dulbecco's modified Eagle's (DMEM) Glutamax (Gibco BRL), 20% fetal bovine serum (FBS) and 1% penicillin/streptomycin, in a 5% CO_2 humidified chamber at 37ºC. Cell viability was assessed by trypan blue exclusion.

Cell transfection and CAT assay

To analyse activities of the CAT reporter plasmids in undifferentiated, untreated (day 3), RA-treated (day 3) and DMSO-treated (day 3) P19 cells, these were seeded at $2x10^5$, $7.5x10^5$, $7.5x10^5$ and $3x10^6$ cells per 60-mm diameter tissue culture-grade dishes in DMEM, 10% FBS 24 hours prior to transfection, respectively. Transient transfection was carried out in serum-free medium Opti-MEM (Life Technologies), using 10 μL of Lipofectamine™2000 Reagent (Life Technologies), to introduce 1.5 μg of reporter construct and 0.5 μg of pSV-β-Galactosidase control vector (Promega). After 5 hours of transfection, medium was changed for DMEM, 10% FBS.

Cells were harvested 48 hours after transfection, washed three times with phosphate-buffered saline (PBS), and then cell extracts were prepared in 1x reporter lysis buffer (Roche). Cell extracts were assayed for CAT activity, using the CAT ELISA kit (Roche). Measurements were performed in duplicate, averaged, and then normalised to the β-galactosidase activity, to correct for transfection efficiency, and to the total protein amount. β-galactosidase activity was measured using the β-Galactosidase Enzyme Activity system (Promega), and the total protein amount was assessed using the Lowry Protein assay kit (SIGMA) for the P19 cells or the Bradforf assay (Sigma Aldrich) for the C2C12 cells.

Deubiquitinating enzyme (DUB) assay

K^{48} and K^{63}- linked multiubiquitin chains (Biomol, International LP) (1 μg) were incubated with purified His-tagged mATX3, mATX3:C14A, mATX3:jos, mATX3:jos:C14A, and mATX3:UIMs proteins (2.5 μM) in a final volume of 20 μL of DUB assay buffer (50 mM HEPES (pH7.4), 500 mM EDTA, 1 mM DTT, 0.1 mg/mL BSA, COMPLETE (Roche Diagnostics), during 15 h at 30ºC. Reactions were stopped by addition of Laemmly sample buffer containing 100 mM DTT.

The substrate Ubiquitin (Ub) 7-amido-4-methylcoumarin (AMC) (Sigma Aldrich) was incubated with 800 nM of each His recombinant protein mATX3, mATX3:C14A, mATX3:jos,

mATX3:jos:C14A in 300 μL of DUB assay buffer. The reaction progress was monitored during 10 min, in a cuvette maintained at 37 ºC by a circulating bath, in a Jasco fluorescence spectrophotometer. Fluorescence emission at 460 nm (λ_{exc}= 380 nm) given by the cleavage of AMC from Ub-AMC.

Immunoblotting

Proteins were extracted from different tissues of adult C57Bl/6 mice, using standard methods (Sambrook et al. 1989). Total protein quantification was assessed using the Lowry Protein assay kit (Sigma). Proteins of spinal cord, brainstem, cerebellum, cerebral cortex, heart, skeletal muscle, testis, kidney, lung, spleen, pancreas, liver and stomach tissues (30 μg) were resolved on a 10% SDS-polyacrylamide gel, and transferred onto a nitrocellulose membrane (Hybond-C, GE Healthcare). The anti-human ataxin-3 specific antiserum (kindly provided by Henry Paulson) was used (1:2000). For detection of the immunocomplexes formed, the secondary antibody peroxidase-conjugated goat anti-rabbit IgG (Stressgen) (1:4000), or goat anti-mouse IgG (Jackson Immunoresearch Laboratories) (1:1000), were used. Staining intensity was developed with the chemiluminescence system (Roche).

The deubiquitinating assays of the K48 and K63- multiubiquitin chains were immediately loaded in a 10% SDS-PAGE polyacrylamide gel. Proteins were transferred in the same abovementioned way and membranes were incubated with a 1:1500 dilution of a monoclonal antibody to ubiquitinylated proteins (clone FK2, Biomol International LP). For the detection of the immunocomplexes it was used a peroxidase-conjugated goat anti-mouse antibody (Santa Cruz Biotechnology) (1:10,000), and a SuperSignal West Pico Chemiluminescent Substrate (Pierce).

Immunohistochemistry

Adult male C57Bl/6 mice were perfused transcardially, under anaesthesia, with fixative solution (4% paraformaldehyde, in 0.1M phosphate buffer, pH 7.4), for 10 minutes. The encephalon and peripheral tissues (skeletal muscle, cardiac muscle, pancreas, spleen, liver and testis) were post fixed for two hours in the same fixative. Mouse embryos were isolated from pregnant C57Bl/6 female mice, at E11.5, E12.5, E13.5, E14.5, E15.5 and E16.5. The day of plug detection was considered to be E0.5 (embryonic day 0.5). Embryos were washed with ice-cold PBS and fixed in 10% buffered formalin, for at least 24 hours, at 4°C. After fixation, the samples (adult tissues and organs and embryos) were paraffin embedded. Nominal 5 mm tissue sections were cut and mounted onto positive charged

slides (X-tra Slides®), deparaffinised on xylene, and rehydrated by passages through graded ethanol series. In formalin-fixed material, heating was performed to allow antigen recovery. Non-specific binding was blocked with normal goat serum (Vectastain® Elite ABC kit, Vector Laboratories). Sections were incubated overnight in primary anti-ataxin-3 antiserum diluted (1:2000) in PBS. Antibody labelling was visualised using the secondary anti-rabbit antibody by the avidin-biotin conjugation method (Vectastain®Elite ABC kit, Vector Laboratories) and 3,3-diaminobenzidine (Vector Laboratories). Sections were counterstained with haematoxylin. Dehydration of sections was assessed through graded ethanols and xylene. Slides were mounted with Histomount®. Positive controls were processed in parallel. Sections were analysed using an Olympus BX-50 microscope, equipped with a Camedia C-2000Z Olympus digital camera. High quality (1600x1200 pixel) images were captured to a PC equipped with the Olympus DP-Soft 3.0. software. Brain sections were referenced to (Paxinos and Franklin 1997).

Ultrastructural analysis and immunogold electron microscopy

Three adult male C57Bl/6 mice with 38 weeks of age were anesthetised and perfused transcardially with PBS followed by a fixative solution (4% paraformaldehyde in PBS, pH 7,3) during 15 min. Tissue fragments were fixed in 2,5% (pontine nuclei), or 4% (testis and quadriceps) glutaraldehyde in 0,2M sodium cacodilate buffer (pH 7,3) overnight (at 4 ºC), postfixed in 1% osmium tetroxhyde in 0,2M sodium cacodilate buffer (pH 7,3) overnight, dehydrated through a graded ethanol series followed by an incubation in propylene oxide (10 min), and embedded in Epon 812 resin at 60 ºC, during 24 hours. Ultrathin sections (~60 nm) were made from the tissue fragments and mounted in nickel grids. For immunogold labelling of endogenous mouse ataxin-3, sections on grids were exposed to a saturated aqueous solution of sodium metaperiodate for 30 min, washed in PBS (10min), incubated in 1% bovine serum albumin (BSA)/ PBS during 30 min, incubated with the antibody anti-humanATX3 (anti-hATX3) antiserum diluted 1:30 in 1% BSA/ PBS during 3 hours at 37ºC, and 1 hour at room temperature, washed 4 times in 1%BSA/ PBS, floated in 10 nm gold labelled goat anti-rabbit IgG(H+L) (RPN421V, Amersham Biosciences) diluted 1:15 in 1%BSA/ PBS for 45 min at room temperature, and washed 4 times in 1% BSA/PBS and a last one in distilled water. Sections were stained with uranyl acetate (5 min) and then with lead citrate (4 min). For negative controls, reactions with the primary antibody preadsorbed with the recombinant His tagged mATX3 protein, and without the primary antibody were used. Ultrathin immunogold labelled sections were visualized in transmission electron microscopes (EM10C and EM902A, Zeiss).

2.4. RESULTS

Cloning of full-length cDNA and analysis of mouse *Mjd* gene organisation

Using one of the cDNA sequences of the human *ATXN3* gene (pMJD1a), we searched for homologous sequences in Gene Bank™ and found one mouse cDNA (Accession number AK008675) with 1097 bp. A full-length mouse cDNA clone with 1100 bp (pMjd1) was obtained by RT-PCR from cerebral cortex total RNA, and verified by sequencing. Analysis of the nucleotide sequence revealed 88, 84, 81, 80 and 68% of identity with the human MJD1-1, MJD5-1, MJD1a, MJD2-1 and H2 cDNA sequences, respectively; and 92% of identity with the rat homologue cDNA. The pMjd1 cDNA contains a coding region of 1065 bp, predicted to encode a 355 amino acid protein - mouse ataxin-3 (mATX3).

A multiple sequence alignment, using CLUSTAL W, of mATX3 with rat ataxin-3 (rATX3) and human ATX3-v1, ATX3-v2, ATX3-v3 (Albrecht M et al. 2003), and ATX3-v4 (see materials and methods) showed a 94, 86, 80, 82, and 83% of identity at the amino acid level, respectively (Figure 2.1).

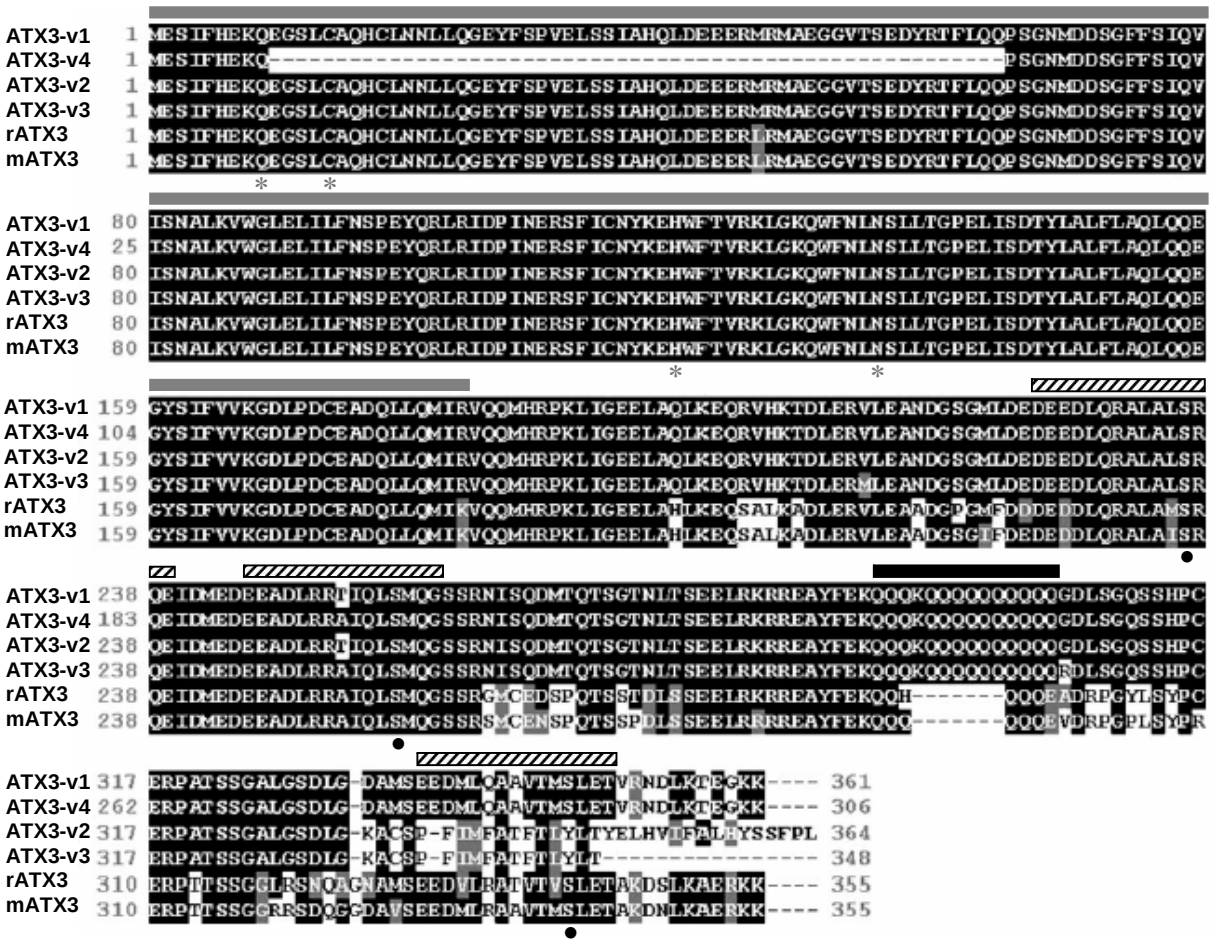

Figure 2.1. (See legend in the next page)

Figure 2.1. Multiple sequence analysis of mouse ataxin-3 (mATX3), rat ataxin-3 (rATX3), and human ataxin-3 (ATX3) variants (CLUSTAL W). Aligned residues that are identical or similar are shaded with a black or grey background, respectively. The Josephin domain is indicated above the sequence alignment by gray *lines*, the UIMs by dashed *lines* and the polyglutamine repeat by a black *line*. The four essential residues Q9, C14, H119 and N134 responsible for the cysteine protease activity are pointed out below the sequence alignment by gray *stars*, and the serine residues S236, S256 and S341 important for each UIM are depicted as black filled *circles*.

This indicates that the obtained sequence is in fact the mouse homologue of human ataxin-3. The cloned mATX3 variant possesses one Josephin domain, containing the four essential residues Q9, C14, H119 and N134 for the catalytic pocket, and three ubiquitin interacting motifs (UIMs), as well as the hATX3-v1 (Figure 2.1). This high conservation suggests conserved functional roles for mATX3.

A probe of 400 bp (nucleotide 1 to 400 of the cloned cDNA), obtained by PCR, was used to screen a BAC mouse library (Incyte Genomics). One positive BAC clone was identified and sequenced by primer walking (Appendix 1, Table A.1). Comparisons of the mouse cDNA clone sequence with the BAC clone sequence enabled us to determine the exon/ intron structure of the mouse *Mjd* gene (Table 2.1). This gene of approximately 36 Kb, localised on chromosome 12, is very similar to its human counterpart, both in number and size of exons and introns. The *Mjd* gene is composed by 11 exons and 10 introns, carrying a $(CAG)_6$ repeat on exon 10 (Table 2.1). Thus, the genomic structure of mouse *Mjd* is highly homologous to that of human *ATXN3*, and it is localised on chromosome 12, in a region syntenic to the human chromosome 14.

Sequence analysis of the 5'-flanking region

Analysis of the 5'- flanking region of the *Mjd* gene revealed that its promoter consists of a sequence lacking TATA boxes or CCAAT boxes, similarly to the human counterpart (Figure 2.2). The G+C-rich region extends from –307 to –8 bp (GC content, 68%). Analysis of the 1173 bp region upstream from the start codon of both mouse and human genes for conservation of putative transcription factor binding regions using the TRES/TRANSFAC program, revealed the presence of putative Sp1, upstream stimulatory factor (USF), Aryl hydrocarbon receptor nuclear translocator (Arnt), Myc-associated factor X (Max), E47 and MyoD regulatory element binding sites, and also of GC box elements in the gene promoters of both species (Table 2.2). Potential transcription factor binding sites for GATA-4, Nkx-2.5, myogenin, myocyte-specific enhancer factor-2 (MEF-2), c-Myb, activating enhancer-binding protein 2-apha (AP-2 alpha), retinoic acid receptor-gamma/retinoid X receptor-beta

Table 2.1. Exon-intron boundaries of the mouse *Mjd* gene

Exon/ Intron	Length (bp)		Acceptor site	Donor site
	Exon	Intron		
Exon 1	67			CCACGAGAAA/gtgagtgtgg
Intron 1		10098		
Exon 2	165		gaaacactag/CAAGAAGGCT	ATTTTTACAG/gtactgattt
Intron 2		226		
Exon 3	45		aattgaacag/CAGCCTTCTG	CTCTATTCAA/gtaagtagtc
Intron 3		2084		
Exon 4	86		cttttgacag/GTTATAAGCA	TTGATCCTAT/gtaagatttt
Intron 4		367		
Exon 5	67		tttcttctag/AAACGAAAGA	AGGCAAGCAG/gtaatatatc
Intron 5		3198		
Exon 6	88		tttttcctag/TGGTTTAACT	CAGCAAGAAG/gtaaataaga
Intron 6		4648		
Exon 7	133		ctctttttag/GTTATTCTAT	AAGAGCAGAG/gtaaaactac
Intron 7		3192		
Exon 8	167		tgttgtttag/TGCCCTCAAA	AGTATGCAAG/gtttggacat
Intron 8		1183		
Exon 9	97		ttgtttttag/GTAGTTCCAG	ACTTTGAAAA/gtaaagtagt
Intron 9		6386		
Exon 10	98		aatgtttcag/GCAACAGCAG	AGCGACCAAG/gtttgctttc
Intron 10		3279		
Exon 11	97		tctttcccag/GAGGCGACGC	

(RAR-γ/ RXR-β), N-Oct-3, SRY-related HMG-box-5 (Sox-5), glucocorticoid receptor (GR), activating protein-1 (AP1) and Myc-associated zinc finger protein (MAZ) were also found in the 5'-flanking region of the mouse *Mjd* gene (Table 2.3). These data suggest that the *Mjd* gene may be developmentally regulated.

Binding of MyoD to the *Mjd* promoter

In order to confirm the binding of the transcription factor MyoD, whose target region is conserved in mouse and human, we expressed and purified a recombinant mouse MyoD-His tag protein and analysed its binding to the –928 bp fragment of the 5' flanking region of the *Mjd* gene, by electrophoretic mobility-shift assay (EMSA). We analysed the binding of various quantities of the recombinant protein (5 and 15 μg) to the DNA and verified that the binding, as revealed by gel retardation assay, increased in proportion with the amount of protein added (Figure 2.3).

To verify that the binding of the recombinant protein to the –928 bp fragment was specific, we performed a competition assay using oligonucleotides corresponding to the MyoD binding region of the *Mjd* gene promoter (localised at position –888 bp) and verified that the presence of these oligonucleotides decreased the binding of the recombinant protein to the promoter fragment (Figure 2.3). This result is consistent with the idea that the *Mjd* gene promoter may indeed be regulated by MyoD, which is a transcriptional activator of muscle-specific genes.

Promoter activity of the 5'-flanking region

To characterise the regions regulating the transcription activity of the mouse *Mjd* gene, we constructed a series of plasmids containing different lengths of the 5'-flanking region of the *Mjd* gene fused to the promoterless *CAT* gene in pCAT3-Basic (Promega): p-237MjdCAT, p-358MjdCAT, p-559Mjd CAT, p-928MjdCAT and p-1173Mjd CAT. Transient transfection assays were performed using undifferentiated mouse embryonic carcinoma P19 cells. CAT activity was normalised for transfection efficiency, with reference to the β-galactosidase activity derived from the cotransfected internal control plasmid. As shown in Figure 2.4A, we observed minimal activity of the promoter with the p-1173MjdCAT construct, and maximal activity with either p-237MjdCAT or p-358MjdCAT plasmid, which presented a

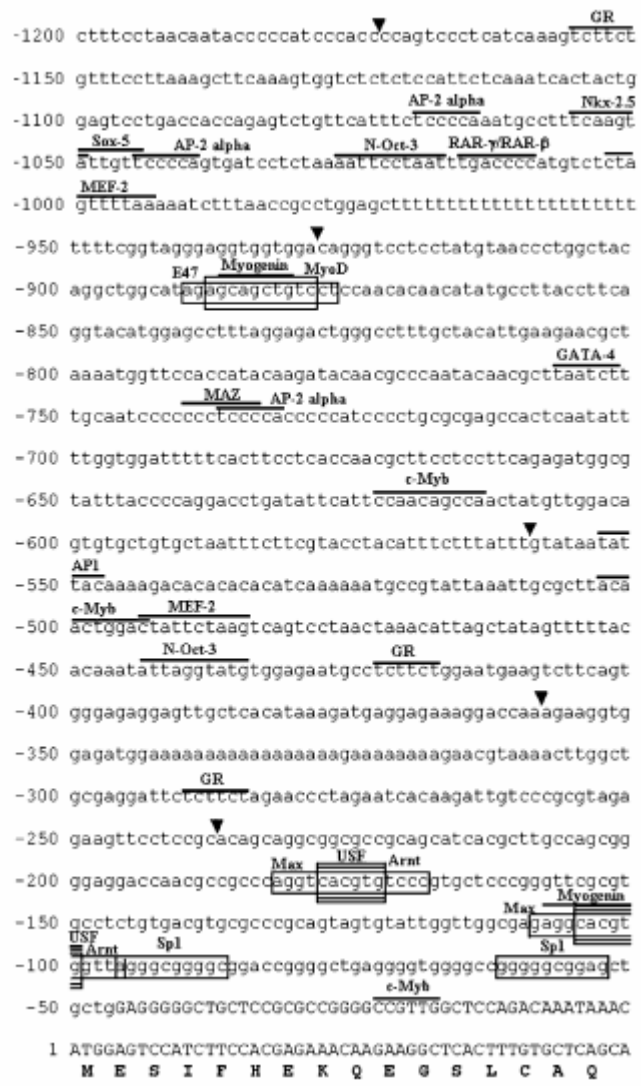

Figure 2.2. Nucleotide sequence of the 5'-flanking region of the mouse *Mjd* gene. The translation start site is *numbered* as +1. *Uppercase letters* represents exon sequences and untranscribed sequences are represented by *lowercase letters*. The coding region of the first exon is shown as codon triplets. For the detection of promoter activity, an *arrowhead* indicates the start point of each construct. Consensus binding sequences of the conserved transcription factor binding sites are *boxed*; for other potential transcription factor binding sites, these are indicated by a *line*.

Table 2.2. Conservation of potential transcriptional factor binding regions between mouse and human promoters (TRES/TRANSFAC)

Transcription factor	Cell specificity	Functional features	Localisation of potential binding sites (bp)	
			mouse promoter	human promoter
Sp1	ubiquitous	activator	-62, -96	-59, -88, -103, -116
USF	ubiquitous	activator	-105, -178	-122, -196
Max	ubiquitous	transcription and differentiation: activator- Max/Myc heterodimers repressor-Mad/Max heterodimers	-109, -182	-196
Arnt	ubiquitous	strong constitutive activator	-105, -178	-123, -197
E47	ubiquitous	acts in conjunction with MyoD, induces transcription and rearrangement of IgH	-890	-262
MyoD	proliferating myoblasts and differentiated myotubes	transcriptional activator of muscle-specific genes	-888	-260

Table 2.3. Potential transcription factor binding regions on the mouse *Mjd* promoter (TESS/TRANSFAC). See text for full names of transcription factors

Transcription factor		Cell specificity	Functional features	Localisation of potential binding sites (bp)
Muscle	**GATA-4**	gonads, heart, intestine, liver, primitive endoderm	cardiac muscle development	-757
	Nkx-2.5	high level in foetal/adult heart, low level in adult spleen, tongue	modest activator, myocardium development	-1056
	Myogenin	myogenic and skeletal muscle cells	muscle-specific transcription activator, induces MEF-2	-887
	MEF-2	myogenic cells, brain	myogenesis activator, induces MyoD	-1003
Nervous system	**AP-2 alpha**	embryo: several regions of nervous system adult: eye, prostate, skin	Activator	-1045, -1070, -737
	RAR-γ/ RXR-β	RAR-γ/RXR-β: striatum RAR-γ: high level in skin	repression of RAR-γ in RA-treated P19 cell aggregates	-1016
	N-Oct-3	CNS: adult and during development	activator	-1027
Other	**c-Myb**	pluripotent hematopoietic stem cells	activator	-23, -503, -623
	Sox-5	post-meiotic germ cells, high level in round spermatids	activator	-1050
	GR	ubiquitous	activator	-290, -423, -1156
	AP1	ubiquitous	activator	-552
	MAZ	ubiquitous	activator, important regulator in TATA-less promoters	-740

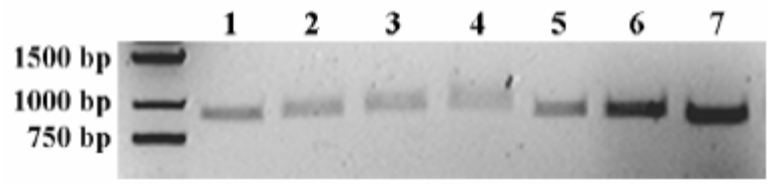

Figure 2.3. Binding of MyoD to the *Mjd* gene promoter. EMSAs were performed with 5 μg (lane 2) or with 15 μg (lane 3) of purified recombinant MyoD incubated with the –928 bp fragment of the promoter. For the competition assay 5 μg of purified recombinant MyoD were incubated with competitor double-stranded oligonucleotides followed by the addition of the –928 bp fragment (lane 5). (Lane 1 and 4) –928 bp fragment of the promoter.

94-fold and a 128-fold increase over the empty pCAT3-Basic plasmid, respectively. The fragments with 237 and 358 bp presented a 1.4-fold increase over the 1173 bp segment of the 5'-flanking region of the gene. We observed a decrease of the promoter activity for the fragments larger than –358 bp, which suggests the existence of repressor-binding sequences in these regions.

These results suggest that the –237 bp region of the cloned 5' region of the *Mjd* gene is sufficient to direct maximal transcription in the P19 cells.

Activation of the mouse *Mjd* gene promoter during differentiation of P19 cells

We next examined the behaviour of the isolated promoter sequence in terms of transcriptional activation during the differentiation of P19 cells onto three different types of cells: neuronal precursors, cardiac/skeletal myocytes and endoderm cells (Jones-Villeneuve et al. 1982; McBurney et al. 1982). To promote cellular differentiation, P19 cells were cultured as aggregates in the presence of medium, retinoic acid (RA) or dimethylsulfoxide (DMSO)-supplemented medium, to obtain endoderm-like cells (untreated), neuron-like cells or cardiac/skeletal myocytes, respectively. A significantly higher activity of the *Mjd* gene promoter was observed in cardiac and skeletal myocytes transfected with constructs p-237MjdCAT and p-1173MjdCAT that presented a 244.4-fold and a 231.5-fold increase of gene activity over cells transfected with the empty pCAT3-Basic plasmid, respectively (Figure 2.4B). Endoderm-like cells presented a 164.7-fold and 144.3-fold increase over the empty vector transfected cells, when transfected with constructs p-237MjdCAT and p-1173MjdCAT,

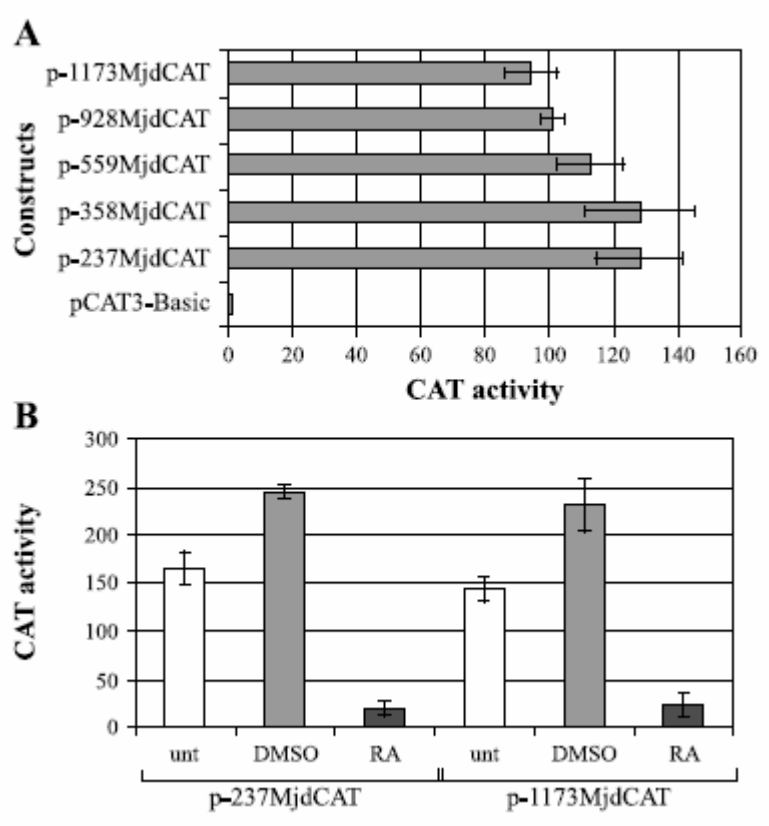

Figure 2.4. Functional analysis of the mouse *Mjd* gene promoter. A) A series of constructs containing different sizes of the 5'-flanking region of the *Mjd* gene were transfected in P19 cells. CAT activity is represented in arbitrary units, normalized for β-galactosidase activity and for total protein amount. B) Activation of the mouse *Mjd* promoter during RA- or DMSO-induced differentiation of P19 cells. Undifferentiated P19 were incubated with medium, or with DMSO- or RA- supplemented medium, on bacterial–grade Petri dishes, for three days, after then dissociated, transfected with p-237MjdCAT and p-1173MjdCAT constructs, and further grown on tissue culture plates. Cells were harvested at day 3, after replating (day 6 after induction of differentiation). Data are expressed as the fold increase in CAT activity compared with transfections using empty CAT plasmid, pCAT3-Basic. The results are the average of 3 independent transfections ± SEM (*error bars*).

respectively. In contrast, neuron-like cells transfected with the same constructs p-237MjdCAT and p-1173MjdCAT showed a 19.3-fold and a 23.0-fold increase respectively, relatively to cells transfected with the empty vector (Figure 2.4B). These data indicate that at early stages of embryogenesis, the *Mjd* gene is preferentially activated in endodermal

(DMSO-treated and untreated) and mesodermal (DMSO-treated) derivatives, including cardiac and skeletal muscle, and relatively less so in neuronal precursors.

Mouse ataxin-3 expression in adult mouse

The expression pattern of mouse ataxin-3 was studied by immunoblotting analysis of several tissues from adult wild-type mice, using the anti-ataxin-3 specific antiserum that cross-reacted with endogenous mouse ataxin-3. Tissue samples from the spinal cord, brainstem, cerebellum, cerebral cortex, heart, skeletal muscle, testis, kidney, lung, spleen, pancreas, liver and stomach, all presented an immunoreactive band of 42 KDa that corresponded to full-length mouse ataxin-3 and another band of approximately 160 KDa, potentially corresponding to an SDS resistant tetramer (Figure 2.5).

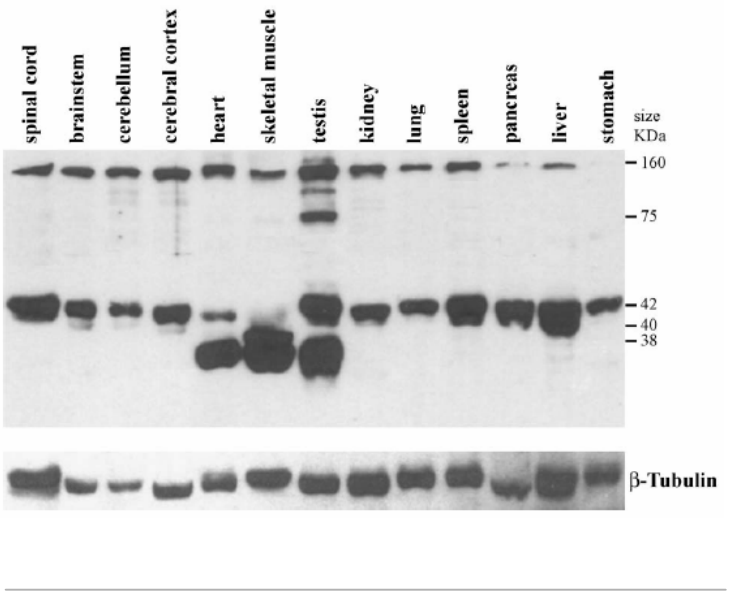

Figure 2.5. Mouse ataxin-3 expression in wild-type C57Bl/6 mice tissues. Protein extracts were resolved on 10% SDS-polyacrylamide gels. Immunoblotting reveals immunoreactive bands of 42 KDa and 160 KDa present in all tissues analysed. Heart, skeletal muscle and testis presented another, lower molecular mass of 38 KDa, while skeletal muscle an additional band of 40 KDa.

Cardiac and skeletal muscle expressed an additional and more prominent lower molecular mass species of 38 KDa that is also present in human counterpart tissues (Paulson et al. 1997). This species and another one of higher molecular mass were also present in testis. Skeletal muscle presented additionally another immunoreactive band of 40 KDa (Figure 2.5). These species could either represent different splice variants of the mouse *Mjd* gene (potentially corresponding to human H2 cDNA variant previously described (Ichikawa et al. 2001), or be the result of natural proteolysis of the endogenous protein, although all tissues were processed in parallel using protease inhibitors. Their conservation in mouse and human (Paulson et al. 1997) suggests that they could be of functional relevance.

To assess the regional and cellular distribution of mouse ataxin-3, we performed immunohistochemistry studies, using the anti-ataxin-3 antiserum, in peripheral tissues and

organs, and in the CNS of wild-type mice. Mouse ataxin-3 seemed to be ubiquitously distributed and to have a cytoplasmatic localisation, as evidenced in the immunostained sections (Figures 2.6, 2.7 and 2.8). The protein was highly expressed in skeletal, cardiac and smooth muscle (Figure 2.6A-D). The flagellum of the spermatozoa stained intensely (Figure 2.6K), and Leydig cells were also reactive to the antibody (Figure 2.6H).

Anti-mouse ataxin-3 immunoreactivity was found ubiquitously in the CNS (Figure 2.7A), and particularly localised in the cytoplasm of both neurons and glial cells. Marked labelling was found on the cytoplasm of neurons in the brainstem (Figure 2.7H) and in the substantia nigra (Figure 2.7I). In the substantia nigra, mouse ataxin-3 was expressed both in the pars compacta and in the pars reticulata. In the cerebellum, immunoreactivity was found that appeared to be located mainly in the cytoplasm, as suggested by the absence of nuclear staining (Figure 2.7F). As shown in Figure 2.7G, staining for mouse ataxin-3 was found in all layers of the cerebral cortex. Myelinated fibres of the white matter were also marked, although the staining was less pronounced. Likewise, in fibre areas, such as the corpus callosum and the anterior commissure, the staining was less intense. Immunolabelling was very intense in the ependymal cells, as observed in the lateral, third and fourth ventricles (Figure 2.7C); the cilia of these cells were also labelled (Figure 2.7D).

Expression of mATX3 during embryonic development

To determine the pattern of expression of mouse ataxin-3 during mouse embryonic development, we performed immunohistochemistry, using anti-ataxin-3 antiserum in sagital sections of embryos, at embryonic (E) days E11.5, E12.5, E13.5, E14.5, E15.5 and E16.5. Mouse ataxin-3 was continuously expressed in several tissues, including the CNS, since the earliest age analysed (E11.5), and exhibited a ubiquitous distribution (Figure 2.8A-F). Ciliated epithelia, like the olfactory (Figure 2.8I) and the cochlear epithelia (Figure 2.8H) were intensely stained.

Subcellular localisation of mATX3

Since there are inconsistent evidences regarding the subcellular localisation of ATX3, we decided to determine the localisation of mATX3 inside the cells of tissues where we found higher levels of this protein. We have used adult mice to perform immunogold staining of mATX3 using the anti-hATX3 antiserum in ultrathin slices of skeletal muscle, testis, and pontine nuclei. The slices were observed at the transmission electron microscope.

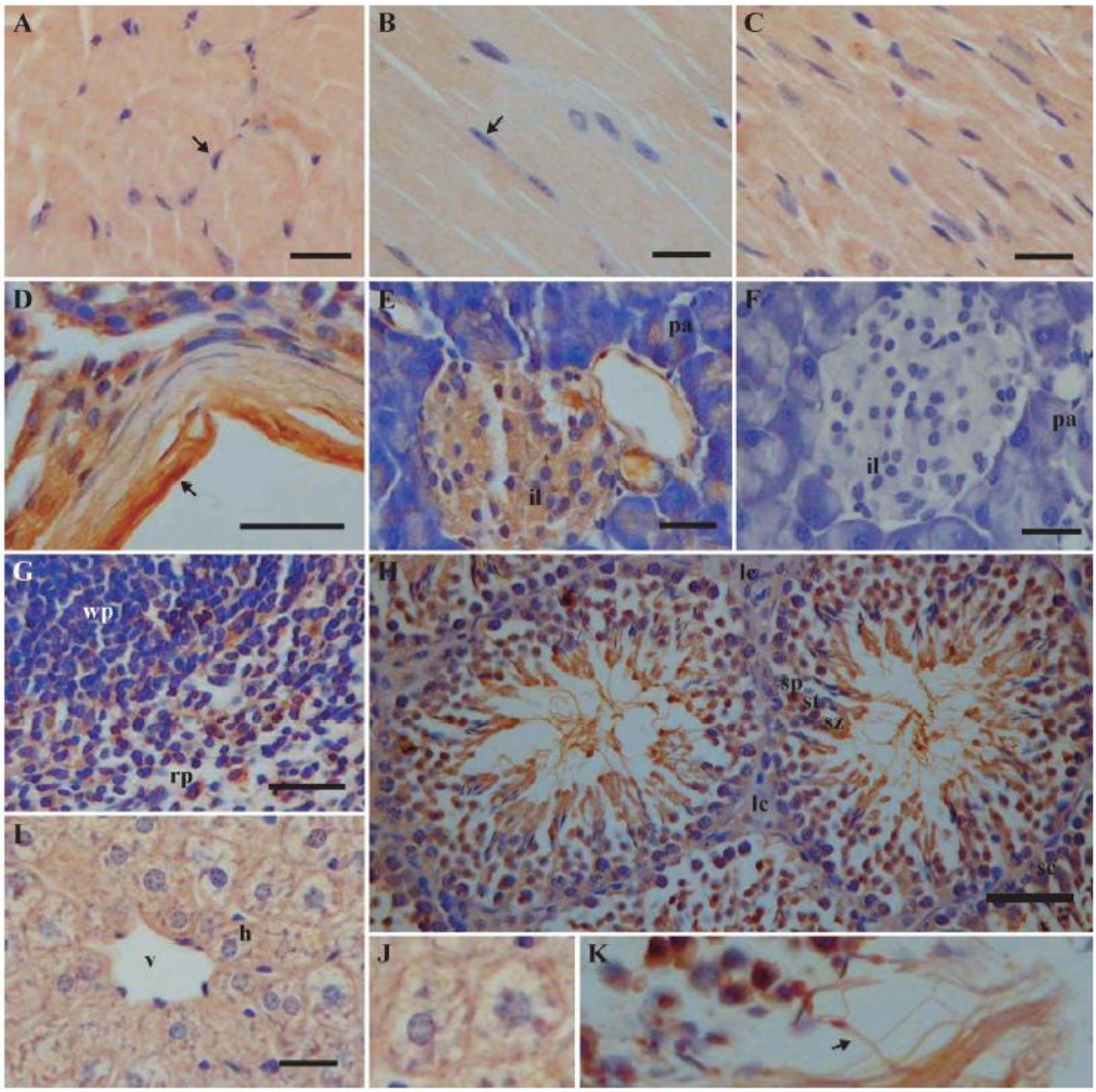

Figure 2.6. Mouse ataxin-3 immunoreactivity in adult mouse tissues. Bright field micrographs of transversal (A) and longitudinal (B) sections of skeletal muscle, (C) cardiac muscle, (D) smooth muscle, (E) pancreas, (F) control of staining, without the primary antibody, in pancreas section, (G) spleen, (H) testis and (I) liver. (A-D) High immureactivity was found in all types of muscles analysed. (E) In the pancreas, staining was ubiquitous and could be clearly observed in the islets of Langerhans, though it was also present in the exocrine component. (G) In the spleen, labelling was found both in the white and red pulp. (H) In the testis, the protein was also widely distributed, both within and outside the seminiferous tubules; in the tubules, it was found on spermatogonia, spermatocytes, spermatids and spermatozoa, and appeared to be absent on Sertoli cells; high reactivity was also found in the surrounding tunica propria (D). (I) In the liver, mouse ataxin-3 immunoreactivity was widely distributed throughout the section. (J) High magnification of two hepatocytes evidencing the more intense perimembrane staining, and (K) high magnification of spermatozoa. The arrows (→) point: in (A, B) a nucleus of muscular cell, showing no anti-mouse ataxin-3 immunoreactivity; in (D) the smooth muscle layer in the tunica propria of the testis; and in (K) the flagellum of a spermatozoon. The black bar on the lower right corner is equivalent to 50 μm. h, hepatocyte; il, islet of Langerhans; lc, Leydig cells; pa, pancreatic acinar cells; rp, red pulp; sc, Sertoli cell; sp, spermatocytes; st, spermatids; sz, spermatozoa; v, venule; wp, white pulp.

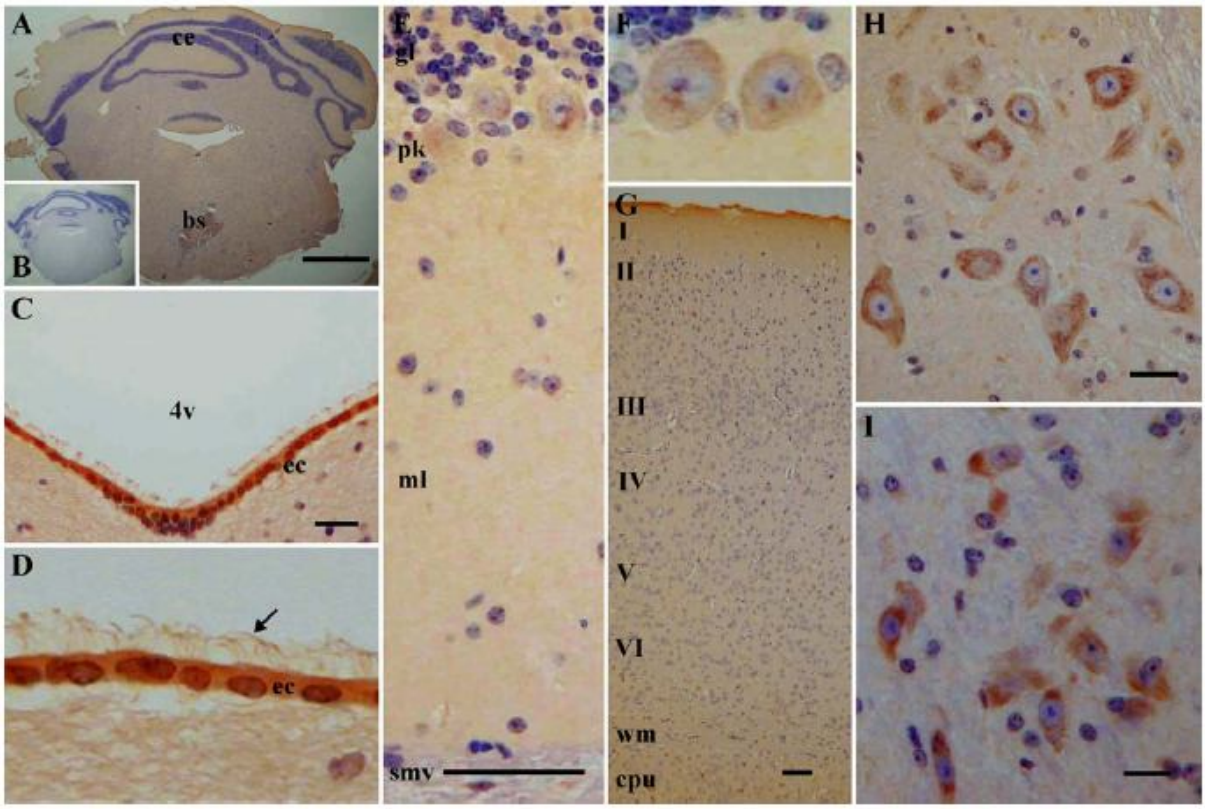

Figure 2.7. Ataxin-3 is ubiquitously expressed in the central nervous system of the adult mouse. (A, B) Low magnification photomicrographs of a coronal section of the cerebellum and brainstem (approximate level: 5.68 mm anterior to bregma) (46), (A) mouse ataxin-3 immunoreactivity, and (B) control of staining, without the primary antibody. Mouse ataxin-3 staining is prominent in ependymal cells, as evidenced in the cells in the fourth ventricle (C) and in the high magnification in (D), also showing the labelled cilia. (E) Low magnification of the anti-ataxin-3 labelling, in the different layers of the cerebellum, evidencing the cytoplasmatic labelling in the Purkinje cells, also shown in higher magnification in (F). Low magnification of immunoreactivity in cerebral cortex layers (G). High magnification of the neuronal immunolabelling in the brainstem (H), and in the substantia nigra (I). The arrow (→) points in (D) the labelled cilia of the ependymal cells. The black bar on the lower right corner is equivalent: in (A) to 1mm, in (G) to 200 μm and in (C, E, H, I) to 50 μm. I-VI, cortical layers I-VI; 4v, fourth ventricle; bs, brainstem; ce, cerebellum; cpu, caudate-putamen; ec, ependymal cells; gl, granule cell layer; ml, molecular cell layer; pk, Purkinje cells; smv, superior medullary velum; wm, white matter.

In the skeletal muscle from mouse quadriceps, mATX3 was distributed throughout the sarcomere being also present in the nucleus and cytoplasm existent between the fibers.

In sarcomeres, mATX3 was present in both myosin-rich (A) and actin-rich (I) bands, A and I, as well in the other sarcomere lines H, M, and Z (Figure 2.9A). Additionally, immunogold labelling for mATX3 was verified: in the sarcoplasmatic reticulum, both outside and inside the L-tubules; in mitochondria, particularly associated to the inner mitochondrial membrane or in the matrix; in the nucleus, associated to both types of chromatin; in both the

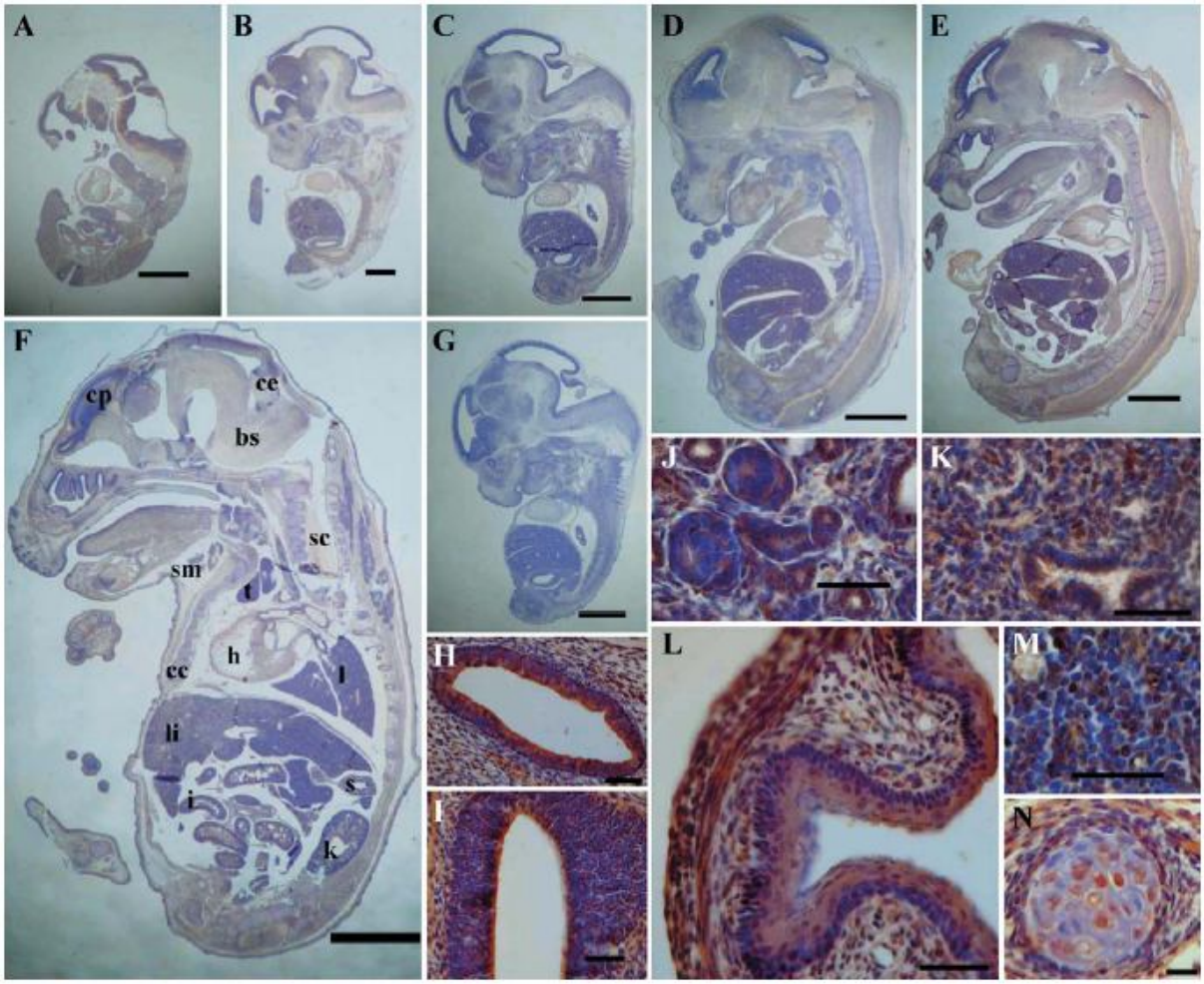

Figure 2.8. Ataxin-3 immunoreactivity during mouse embryonic development. Sagital micrographs of mouse embryos at (A) embryonic day 11.5 (E11.5), (B) E12.5, (C) E13.5, (D) E14.5, (E) E15.5 and (F) E16.5. (F) At the embryonic day E16.5, the developing cardiac, skeletal and smooth muscle were visibly labelled for mouse ataxin-3, immunoreactivity was also found in the respiratory and the digestive tracts, specially marking the non-keratinizing stratified squamous epithelia of the oral cavity and nasopharynx, and the intestinal villi, in the apical portion of enterocytes; as well as in the adrenal glands, the pancreas and the salivary glands (sublingual and submaxilary). (G) Control of staining, without the primary antibody, in a sagital section of an E13.5 mouse embryo. (H-N) High magnifications of E16.5 embryo. The black bar in the lower right corner is equivalent: in (A, B) to 1mm, in (C-G) to 2 mm and in (H-N) to 50μM. Intense ataxin-3 staining is evidenced in the cochlear (H) and in the olfactory epithelia (I). Ataxin-3 is marked in the developing (J) kidney, (K) lung, (L) stomach (M) thymus (both in the medulla and in the cortex) and (N) ossification areas (the periosteum was stained, as well as the cytoplasm of osteoprogenitor cells, whereas larger and more cuboidal osteoblasts appeared to exhibit no staining). bs, brainstem; cc, costal cartilage; ce, cerebellar primordium; cp, cortical plate; h, heart; i, intestine; k, kidney; l, lung; li, liver; s, stomach; sc, spinal cord; sm, submaxilar gland; t, thymus.

rough and the smooth endoplasmic reticulum; in the Golgi apparatus, being also present in secretory vesicles; and also in the cytosol (Figure 2.9A). The immunoelectron microscopy for

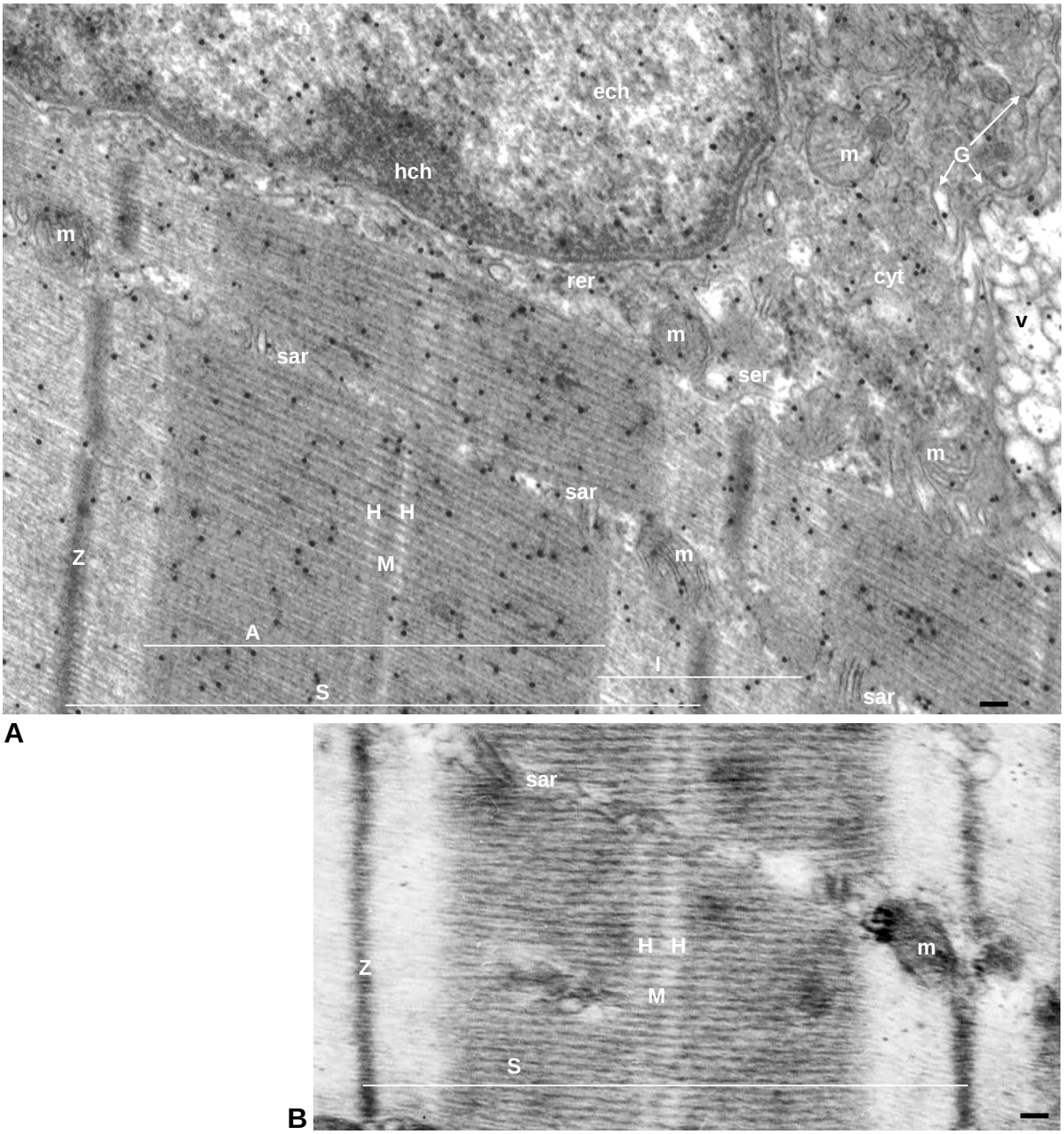

Figure 2.9. Mouse ataxin-3 is widely distributed at the subcellular level in the skeletal muscle. (A) Transmission electron photographs showing the ultrastructure of mouse skeletal muscle and the localisation of mATX3 labelled with immunogold particles (black dots). (B) Photograph corresponding to the negative control using the anti-hATX3 antibody pre-adsorbed with the recombinant mATX3 protein and showing no immunogold particles. The black bar on the lower right corner is equivalent to 1 μm. A, band A; cyt, cytoplasm; ech, euchromatin; G, Golgi apparatus; H, line H; hch, heterochromatin; I, band I; M, line M; m, mitochondria; n, nucleus; rer, rough endoplasmic reticulum; S, sarcomere; sar, sarcoplasmatic reticulum; ser, smooth endoplasmic reticulum; v, vesicle; Z, line Z.

mATX3 in mouse testis revealed that the protein was expressed in all types of cells in conformity with the immunohistochemistry results. Similarly to that observed in skeletal muscle, in the seminiferous tubules mATX3 was localised in several cellular compartments, such as the nucleus, mitochondria, vesicles, smooth endoplasmic reticulum (Figure 2.10). Interestingly, the characteristic form of the spermatid mitochondria showed very well that mATX3 is mainly associated to the inner mitochondrial membrane, being also found in the matrix (Figure 2.10). In the specific spermatozoon structures, mATX3 showed to be present in the axial filaments (flagellum) associated to both the microtubules that compose the axonems in a 9+2 arrangement, and the peripheral mitochondria layer of the axonem; and in the head, either in the highly condensed chromatin or in the acrosome (Figure 2.10).

Similarly to the other studied tissues, mATX3 was not associated to any specific structure in cells/ neurons of the pontine nuclei, one of the most affected cerebral regions in MJD patients. Mouse ATX3 showed to be present in nerve fibers (myelinated and non-myelinated), in neuronal cell bodies, and in various glial cell types (Figure 2.11). In nerve fibers, mATX3 was present in both pre and pos-synaptic terminals, being also associated to some synaptic vesicles, specifically to their membranes (Figure 2.11A). In cellular bodies mATX3 localised both in the cytoplasm, particularly in the rough endoplasmic reticulum, Golgi apparatus, and mitochondria (Figure 2.11B); and in the nucleus, being almost exclusively associated to heterochromatin (Figure 2.11B). Observation of the large neuronal mitochondria confirmed that mATX3 was mainly localised in the inner mitochondrial membrane (Figure 2.11C), like in the other tissues analysed. Analysis of the highly dense cytoskeleton of axons revealed that mATX3 was associated to this structure (Figure 2.11D).

At the electron microscope, the ultrastructure analysis of the immunogold labelling slices revealed that mATX3 was widely distributed through mouse skeletal muscle, testis and pontine nuclei.

Mouse ATX3 conserves the deubiquitinylation activity and is able to hydrolyse monoubiquitinated proteins

As above mentioned, ATX3 is a protein highly conserved through evolution, and mATX3. Mouse ataxin-3 possesses one Josephin domain, containing the four essential residues Q9, C14, H119 and N134 for the catalytic pocket, and three ubiquitin interacting motifs (UIMs), as well as the hATX3-v1 (Figure 2.12A). This high conservation suggests conserved functional roles for mATX3. Until now, only a function of deubiquitinating enzyme (DUB) was attributed to ATX3, specifically to its Josephin domain. To test the conservation of the DUB function in mATX3, we have generated a series of bacterial expression plasmids for His-tagged mATX3, mATX3:C14A, mATX3:jos, mATX3:jos:C14A and mATX3:UIMS proteins

Figure 2.10. Mouse ataxin-3 is localised in several types of cells from testis, namely in spermatids and spermatazoons. Transmission electron photographs showing the ultrastructure of mouse testis and the localisation of mATX3 labelled with immunogold particles (black dots). The black bar on the lower right corner is equivalent to 2.2 μm. acrs, acrosome; ax, axonem; ax f, axial filament; m, mitochondria; mt, microtubule; n, nucleus; ser, smooth endoplasmic reticulum; Sper, spermatid; Spt, spermatozoon; v, vesicle.

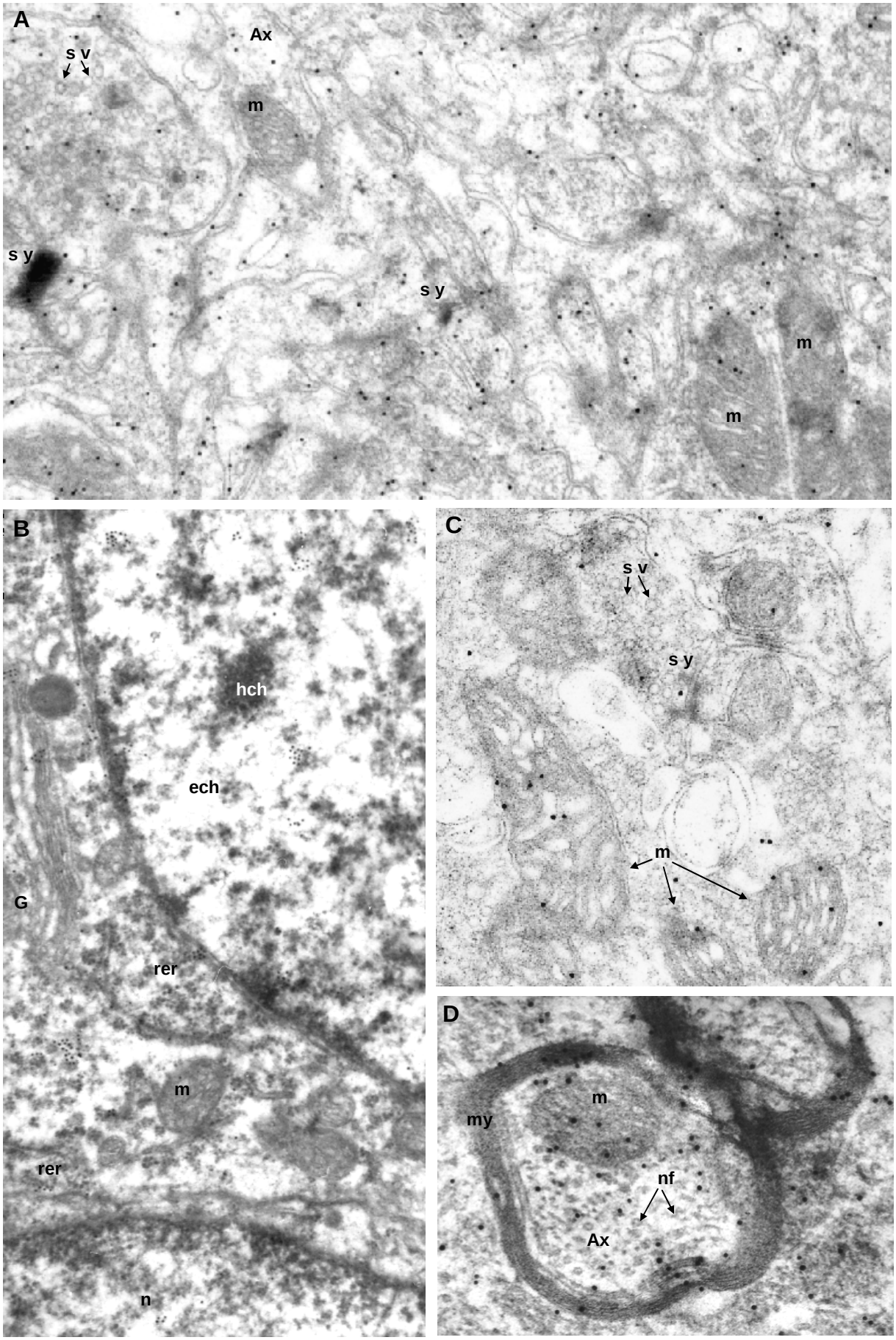

Figure 2.11. (See legend in the next page)

Figure 2.11. Mouse ataxin-3 is widely distributed at the subcellular level in the pontine nuclei. (A-D) Transmission electron photographs showing the ultrastructure of mouse pontine nuclei and the localisation of mATX3 labelled with immunogold particles (black dots). (A) Region of nerve fibers showing that mATX3 is present in several structures and that is both in pre- and pos- synaptic terminals, being also localised in some synaptic vesicles. (B) Ultrastructure of a region showing part of two cellular bodies. (C) Mitochondria of high dimensions and synapse. (D) Myelinated fiber showing the richness in neurofilaments of the axons. Ax, axon; ech, euchromatin; G, Golgi apparatus; hch, heterochromatin; m, mitochondria; my, myelin; n, nucleus; nf, neurofilament; rer, rough endoplasmic reticulum; sv, synaptic vesicle; sy, synapse.

(Figure 2.12A). These recombinant proteins were expressed in *E. coli*, purified by ionic change chromatography, and additionally by gel filtration chromatography in order to isolate the monomeric species.

The protein monomers were incubated with both K^{48}-linked or K^{63}-linked polyubiquitin chains, and their capacity to hydrolyse these chains was assessed by immunoblotting. As for the human protein, mATX3, and the Josephin domain (mATX3:jos) alone, were able to cleave either K^{48} or K^{63} chains; moreover, cysteine 14 revealed to be essential for this activity (Figure 2.12). Furthermore, in this assay, we demonstrated that mATX3 monomers can cleave chains containing two or more ubiquitins *in vitro* (Figure 2.12B).

In order to study the potential cleavage of monoubiquitinated proteins, we performed fluorimetric assays using as substrate Ub-AMC and as enzymes mATX3, mATX3:jos, or the corresponding proteins with the catalytic cysteine 14 mutated for an alanine. Both the entire protein and only the Josephin domain were able to cleave the ubiquitin from the AMC molecule, while the respective mutated C14A proteins were not (Figure 2.12C), showing that mATX3 has the ability to hydrolyse monoubiquitinated substrates *in vitro*.

Figure 2.12. (next page) Mouse ataxin-3 conserves the deubiquitinating activity observed for the human ataxin-3. A) Scheme of the recombinant His-tagged proteins used in this study: mATX3, the full-length protein; mATX3:C14A, the full-length protein carrying the C14A point mutation; mATX3:jos, the Josephin domain of mATX3; mATX3:jos:C14A, the Josephin domain with the C14A mutation; and mATX3:UIMs, the C-terminal of mATX3 containing the three UIMs. B) Polyubiquitin immunoblot showing the deubiquitinating activity of each used protein. mATX3, as well as its Josephin domain for itself (mATX3:jos) were able to cleave both K^{48} and K^{63}-linked polyubiquitin chains, preferentially with two or more ubiquitins. The mutation of the catalytic cysteine in these two proteins (mATX3:C14A and mATX3:jos:C14A) abolished their DUB activity. The C-terminal of mATX3 containing the UIMs (mATX3:UIMs) is not capable to hydrolyse polyubiquitin chains. C) Fluorimetric assay showing that mATX3 is able to hydrolyse Ub-AMC substrates by its Josephin domain (mATX3:jos) carrying a functional catalytic Cysteine 14, since both mutated mATX3:C14A and mATX3:jos:C14A can not cleave Ub-AMC substrates.

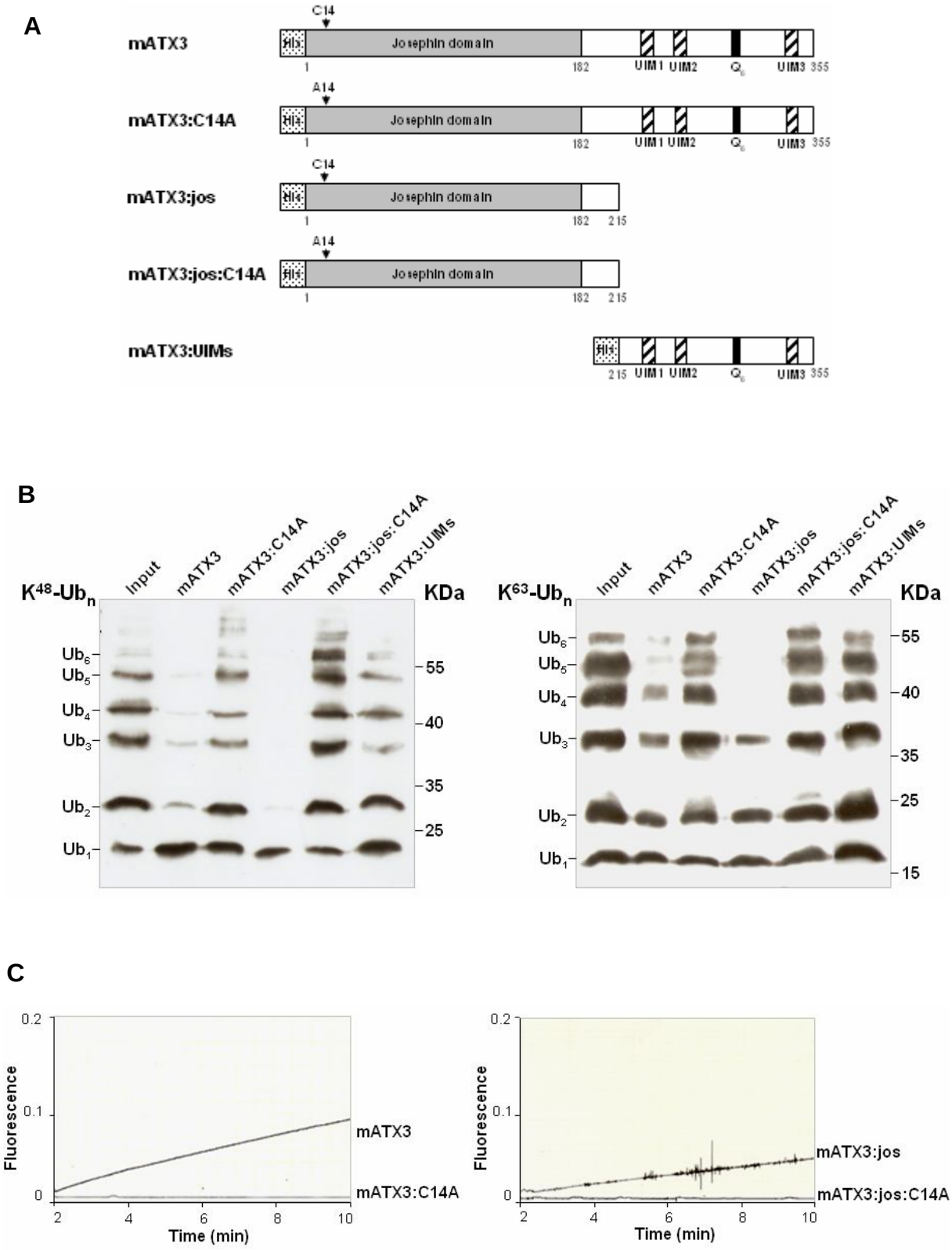

Figure 2.12. (See legend in the previous page)

Additionally, we verified that the entire protein shows a higher capacity to cleave monoubiquitinated substrates than the Josephin domain on its own, which suggests that although the C-terminal of the protein (mATX3:UIMs) does not cleave the ubiquitin chains itself, it must be important to bind ubiquitin molecules and accelerate the hydrolysis reaction (Figure 2.12C). This result suggests that ATX3 could, among other functions, rescue proteins from degradation by totally deubiquitinating a given substrate.

2.5. DISCUSSION

In this study, we determined the entire genomic structure of the mouse *Mjd* gene, characterised the functional promoter activity for the 5'-flanking region in transient transfection assays, and investigated the expression of the gene in mouse embryonic carcinoma P19 cells and its developmental regulation in mice. Our results showed that the mouse *Mjd* gene, a gene with 36 Kb, has a very similar organisation to the human *ATXN3*: both the number and size of exons and introns — 11 exons and 10 introns — are identical (Ichikawa et al. 2001). The *Mjd* gene contains a CAG repeat localised in exon 10, as occurs in the human gene. The *Mjd* cDNA has a high sequence similarity to its rat and human counterparts. At the amino acid level, mouse ataxin-3 revealed 94% and 82-86% of identity with rat and human proteins. The $(CAG)_n$ repeat in the mouse *Mjd* gene, as well as in the rat gene (Schmidtt et al. 1997), is shorter than their human counterpart containing six triplet units, as compared to the range of 10-51 repeats in the human normal population (Maciel et al. 2001). Reduced length of polyglutamine tracts and high conservation at the amino acid level have also been observed in mouse homologues of other genes involved in human polyglutamine disorders, such as *SCA1* (Banfi et al. 1996), *SCA2* (Nechiporuk et al. 1998), *SCA7* (Strom et al. 2002), and *HD* (Barnes et al. 1994; Lin et al. 1994). This suggests that the polyglutamine stretch may have no relevance for the function in the wild-type protein and that the expansion of repeats may be characteristic of primates, since no natural models of expanded polyQ are known in rodents.

Analysis of the 1173-bp regulating region, upstream of the mouse *Mjd* gene, revealed the presence of putative binding sites for the transcription factors Sp1, USF, Max, Arnt, E47 and MyoD, which were conserved in the 5'-flanking region of the human gene, and the presence of potential binding sites for GATA-4, Nkx-2.5, myogenin, MEF-2, c-Myb, AP-2 alpha, RARγ/ RXRβ, N-Oct-3, Sox-5, GR, AP1 and MAZ. Similarly to the human *ATXN3* promoter gene, no TATA or CCAAT boxes were found on this 5'-flanking region of the *Mjd* gene. This and the presence of both constitutive and tissue-specific transcription factor

regulatory sites suggest that the *Mjd* promoter is unusual, since it presents characteristics of both housekeeping and regulated genes. Interestingly, the results of the functional studies of this TATA-less promoter region correlate very well with the predicted role of these putative transcription factor binding regions. Analysis of the promoter activity, using a series of constructs containing different lengths of the 5' upstream region of the *Mjd* gene, and CAT as a reporter gene, showed minimal activity of the promoter for the –1173 bp fragment, whereas fragments –237 and –358 bp presented maximal activity. The progressive decrease of activity for fragments larger than –358 bp suggests the existence of repressor binding sites in these regions. Sequence analysis of segments –237 and –358 bp revealed the repeated presence of similar regulatory regions on both fragments, except for the presence on the –358 bp segment of a putative GR binding region at position –290 bp. The similarity of results for the two constructs may relate to the absence of glucocorticoid exposure in the P19 system used in this study. The –237 bp region, containing putative binding sites for several ubiquitous transcription factors, such as Sp1, USF, Max and Arnt, which are conserved in the human promoter, seems to be sufficient to direct maximal transcription in the P19 cells.

Having identified the minimal promoter region and potential regulatory elements, we then studied the *Mjd* promoter activity, both in RA-induced (neuronal) and DMSO-induced (cardiac/skeletal myocytes) differentiated P19 cells (Jones-Villeneuve et al. 1982; McBurney et al. 1982). Cells transfected with constructs p-237MjdCAT and p-1173MjdCAT exhibited an increase in the promoter activity of the *Mjd* gene when treated with DMSO — there was a 1.5-fold and 1.6-fold higher activity, respectively, in relation to untreated cells. This is in agreement with the presence on the promoter of several putative binding regions for muscle-specific transcription factors including myogenin, MyoD/E47, MEF-2, GATA-4 and Nkx-2.5. Of these, the MyoD binding site is also present in the human promoter. We confirmed the binding of the transcription factor MyoD to the mouse *Mjd* promoter by gel shift assay. These results are in conformity with the immunoblotting results that showed a high expression of the *Mjd* gene product — mATX3 — in cardiac and skeletal muscle. These tissues expressed smaller isoforms of the protein, with 38 and 40 KDa, which are conserved in humans (9), suggesting the functional relevance of these isoforms. The expression of mouse-ataxin-3 in cardiac, skeletal and smooth muscle was also confirmed by immunohistochemistry, both in adult mouse and during development, showing a cytoplasmatic localisation.

Untreated pre-aggregated P19 cells that correspond to endoderm-like cells (Skerjanc 1999) presented a relatively high activity of both *Mjd* promoter regions (-237 and –1173 bp), suggesting that the *Mjd* gene could be of functional relevance since the first stages of cell differentiation.

Neuron-like cells presenting morphologic and metabolic characteristics of normal neurons were obtained by RA-induced P19 differentiation. Intriguingly, transient transfection

of these cells with constructs p-237MjdCAT and p-1173MjdCAT originated an activity 8.5-fold and 6.3-fold weaker than the untreated cells, respectively. The weaker activity of the minimal promoter (-237 bp) could be explained by the presence of two conserved putative binding sites for Max, at positions –109 and –182 bp. The Max and Mad genes are known to be up-regulated during RA-induced differentiation (Sarkar and Sharma 2002), thus Max/Mad heterodimers could bind and act as repressors of transcription. Simultaneously, down-regulation of the activator gene c-Myc, which is later expressed at high level (at day 14 of differentiation) (Sarkar and Sharma 2002), could also contribute to the observed decrease in promoter activity. Alternatively, a decrease in transcription may occur through the AhR/Arnt pathway, potentially acting at the conserved –105 and –178 bp binding sites. In fact, Aryl hydrocarbon receptor (AhR) has been shown to be down-regulated in RA-treated cells (Wanner et al. 1995). In spite of the presence on the p–1173MjdCAT construct of several potential binding regions for AP2-alpha, N-Oct-3 and RARγ/RXRβ, which are activators for neuron-specific genes, CAT activity on RA-differentiated cells transfected with this construct was rather similar to the one obtained for the minimal promoter construct. It is possible that the potential activation of transcription by these factors is not sufficient to overcome the transcription repression of the *Mjd* gene by the Max/Mad pathway, at least at this stage (day 6) of RA-induced differentiation. This does not exclude that at later stages of embryonic development, which are not mimicked by P19 cells, these transcription factors could eventually become activated. The presence of additional neuronal-specific enhancers of transcription upstream of the –1173 bp promoter region of the *Mjd* gene also cannot be excluded, and could account for the high expression of mouse ataxin-3 observed in the CNS during both adult and embryonic stages of the mouse.

In the CNS of the adult mouse, mATX3 was ubiquitously expressed and was localised in the cytoplasm of both neurons and glial cells. Relevant reactivity was found in the brainstem (mainly in neurons), in the substantia nigra, and in both the granular and molecular layers of the cerebellum. However, a very intense expression was also observed in other types of cells of the CNS, which are not affected in MJD. We suggest that the pathogenic mechanism in MJD may be independent of the function of ATX3, being not only due to a prominent expression of the mutant protein in the affected regions, but also to other factors that contribute to a selective neuronal loss.

The study of the expression pattern of mATX3 during embryonic development, revealed that it is expressed since the early stages, and confirmed the ubiquitous expression observed in adult mice. In addition the immunoelectron microscopy studies revealed that mATX3 was present in both the nucleus and the cytoplasm, and that it was not associated to a specific cellular compartment. Specifically in mitochondria, mATX3 was mainly present in the inner membrane.

The intense immunoreactivity of mATX3 in ependymal cells, in the flagellum of the spermatozoa and in ciliated olfactory and cochlear epithelia suggests that this protein may have an important function in cell structure and/or motility. Additionally, the presence in the promoter region of conserved binding sites for muscle-specific transcription factors, and the high activity of the *Mjd* promoter in DMSO-treated cells, in conjunction with the very intense expression of mATX33 in cardiac, skeletal and smooth muscle, suggests that the function of the *Mjd* gene may be relevant in these tissues. The subcellular localisation of mATX3 in the skeletal muscle, testis and pontine nuclei revealed that was associated to different cytoskeleton structures such as the sarcomere, the axonem of the spermatozoon flagellum and the axon cytoskeleton reinforcing the abovementioned hypothesis. Further functional studies are necessary to determine whether mATX3 may be a cytoskeleton-associated protein that could be important for motility and/or for cellular transport.

The human ATX3 protein possesses DUB activity, which suggests a role in the UPS (Burnett et al. 2003; Doss-Pepe et al. 2003; Chai et al. 2004; Berke et al. 2005). This suggests the orthology of the mouse *Mjd* gene given that mATX3 protein conserves the only biochemical function until now attributed to human ATX3. Furthermore, we demonstrated that the monomeric state is important for the complete cleavage of polyubiquitin chains, since mATX3 monomers did cleave chains containing two or more ubiquitins, whereas in previous reported studies (Burnett et al. 2003; Doss-Pepe et al. 2003; Rodrigues et al. 2007), in which ATX3 proteins, like the human and the *C. elegans* ataxin-3, were not purified to isolate the monomeric species, they could only cleave chains with four or more ubiquitins. Moreover, we have verified that mATX3 was able to cleave the ubiquitin moiety from monoubiquitinated species like other Josephin proteins (Tzvetkov and Breuer 2007).

In summary, our studies indicate that the *Mjd* gene is highly conserved between species, within coding and 5' regulatory regions, and its regulated expression during development suggests that ATX3 may have an important biological function. Given this conservation, the study of the mouse *Mjd* gene may provide fundamental insights to the function of human ATX3.

Chapter 3

Mjd, a stress-responsive gene?

3.1. SUMMARY

DAF-16 is a *C. elegans* stress-responsive transcription factor. Similarly to the human species, the mouse has three DAF-16 homologue genes: *Foxo1*, *Foxo3* and *Foxo4*. We have previously observed that DAF-16 binds *in vitro* to the *C. elegans atxn-3* promoter. Sequence analysis of the 5' flanking region of the mouse *Mjd* gene revealed several potential binding sites for Foxo transcription factors. We speculated that the *Mjd* gene might be regulated by this pathway. We have studied the expression of the *Mjd* gene, by real-time RT-PCR, in the skeletal muscle and total brain of C57Bl6/J mice submitted to two different stress conditions, cold (4ºC during 24 hours), and starvation (deprivation of food during 24 hours) predicted to affect Foxo transcription factors activity and expression of the downstream target genes. No differences in the expression of the *Mjd* gene were found in the brain of the stressed mice, although there was a tendency for a decrease of expression. We have also tested the expression levels of the *Foxo* genes in brain, and found that only the *Foxo3* and *Foxo4* gene showed altered (decreased) expression, and uniquely in the starvation situation. In contrast, in the skeletal muscle of starved and cold-exposed mice we found a ~two-fold increase of the *Foxo1* and *Mjd* genes. *Foxo3* and *Foxo4* were decreased in the skeletal muscle of cold-stressed mice. These results suggest that the *Mjd* gene seems to be a stress-responsive gene, possibly under the regulation of transcription factor Foxo1. Further studies should be performed to confirm that the observed activation of the *Mjd* gene under stress conditions in skeletal muscle is due to the direct binding of Foxo1 to the *Mjd* gene promoter. Additional analysis of the expression of the *Mjd* gene in specific regions of brain should also be performed, which may allow increased sensitivity to expression changes. The relevance of this regulation to clinical manifestations such as the cachexia present in MJD patients, or to the fact that MJD is an ageing-related disorder also remains to be explored.

3.2. INTRODUCTION

MJD is a late onset disorder caused by a dominant inherited expanded CAG repeat in the *ATXN3* gene encoding a mutant polyQ-containing protein. The pathogenic mechanism of this disease is not known yet. However, and even being a genetic disorder, given the fact that both normal and mutant ataxin-3 are recruited to intracellular aggregates during the patient life and that the clinical symptoms generally appear at midlife, MJD could be considered an aging disorder and several aging-modulating factors could contribute to its variable clinical presentation. MJD is characterised mainly by ataxia, often associated to

other symptoms, namely in the case of patients with later onset, a peripheral neuropathy and distal muscular atrophy (Coutinho and Andrade 1978).

The FOXO transcription factors are mostly known for their association with longevity. In fact, it is known that life span is partially determined by the genetic background of an organism (Mori 1997). The genes determining life span were extensively studied in *C. elegans* (Guarente and Kenyon 2000; Antebi 2007). These genes were divided in two classes: one class related to the specific insulin signaling pathway (*daf-2*, *age-1*, *akt-1,2*, and *daf-16*); and the other related to biological rhythm (*clk-1,2,3* and *gro*) (Guarente and Kenyon 2000; Antebi 2007).

DAF-16 is a forkhead box "Other" (FoxO) protein, a subgroup of the forkhead transcription factor family (Lin et al. 1997; Ogg et al. 1997). This transcription factor is a target of the insulin-like signaling pathway, which plays a crucial role in the regulation of development, metabolism and longevity in response to stress conditions (Lee et al. 2001; Lin et al. 2001). Apparently, the mammalian insulin-signaling pathway is very similar to that of the *C. elegans*, which suggests that this systemic aging control mechanism may be conserved in evolution. In this case, mammalian homologues of *daf-16* could regulate aging-related molecules. In fact, in the past few years it was shown that FoxO proteins are key factors in inducing various target genes, including the regulators of metabolism, cell cycle, cell differentiation, cell death, and oxidative stress response (Tran et al. 2003; Accili and Arden 2004; Van Der Heide et al. 2004; Barthel et al. 2005).

Similarly to human, the mouse has three *daf-16* homologue genes: *Foxo1*, *Foxo3*, and *Foxo4* (previously known as *Fkhr*, *Fkhrl1*, and *Afx*, respectively) (Biggs et al. 2001). These *Foxo* genes have slightly different expression patterns: all of them are expressed in the adult mouse brain, spleen, lung, liver, skeletal muscle, kidney, and white adipose tissue; additionally, *Foxo1* is also expressed in brown adipose tissue, *Foxo3* in heart and testis, and *Foxo4* in heart and brown adipose tissue (Furuyama et al. 2000). In particular, the expression of *Foxo1* and *Foxo3* in the brain starts relatively late, between the E12.5 and E14 stages, and in the adult *Foxo1* expression is restricted to the striatum and hippocampus, whereas *Foxo3* is widely expressed throughout the brain (Hoekman et al. 2006). The consensus binding site for DAF-16 and the mouse homologues (DBE, for daf-16 family member binding element) is an 8-bp [TTGTTTAC] sequence (Figure 3.1) (Furuyama et al. 2000).

The transactivation of target genes by the FoxO proteins is regulated by phosphorylation by the kinase acute transforming retrovirus thymoma (Akt), which promotes their shuttling to the cytoplasm and thus an inhibition of their activity (Biggs et al. 1999; Brunet et al. 1999; Guo et al. 1999; Kops et al. 1999; Brunet et al. 2001; Rena et al. 2002). Once in the cytoplasm, and in particular Foxo1 is sent to proteasomal degradation

(Matsuzaki et al. 2003) following ubiquitination by Skp2 (Huang et al. 2005). The activity of the Foxo proteins is also modulated by acetylation/ deacetylation. Actually, the cAMP response element binding protein binding protein (CBP or CREBBP) and p300 interact with FoxO proteins, and can acetylate residues of the DNA binding domain limiting their function (van der Heide and Smidt 2005). In contrast, sirtuins are able to deacetylate FoxO transcription factors having different effects in their ability for transactivation that may also depend of the stress condition (Brunet et al. 2004; Motta et al. 2004).

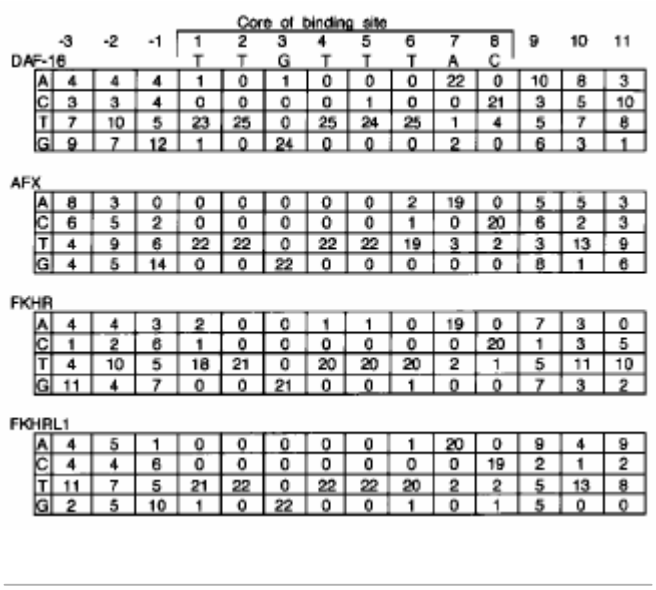

Figure 3.1. Matrices of the selected binding sequences for DAF-16, AFX (Foxo4), FKHR (Foxo1), and FKHRL1 (Foxo3) transcriptional factors. The number of sequences on which this summary was based is: 25 for DAF-16, 22 for AFX, 21 for FKHR, and 22 for FKHRL1. The core sequence, TTGTTTAC, was shared and the sequence was designated as DEB. *(adapted from Furuyama et al. 2000)*

In insulin-sensitive tissues, such as the skeletal muscle, and in the fed state, insulin negatively regulates FoxO-mediated transactivaton of target genes by its phosphorylation by Akt. FoxO proteins have also been implicated in the regulation of differentiation of muscle cells (Hribal et al. 2003).

Additionally, it was observed that FoxO proteins play an important role in the activation of protein turnover in the skeletal muscle through the regulation of atrogin, an F-box protein which targets proteins for ubiquitinylation and degradation by the proteasome (Sandri et al. 2004; Stitt et al. 2004). In conformity, recently was reported that Foxo1 is able to inhibit mammalian target of rapamycin (mTOR) signaling relevant for autophagy, and protein synthesis in the skeletal muscle, by inducing the expression of eukaryotic initiation factor 4E-binding protein (4E-BP1), which in turn is the inhibitory protein of eukaryotic initiation factor-4E (eIF4E), thus repressing the translation process (Southgate et al. 2007). Indeed, *Foxo1* and *Foxo3* are upregulated in fasting and in insulin-deficient rat skeletal muscle (Furuyama et al. 2002), as well as in starved mice skeletal muscle (Furuyama et al. 2003).

Skeletal muscle is the major protein reservoir in the body. This tissue possesses a high plasticity and muscle proteins can be mobilised into free amino acids under disuse conditions (i.e. immobilisation, denervation, etc.), stress conditions (starvation, etc.), and in several pathological states. The free amino acids provided by the skeletal muscle, in the

latter conditions, are used to provide energy through gluconeogenesis, as precursors of protein synthesis in the liver, and to maintain protein synthesis in vital organs such as heart, brain and lungs. In these cases, muscle mass is controlled by a tight regulation of protein synthesis and degradation by the ubiquitin proteasome system (UPS). In fact, the ubiquitination/ deubiquitination machinery is upregulated in muscle wasting, namely some E2 and E3 ligases, and DUBs (Furuyama et al. 2002; Lecker et al. 2004; Attaix et al. 2005; Combaret et al. 2005; Wing 2005). Several signaling pathways regulate the UPS in muscle (Figure 3.2). In particular, the insulin/ IGF-1 signaling pathway regulates the phosphorylation of FoxO transcription factors and consequently of their transactivation of UPS-related genes such as atrogins (Attaix et al. 2005).

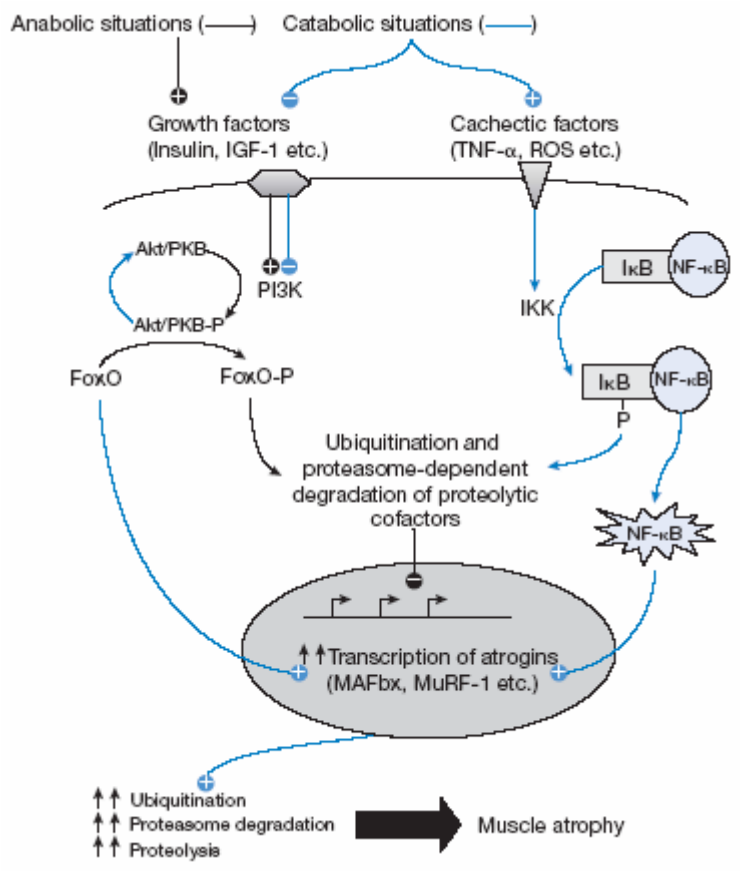

Figure 3.2. Signalling pathways that regulate the UPS in catabolic (blue lines) or in anabolic conditions (black lines). In catabolic conditions and given the low circulating levels of insulin and/or IGF-1both Akt/PKB (protein kinase B) and the FoxO transcription factors are poorly phosphorylated (P). All these events lead to increased transcription of atrogins (i.e. atrophy genes), which ultimately results in a stimulation of the UPS. In contrast, in anabolic situations (black lines) insulin and/or IGF-1 activate PI3K. In that case, both Akt and FoxO are highly phosphorylated, and the latter event is ultimately responsible for repressed transcription of atrogins. In addition, the high levels of phosphorylated Akt induce increased protein synthesis. *(adapted from Attaix et al. 2005)*

All organisms are subjected to several stress-conditions in Nature. In mammals, that are homeothermic organisms, cold exposure consists in another stress-condition that leads to a metabolic heat gain given by an increase in food intake, and also by mobilisation of body reserves (Mount 1978). Therefore, increased rates of protein synthesis/ degradation could contribute to metabolic heat production by animals in cold environments. However, individual tissues respond differently to cold exposure. In particular, in rat skeletal muscles short-term cold exposure leads to a decrease of protein synthesis but without alterations in the protein degradation levels (Samuels et al. 1996). Since the role of the Foxo transcription factors is unknown in response to cold-exposure, we thought it would be interesting to study their expression levels, as well as their gene targets in this specific stress-condition.

We have previously observed that daf-16/Foxos consensus binding sequences were conserved in the human *ATXN3* promoter and in its corresponding mouse and *C. elegans* homologue genes *Mjd* and *atxn-3*, respectively (Santos 2005). We have expressed a recombinant His-tagged DAF-16 protein and confirmed its *in vitro* binding to the -1000 bp 5´-flanking region of the *C. elegans atxn-3* gene by EMSA (Santos 2005).

Several evidences led us to raise a question: *is Mjd a stress-responsive gene*? These evidences were: (1) the fact that Foxo proteins promote protein degradation in insulin-deficient conditions in skeletal muscle; (2) the fact that mouse ataxin-3 has DUB activity (Chapter 2), is highly expressed in the skeletal muscle (Costa et al. 2004), and potentially involved in the UPS, which seem to be very important in the response to stress-conditions; (3) our observation of the *in vitro* binding of the *C. elegans* homologue DAF-16 to the worm *atxn-3* promoter; and (4) the knowledge that MJD is a late-onset disease, and aging-related factors regulating the expression of the *ATXN3* gene could contribute to the pathology.

Thus, in this chapter our main objective was to investigate the possibility that Foxo proteins regulate the expression of the *Mjd* gene. For that, we have determined by bioinformatic analysis the potential binding sites of Foxo proteins to the mouse *Mjd* promoter, and analysed the mRNA expression levels of the *Mjd*, *Foxo1*, *Foxo3*, and *Foxo4* genes in the skeletal muscle and total brain of mice submitted to two different stress-conditions: starvation, and short-term cold exposure. Our results are consistent with the hypothesis raised, however further analyses should be performed to confirm it.

3.3. MATERIALS AND METHODS

Computational methods

Several binding sequences (18) for the three mouse Foxo transcription factors were searched in the four possible DNA chain directions, in the approximately 4 Kb of the 5'-flanking region of the mouse *Mjd* gene. These sequences were based in the matrices for the DNA consensus binding sequences of these proteins previously reported (Furuyama et al. 2000).

Animals

Young adult C57Bl6/J mice (Harlan Interfauna Iberica, SA) with 11-13 weeks of age were housed at a temperature of 22 ± 1 ºC, and a relative humidity of 50 ± 5 % in a 12:12 light-dark cycle, and consumed a regular diet and tap water *ad libitum*. A group of 8 animals ("control") was maintained in standard conditions, a group of 8 animals ("starvation") was submitted to starvation with free access to water at normal temperature during 24 hours, and a group of 7 animals ("cold exposure") was maintained with food *ad libitum*, and with total access o water, at 4 ± 1 ºC, during 24 hours. The animals were anesthetised and peripheral blood by heart punction was collected. The blood was centrifuged at 13000 rpm during 5 min and serum was stored at -20ºC. Mice were then perfused with PBS, and the brain and skeletal muscle from the gastrocnemius were directly stored at -80ºC.

Quantification of the glucose levels in the serum

Serum glucose levels from the "control" and the "starvation" groups were determined using the kit Glucose-TR (Trinder.GOD-POD) using the manufacturer instructions. Briefly, 10 µL of serum from each animal were incubated with 1 mL of WR reagent at 37 ºC, during 10 min. After that, absorbance values were acquired at 505 nm. Duplicates of all samples were performed and glucose concentration (mg/mL) was achieved by comparison with a standard curve.

RNA extraction and cDNA synthesis

Total RNA was isolated from each mouse brain and skeletal muscle, using Trizol reagent (Invitrogen), and 2.5 µg was used to perform reverse transcription using the

SuperScript™ First-Strand Synthesis System for RT-PCR (Invitrogen) with an oligo(dT) primer.

Quantitative real-time RT-PCR

Gene expression was assessed by quantitative real-time RT-PCR, using the QuantiTec SYBR Green PCR kit (Qiagen), 2 μL of total cDNA, and 500 nM of each primer. The pair of primers used to amplify the genes *Mjd*, *Foxo1*, *Foxo3*, *Foxo4*, and *Hprt* was respectively: mmMJD14/ mmMJD21, Fkhr(1)/ Fkhr(2), Fkhrl1(1)/ Fkhrl1(2) and Afx(1)/ Afx(2), Hprt(3)/ Hprt(4) (Appendix 1, Table A.1). The reactions were carried out in a real-time cycler LightCycler (Roche) using standard cyclic conditions indicated in the abovementioned kit.

Statistical analysis

Quantitative real-time RT-PCR data was compared between two groups of experiments using the t-test, which was calculated using the SPSS version 14.0 package. A significant $P < 0.05$ value was considered.

3.4. RESULTS

Localisation of potential binding sites of Foxos in the 5' flanking region of the *Mjd* gene

Based in the matrices reported for the 8-bp length DBE binding sequences of mouse Foxos (Figure 3.1) (Furuyama et al. 2000), and taking into account the four possible DNA reading sequences, we have determined 18 potential sequences and ordered these by their probability of occurrence (Table 3.1). We have searched the 4054 bp of the 5' flanking region of the *Mjd* gene and found 18 potential FoxO binding sequences with variable probability of occurrence (Figure 3.3 and Table 3.2). However, some near and even superimposed sequences could correspond to a single binding site. Taking this into account, the sequences at positions (-2233, -2235, and -2239 bp), (-2349 and -2352 bp), (-2552, and -2555 bp), (-3496, and -3499 bp), (-3690, and -3696 bp), and (-3918, and -3921) could indeed correspond to unique FoxO binding sites. Based in the matrices reported for the 8-bp length DBE binding sequences of mouse Foxos (Figure 3.1) (Furuyama et al. 2000), and taking into account the four possible DNA reading sequences, we have determined 18 potential

Table 3.1. Decreasing order for the probability of occurrence of the potential Foxo binding sequences

Ranking by probability of occurrence	Potential Foxo binding sequences			
1	ttgtttac	aacaaatg	catttgtt	gtaaacaa
2	ttgttttc	aacaaaag	cttttgtt	gaaaacaa
3	ttgtttat	aacaaata	tatttgtt	ataaacaa
4	ttgttttt	aacaaaaa	tttttgtt	aaaaacaa
5	ttgtttag	aacaaatc	gatttgtt	ctaaacaa
6	ttgttttg	aacaaaac	gttttgtt	caaaacaa
7	ttgttgac	aacaactg	cagttgtt	gtcaacaa
8	ttgttgtc	aacaacag	ctgttgtt	gacaacaa
9	ttgttgat	aacaacta	tagttgtt	atcaacaa
10	ttgttgtt	aacaacaa	ttgttgtt	aacaacaa
11	ttgttgag	aacaactc	gagttgtt	ctcaacaa
12	ttgttgtg	aacaacac	gtgttgtt	cacaacaa
13	ttgttaac	aacaattg	caattgtt	gttaacaa
14	ttgttatc	aacaatag	ctattgtt	gataacaa
15	ttgttaat	aacaatta	taattgtt	attaacaa
16	ttgttatt	aacaataa	ttattgtt	aataacaa
17	ttgttaag	aacaattc	gaattgtt	cttaacaa
18	ttgttatg	aacaatac	gtattgtt	cataacaa

sequences and ordered these by their probability of occurrence (Table 3.1). Given this, we can consider 11 potential binding regions for Foxo transcription factors in the ~4 Kb of the 5'-upstream region of the *Mjd* gene.

Starved mice presented diminished levels of serum glucose

In order to study the *Mjd* and *Foxo*s expression levels in brain and in skeletal muscle of mice subjected to starvation and sort-term cold exposure, we have maintained a group of 8 animals in standard conditions ("control"), a group of 8 animals ("starvation") in starvation with free access to water at normal temperature during 24 hours, and a group of 7 animals ("cold exposure") fed *ad libitum*, and with total access of water, at 4 ± 1 ºC, during 24 hours.

We measured the levels of glucose in serum from both control and starved mice, and confirmed the decrease of glucose in the last ones (Figure 3.4), which may indicate a reduction of circulating insulin. In order to confirm the effect of cold-exposure, we are currently measuring the *Ucp3* mRNA levels (known to be increased in this condition), by quantitative real-time RT-PCR, in the skeletal muscle of mice subjected to this stress.

Figure 3.3. The putative Foxo binding sequences are highlighted in the ~4 kb of the 5' flanking region of the *Mjd* gene.

Table 3.2. Localisation and probability of occurrence of potential Foxo binding sequences to the *Mjd* 5' flanking region

Localisation (bp)	Ranking by probability of occurrence
-1048	18
-1188	18
-1634	4
-2233	6
-2235	10
-2239	11
-2349	1
-2352	7
-2390	2
-2552	1
-2555	9
-3050	15
-3496	15
-3499	13
-3690	4
-3696	4
-3918	18
-3921	2

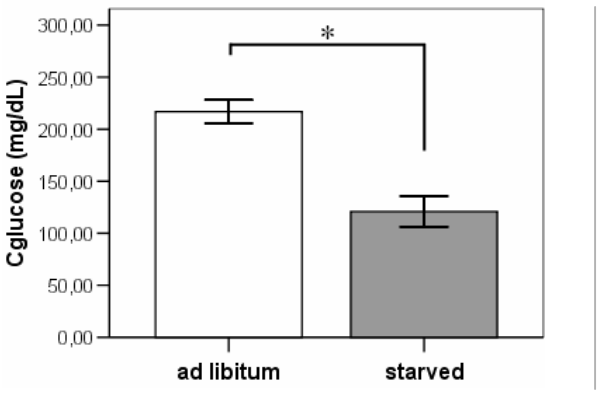

Figure 3.4. Mice subjected to starvation during 24 hours presented significant decreased levels of glucose in the serum. The results correspond to the average of the levels obtained for 8 animals in each group ± SEM (error bars). ∗, statistical significance ($p<0.05$).

Foxo3 and *Foxo4* expression levels decrease in the brain of starved mice

The expression levels of the *Foxo1*, *Foxo3*, or *Foxo4* genes of mice subjected to starvation or cold exposure in the brain had not been described previously in the literature. To achieve the mRNA level of these genes we have extracted total RNA from total brain of control (n=8), starved (n=8), and cold-exposed (n=7) mice, and performed quantitative real-time RT-PCR for each gene (Figure 3.5). *Foxo1* showed a slight but not significant decrease in stressed mice, either starved or cold-exposed, in relation to controls (Figure 3.5). *Foxo3* and *Foxo4* were diminished 2.69 and 2.80-fold, respectively, in the brain of mice subjected to starvation (Figure 3.5 and Table 3.3). In addition, we also observed a trend towards a

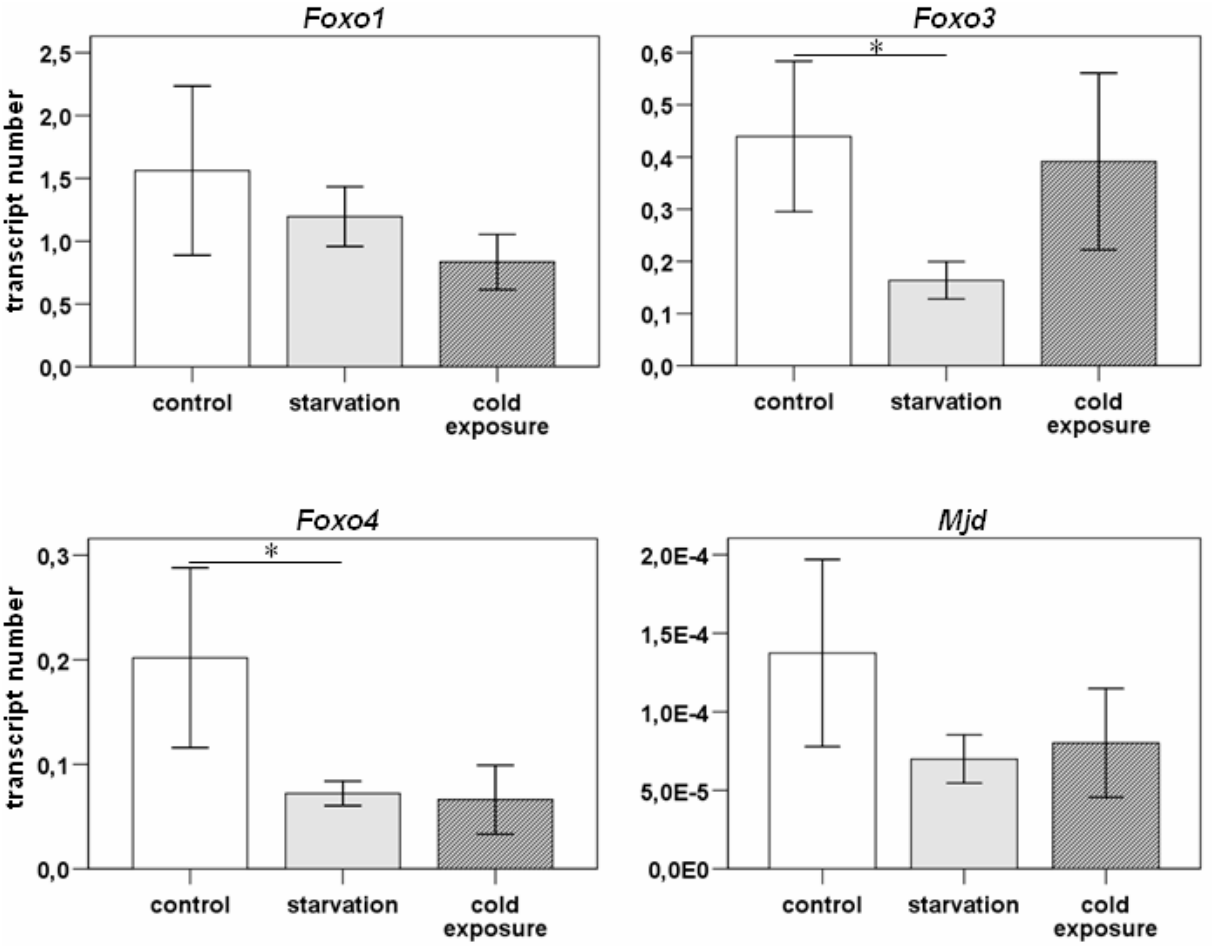

Figure 3.5. *Foxo3* and *Foxo4* gene levels showed to be decreased in the whole brain of starved mice. Transcript levels of *Mjd*, *Foxo 1*, *Foxo3*, and *Foxo4* genes in the total brain of mice from the "control", "starvation", and "cold-exposure" groups were measured by quantitative real-time RT-PCR. The results were normalised for the *Hprt* gene and correspond to the average of the results obtained for the mice of each group ± SEM (error bars). (∗) statistical difference.

decrease of the levels of *Foxo4* in cold-exposed mice (Figure 3.5). The *Mjd* gene levels showed a similar trend as *Foxo1* for a decrease, but not significant, in stressed mice (Figure 3.5 and Table 3.3).

Mjd, *Foxo1*, *Foxo3*, and *Foxo4* genes showed specific patterns of altered expression in the skeletal muscle of stressed mice

In order to define the expression levels of *Foxo1*, *Foxo3*, or *Foxo4* genes in the skeletal muscle of mice subjected to starvation and cold exposure, we have extracted total RNA from the skeletal muscle of the same abovementioned mice, and performed quantitative real-time RT-PCR for each gene (Figure 3.6). In starvation conditions only *Foxo1* levels

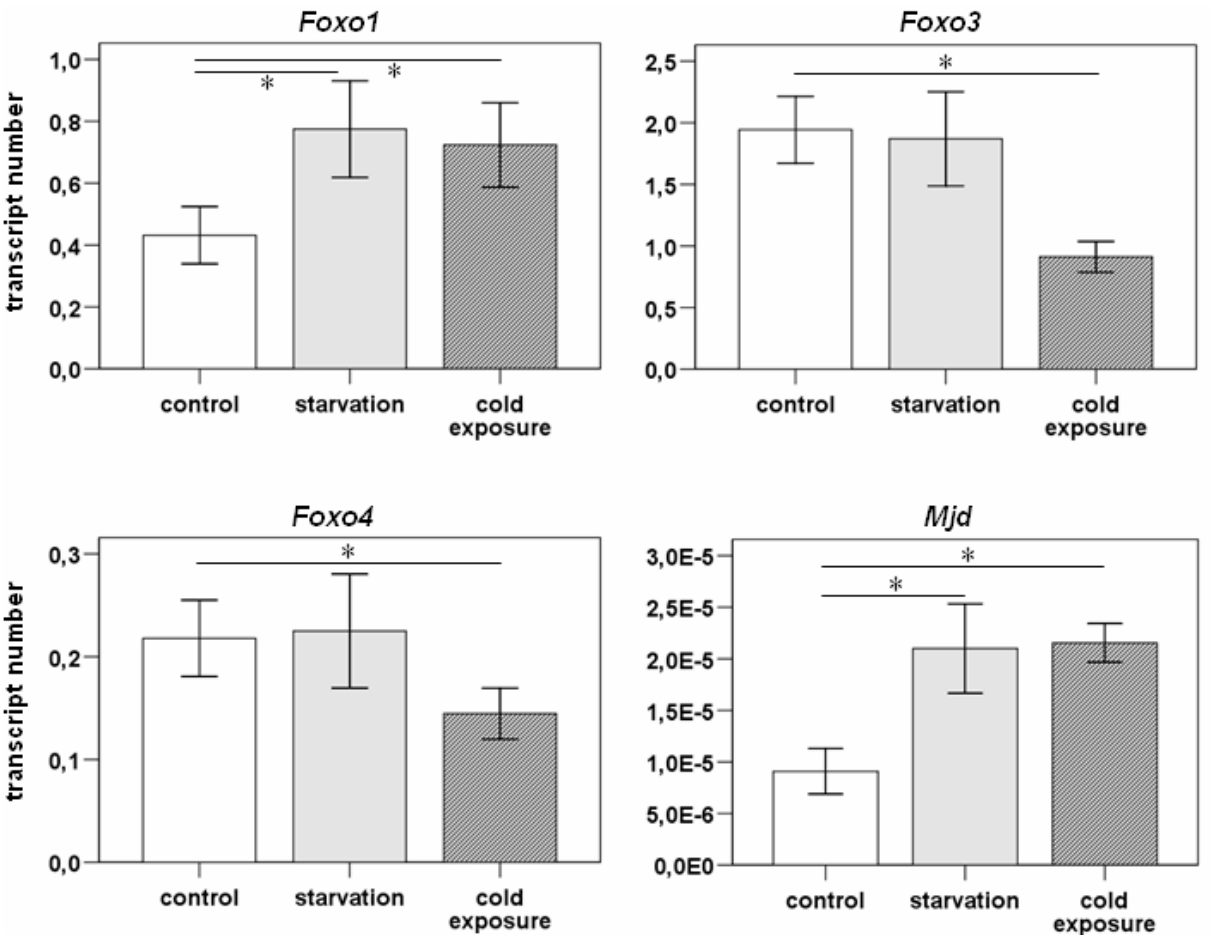

Figure 3.6. *Mjd*, *Foxo1*, *Foxo3*, and *Foxo4* genes showed specific patterns of altered expression in the skeletal muscle of stressed mice. Transcript levels of *Mjd*, *Foxo1*, *Foxo3*, and *Foxo4* genes in the skeletal muscle of mice from the "control", "starvation", and "cold-exposure" groups were measured by quantitative real-time RT-PCR. The results were normalised for the *Hprt* gene and correspond to the average of the results obtained for the mice of each group ± SEM (error bars). (∗) statistical difference ($p < 0.05$).

changed significantly, being 1.79-fold increased (Figure 3.6). The *Mjd* levels also showed to be 2.32-fold increased in starved mice (Figure 3.6 and Table 3.3).

In the skeletal muscle of cold-exposed mice all the four studied genes showed significant alterations of expression: (1) *Foxo1* showed the same tendency observed in starved mice increasing 1.68-fold; (2) *Foxo3* and *Foxo4* expression was diminished 2.13 and 1.51-fold, respectively; and (3) *Mjd* presented the same trend observed in starved mice increasing 2.38-fold (Figure 3.6 and Table 3.3).

Table 3.3. Fold-change of the *Mjd*, *Foxo1*, *Foxo3*, and *Foxo4* gene levels in the brain and skeletal muscle of mice in stress conditions. (↑) increase; (↓) decrease.

Tissue	Stress	Fold-change			
		Mjd	***Foxo1***	***Foxo3***	***Foxo4***
whole brain	starvation	-	-	↓ 2.69	↓ 2.80
	cold exposure	-	-	-	-
skeletal muscle	starvation	↑ 2.32	↑ 1.79	-	-
	cold exposure	↑ 2.38	↑ 1.68	↓ 2.13	↓ 1.51

3.5. DISCUSSION

In this chapter, we tried to explore the hypothesis that *Mjd* could be a stress-responsive gene, regulated by Foxo transcription factors. Since the *daf-16* mouse homologue genes, *Foxo1*, *Foxo3* and *Foxo4*, are stress-responsive transcription factors known to respond to particular conditions with altered insulin/ IGF1 levels, we attempted to investigate the effect of these conditions upon expression of the *Mjd* gene.

As previously described, we have verified that the recombinant DAF-16 protein binds *in vitro* to the *C. elegans atxn-3* promoter (Santos 2005). In order to identify the DBEs in the mouse *Mjd* promoter region, and based in the matrixes previously reported (Furuyama et al. 2000), we have determined all the FoxO possible binding sequences, and searched these, in the -4054 bp 5' flanking region of the *Mjd* gene. We found 11 potential binding sequences, some of them with a high probability of occurrence, which means that the mouse *Mjd* gene might be regulated by FoxO transcription factors. However, further experiments should be performed in order to prove the direct binding of FoxO proteins to the *Mjd* promoter by EMSA

and chromatin immunoprecipitation, and to evaluate the expression levels of the endogenous *Mjd* gene, or of the CAT gene under the regulation of the *Mjd* promoter, using the constructs defined in Chapter 2, in cells overexpressing a FoxO protein, for instance C2C12 cells overexpressing Foxo1 (Bastie et al. 2005).

Another way, however indirect, to verify *in vivo* if the *Mjd* gene is regulated by FoxO transcription factors, is to measure the *Mjd* level in a certain tissue of mice submitted to a known condition that upregulates FoxOs. Since it was previously reported that in starvation conditions, *Foxo1* and *Foxo3* were upregulated in mice skeletal muscle (Furuyama et al. 2003), we have stressed a group of mice exactly in the same way (food deprivation during 24 hours), and evaluated the expression levels of the *Mjd*, *Foxo1*, *Foxo3*, and *Foxo4* genes in the same tissue. Our results confirmed the maintenance of the levels of *Foxo4* and the upregulation of *Foxo1* (1.79-fold) in the skeletal muscle of starved mice, although we did not observe any expression level difference of *Foxo3* gene in relation to control mice. This difference could be explained by the number of analysed mice, given that we have studied groups of eight mice, whereas the previous study analysed groups of four mice each (Furuyama et al. 2003); or by the use of different methods to quantify gene expression, since we used real-time RT-PCR and the other researchers used Northern blotting. Although Northern blotting is a sensitive technique it is less precise than real-time RT-PCR; most probably the reduced number of analysed mice (half of ours) in the published study (Furuyama et al. 2003) may be responsible for this difference.

As discussed above, it is expected that the low levels of blood insulin during starvation will decrease the activity of Akt, and subsequently to an increase of unphosphorylated Foxo1, which is localised into the nuclei exerting its transcriptional activity (Biggs et al. 1999; Brunet et al. 1999). Although it was reported that the level of phosphorylated Foxo1 was increased in skeletal muscle of starved mice (Furuyama et al. 2003), probably because of its phosphorylation by kinases other than Akt, in starvation conditions the increase of the expression levels of total *Foxo1* was much higher and the amount of unphosphorylated Foxo1 would still be greatly larger than during *ad libitum* feeding (Furuyama et al. 2003). Thus, the change in the expression level of *Foxo1* might be more important than that of phosphorylation in the regulation of target genes in the skeletal muscle during starvation.

Interestingly, we verified that the levels of the *Mjd* gene were also increased in the skeletal muscle of starved mice. Since mATX3, the protein encoded by the *Mjd* gene, possesses DUB activity (Chapter 2), and is probably involved in the UPS, this result is in accordance with the previous studies that reported an increase of proteins involved in the ubiquitination/ deubiquitination machinery in muscle wasting (Furuyama et al. 2002; Lecker et al. 2004; Attaix et al. 2005; Combaret et al. 2005; Wing 2005).

Given that MJD is a neurodegenerative disorder, and even knowing that brain is exclusively dependent of glucose metabolism and that starvation may not have a direct effect in the brain, we decided to evaluate the levels of the same genes in the brain of mice subjected to starvation. Effectively, we verified for the first time that, although not significant, there was a trend towards a decrease of the gene expression levels of *Foxo1*, and that *Foxo3* and *Foxo4* showed to be significantly decreased 2.69 and 2.80-fold, respectively. The *Mjd* gene showed only a tendency for a decrease of its expression levels. Interestingly, as in the skeletal muscle, the expression pattern of *Mjd* and *Foxo1* in brain seem to follow the same direction, but in this case towards a decrease in expression. Thus, we may speculate that Foxo1 could indeed activate the *Mjd* transcription. Nonetheless, the levels of *Foxo3* and *Foxo4* mRNAs were also more significantly diminished in starved brains which could mean that these could also regulate the *Mjd* gene.

Although no expression levels studies were reported regarding FoxO proteins in cold-stressed mammals, we decided to investigate the expression levels of *Foxo1*, *Foxo3*, and *Foxo4* mRNAs in both skeletal muscle and brain of short-term cold exposed mice (4ºC, during 24 hours). We have not observed significant differences in the expression levels for any of the studied genes in the whole brain of cold-stressed mice in relation to controls. However, *Foxo1*, and *Foxo4* levels tend towards a decrease of expression in cold-exposed mice as did the *Mjd* gene. This suggests that these genes might be more mildly stress-responsive genes in the brain of cold-stressed mice. Additional analysis of the expression levels of these genes in specific regions of the brain, in particular the ones affected in MJD, should be performed, potentially allowing an increased sensitivity to expression changes.

The evaluation of the expression of these genes in the skeletal muscle of cold-stressed mice revealed that all of them were significantly altered. Interestingly, *Foxo1* was increased in cold-exposed mice, following the same trend observed in the starved ones, whereas *Foxo3* and *Foxo4* showed a decreased expression. The *Mjd* expression levels were increased. Once again, *Mjd* and *Foxo1* seem to share the same expression profile, which corroborates the hypothesis of that *Mjd* transcription could be activated by *Foxo1*.

In this study we defined the expression profile of the *Mjd*, *Foxo1*, *Foxo3*, and *Foxo4* genes in the skeletal muscle and total brain of mice submitted to two different stress conditions: starvation and cold exposure. Of great importance is the fact that in the skeletal muscle these two conditions have different effects in the protein metabolism. In the starved mice a decrease in protein synthesis and an increase of protein degradation was reported (Sandri et al. 2004; Stitt et al. 2004), whereas in short-term cold exposed rats only a decrease in protein synthesis was observed, with no alterations in protein degradation (Samuels et al. 1996).

Given that in relation to the *Foxo1* and *Mjd* genes we have only observed a significant increase in the skeletal muscle of mice subjected to both stress conditions, and that the common effect between these two is the decrease of protein synthesis, we may speculate that mATX3 could be important for either: (1) the recovery of certain important muscle proteins from degradation; (2) the regulation of Foxo1 itself, since mATX3 interacts with both CBP and p300 (Li et al. 2002), which in turn modulate Foxo1 activity by acetylation (van der Heide and Smidt 2005); (3) the regulation by the UPS of the levels of Foxo1 (Matsuzaki et al. 2003; Huang et al. 2005); and/or (4) the regulation of protein synthesis acting in conjunction with Foxo1 in the inhibition of eIF4E (Southgate et al. 2007), given that we identified this elongation factor as a direct molecular partner of mATX3 (see Chapter 4).

Here we have also shown for the first time that FoxO proteins are involved in the cellular response to cold-stress, in particular in the skeletal muscle, and that the fact that the *Mjd* gene is upregulated in stress-conditions may lead us to speculate that stresses during a patient's lifetime could lead to an increase of mutant ATX3 inside cells, which could potentially lead to a worst phenotype. In particular in the skeletal muscle, stress and a deregulation of ATX3 activity may contribute to the distal muscular atrophy or to the cachexia observed in MJD patients. Nevertheless, the relevance of this regulation to this clinical feature or to the fact that MJD is an ageing-related disorder remains to be explored.

Chapter 4

New molecular partners of ataxin-3

GENERAL CONSIDERATIONS

Several molecular processes need to occur inside any cell to keep it alive. These intracellular events are mediated by quite a few types of biomolecules. The functionality of proteins is very high, since they are present in all compartments of the cell, in a vast number, often adopting several different three-dimensional structures and playing different functions in cellular metabolism. Proteins, besides being able to interact with all the other types of biomolecules, can also interact with other proteins. However, each protein-protein interaction is a specific molecular event, with a precise functional purpose, in a cellular pathway.

Currently, in spite of knowing that ATX3 protein possesses DUB activity *in vitro*, and that it interacts with about 27 proteins (Chapter 1, section 1.3.6), its biological or physiological function remains to unveil. In Chapter 2, we have characterised the mouse *ATXN3* homologue gene (*Mjd*), verified its orthology in relation to the human, since mATX3 preserves the DUB activity, and determined its subcellular localisation in some mouse tissues. In general, mATX3 can be found in almost all cellular compartments, including the nucleus, cytoplasm, mitochondria, endoplasmic reticulum and Golgi apparatus. In order to use the mouse as a model to study either the normal function of ATX3, or its role in pathogenesis, it is crucial (i) to confirm some known human ATX3-protein interactions in mouse, and (ii) to search for new protein partners of mATX3.

The identification of the molecular partners of mATX3 will be important to characterise the biological role(s) of mATX3. Furthermore, the characterisation and potential manipulation of the mATX3-protein interactions, for example it's possible DUB substrates, may be important in the disease context and could represent putative targets of therapeutic intervention.

This chapter describes the preliminary results of an exploratory investigation regarding (i) the search of new mATX3 protein interactors, and (ii) some novel hypotheses related to the mATX3 role in specific pathways or systems, raised by our own and other researcher's results. The majority of the results described here will need to be further investigated in the future. However we believe that their presentation in a structured manner can be of use in the planning of these future studies.

This chapter is divided in four sub-chapters:

- **Chapter 4.1** Screening of protein interactors of mouse ataxin-3 using the yeast two-hybrid system
- **Chapter 4.2** Ataxin-3 and the SCF complex
- **Chapter 4.3** Ataxin-3 and microtubules: a role in mitosis?
- **Chapter 4.4** Ataxin-3 in sarcomeres

Chapter 4.1

Screening of protein interactors of mouse ataxin-3 using the yeast two-hybrid system

4.1.1. SUMMARY

Currently 27 protein interactors of ATX3 are known. In order to further define the interactome of this protein we screened two mouse cDNA libraries using the y2h system to identify new protein partners of the mouse homologue ATX3. We have identified 81 new mATX3 interactors, and further confirmed the direct interaction of mATX3 with 18 of them by y2h co-transformation and mating assays. In order to obtain an integrative view of the relationship between mATX3 and its interactors, we performed a bioinformatic analysis of all the known (27) and the new mATX3 interactors thus confirmed (18) using databases that contain gene/protein information from different species. We have found the interactors of ATX3 to integrate three different functional networks.

Overall, the main functional pathways in which ATX3 seems to be involved are, as previously proposed, transcription regulation and protein degradation. Additionally, our novel results suggest that ATX3 may also be involved in the following processes: protein synthesis, cell cycle, cellular proliferation and differentiation, cellular movement and spermatogenesis.

4.1.2. INTRODUCTION

The ubiquitous cellular and subcellular expression pattern of mATX3 in all tissues analysed (Chapter 2) led us to hypothesise that a very large number of its interactions remained unidentified. One strategy for the identification of interacting proteins is the yeast two-hybrid (y2h) system (Fields and Song 1989). This *in vivo* system is used to screen cDNA libraries for clones encoding proteins that are able to bind to a protein of interest (Chien et al. 1991). In this study the GAL4-based yeast two-hybrid system (Durfee et al. 1993) was used to identify novel protein interactors of mATX3.

The yeast two-hybrid system is based on the fact that eukaryotic transcription factors are constituted by two physically separated and functionally independent domains: the DNA-binding domain (DNA-BD) that binds to a specific promoter sequence, and an activation domain (AD) that allows RNA polymerase II complex to transcribe the gene downstream of the DNA-binding site (Keegan et al. 1986). In general these two domains are part of the same protein (as is the case of the GAL4 yeast transcription factor), both being necessary for the transcription of a gene. Physically separated DNA-BD and AD peptides expressed in the same cell do not interact with each other and consequently do not activate gene transcription (Ma and Ptashne 1988). On the other hand, gene transcription can be restored if these domains are in close physical proximity at the corresponding promoter region.

In the GAL4-based two-hybrid system, one hybrid (the bait) is a fusion protein between the GAL4 DNA-BD (GAL4BD) and the protein/peptide of interest that in this case is mATX3 (GAL4BD::mATX3); and the second hybrid (prey) consists in the GAL4 activation domain (GAL4AD) fused to a cDNA library clone (GAL4AD::prey). When the two hybrid proteins expressed in yeast are able to interact, the two domains of GAL4 will get in close physical proximity and will activate the transcription from promoters containing UAS_G GAL4-binding sites. Some specific yeast strains are normally used in the screenings of cDNA libraries for bait interactions. In particular, the commonly used Y190 yeast strain provides a double selection system since is a carrier of two chromosomal reporter genes whose expression is regulated by GAL4: (1) the *E.coli lacZ* gene under the control the *GAL1* promoter; and (2) the *HIS3* gene, whose regulatory region was replaced by $GAL1_{UAS}$. Given that the Y190 strain is deleted for *GAL4* and its negative regulator *GAL80*, the expression of both reporter *HIS3* and *lacZ* genes should be off in the absence of exogenous GAL4. Therefore, in this system a positive interaction between the GAL4BD::mATX3 bait and a hybrid GAL4AD::prey will result in the activation of the reporter genes, generating β-galactosidase expressing and histidine prototrophic (His^+) yeast colonies.

4.1.3. MATERIALS AND METHODS

Yeast strains

The *Saccharomyces cerevisiae* strains used in the yeast two-hybrid system assays (GAL4 2H-2) were Y190 and Y187 (Harper et al. 1993).

The genotype of the Y190 strain is *MATa*, *ura3-52*, *his3-200*, *ade2-101*, *lys2-801*, *trp1-901*, *leu2-3*, *112*, *gal4Δ*, *gal80Δ*, *cyh^{r}2*, *MEL1*, *LYS2::GAL1*$_{UAS}$-*HIS3*$_{TATA}$-*HIS3*, *URA3::GAL1*$_{UAS}$- *GAL1*$_{TATA}$-*lacZ*. This strain contains two reporter genes (*HIS3* and *lacZ*), each regulated by a different GAL4-dependent promoter to reduce the incidence of background. The *HIS3* reporter is under the control of the *GAL1*$_{UAS}$, and a minimal promoter containing both *HIS3* TATA boxes, TR (regulated) and TC (constitutive). The *lacZ* reporter is regulated by the intact *GAL1* promoter, including the *GAL1*$_{UAS}$ and the *GAL1* minimal promoter. The genotype of the Y187 strain is *MATα*, *ura3-52*, *his3-200*, *ade2-101*, *trp1-901*, *leu2-3*, *112*, *gal4Δ*, *met$^-$*, *gal80Δ*, *MEL1*, *URA3::GAL1*$_{UAS}$- *GAL1*$_{TATA}$-*lacZ*. This yeast strain possesses only the *lacZ* reporter gene above described.

Yeast culture medium

Complete medium (YPAD) and selection medium (SD) used for yeast growth and manipulation were prepared as described in the Yeast Protocols Handbook (Clontech). SD-WLH was prepared with all amino acids except tryptophan (W), leucine (L) and histidine (H). These nutrients were added separately depending on the necessary selection medium. The leaky expression of IGP dehydratase (*HIS3* product), in the Y190 yeast strain, was controlled by including 3-amino-1,2,4-triazole (3-AT, Sigma) in the medium. The minimum concentration of 3-AT required for library screening, co-transformation and mating assays was titrated.

Yeast two-hybrid bait constructs

In order to search for new interactors of mATX3 using the yeast two-hybrid GAL4-based system, several mATX3 bait constructs were prepared (Table 4.1.1). The pGBT9 low expression vector was used for the construction of these baits. The bait plasmids encode the DNA-binding domain of the GAL4 transcription factor (GAL4BD) in N-terminal fusion with the full-length mATX3 (pGBT9Mjd), the N-terminal fragment of mATX3 (aa 1-215, pGBT9Mjd:jos), the C-terminal of mATX3 (aa 216-355, pGBT9Mjd:UIMs), the full-length mATX3 carrying a point mutation C14A (pGBT9Mjd:C14A), and the N-terminal segment of mATX3 carrying the C14A mutation (pGBT9Mjd:jos:C14A). These constructs carry the *TRP1* marker, which confers the ability for yeast cells to grow in the absence of tryptophan (W). Only the pGBT9Mjd plasmid was used in the screening of mouse cDNA libraries, whereas the other bait plasmids were prepared for further mapping of the interaction region.

The bait plasmids pGBT9Mjd, pGBT9Mjd:jos, pGBT9Mjd:UIMs, pGBT9Mjd:C14A and pGBT9Mjd:jos:C14A were constructed by recombination between a Gateway converted version of the pGBT9 vector (provided by RZPD) and the corresponding plasmids pDONR207Mjd, pDONR207Mjd:jos, pDONR207Mjd:UIMs, pDONR207Mjd:C14A, and pDONR207Mjd:C14A (Chapter 2). The open reading frames (ORF) of bait coding sequences were introduced in the pGBT9 vector in frame with the GAL4BD coding sequence. These bait constructs have a *TRP1* gene that allows auxotrophic yeasts to grow in media lacking tryptophan. All the constructs were checked for correct in frame cloning by automated sequencing using the GAL4BD-F and GAL4BD-R primers (Appendix 1, Table A.1),and then tested for their toxicity in yeast and for self-activation of the two reporter genes, *HIS3* and *lacZ*. In this chapter, only the bait construct pGBT9Mjd, expressing the fusion protein GAL4BD::mATX3, was used.

Table 4.1.1. Yeast two-hybrid bait constructs

GAL4BD::bait fusion	
vector	**protein**
pGBT9Mjd	GAL4BD::mATX3[aa1-355]
pGBT9Mjd:jos	GAL4BD::mATX3[aa1-215]
pGBT9Mjd:UIMs	GAL4BD::mATX3[aa216-355]
pGBT9Mjd:C14A	GAL4BD::mATX3[aa1-355]:C14A
pGBT9Mjd:jos:C14A	GAL4BD::mATX3[aa1-215]:C14A

aa, amino acids

Screening of mouse y2h library

The pGBT9Mjd bait plasmid was sent to the RZPD Company and used by them to perform the screening of two mouse libraries. A yeast strain carrying a fluorogenic reporter gene was transformed with the bait plasmid, and the minimum amount of 3-AT required for stringency of the *HIS3* reporter gene was titrated. In order to eliminate auto-activation of the GAL4 system, selective media containing 45 mM 3-AT showed to be stringent enough for this bait. The two Matchmaker cDNA GAL4 libraries (Clontech) – Mouse 11-Day Embryo and Mouse Testis – pre-transformed into the yeast strain Y187, were each screened twice, by mating with the yeast strain Y190 pre-transformed with the bait. Selective media used in the two screenings of each library were SD-WLH 45 mM 3-AT and SD-WLH 50 mM 3-AT. Positive clones were selected, grown in microtiter plates, and hybrids interaction measured by a quantitative readout of the fluorogenic reporter gene. The inserts of the positive preys were amplified by PCR and sequenced only once. RZPD sent data in a table form indicating the name of the interacting proteins, their partial sequences, and the number of times each one was isolated from both screenings.

Bioinformatic analysis

All sequences of the fusion prey transcripts were checked for the reading frame. The interacting region of each prey with mATX3 was determined using the GenBank database and the ExPASy Translate Tool. The newly identified and previously known mATX3 protein interactors were analysed in conjunction for their putative molecular network pathways using the trial version of the Ingenuity Pathways Analysis Inc. 5.0 software, which in turn uses all the information known for a specific gene/protein including the one from their homologues in other species.

Yeast two-hybrid prey constructs

Total RNA was isolated from adult C57Bl/6 mouse brain and testis, using Trizol reagent (Invitrogen Life Technologies). Total RNA (2.5 μg) from each tissue was used to perform reverse transcription using the SuperScript™ First-Strand Synthesis System for RT-PCR (Invitrogen Life Technologies) with an oligo(dT) primer. The coding sequences of the preys Ap3b1[aa 1-138], Atp5j, Bcl7c, Brf1, Ccdc113, Cul1[aa 714-776], Eef1b2, Eif4e, Etfb, Gtf2e2, Kif2c, Lrcc40, Pcmt1, Rpl6, Rps9, Spatc1, Thg1l, Tsga10ip, and Twa1 were amplified in frame by RT-PCR using the corresponding pair of primers including the 5' (attB1) and 3' (attB2) attB site-specific recombination sequences (Gateway Cloning System) (Appendix 1, Table A.2), and 1 μL of total cDNA from the respective tissue or of the plasmids pCMV-SPORT6-Ap3b1, pCMV-SPORT6-Cul1, or pCMV-SPORT6-Kif2c (Open Biosystems) (Table 4.1.2).

For PCR products smaller than 700 bp, PCRs were performed using the enzyme Taq DNA Polymerase (Fermentas) under the following conditions: one cycle of 5 min at 95°C, followed by 35 cycles of one min at 95°C, one min at 55°C, one min at 72°C, and ending with 5 min at 72°C. To amplify PCR products higher than 700 bp the enzyme BIO-X-ACT-LONG (Bioline) was used in the conditions: one cycle of 5 min at 95°C, followed by 35 cycles of one min at 95°C, one min at 55°C, three min at 68°C, and ending with 15 min at 68°C. The RT-PCR products were purified from 1% agarose gels using the GFX™ PCR DNA and Gel Band Purification Kit (Amersham Pharmacia Biotech) or the QIAQuick Gel Extraction kit (Qiagen) and cloned in the pDONR207 vector using the Gateway Cloning System (Invitrogen Life Technologies) accordingly to manufacturer´s instructions.

The prey plasmids were obtained by recombination between a Gateway version of the pGAD424 vector (provided by RZPD) and the corresponding pDONR207 prey plasmids (Table 4.1.2), using the Gateway Cloning System (Invitrogen Life Technologies). Prey coding sequences were introduced in the pGAD424 vector in frame with the GAL4AD coding sequence. A pGADMjd plasmid was also prepared similarly from the pDONR207Mjd plasmid. These prey constructs have a *LEU2* gene that allows auxotrophic yeasts to grow in media lacking leucine. Each construct was checked for the correct in frame cloning by automated sequencing using the GAL4AD-F and GAL4AD-R primers, and when necessary, gene specific primers such as Brf1(1), Kif2c(1), Lrrc40(1), or Tsga10ip(1) (Appendix 1, Table A.1) and then tested for their toxicity in yeast and for their self-activation of the two reporter genes, *HIS3* and *lacZ*.

Table 4.1.2. Selected prey proteins from the library screenings with the pGBT9Mjd bait plasmid and details about the construction of the prey pGAD plasmids.

Prey	RT-PCR primers	PCR product size (bp)	RT-PCR template	Cloning vector	GAL4AD::prey fusion	
					vector	protein
Ap3b1[aa1-138]	attB1Ap3b1/ attB2Ap3b1[138]	475	pCMV-SPORT6-Ap3b1	pDONR207 Ap3b1[aa1-138]	pGADAp3b1[aa1-138]	GAL4AD::Ap3b1[aa1-138]
Atp5j	attB1Atp5j/ attB2Atp5j	388	mouse testis total cDNA	pDONR207Atp5j	pGADAtp5j	GAL4AD::Atp5j
Bcl7c	attB1Bcl7c/ attB2Bcl7c	715	mouse testis total cDNA	pDONR207Bcl7c	pGADBcl7c	GAL4AD::Bcl7c
Brf1	attB1Brf1/ attB2Brf1	2092	mouse brain total cDNA	pDONR207Brf1	pGADBrf1	GAL4AD::Brf1
Ccdc113	attB1Ccdc113/ attB2Ccdc113	1195	mouse testis total cDNA	pDONR207Ccdc113	pGADCcdc113	GAL4AD::Ccdc113
Cul1[aa714-776]	attB1Cul1[714]/ attB2Cul1	253	pCMV-SPORT6-Cul1	pDONR207Cul1[aa714-776]	pGADCul1[aa714-776]	GAL4AD::Cul1[aa714-776]
Eef1b2	attB1Eef1b2/ attB2Eef1b2	739	mouse brain total cDNA	pDONR207Eef1b2	pGADEef1b2	GAL4AD::Eef1b2
Eif4e	attB1Eif4e/ attB2Eif4e	715	mouse brain total cDNA	pDONR207Eif4e	pGADEif4e	GAL4AD::Eif4e
Etfb	attB1Etfb/ attB2Etfb	829	mouse testis total cDNA	pDONR207Etfb	pGADEtfb	GAL4AD::Etfb
Gtf2e2	attB1Gtf2e2/ attB2Gtf2e2	940	mouse testis total cDNA	pDONR207Gtf2e2	pGADGtf2e2	GAL4AD::Gtf2e2
Kif2c	attB1Kif2c/ attB2Kif2c	2227	pCMV-SPORT6-Kif2c	pDONR207Kif2c	pGADKif2c	GAL4AD::Kif2c
Lrrc40	attB1Lrrc40/ attB2Lrrc40	1870	mouse testis total cDNA	pDONR207Lrrc40	pGADLrrc40	GAL4AD::Lrrc40
Pcmt1	attB1Pcmt1/ attB2Pcmt1	745	mouse testis total cDNA	pDONR207Pcmt1	pGADPcmt1	GAL4AD::Pcmt1
Rpl6	attB1Rpl6/attB2Rpl6	952	mouse testis total cDNA	pDONR207Rpl6	pGADRpl6	GAL4AD::Rpl6
Rps9	attB1Rps9/attB2Rps9	646	mouse testis total cDNA	pDONR207Rps9	pGADRps9	GAL4AD::Rps9
Spatc1	attB1Spatc1/ attB2Spatc1	1504	mouse testis total cDNA	pDONR207Spatc1	pGADSpatc1	GAL4AD::Spatc1
Thg1l	attB1Thg1l / attB2Thg1l	958	mouse testis total cDNA	pDONR207Thg1l	pGADThg1l	GAL4AD::Thg1l
Tsga10ip	attB1Tsga10ip/ attB2Tsga10ip	1824	mouse testis total cDNA	pDONR207Tsga10ip	pGADTsga10ip	GAL4AD::Tsga10ip
Twa1	attB1Twa1/ attB2Twa1	748	mouse brain total cDNA	pDONR207Twa1	pGADTwa1	GAL4AD::Twa1

aa, amino acids

GST::prey expressing constructs

Glutathione-S-transferase (GST)-tag prey protein expression plasmids were obtained by recombination between the corresponding pDONR207 plasmids (Table 4.1.2) and the pDEST15 vector using the Gateway Cloning System (Invitrogen) (Table 4.1.3).

Table 4.1.3. GST::prey expressing constructs

GST::prey fusion	
vector	**protein**
pDEST15Ap3b1[aa1-138]	GST::Ap3b1[aa1-138]
pDEST15Atp5j	GST::Atp5j
pDEST15Bcl7c	GST::Bcl7c
pDEST15Brf1	GST::Brf1
pDEST15Ccdc113	GST::Ccdc113
pDEST15Cul1[aa714-776]	GST::Cul1[aa714-776]
pDEST15Eef1b2	GST::Eef1b2
pDEST15Eif4e	GST::Eif4e
pDEST15Etfb	GST::Etfb
pDEST15Gtf2e2	GST::Gtf2e2
pDEST15Kif2c	GST::Kif2c
pDEST15Lrrc40	GST::Lrrc40
pDEST15Pcmt1	GST::Pcmt1
pDEST15Rpl6	GST::Rpl6
pDEST15Rps9	GST::Rps9
pDEST15Spatc1	GST::Spatc1
pDEST15Thg1l	GST::Thg1l
pDEST15Tsga10ip	GST::Tsga10ip
pDEST15Twa1	GST::Twa1

aa, amino acids

Auto-activation assay

In order to assess the ability of the bait construct (pGBT9Mjd) to auto-activate the yeast reporter genes, pre-transformed Y190 yeasts were spread and plated as dots in selective medium SD-WH supplemented with different concentrations of 3-AT: 20, 30, 40, 50, 60, 70, 80, 90, 100, 110, 120, and 130 mM. Plates were incubated at 30ºC during five days, then assayed for β-galactosidase expression, and the minimum concentration of 3-AT required to eliminate self-activation of the GAL4 system determined.

To assess the capacity of the prey constructs to auto-activate the reporter genes, pre-transformed Y190 yeasts with each prey construct were plated as dots in selective medium

SD-LH supplemented with 90 mM of 3-AT. Plates were incubated and assayed as mentioned above.

Yeast transformation

All yeast transformations were performed using the high efficiency lithium acetate method (Gietz et al. 1995). Y190 and Y187 strains without plasmids were grown in YPAD medium, overnight at 30ºC and at 200 rpm, while pre-transformed strains were grown in the appropriate SD medium to keep selective pressure of the plasmid. Overnight cultures were diluted in the respective medium to a cell optical density of 0.3 at 600 nm, and then incubated at 30ºC, at 200 rpm, until reach an optical density (OD) of 0.6. Cells were harvested by centrifugation at 1800 rpm for 5 min, first washed with sterile water and then with freshly made 100 mM LiAc. The following components were added to yeast pellets by order: 240 μL PEG (50% w/v), 36 μL 1M LiAc, 25 μL denatured salmon sperm DNA (2mg/mg), and 50 μL plasmid (1 μg) diluted in sterile water. Each tube was vortexed vigorously until the cell pellet was completely ressuspended, and then cells were incubated at 30 ºC during 30 min. Yeast cells where subsequently heat-shocked at 42ºC for 20 min. Finally, cells were centrifuged one min at 3000 rpm, and ressuspended in 1 mL of YPAD. 20 μL of the transformed yeast culture were plated onto the appropriated selective medium, and plates were incubated at 30ºC during five days.

Yeast mating

Yeast mating assays were performed using a previously described method (Bendixen et al. 1994). Briefly, one fresh yeast colony from each of the two mating types was used to inoculate 500 μL of YPAD, vortexed, and then incubated overnight at 30ºC, at 200 rpm. In the day after, 20 μL of the mating culture were spread in SD-WLH to select diploids, and in SD-WLH 30 mM 3-AT plates to select diploids with a positive two-hybrid interaction, after an incubation period of five days at 30ºC.

β-Galactosidase (β-gal) colony-lift filter assay

The β-galactosidase expression test was performed by colony-lift filter assay (Breeden and Nasmyth 1985). The assay was performed directly on fresh plates containing single colonies or dots of yeast transformants. Selective media supplemented with 90 mM and 30 mM of 3-AT were used in co-transformation and mating assays, respectively. A nylon

membrane (Hybond-N, GE Healthcare) was placed over the plate surface in contact with the yeast colonies. When the membrane was uniformly soaked, it was lifted and submerged in liquid nitrogen for 10 seconds to allow cell permeabilisation. After that, the membrane was thawed at room temperature and placed, with colony side up, on a Petri dish containing a filter paper pre-soaked in Z buffer (16.1 mg/mL $Na_2HPO_4.7H_2O$, 5.5 mg/mL $NaH_2PO_4.H_2O$, 0.75 mg/mL KCl, 0.246 mg/mL Mg_2SO_4, pH 7.0), supplemented with 1 mg/mL 5-bromo-4-chloro-3indolyl-β-D-galactopyranoside (X-Gal) and 38.6 mM β-mercaptoethanol (β-ME). Filters were incubated 1-12 hours at 30ºC, and then analysed for the presence of blue colonies (*lacZ* positive transformants).

4.1.4. RESULTS

Assessment of the mATX3 bait auto-activation

The use of yeast two-hybrid system as a tool to identify protein interactors requires that the hybrid proteins cannot by themselves activate the reporter genes. Autonomous activation of reporter transcription could be explained by: (1) the ability of some proteins, with no apparent function in transcription, to lead to a certain level of self-activation when fused to a DNA-binding domain; or by (2) the non-specific binding of AD-fusion proteins to promoters. The hybrid pGBT9Mjd construct was evaluated for its ability to self-activate the transcription of the Y190 strain reporter genes: *GAL1*$_{UAS}$-*HIS3* and *GAL1-lacZ*. Furthermore, the Y190 yeast strain is slightly prototrophic for histidine, but the addition of a competitive inhibitor of the *HIS3* gene product (IGP dehydratase), 3-AT, increases the sensitivity of the reporter gene, turning Y190 cells auxotrophic to histidine (Brent and Finley 1997).

The auto-activation of the pGBT9Mjd bait plasmid was tested using different methodologies depending on the yeast two-hybrid approach. The mouse y2h libraries screenings were performed by the company RZPD (Germany) and, in this case, a yeast strain containing a fluorogenic reporter gene was transformed with the bait plasmid and the concentration of 3-AT necessary to eliminate self-activation was titrated by fluorescence. The GAL4::mATX3 hybrid protein was found to auto-active the GAL4 system and a concentration of 45 mM of 3-AT was determined as that required to eliminate the auto-activation.

Direct protein interactions were evaluated by us using yeast co-transformation and mating assays. In this case, at a concentration of 90 mM of 3-AT we could still detect growth of some colonies, however these did not show β-gal activity (Figure 4.1.2). So, 90mM 3-AT

was defined as the working concentration to eliminate self-activation of the pGBT9Mjd plasmid in the Y190 strain when assessing for direct protein interactions.

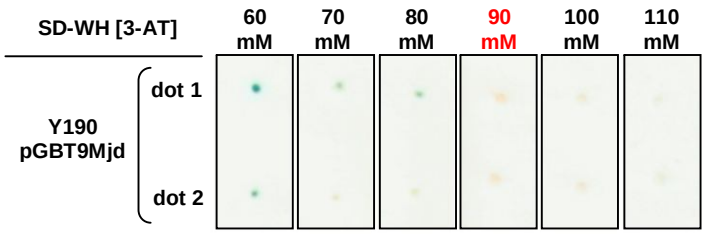

Figure 4.1.2. The pGBT9Mjd plasmid, encoding for the GAL4BD::mATX3 hybrid protein, does not auto-activate the GAL4-based reporter genes in the Y190 yeast strain if the selective medium SD-WH is supplemented with a concentration of 90 mM of 3-AT or higher. Two independent colony filter assays for β-gal activity are represented for dots of cells pre-transformed with the bait plasmid. LacZ reporter expression is indicated by the blue colour of the colonies, which is only observed in plates with 3-AT concentrations lower than 80 mM.

Identification of new protein interactors of mATX3

In order to identify mouse proteins that interact with mATX3, the pGBT9Mjd bait plasmid was sent to the RZPD Company and used to perform library screenings. A yeast strain carrying a fluorogenic reporter gene was transformed with the bait plasmid. Two mouse GAL4AD-fusion cDNA expression libraries were screened, one representative of 11-day mouse embryo transcripts and the other of mouse testis transcripts. These libraries were pre-transformed into the Y187 yeast strain, and screenings were performed by mating with another yeast strain pre-transformed with the bait. Colonies able to grow on the selective medium were collected, and further tested in a quantitative readout for the activation of the fluorogenic reporter gene. The positive prey plasmid inserts were amplified by PCR and identified by sequencing.

In the four library screenings performed (each library was screened twice), a total of 81 new protein interactors of mATX3 were identified (Tables 4.1.4, 4.1.5, and 4.1.6). The company subdivided the positive interacting proteins in three classes taking into account their probability of being truly mATX3 interactors: (class 1) prey proteins that appeared more than once (Table 4.1.4); (class 2) prey proteins that appeared only once (Table 4.1.5); and (class 3) promiscuous prey proteins that appeared to interact with several baits, or resulting

from fusion transcripts that were fragments of the 3' UTR, or cloned in the reverse orientation (Table 4.1.6).

We have focused on the most probable interactors, the class 1 (27) and class 2 (29) preys. For these, we have analysed their sequences and identified the reading frame of the cDNA insert in relation to the GAL4AD sequence, translated the DNA to protein sequences, and consequentially determined the interacting sequence of each prey protein with mATX3 (Tables 4.1.4, and 4.1.5). The analysis of some sequences did not allow the determination of the reading frame, or the interacting protein sequence, due to the fact that they corresponded to genomic DNA, or were not found in the databases. From the initial 56 preys (classes 1+2), we were able to determine the reading frame and the peptide interacting region for 35 proteins. Among these, we have selected 29 preys for cDNA cloning, to further perform both yeast two-hybrid co-transformation and mating assays (Tables 4.1.4 and 4.1.5). The criteria used to select these preys were: (1) the class of the preys, class 1 being preferential; (2) the reading frame of the inserts, "frame 1" being the favoured one; and (3) the interaction relevance in relation to our ongoing functional studies. Reading frames are not the best criterion to judge preys, since each prey insert was only sequenced once with reduced quality, and translational frame-shifting can compensate for shifted frames in some rare cases.

A group of proteins showed to directly interact with mATX3

In order to clone the identified interactors, we have designed primers and amplified the total coding region of the selected cDNAs, with the exception of Ap3b1 and Cul1 cDNAs (given their big length), for which only the fragments encoding the interacting domain were amplified. Among the 29 chosen cDNAs, we were able to clone 19 cDNA preys (Tables 4.1.4 and 4.1.5) into the pGAD424 vector which, as the bait vector pGBT9, is a low expression plasmid. The prey plasmids [(pGADAp3b1[aa 1-138], pGADAtp5j, pGADBcl7c, pGADBrf1, pGADCcdc113, pGADCul1[aa 714-776], pGADEef1b2, pGADEif4e, pGADEtfb, pGADGtf2e2, pGADKif2c, pGADLrcc40, pGADPcmt1, pGADRpl6, pGADRps9, pGADSpatc1, pGADThg1l, pGADTsga10ip, and pGADTwa1)] encode the DNA-activation domain of the GAL4 protein (GAL4AD) in N-terminal fusion (in frame) with the prey cDNAs (Table 4.1.2). We have also prepared a pGADMjd plasmid to test whether mATX3 interacts with itself forming dimers. These constructs carry the *LEU2* gene, which confers auxotrophic yeast the ability to grow in the absence of leucine (L). All these plasmids were tested for auto-activation of the reporter genes *GAL1*$_{UAS}$*-HIS3* and *GAL1-lacZ*, and no

Table 4.1.4. Positive class 1 preys, those identified more than once as mATX3 interactors in the mouse libraries screenings

Prey gene symbol	Prey protein [aa]	Times isolated	Different screens	Library found	Reading frame	Interacting sequence
4930455F23Rik	[509]	14	3	embryo ; testis	1	[198-509]
Dbil5	Dbil5 [87]	12	2	testis	1 (3 Stop)	[aa1-87]
5730409G07Rik	Thg1l	10	3	embryo ; testis	1	[aa12-235]
Bcl7c	Bcl7c [217]	8	3	embryo ; testis	1/3	[aa85-217]
LOC630138	-	7	2	embryo ; testis	ND	ND
2900024C23Rik	[428]	6	2	embryo ; testis	2	[1-110]
Cul1	Cul1 [776]	3	2	embryo ; testis	1	[aa714-776]
Rpl6	Rpl6 [296]	6	2	embryo	3	[aa239-296]
2310003C23Rik	Twa1 [228]	5	1	embryo	1	[aa163-228]
Ccdc113	Ccdc113 [377]	4	1	testis	1	[aa122-345]
na-ENSMUSG00000063362	Alg11 [450]	4	2	embryo	1	[aa41-92]
na-Mm.393660	-	4	2	testis	ND	ND
Prm2	Prm2 [107]	4	2	testis	1/2 (1 Stop)	[aa1-107]
Spatc1	Spatc1 [480]	4	2	testis	2	[aa245-480]
Atp5j	Atp5j [108]	3	2	testis	1	[aa1-108]
LOC627889	[295]	3	1	embryo	3	[aa253-295]
Soat2	Soat2	3	1	testis	ND	ND
E430028B21Rik	[608]	2	1	embryo	3	[aa507-608]
Gtf2e2	Gtf2e2 [292]	2	2	embryo ; testis	1	[aa1-198]
Lrrc40	Lrrc40 [602]	2	2	testis	1	[aa562-602]
Map2k6	Map2k6	2	2	embryo	2/3 (2 Stop)	ND
Rps9	Rps9 [194]	2	2	embryo	1	[aa114-194]
Serbp1	Serbp1 [407]	2	2	embryo	3	[aa1-214]
na-Mm.393935	-	2	1	embryo	ND	ND
Tpr	Tpr [2357]	2	1	embryo	3	[aa2012-2256]
Tsga10ip	Tsga10ip [587]	2	1	testis	1	[aa327-373]
Wdr34	Wdr34	2	1	embryo	ND	ND

All preys selected for cloning are shaded; successful prey cloning is shaded in dark grey; unsuccessful prey cloning is shaded in light grey; *ND*, not determined; *Stop*, stop codon before 1st methionine; *aa*, amino acids

significant colony growth in selective plates SD-LH supplemented with 90 mM of 3-AT was observed, neither β-gal activity was detected in eventually grown colonies.

In co-transformed Y190 yeast cells, GAL4BD::mATX3 showed to specifically interact with GAL4AD::Ap3b1[aa1-138], GAL4AD::Atp5j, GAL4AD::Bcl7c, GAL4AD::Ccdc113, GAL4AD::Cul1[aa714-776], GAL4AD::Eef1b2, GAL4AD::Eif4e, GAL4AD::Etfb, GAL4AD::Gtf2e2, GAL4AD::Lrcc40, GAL4AD::mATX3, GAL4AD::Pcmt1, GAL4AD::Rpl6, GAL4AD::Rps9, GAL4AD::Spatc1, GAL4AD::Thg1l, GAL4AD::Tsga10ip, and GAL4AD::Twa1 (Figure 4.1.3). Co-transformed yeasts expressing GAL4BD::mATX3 and GAL4AD::Brf1

Table 4.1.5. Positive class 2 preys, those identified only once as mATX3 interactors in the mouse libraries screenings

Prey gene symbol	Prey protein [aa]	Library found	Reading frame	Interacting sequence
1700011H22Rik	-	testis	ND	ND
1700023E05Rik	-	testis	ND	ND
1700111A04Rik	-	testis	ND	ND
9530048O09Rik	-	embryo	ND	ND
Ap3b1	Ap3b1 [1105]	embryo	2	[aa19-138]
Brf1	Brf1 [676]	embryo	1	[aa221-350]
Ccnl2	Ccnl2 [518]	embryo	1	[aa138-196]
Ddt	Ddt [118]	embryo	2	[aa1-118]
Ebna1bp2	Ebna1bp2 [306]	embryo	2	[aa1-207]
Eef1b2	Eef1b2 [225]	embryo	3	[aa40-225]
Eif4e	Eif4e [217]	embryo	1	[aa47-217]
Entpd4	Entpd4	embryo	ND	ND
Etfb	Etfb [255]	embryo	1	[aa7-227]
Immt	Immt [757]	embryo	3	[aa548-757]
Kif2c	Kif2c [721]	testis	1	[aa645-721]
LOC329575	-	embryo	ND	ND
LOC620213	-	embryo	ND	ND
Mycbpap	Mycbpap [713]	testis	1	[aa351-554]
na-Mm.394565	-	embryo	ND	ND
na-Mm.398263	-	testis	ND	ND
Pdzd11	Pdzd11 [140]	embryo	2	[aa1-140]
Pla2g12a	Pla2g12a [153]	embryo	2 (1 Stop)	[aa1-153]
Rbbp4	Rbbp4 [425]	embryo	3	[aa399-425]
Ublcp1	Ublcp1 [318]	embryo	3 (1 Stop)	[aa1-174]
Zfp503	Zfp503 [652]	embryo	2	[aa530-652]
Ddit3	Ddit3 [168]	testis	1 (1 Stop)	[aa1-168]
Ik	Ik [557]	embryo	1	[aa272-425]
Pcmt1	Pcmt1 [227]	testis	1	[aa1-217]
Pkm2	Pkm2 [531]	testis	1 (5 aa)	[aa527-531]

All preys selected for cloning are shaded; successful prey cloning is shaded in dark grey; unsuccessful prey cloning is shaded in light grey; *ND*, not determined; *Stop*, stop codon before 1st methionine; *aa*, amino acids

grew poorly indicating toxicity (Figure 4.1.3).

These interactions were further confirmed by yeast mating assays. Y190 cells expressing GAL4BD::mATX3 were mated with Y187 yeasts expressing the hybrid prey proteins: GAL4AD::Ap3b1[aa1-138], GAL4AD::Atp5j, GAL4AD::Bcl7c, GAL4AD::Brf1, GAL4AD::Ccdc113, GAL4AD::Cul1[aa714-776], GAL4AD::Eef1b2, GAL4AD::Etfb, GAL4AD::Gtf2e2, GAL4AD::Lrcc40, GAL4AD::mATX3, GAL4AD::Pcmt1, GAL4AD::Rpl6, GAL4AD::Rps9, GAL4AD::Spatc1, GAL4AD::Thg1l, GAL4AD::Tsga10ip, and

Table 4.1.6. Positive class 3 preys identified as mATX3 interactors in the mouse libraries screenings but putative false positives.

Prey gene symbol	Prey protein	Times isolated	Different screens	Library found
Ccdc57	Ccdc57	1	1	embryo
Cfp	Cfp	1	1	embryo
Eef2	Eef2	1	1	embryo
na-ENSMUSG00000049202	-	1	1	testis
Ccnd1	Ccnd1	3	1	embryo
Ube2v2	Ube2v2	2	1	testis
Ran	Ran	1	1	embryo
Cox2	Cox2	1	1	embryo
Fhod1	Fhod1	1	1	embryo
Cugbp2	Cugbp2	13	2	embryo
Zfx	Zfx	5	3	embryo ; testis
Fyco1	Fyco1	3	2	embryo
Gpm6A	Gpm6A	3	2	testis
Col5a2	Col5a2	2	1	embryo
5730455P16Rik	-	1	1	testis
Ap3s2	Ap3s2	1	1	testis
Cmtm6	Cmtm6	1	1	testis
Dnajc5	Dnajc5	1	1	embryo
Grpel2	Grpel2	1	1	embryo
Pcmtd2	Pcmtd2	1	1	embryo
Prei3	Prei3	1	1	testis
Rhoa	Rhoa	1	1	embryo
Sbno1	Sbno1	1	1	testis
Tox	Tox	1	1	embryo
Hmgb2l1	Hmgb2l1	1	1	embryo

GAL4AD::Twa1. In addition, mating assays were performed between Y187 cells expressing the bait GAL4BD::mATX3 protein and Y190 yeasts expressing each of the above mentioned prey proteins, with the exception of GAL4AD::Ccdc113 and GAL4AD::Spatc1 (Figure 4.1.4). Furthermore, mated yeasts expressing GAL4BD::mATX3 and GAL4AD::Brf1 did not show any cellular toxicity and confirmed the protein interaction.

In total, 18 novel proteins (Table 4.1.7) were shown to interact with mATX3 in yeast co-transformation and mating assays. Among these proteins, 12 belong to class 1 and the remaining six to class 2. Additionally, bacterial GST::prey protein expressing plasmids were prepared to confirm each of these interactions by GST pull-down assay in the future (Table 4.1.3).

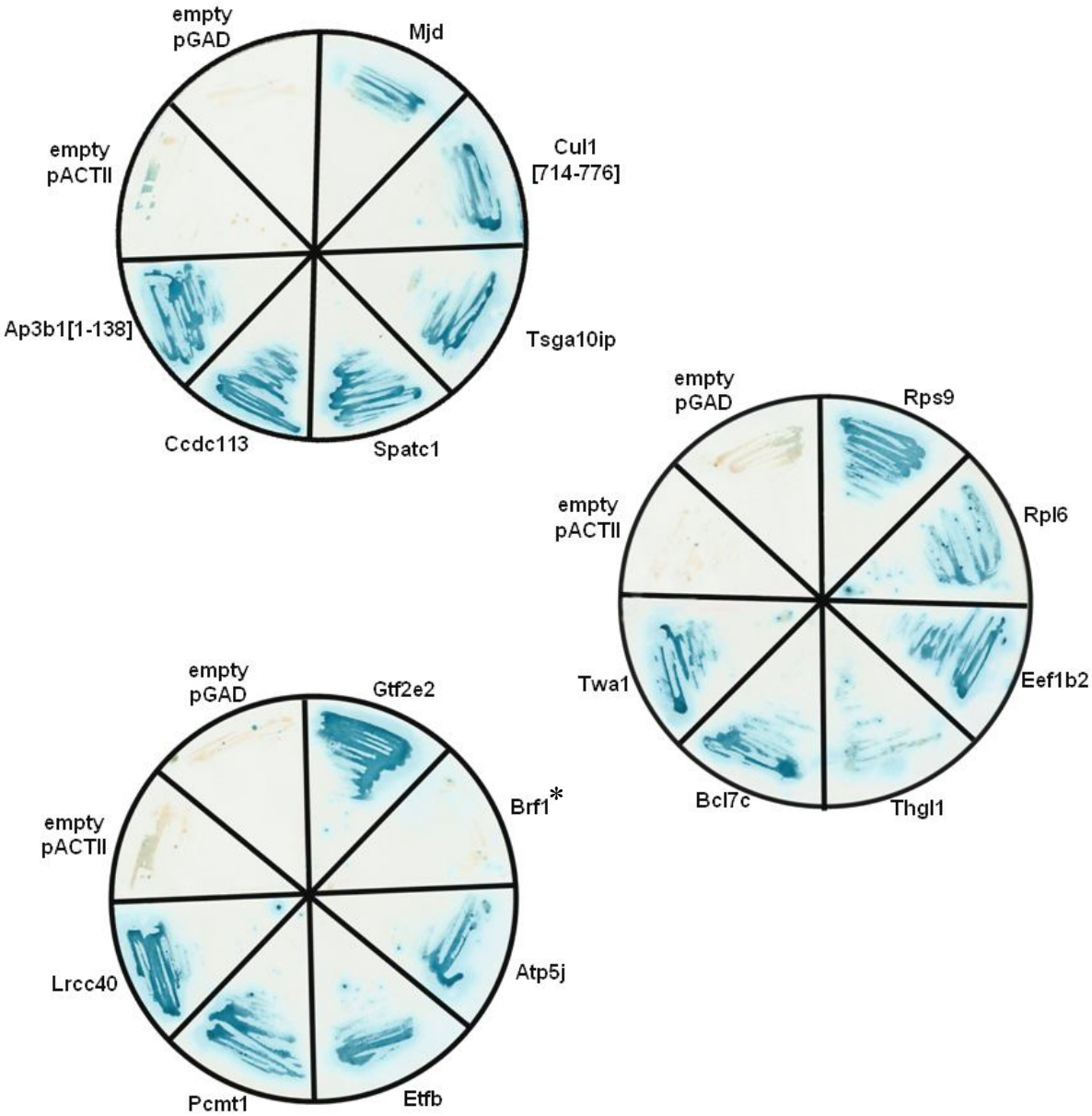

Figure 4.1.3. Several new protein interactions of mATX3 were confirmed by yeast two-hybrid co-transformation. The interaction between GAL4BD::mATX3 and each GAL4AD::prey protein is shown by the blue colony streaks of yeast cells co-transformed with both bait and prey plasmids, and plated in SD-WLH 90mM 3-AT. Blue colour is indicative of β-gal activity and therefore expression of the lacZ reporter gene. pGADBrf1 showed considerable toxicity in the yeast co-transformation assay (*). The empty GAL4AD expression vectors pGAD424 and pACTII were co-transformed with the pGBT9Mjd plasmid (expressing GAL4BD::mATX3) in Y190 cells to provide negative controls.

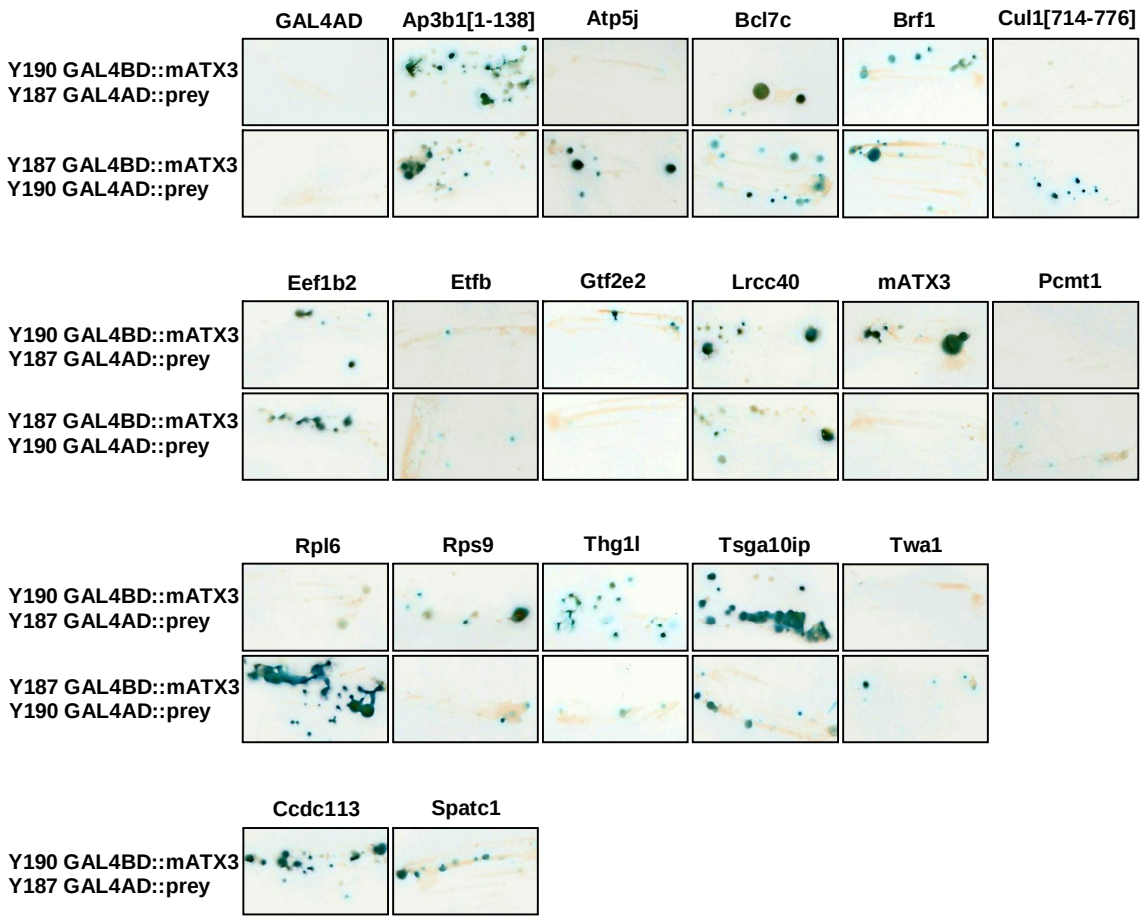

Figure 4.1.4. The new protein interactions with mATX3 were additionally confirmed by yeast two-hybrid mating assay. The interaction between GAL4BD::mATX3 and each GAL4AD::prey protein is shown by the blue colonies of diploid cells that grew in the selective medium SD-WLH 30mM 3-AT. Blue colour is indicative of β-gal activity and therefore expression of the lacZ reporter gene. The mating assays were performed in the two possible directions using pre-transformed Y190 and Y187 yeast for all the bait and prey plasmids. Streaks of mating diploids expressing the bait and GAL4AD alone were included as negative control.

The partners of mATX3: functions and molecular networks

Among the 18 mATX3 interactors confirmed by y2h assays, the function was eligible for 12, using the databases of the Ingenuity Pathways Analysis software. These new putative molecular partners of mATX3 were analysed for their subcellular localisation, type and functional involvement in cellular processes in conjunction with the previously 27 reported ATX3 interactors (Table 4.1.8). We determined the potential functional networks in which all the ATX3 interactors may be involved (Table 4.1.8). Three networks

Table 4.1.7. Description of the new protein interactors of mATX3

Protein	
Name	**Description**
Ap3b1	adaptor-related protein complex 3, beta 1 subunit
Atp5j	ATP synthase, H+ transporting, mitochondrial F0 complex, subunit F6
Bcl7c	B-cell CLL/lymphoma 7C
Brf1	BRF1 homolog, subunit of RNA polymerase III transcription initiation factor IIIB (*S. cerevisiae*)
Ccdc113	coiled-coil domain containing 113
Cul1	cullin 1
Eef1b2	eukaryotic translation elongation factor 1 beta 2
Eif4e	eukaryotic translation initiation factor 4E
Etfb	electron-transfer-flavoprotein, beta polypeptide
Gtf2e2	general transcription factor IIE, polypeptide 2, beta 34kDa
Lrrc40	leucine rich repeat containing 40
Pcmt1	protein-L-isoaspartate (D-aspartate) O-methyltransferase
Rpl6	ribosomal protein L6
Rps9	ribosomal protein S9
Spatc1	spermatogenesis and centriole associated 1
Thg1l	tRNA-histidine guanylyltransferase 1-like (S. cerevisiae)
Tsga10ip	testis specific 10 interacting protein
Twa1	two hybrid associated protein No. 1 with RanBPM

were identified concerning the following functions: (A) gene expression, protein synthesis and degradation (Figure 4.1.5); (B) cancer, protein synthesis (Figure 4.1.6); and (C) cancer and reproductive system (Figure 4.1.7).

Network (A) was the one that comprised the highest number of ATX3 interactors (21), being composed in the majority by known interactors (18). This network was composed mainly by transcription regulators. The three new interactors of this network were two transcription regulators (Brf1 and Gtf2e2), and one enzyme (Pcmt1) (Table 4.1.8). All these proteins were shown to be involved in the regulation of gene expression and protein synthesis and degradation.

Network (B) was comprised by four known and five newly found interactors. This group was mainly composed by enzymes (CHIP, Cul1, and PARK2) involved in protein quality control. The others were regulators of translation (Eef1b2 and Eif4e), and ribosomal subunits (Rpl6 and Rps9). Cul1, a member of the SCF complex, and its respective regulator NEDD8, participate in the degradation of proteins involved in cell cycle, among others. Tubulin, the component of microtubules, also makes part of this network since microtubules are crucial in cell division. Several of these novel interactors were also shown to be important in embryonic development.

Table 4.1.8. Predictive functional networks for the known and the novel ATX3 interactors. Novel interactors are shaded.

Network	Cellular Functions	ATX3 or mATX3 interactor			
		Name	**Reference**	**Subcellular localisation**	**Type**
A	Gene expression Protein synthesis and degradation	**Brf1**	this study	n, cyt	t reg
		CREBBP	Li et al. 2002	n, cyt	t reg
		Derlin-1	Wang et al. 2006	cyt, end ret	receptor
		Gtf2e2	this study	n	t reg
		HDAC3	Evert et al. 2006	n, cyt	t reg
		HDAC6	Burnett et al. 2005	n, cyt	t reg; cytosk as
		HHR23A	Wang et al. 2000	n	DNA repair reg
		HHR23B	Wang et al. 2000	n, cyt	DNA repair reg
		NCOR1	Evert et al. 2006	n, cyt	t reg
		PCAF	Li et al. 2002	n, cyt	t reg
		Pcmt1	this study	cyt	enzyme
		p300	Li et al. 2002	n	t reg
		p45	Wang et al. 2007	n, cyt, plas memb	t reg
		SELS	Wang et al. 2006	cyt, end ret	enzyme binding
		SUMO1	Shen et al 2006	n, cyt	Ub-like
		SYVN1	Wang et al. 2006	cyt, end ret	transporter
		TBP	Araujo et al. 2007	n, cyt	t reg
		UBB	Ferro et al. 2007	cyt	protein binding
		UBE4B	Matsumoto et al. 2004	n, cyt	enzyme
		VCP	Dai et al. 2000	n, cyt, end ret	chaperone
		WT1	Araujo et al. 2007	n	transcription reg
B	Protein synthesis Cancer	**CHIP**	Jana et al. 2005	cyt, end ret	E3 Ub ligase
		Cul1	this study	n, cyt	SCF component
		Eef1b2	this study	cyt	translation reg
		Eif4e	this study	n, cyt, plas memb	translation reg
		NEDD8	Ferro et al. 2007	n, cyt	Ub-like
		PARK2	Tsai et al. 2003	n, cyt, memb fract	E3 Ub ligase
		Rpl6	this study	rib	struct const
		Rps9	this study	rib	struct const
		TUBB	Zhong et al 2006	cyt	struct const

cyt, cytoplasm; *cytosk as*, cytoskeleton associated; *end ret*, endoplasmic reticulum; *memb fract*, membrane fraction; *n*, nucleus; *plas memb*, plasma membrane; *reg*, regulator; *rib*, ribosome; *struct const*, structural constituent; *t reg*, transcription regulator; *Ub*, ubiquitin.

The functional network (C) was constituted by 8 (four new and four known) ATX3 interactors. This was a heterogeneous network defined by proteins from different functional families: vesicle transporter (Ap3b1), transcription regulator (FOXO4), one ion channel (ACCN2), a protein associated to the cytoskeleton (PLIC-1), and speriolin (Spatc1)

Table 4.1.8. (continued)

Network	Top Functions	ATX3 or mATX3 interactor			
		Name	**Reference**	**Subcellular localisation**	**Type**
C	**Cancer** **Reproductive system**	**ACCN2**	Shen et al. 2006	plas memb	ion channel
		Ap3b1	this study	cyt, memb fract	transporter; cytosk as
		ARHGDIA	Shen et al. 2006	cyt	GTPase activator
		Atp5j	this study	mit	ATPase
		Etfb	this study	mit	transporter
		FOXO4	Araujo et al. 2007	n, cyt	t reg
		PLIC-1	Heir et al. 2006	n, cyt	cytosk as
		Spatc1	this study	cyt	Cdc20 binding

cyt, cytoplasm; *cytosk as*, cytoskeleton associated; *memb fract*, membrane fraction; *mit*, mitochondria; *n*, nucleus; *plas memb*, plasma membrane; *t reg*, transcription regulator; Ub, ubiquitin.

that co-localises with Cdc20 and is involved in spermatogenesis (Table 4.1.8). The novel mitochondrial interactors (Atp5j and Etfb) were also included in this network since both cell cycle and spermatogenesis processes require a high quantity of energy produced by mitochondria. ARHGDIA is a GTPase activator that may be important in the regulation of microtubule dynamics, crucial for cell movement. Proteins implicated in microtubule dynamics, protein synthesis, and vesicle transport were also shown to be very important in the cell cycle process.

ATX3 seem to interact with different types of proteins, that are expressed in different cell compartments, and playing different functions in specific cellular pathways.

4.1.5. DISCUSSION

Presently, the y2h technique is an important and largely applied tool in protein-protein interaction studies, and its data may be complemented and confirmed by other methodologies: GST pull-down, co-immunoprecipitation and co-localisation of the endogenous proteins.

In fact, the y2h system in conjunction with other technologies for the detection of protein-protein interactions,, and in addition to the complete genome sequencing of several organisms, allowed the high throughput determination of all protein-protein interactions specific for an organism in a certain physiological condition, the interactome. Several interactomes are already known specifically for *S. cerevisiae* (Uetz et al. 2000; Ito et al. 2001), *H. pylori* (Rain et al. 2001), *C. elegans* (Walhout et al. 2000; Li et al. 2004),

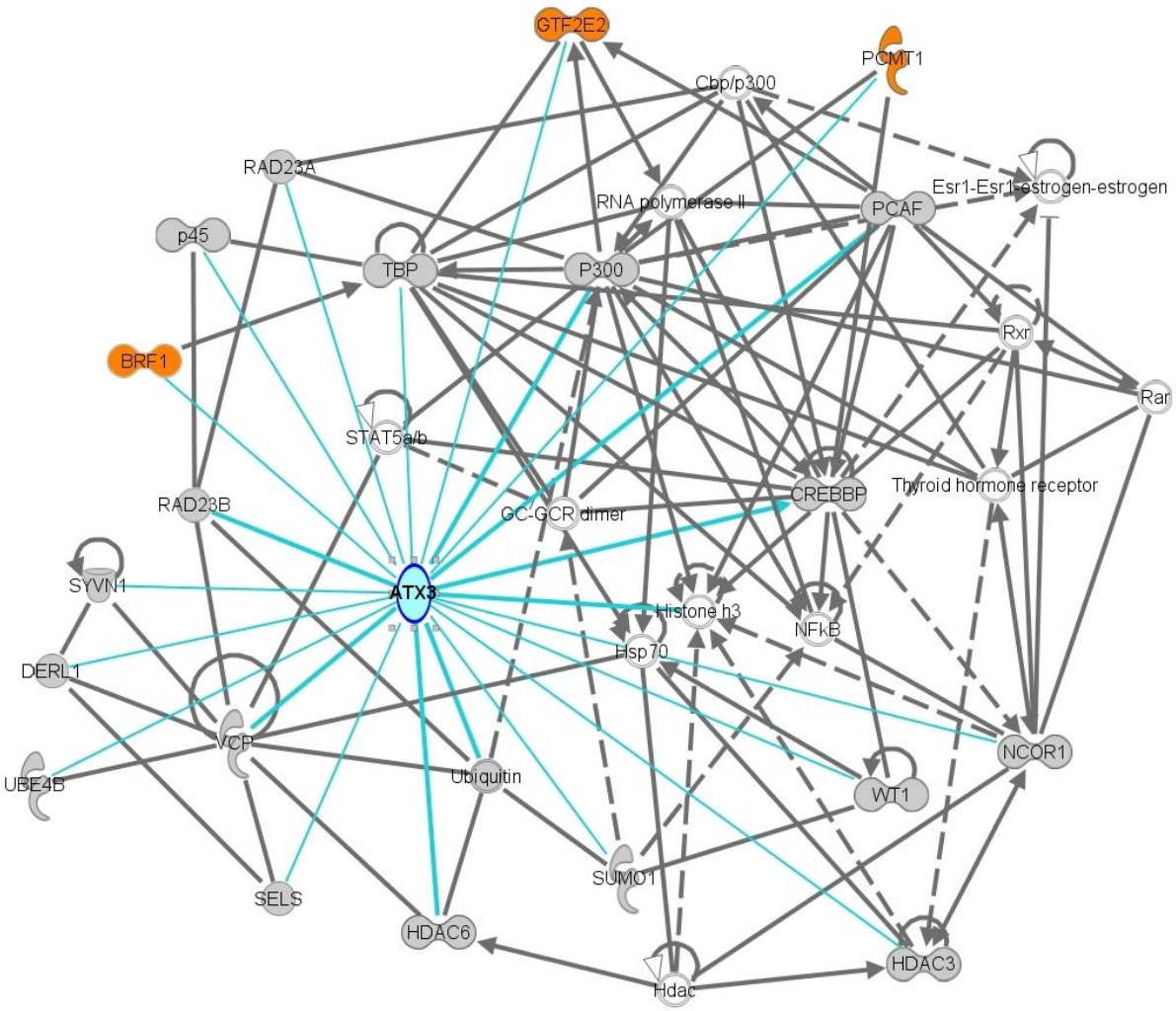

Figure 4.1.5. Scheme of a predicted functional network (A) including some of the ATX3 interactors. The biological mechanisms involved in this network of interacting proteins are (1) gene expression and (2) protein synthesis and degradation. The known ATX3 interactors are highlighted in grey, and the new mATX3 interactors are shaded in orange. ATX3 is delimited by a dark blue line and ATX3 interactions are represented as light blue lines. Connecting lines represent binding between two proteins, full-line arrows indicate direct interactions and "action on" the pointed protein, and dashed arrows represent indirect interactions. For full-name of the previously known interactors and newly identified interactors see Tables 1.2. (Chapter 1) and 4.1.7, respectively. *RAD23A*, HHR23A; *RAD23B*, HHR23B. Network analysis was performed using the Ingenuity Pathways Analysis Inc. 5.0 software.

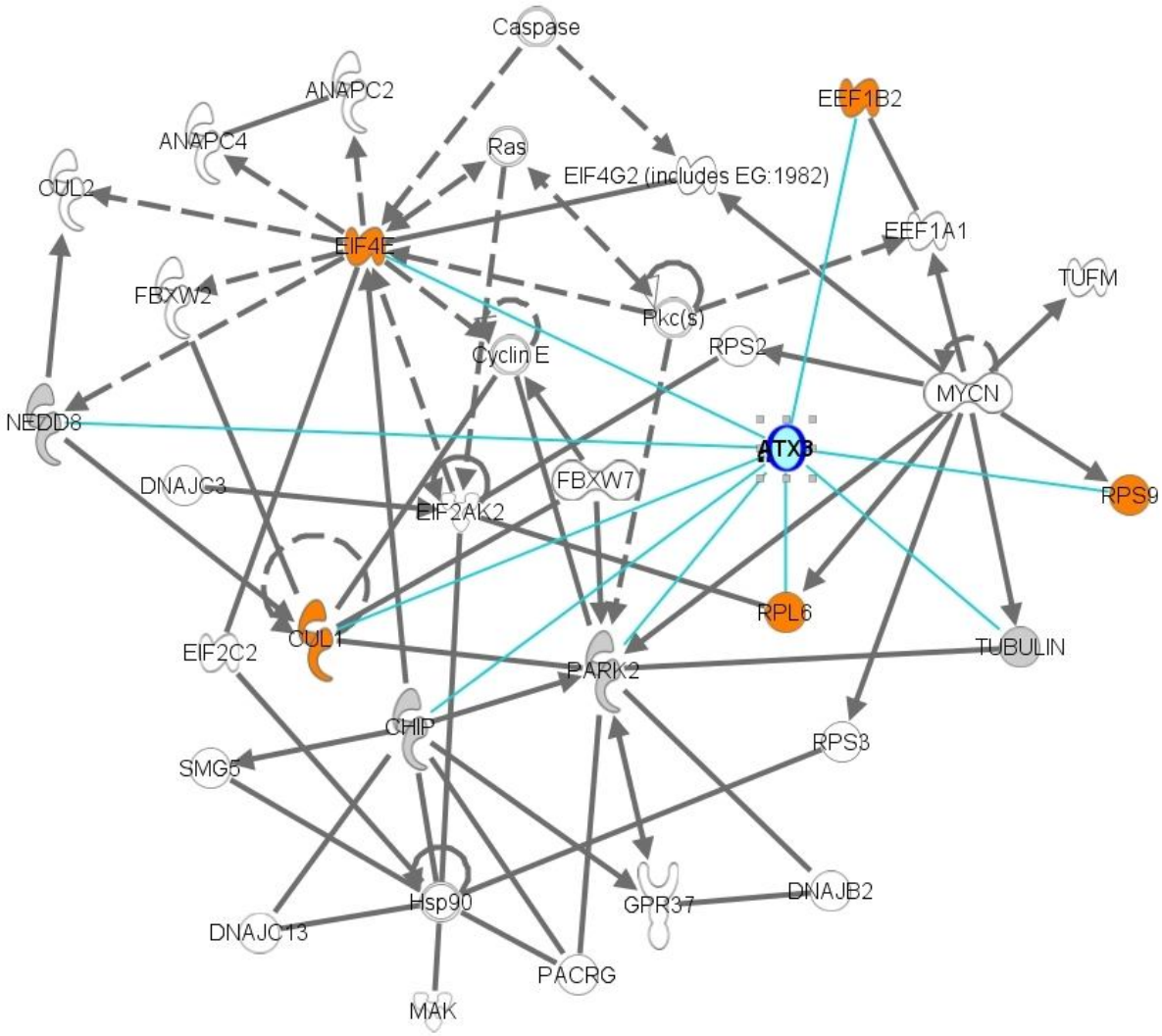

Figure 4.1.6. Scheme of a predicted functional network (B) including some of the ATX3 interactors. The biological mechanisms involved in this network of interacting proteins are (1) cancer and (2) protein synthesis. The known ATX3 interactors are highlighted in grey, and the new mATX3 interactors are delimited by an orange line. ATX3 is delimited by a dark blue line and ATX3 interactions are represented as light blue lines. Connecting lines represent binding between two proteins, full-line arrows indicate direct interactions and "action on" the pointed protein, and dashed arrows represent indirect interactions. For full-name of the previously known interactors and newly identified interactors see Tables 1.2. (Chapter 1) and 4.1.7, respectively. Network analysis was performed using the Ingenuity Pathways Analysis Inc. 5.0 software.

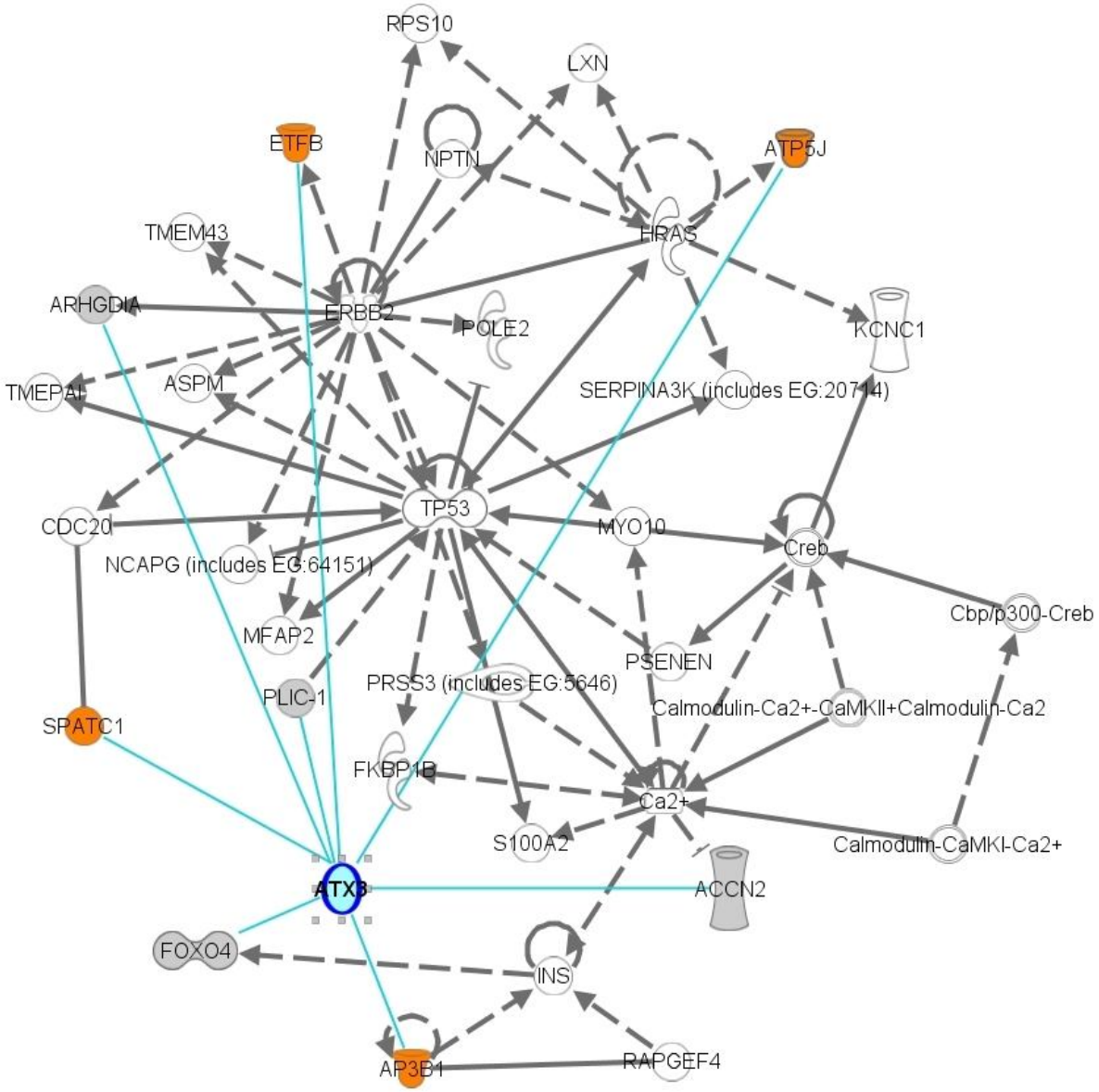

Figure 4.1.7. Scheme of a predicted functional network (C) including some of the ATX3 interactors. The biological mechanisms involved in this network of interacting proteins are (1) cancer and (2) reproductive system. The known ATX3 interactors are highlighted in grey, and the new mATX3 interactors are delimited by an orange line. ATX3 is delimited by a dark blue line and ATX3 interactions are represented as light blue lines. Connecting lines represent binding between two proteins, full-line arrows indicate direct interactions and "action on" the pointed protein, and dashed arrows represent indirect interactions. For full-name of the previously known interactors and newly identified interactors see Tables 1.2. (Chapter 1) and 4.1.7, respectively. Network analysis was performed using the Ingenuity Pathways Analysis Inc. 5.0 software.

D. melanogaster (Giot et al. 2003), and *H.sapiens* (Colland et al. 2004; Rual et al. 2005). Furthermore, interactomes have been recently defined for some polyQ containing proteins, namely huntingtin (Goehler et al. 2004; Kaltenbach et al. 2007) and ataxin-1 (Lam et al. 2006), using the y2h system.

In this study, we identified new protein partners of mATX3 using the y2h system to screen two mouse cDNA expression libraries (11-day embryo and testis) with a bait plasmid encoding mATX3. Yeast growth conditions were optimized for the use of the bait GAL4BD::mATX3 hybrid in either the libraries screenings, or in co-transformation and mating assays. Y190 yeast cells expressing the GAL4BD fusion with the full length mATX3 showed a normal growth, which means that this bait is not toxic. However, these yeasts exhibited some autonomous transactivation of the reporter genes *HIS3* and *lacZ*. This auto-activation was abolished by the addition of 3-AT to the selective medium, turning this bait suitable to be used in the y2h assays.

The four y2h screenings performed, two for each mouse cDNA library, resulted in the identification of 81 mATX3 potential interactors. Of these, we were able to clone and confirm the interaction of 18 new proteins with mATX3 using y2h co-transformation and mating assays: Ap3b1, Atp5j, Bcl7c, Brf1, Ccdc113, Cul1, Eef1b2, Eif4e, Etfb, Gtf2e2, Lrcc40, Pcmt1, Rpl6, Rps9, Spatc1, Thg1l, Tsga10ip, and Twa1. Although one of the selection criteria was the number of times the prey proteins were identified, and thus the majority of these (12) y2h confirmed prey interactors belonging to the class of proteins identified more than once, the six remaining preys were also confirmed. This suggests that preys that are identified only once may be true interactors. In the selected group we also have chosen preferably preys that were found to be in the correct open reading frame (frame 1) in relation to the GAL4AD domain. However, from the 18 confirmed proteins, four of the corresponding cDNA fragments were apparently inserted into the prey plasmids in other frames (frames 2 or 3), which confirms that the reading frame was not a good criterion to evaluate preys, since in rare cases translation frame-shifting can compensate for shifted frames, and, particularly in this case, some sequencing errors may also have occurred since the prey inserts were only sequenced once. In order to confirm these interactions by another methodology, we have prepared GST::prey expressing plasmids to be used in GST pull-down assays, which are currently being performed.

Surprisingly, none of the previously 27 known ATX3 interactors appeared in our library screenings for mATX3. Nevertheless, several of the new interactors were functionally related with known ATX3 interactors. In order to have an integrative view of the functional pathways that ATX3 is involved, we performed a bioinformatic analysis of all the ATX3 interactors, the known (27) and the here newly described for mATX3, for which we have

confirmed the interaction by y2h assays (18). Among the total of 45 ATX3 protein interactors, 43 of the genes were “mapped” in the used database, and the establishment of functional networks was possible only for 39.

Along with the interactors for which the genes were unmapped we were able to identify two of them by protein alignments, and confirmed their interaction with mATX3 by y2h. One of them was the Thg1l, also known as the interphase cytoplasmic foci protein 45, which is involved in tRNA modification and processing, and implicated in cell cycle regulation as the interference of human THG1L mRNA by siRNA induces cell proliferation and increases the number of polycentrosomal and multinucleated cells (Guo et al. 2004). The other interactor was Twa1 that shares a homologous domain with Muskelin (Adams et al. 1998) and RanBPM, which is called the LisH-CTLH domain and is detected in proteins involved in microtubule dynamics, cell migration, nucleokinesis and chromosome segregation (Emes and Ponting 2001).

The four proteins for which the genes were known but that the analysis program was not able to insert into a functional network, were: Bcl7c, Ccdc113, Lrrc40, and Tsga10ip. In this study we were able to confirm the interaction of mATX3 with Bcl7c, Ccdc113, Lrrc40 and Tsga10ip. Although the function of Bcl7c is unidentified, it is known that is involved in cell apoptosis (Cregan et al. 2004). Ccdc113 is a protein with a coiled-coil domain of unknown function. Lrrc40 is a leucine rich repeat (LRR) containing protein with no attributed function. However, LRR as well as WD-40 repeats are common structures in the protein-protein substrate interacting domains of F-box proteins (Bai et al. 1996), which are components of the SCF and SCF-like E3 ubiquitin ligases responsible for the recruitment of the substrates for ubiquitination. Tsga10ip is a testis-specific protein of unknown function.

The remaining 39 ATX3 protein partners showed to be part of three different functional networks.

The first network (A) comprised the highest number of ATX3 interactors, the majority being known interactors, and was functionally related to gene expression, and protein synthesis and degradation. This system includes some of the interacting proteins that pointed to a function of ATX3 in **transcription regulation**.

ATX3 may act as a transcriptional repressor inhibiting the CREB-dependent transcription pathway by its binding to CREBBP, p300, and PCAF (Li et al. 2002); or promoting the deacetylation of histones either by its binding to the acetylation site of histones (Li et al. 2002), or recruiting HDAC3 and NCOR1 to specific promoter regions (Evert et al. 2006). Interestingly, Pcmt1, a newly found mATX3 interactor in this study, is a RNA-binding protein with a methyltransferase activity and was shown to interact with CREBBP and p300, bridging the CBP/p300-anchored coactivator complex with the peroxisome proliferator-activated receptor (PPAR)–binding protein (PBP)-anchored coactivator complex, but

differentially modulating their coactivator functions, by repressing the CREBBP/p300 effect to enhance the activity of PBP and PRIP (peroxisome proliferator-activated receptor (PPAR)–interacting protein (Misra et al. 2002) (Figure 4.1.8). CREBBP/p300 and PBP/PRIP are coactivator complexes of many transcription factors, but also of nuclear receptors (ligand-regulated transcription factors) for steroid and thyroid hormones, PPARs, vitamin D3, and retinoic acid among others (Vo and Goodman 2001; Crawford et al. 2002). Some evidences respecting these ATX3 interactions, may lead us to suggest that ATX3 may be for example repressing the estrogen receptor signaling pathway either by repressing CREBBP-mediated transcription, which in turn is known to activate the estrogen receptor signaling (Vadlamudi et al. 2001), or by its interaction with NCOR1 that was shown to inhibit this pathway (Huang et al. 2002).

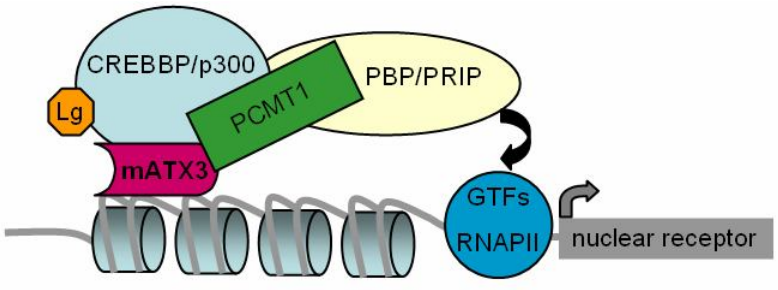

Figure 4.1.8. Scheme for the possible functional relevance of the mATX3/ Pcmt1 interaction. *Lg*, ligand; *GTFs*, general transcription factors; *RNAPII*, RNA polymerase II.

ATX3 may also be interfering with the activity of some transcription factors by its direct binding. Three interactions between ATX3 and transcription factors (FOXO4, WT1, and TBP) were previously reported (Araujo et al. 2007). The WT1 transcription factor, a recently found ATX3 interactor (Araujo et al. 2007), is involved in the G1 phase arrest and consequently in cell growth, proliferation, differentiation and development events. Here, we also report two novel interactions of ATX3 with transcriptional factors, Brf1 and Gtf2e2. Brf1 is one of the three subunits of the TFIIIB complex (Colbert and Hahn 1992), TBP and Bdp1 being the others. Brf1 was shown to interact with TBP (Wang and Roeder 1995). TFIIIB makes part of the RNA polymerase III transcription factor complex that manufactures transfer RNAs (tRNAs), 5S ribosomal RNA (rRNA), and other small structural RNAs essential for the biosynthetic process. Transcription by RNA polymerase III is closely coupled with the cell growth rate, and consequently with proliferation, differentiation, and development processes. Upon a proliferation stimulus, the mitogen-activated extracellular signal-regulated kinase (ERK) phosphorylates Brf1, which in turn enhances the promoter recruitment of TFIIIB and RNA polymerase III augmenting the production of biosynthetic RNAs (Felton-Edkins et al. 2003). Conversely, the retinoblastoma (Rb) protein inhibits the RNA polymerase III- directed

transcription by binding to TFIIIB (Larminie et al. 1997; Hirsch et al. 2004). Of great interest is the fact described here that mATX3 may also interact with Rbbp4, a Rb-binding protein (Nicolas et al. 2000) (Figure 4.1.9). This protein also interacts with HDAC3 and represses transcription by increasing the methylation of histone H3 (Kuzmichev et al. 2002). These evidences may suggest that ATX3 could make a structural bridge between the TFIIIB complex (interacting with TBP and Brf1) and the repressing complex containing its interactors Rbbp4 and HDAC3, the Rb protein, between others (Nicolas et al. 2001). Alternatively, these proteins might also be targets of the enzymatic activity of ATX3, acting as a DUB in order to regulate their levels, or acting as a deneddylase namely of Rbbp4 that was recently found to be neddylated by NEDD8 (Jones et al. 2008) in order to interfere with its stability. These evidences may imply that ATX3 is inhibiting cell growth by repressing the RNA polymerase III-mediated transcription (Figure 4.1.9). The involvement of ATX3 in this process may be achieved by the analysis of the RNA polymerase III transcription in cells (proliferating or fully differentiated) overexpressing ATX3 or lacking this protein.

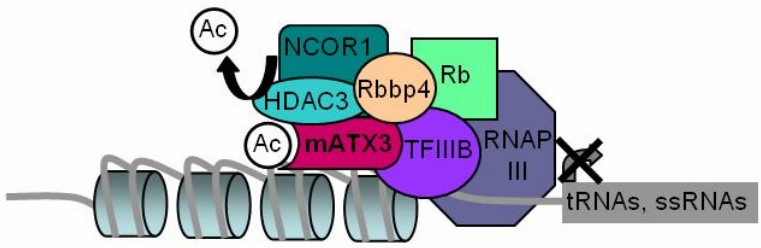

Figure 4.1.9. Scheme for the possible functional relevance of the mATX3/Brf1 and mATX3/Rbbp4 interaction. *Ac*, acetyl group; *RNAPIII*, RNA polymerase III.

Gtf2e2, also known as TFIIE-B, is a general RNA polymerase II transcription factor that also binds to TBP (Watanabe et al. 2003), and is activated through acetylation by p300 and PCAF (Struhl 1998; McKenna and O'Malley 2000). It would be interesting to perform functional studies to evaluate the effect of the interaction between mATX3 and Gtf2e2 in its cellular role.

The ATX3 interactors that suggest its role in **protein synthesis and degradation** also belong to network (A). All of these interactors were already known. They were particularly involved in the retro-translocation of polyubiquitinated substrates from the endoplasmic reticulum to the 26S proteasome (VCP, HHR23A, HHR23B, derlin-1, synoviolin and selenoprotein S) (Hirabayashi et al. 2001; Kobayashi et al. 2002; Doss-Pepe et al. 2003; Boeddrich et al. 2006; Zhong and Pittman 2006). The two remaining ATX3 interactors were UBE4B, an E3 ligase that also binds to VCP (Kaneko et al. 2003), and p45, a proteasome subunit that binds to HHR23B (Hiyama et al. 1999).

ATX3 showed to be involved in a second network, related also to protein synthesis and to cancer, potentially in **cell cycle regulation** (network B). This network is also linked with the possible role of ATX3 in the protein surveillance machinery, either by its DUB (Burnett et al. 2003) or its deneddylase activities (Ferro et al. 2007). In addition, two E3 ubiquitin ligases, previously shown to interact with ATX3, make part of this network, CHIP (a co-chaperone) (Jana et al. 2005) and parkin (the most commonly mutated protein in familial Parkinson's disease) (Tsai et al. 2003). Cullin 1 (Cul1) was one of the novel interactors found here, which makes part of the Skp1-Cullin-F-box (SCF) complex – an E3 ubiquitin ligase. SCF complex promotes specific protein ubiquitination and degradation that are important for cell cycle progression, cell differentiation, DNA repair and signal transduction. Interestingly, Cullin 1 is activated by conjugation with NEDD8, the recently found ATX3 interactor (Ferro et al. 2007). Additionally, the deneddylase activity of mATX3 (Chapter 4.2) may suggest a direct regulation of the SCF complex activity. The ribosomal subunits Rpl6 and Rps9, also make part of this network, and interestingly it was recently found that ribosomal proteins are potential targets of neddylation in order to regulate their stability (Xirodimas et al. 2008), Rpl6 being one of these. These evidences point for a potential regulation of the stability of these ribosomal proteins by ATX3 acting as a deneddylase.

As part of this network, the translation initiation factor Eif4e, a new partner of mATX3, also plays important roles in cell growth, proliferation, differentiation, G1/S phase transition, apoptosis and development. Interestingly, Eif4e is degraded by the UPS via the E3 ubiquitin ligase CHIP that increases its ubiquitination (Murata and Shimotohno 2006). The fact that ATX3 interacts with both CHIP and Eif4e suggests that ATX3 may be regulating the degradation of Eif4e though the UPS exerting its DUB function.

Tubulin was also found to interact with ATX3 (Zhong and Pittman 2006) and makes part of this network most probably because microtubules and the cytoskeleton in general are very important structures in cell cycle. Parkin strongly binds both α and β tubulins in order to stabilise microtubules (Yang et al. 2005). Furthermore, Eef1b2, found here to be a mATX3 interactor, promotes the GDP exchange reaction to the translation elongation factor Eef1a, essential in the elongation step in protein synthesis, in particular in cell cycle (Le Sourd et al. 2006).

The here found cellular network (C), in which ATX3 is involved, concerns cancer and reproductive system. In fact, observing the respective scheme (Figure 4.1.6) it is easy to identify a central protein that play important roles in cell cycle and cell death, the tumor protein p53 (TP53). The TP53, through mediates the p53-dependent cell cycle G1 phase arrest in response to a variety of stress stimuli. CDKN1A is a potent cyclin-dependent kinase inhibitor that binds to and inhibits the activity of cyclin-CDK2 or -CDK4 complexes, and thus functions as a regulator of cell cycle progression at G1. The expression of this gene is tightly

controlled by the TP53, through which this protein mediates the p53-dependent cell cycle G1 phase arrest in response to a variety of stress stimuli.

Of great interest, is the fact several newly and also a few known ATX3 interactors are directly or indirectly related to several molecular factors that in general are associated to an inhibition of cell division, either in the context of differentiation or as a cell response to a specific stimulus. FOXO4, a recently identified ATX3 interactor, is a stress response transcription factor (see Chapter 3) that interestingly, and in conjunction with the other FOXO proteins (FOXO1 and FOXO3) is necessary to activate the transcription of the cyclin-dependent kinase inhibitor 1A (*CDKN1A*) gene (Gomis et al. 2006). PLIC-1, a cytoskeleton associated protein was recently shown to bind ATX3, mediating its shuttling to aggresomes in special of the expanded ATX3 (Heir et al. 2006). However, it was also demonstrated that PLIC-1 is involved in the decrease of the degradation of TP53 (Kleijnen et al. 2000). Since ATX3 is potentially involved in the UPS, it is possible that it could mediate the degradation process of TP53 in conjunction with PLIC-1.

Apparently, from the analysis of the scheme of network (B), we may propose that ATX3 is involved in cell cycle control, most probably in cell division inhibition, or regulating important molecules for this process. The newly identified interactors of mATX3 that may be implicated in this cellular event could be either substrates of the ATX3 DUB or deneddylase activity or simply its molecular partners in a specific pathway. These were the ribosomal proteins Rpl6 and Rps9, the adaptor protein Ap3b1 involved in intracellular molecular transport and in the protein targeting to lysosome, the nuclear transporter Tpr, the enzyme Ddt, and the cytokine IK.

Proteins of this network are also implicated in cellular movement and in the reproductive system development and function. Two interlinked molecular factors play central roles in this network, ERBB2 and HRAS, both involved in cell cycle progression, cell proliferation, growth, migration and apoptosis. ARHGDIA was described as an ATX3 interactor in 2006, but no further studies were performed (Shen et al. 2006). This protein has Rho GDP-dissociation inhibitor activity and is implicated in cell morphology, movement (Bruneel et al. 2005), adhesion (Leffers et al. 1993), motility (Kaibuchi et al. 1999), exocytosis and apoptosis. Furthermore, ARHGDIA is directly linked with the actin cytoskeleton regulation by decreasing actin polymerisation (Leffers et al. 1993) and is regulated by phosphorylation by ERBB2 (Bose et al. 2006).

The new mATX3 interactors making part of network (D) were Atp5j, Etfb, and Spatc1. Atp5j is the subunit F6 of the mitochondrial ATP synthase required for the interaction of the multi-subunit complexes F1 and F0. Interestingly, the mRNA levels of Atp5j were shown to be positively regulated by HRAS (Yoon et al. 2002). Etfb is a mitochondrial electron-transfer-flavoprotein that is also regulated by ERBB2 (Landis et al. 2005). These interactions may

suggest a common involvement of these proteins, and ATX3, with ERBB2. The spermatogenesis and centriole-associated 1 (Spatc1), also known as speriolin, binds to γ-tubulin, and to the spindle checkpoint protein Cdc20, potentially regulating or stabilising it during meiosis (Goto and Eddy 2004). In fact, Cdc20 mRNA levels are also regulated by ERBB2 (Wilson et al. 2005). The interaction of mATX3 with Spatc1 suggests that mATX3 may play a role in spermatogenesis which can explain the high expression of mATX3 in mouse testis previously found by us (Costa et al. 2004). In general, we may propose that ATX3 is involved in the response of the ERBB2, HRAS and TP53, specifically related to cellular movement, growth and proliferation, and to spermatogenesis.

In conclusion, through the screening of two mouse cDNA library using the y2h system and mATX3 as bait, we have identified 81 putative mATX3 interactors. Among these, 56 were found to be the most probable mATX3 interactors, and we were able to identify for 35 the reading frame and the interacting region with mATX3. Direct interaction of mATX3 with 18 protein partners was confirmed by y2h co-transformation and mating assays. Overall, the main functional pathways that ATX3 seems to be involved in transcription regulation (acting either as a transcription repressor, or interacting with transcription factors), protein degradation, protein synthesis, cell cycle, cellular proliferation and differentiation, cellular movement and spermatogenesis. These preliminary results open completely new avenues of research in the search for the physiological role of ataxin-3.

Chapter 4.2

Ataxin-3 and the SCF complex

4.2.1. SUMMARY

A few years ago, it was shown that ATX3 is a deubiquitinating enzyme (DUB), and recently our group showed that human ATX3 interacts with the ubiquitin-like protein NEDD8, and also presents deneddylase activity. NEDD8 is essential for the activation of SCF-like E3 ubiquitin ligase complexes, which in turn mediate the degradation of several proteins by the ubiquitin proteasome system (UPS).

In this study we have expressed the recombinant mouse ATX3 (mATX3) protein and purified it into the monomeric state. We have verified that mATX3 interacts with mouse Nedd8 using yeast two hybrid (y2h) assays, and that it also presents deneddylase activity *in vitro,* using a fluorogenic NEDD8 substrate. As in the human, mATX3 deneddylase activity were found to be undertaken by its josephin domain, in which cysteine 14 showed to be fundamental for this activity.

Interestingly, in an y2h screening for mATX3 interactors, we found that cullin1 (Cul1), a member of the SCF complex, was also a molecular partner of mATX3. Cul1 is activated by neddylation of the Lys 720 residue. The interaction region of Cul1 with mATX3 corresponded to the last 62 C-terminal residues (714-776). Since this Cul1 region comprised the neddylation residue Lys 720, we have mutated this residue for an arginine and verified that mATX3 also interacts with this mutated protein in y2h assays. Thus, the interaction of mATX3 with Cul1 seems to be independent of its neddylation state. Nevertheless, ATX3 may also compete with NEDD8 for the binding site in Cul1.

These results suggest that ATX3 may be potentially regulating the SCF complex by interacting with Cul1 and Nedd8. Further work is necessary to verify this hypothesis.

4.2.2. INTRODUCTION

The ubiquitin (Ub)-dependent degradation of regulatory proteins plays important roles in the control of several physiological processes (see Chapter 1). This process begins with the attachment of a multisubunit chain to a target protein, which involves the activities of Ub-activating (E1), Ub-conjugating (E2), and Ub-protein ligases (E3) enzymes. The specificity of ubiquitin-dependent proteolysis derives from hundreds of E3 ubiquitin ligases that recognise specific substrates through particular interaction domains. There are two main classes of E3 enzymes that differ basically on the composition by one of the two characteristic protein motifs: the HECT domain or the RING domain (Pickart 2001). More recently, a third class was proposed: the U-box domain (Hatakeyama and Nakayama 2003). The HECT domain E3 enzymes function themselves as ubiquitin carriers, which mean that the HECT catalytic

domain forms a thioester intermediate with ubiquitin before its transfer for the bound substrate (Scheffner et al. 1993). Conversely, the RING domain class E3 does not have catalytic activity by itself, but uses the Zn-binding RING structural motif to recruit and direct an E2 enzyme towards specific substrates, which are mostly recognised by associated substrate recruitment subunits (Jackson et al. 2000). The prototype of a U-box protein is the yeast Ufd2, that was first identified as a Ub-chain assembly factor (E4). The U-box domain protein in conjunction with an E1 and an E2, mediate polyubiquitination in the absence of a HECT or a RING-type E3 (Hatakeyama and Nakayama 2003).

Cullins function as central proteins in the organisation of a large family of multisubunit RING domain E3 ubiquitin ligases, named cullin-RING ligases (CRLs) (Willems et al. 2004; Petroski and Deshaies 2005). Cullins interact with the RING finger protein Rbx1 (also known by ROC1 and Hrt1) to form the integral core of the E3 Ub-ligase complex (Ohta et al. 1999). The cullin1 (Cul1)- containing SCF (Skp1-Cul1/Cdc53-F-box protein) complexes are the best characterised of the cullin-containing E3 ligases, and their promotion of specific protein ubiquitination and degradation by the UPS is fundamental for cell-cycle regulation, cell differentiation, DNA repair, and signal transduction (Willems et al. 2004).

In the SCF complex, Rbx1 interacts with the C-terminal of Cul1 recruiting the E2 ligase, while Skp1 function as an adaptor between an F-box protein and the N-terminal of Cul1 (Skowyra et al. 1997). F-box proteins, in turn, recruit substrates for ubiquitination through their specific protein-protein interaction domains, such as the WD-40 repeats or leucine-rich repeats (LRR) (Bai et al. 1996; Skowyra et al. 1997) (Figure 4.2.1).

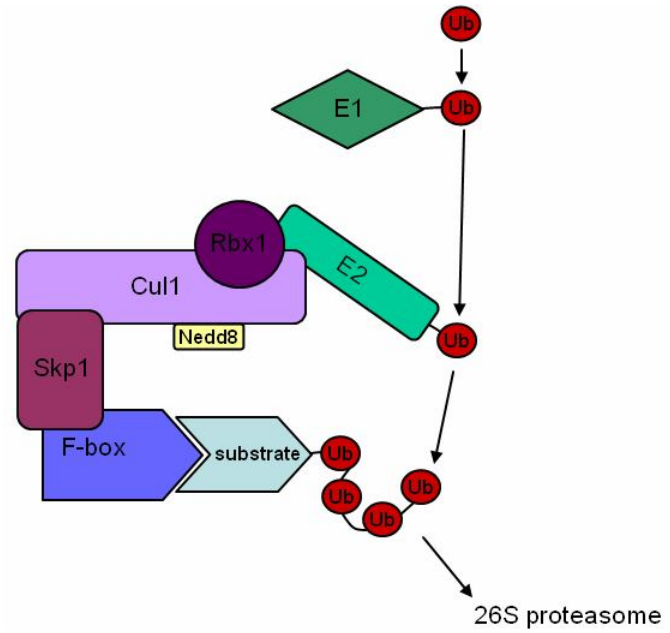

Figure 4.2.1. Mechanism of action of the SCF complex, an E3 ubiquitin ligase, in the UPS.

The ubiquitin ligase activity of CRLs is regulated by the Ub-like protein NEDD8 that covalently binds to a lysine residue in cullins (Hori et al. 1999; Kamura et al. 1999). Neddylation, the process of NEDD8 conjugation, increases the cullin-organised E3 ligase activity, in part by increasing their affinity for E2 ligases (Wu et al. 2000; Kawakami et al. 2001; Pan et al. 2004). However, this cullin-NEDD8 binding is reversible, through the process of deneddylation that consist in the removing of NEDD8 from cullins. Neddylation was found to be important, not only for the activity of cullin-containing complexes, but also for modulating the stability of cullin proteins, in the way that neddylation confers instability to activated cullins, whereas deneddylation protects them from degradation, thus maintaining the adequate cellular cullin levels for CRL activities in vivo (Wu et al. 2005). In this context, it was shown that the TBP-interacting protein 120/cullin-associated and neddylation-dissociated (CAND) A (TIP120A) regulates Cul1 neddylation by its binding to Cul1 inhibiting its neddylation (Hwang et al. 2003).

Deneddylation is undertaken by several deubiquitinating enzymes (DUBs) namely USP21, CNS/COP9 signalosome, and NEDP1/SENP8/DEN1 (Parry and Estelle 2004). Recently, our research unit found that the human DUB ATX3 interacts with NEDD8 and also presents deneddylase activity (Ferro et al. 2007). Interestingly, NEDD8 was also found to be part of Ub-containing intranuclear inclusions present in patients with several neurodegenerative disorders, namely MJD (Mori et al. 2005).

In this study we aimed to: (1) validate the conservation of the ATX3/ NEDD8 interaction in the mouse; (2) determine the conservation of mATX3 deneddylase activity; (3) verify the effect of Cul1 neddylation in the Cul1/ mATX3 interaction.

4.2.3. MATERIALS AND METHODS

Yeast strain and culture medium

The *Saccharomyces cerevisiae* strain used in the yeast two-hybrid system assays (GAL4 2H-2) was the Y190 (Harper et al. 1993). The genotype of this strain is *MATa*, *ura3-52*, *his3-200*, *ade2-101*, *lys2-801*, *trp1-901*, *leu2-3*, *112*, *gal4Δ*, *gal80Δ*, *cyh^{r}2*, *MEL1*, *LYS2::GAL1$_{UAS}$-HIS3$_{TATA}$-HIS3*, *URA3::GAL1$_{UAS}$- GAL1$_{TATA}$-lacZ*. This strain contains two reporter genes (*HIS3* and *lacZ*), each regulated by a different GAL4-dependent promoter to reduce the incidence of background. The *HIS3* reporter is under the control of the *GAL1$_{UAS}$*, and a minimal promoter containing both *HIS3* TATA boxes, TR (regulated) and TC

(constitutive). The *lacZ* reporter is regulated by the intact *GAL1* promoter, including the $GAL1_{UAS}$ and the *GAL1* minimal promoter.

Complete medium (YPAD) and selection medium (SD) used for yeast growth and manipulation were prepared as described in the Yeast Protocols Handbook (Clontech). The base of SD (SD-WLH) was prepared with all amino acids except tryptophan (W), leucine (L) and histidine (H). These nutrients were added separately depending on the necessary selection medium. The background expression of IGP dehydratase (*HIS3* product), in the Y190 yeast strain, was controlled by including 90 mM of 3-AT (Sigma) in the medium.

Yeast two-hybrid constructs

The bait plasmid used in the co-transformation assays was pGBT9Mjd. This construct, expressing the GAL4BD::mATX3 fusion protein (GAL4BD N-terminal to the full-length of mATX3) (Chapter 4.1) has a *TRP1* gene that allows auxotrophic yeasts to grow in media lacking tryptophan (SD-W).

Total RNA was isolated from adult C57Bl/6 mouse brain, using Trizol reagent (Invitrogen Life Technologies). Total RNA (2.5 μg) was used to perform reverse transcription using the SuperScript™ First-Strand Synthesis System for RT-PCR (Invitrogen Life Technologies) with an oligo(dT) primer. The coding sequences of the preys Nedd8 and Cul1 were amplified in frame by RT-PCR using the pair of primers including the 5' (attB1) and 3' (attB2) attB site-specific recombination sequences (Gateway Cloning System) attB1Nedd8/ attB2Nedd8 or attB1Cul1/ attB2Cul1 (Appendix 1, Table A.2), and 1 μL of total cDNA from mouse brain or of the plasmid pCMV-SPORT6-Cul1 (Open Biosystems), respectively.

PCR was performed using the enzyme BIO-X-ACT-LONG (Bioline) in the following conditions: one cycle of 5 min at 95°C, followed by 35 cycles of one min at 95°C, one min at 55°C, three min at 68°C, and ending with 15 min at 68°C.

The RT-PCR products (Nedd8, 304 bp; Cul1, 2392 bp) were purified from 1% agarose gels using the QIAQuick Gel Extraction kit (Qiagen), and cloned in the pDONR207 vector using the Gateway Cloning System (Invitrogen Life Technologies), using the manufacturer's instructions. To obtain the pDONR207Cul1:K720R plasmid a point mutation was introduced, corresponding to the alteration of the lysine for an arginine residue at position 720, into the pDONR207Cul1 plasmid using the mutagenesis primer Cul1-K720R (Appendix 1, Table A.4), the Pfu Turbo enzyme (Stratagene) and the DpnI endonuclease enzyme according to the published conditions (Makarova O et al. 2000).

The y2h prey constructs were obtained by recombination of a Gateway version of the pGAD424 vector (provided by RZPD) with the corresponding pDONR207Nedd8,

pDONR207Cul1, and pDONR207Cul1:K720R plasmids, using the Gateway Cloning System (Invitrogen Life Technologies). Prey coding sequences were introduced in the pGAD424 vector in frame with the GAL4AD coding sequence. These y2h prey constructs pGADNedd8, pGADCul1, and pGADCul1:K720R (Table 4.2.1) have a *LEU2* gene that allows auxotrophic yeast to grow in media lacking leucine. The plasmid pGADCul1[aa714-776] described in Chapter 4.1 was also used.

Each construct was confirmed by automated sequencing using primers GAL4AD-F and GAL4AD-R, and in the case of pGADCul1 with primers Cul1(1), and Cul1(2) (Appendix 1, Table A.1) to verify the correct in frame cloning, and tested for their toxicity in yeast and for self-activation of the two reporter genes, *HIS3* and *lacZ*.

GST::prey expressing constructs

Recombinant glutathione-S-transferase (GST)-tag prey protein expression plasmids were obtained by recombination of the corresponding pDONR207 plasmids with the pDEST15 vector using the Gateway Cloning System (Invitrogen) in order to obtain the constructs pDEST15Nedd8 and pDEST15Cul1 (Table 4.2.1).

Table 4.2.1. GAL4AD::prey and GST::prey expressing constructs

Fusion protein	
vector	**protein**
pGADNedd8	GAL4AD::Nedd8
pGADCul1	GAL4AD::Cul1
pGADCul1:K720R	GAL4AD::Cul1:K720R
pDEST15Nedd8	GST::Nedd8
pDEST15Cul1	GST::Cul1

Yeast transformation

All yeast transformations were performed using the high efficiency lithium acetate method (Gietz et al. 1995). Y190 without plasmids were grown in YPAD medium overnight at 30ºC, at 200 rpm, while pretransformed strains were grown in the appropriate SD medium to keep selective pressure of the plasmid. Overnight cultures were diluted in the respective medium to a cell density of 0.3 at 600 nm, and then incubated at 30ºC, at 200 rpm, until reached at an optical density (OD) of 0.6 at 600 nm. Cells were harvested by centrifugation at 1800 rpm for 5 min, first washed with sterile water and then with fresh made 100 mM LiAc.

The following components were added to yeast pellets, in this order: 240 μL PEG (50% w/v), 36 μL 1M LiAc, 25 μL denatured salmon sperm DNA (2mg/mg), and 50 μL plasmid (1 μg) diluted in sterile water. Each tube was vortexed vigorously until the cell pellet was completely ressuspended, and then cells were incubated at 30 ºC during 30 min. Yeast cells where subsequently heat-shocked at 42ºC for 20 min. Finally, cells were centrifuged one min at 3000 rpm, and ressuspended in 1 mL of YPAD. A volume of 20 μL of the transformed yeast culture was plated onto the appropriated selective medium, and plates were incubated at 30ºC during five days.

β-Galactosidase (β-gal) colony-lift filter assay

The β-galactosidase expression test was performed by colony-lift filter assay (Breeden and Nasmyth 1985). The assay was either performed directly on fresh plates with single colonies or with dots of yeast transformants grown on the specific selective medium supplemented with 90 mM of 3-AT. A nylon membrane (Hybond-N, GE Healthcare) was placed over the surface of the plate containing the yeast cells to be assayed. When the membrane was uniformly wetted, it was lifted and submerged in liquid nitrogen for 10 seconds to allow cell permeabilisation. After that, the membrane was thawed at room temperature and placed, colony side up, on a Petri dish containing a filter paper pre-soaked in Z buffer (16.1 mg/mL $Na_2HPO_4.7H_2O$, 5.5 mg/mL $NaH_2PO_4.H_2O$, 0.75 mg/mL KCl, 0.246 mg/mL Mg_2SO_4, pH 7.0), supplemented with 1 mg/mL X-Gal (5-bromo-4-chloro-3indolyl-β-D-galactopyranoside) and 38.6 mM β-ME (β-mercaptoethanol). Filters were incubated 1-12 hours at 30ºC, and then analysed for the presence of blue colonies (*lacZ* positive transformants).

Expression and purification of recombinant His-tagged proteins

The recombinant hexahistidine-tagged mATX3, mATX3:C14A, mATX3:jos, and mATX3:jos:C14A proteins were expressed in *Escherichia coli* BL21SI cells (Invitrogen). Cells were grown at 37ºC in LB/ON (without NaCl) medium containing 100 mg/l of ampicillin and 0.2% (w/v) of glucose until a cell density of 0.6 at 600 nm was reached, then the recombinant protein expression was induced by the addition of NaCl to a final concentration of 0.3 M and culture was further grown for 3 hours at 30ºC. Cells were harvested, ressuspended in buffer L (20 mM sodium phosphate (pH 7.5), 500 mM NaCl) (Gales et al. 2005), 10 mM imidazole, 50 mg/L lysozime and stored at -20ºC. Phenylmethylsulphonyl fluoride (PMSF) was added to the protein extract to a final concentration of 1mM, and after centrifugation the supernatant

was collected and the recombinant protein was purified using the HiTrap Kit (GE Healthcare) being eluted in three fractions of buffer L containing 50 mM, 100 mM or 500 mM imidazole.

The fractions of the proteins mATX3, mATX3:C14A, mATX3:jos, and mATX3:jos:C14A, considered appropriate for further purification, were selected by SDS-PAGE analysis, applied to a HiPrep 26/60 Sephacryl S-200 high resolution column (GE Healthcare) equilibrated in buffer A (20 mM HEPES (pH7.5), 50 mM NaCl, 5% glycerol, 1 mM EDTA, 1 mM DTT), and protein was eluted with a flow rate of 0,5 mL/min, at 4 ºC, being monitored at 280 nm. After SDS-PAGE analysis, the fractions containing only protein monomers were pooled and concentrated in on Millipore Amicon Ultra-15 concentrators (cut-off 10 KDa, Millipore) to 1-2 mg/mL. Purified monomeric proteins were diluted into a 20 μM working solution and maintained in ice for enzymatic assays and then stored at -80 ºC.

Deneddylation assay

The fluorogenic substrate NEDD8 7-amido-4-methylcoumarin (AMC) (Biomol) was incubated with 800 nM of each His recombinant protein mATX3, mATX3:C14A, mATX3:jos, mATX3:jos:C14A in 300 μL of the assay buffer (50 mM HEPES, pH7.4, 500 mM EDTA, 1 mM DTT, 0.1 mg/mL BSA, COMPLETE (Roche Diagnostics)). The reaction progress was monitored during 10 min, in a fluorescence cuvette maintained at 37 ºC by a circulating bath, in a Jasco fluorescence spectrophotometer. Fluorescence emission at 460 nm (λ_{exc}= 380 nm) given by the cleavage of AMC from NEDD8-AMC.

4.2.4. RESULTS

Mouse ataxin-3 interacts with Nedd8 and presents deneddylation activity

To evaluate if the interaction of ATX3 and NEDD8 was conserved in the mouse we have used the y2h strategy, namely the GAL4 system. We have constructed an y2h prey plasmid pGADNedd8 (expressing the GAL4AD::Nedd8 fusion protein) and used the bait plasmid pGBT9Mjd (expressing the GALBD::mATX3 fusion protein). The pGADNedd8 was tested for auto-activation of the reporter genes *GAL1*$_{UAS}$*-HIS3* and *GAL1-lacZ*, and no substantial colony growth in selective plates SD-LH supplemented with 90 mM of 3-AT was observed; no β-gal activity was verified in the grown colonies. In co-transformed Y190 yeast cells, GAL4BD::mATX3 showed to specifically interact with GAL4AD::Nedd8 (Figure 4.2.2A). Co-transformations of the bait plasmid pGBT9Mjd with the empty pGAD424 vector showed

no positive interaction (Figure 4.2.2A). Additional confirmation of this mATX3/ Nedd8 interaction by GST-pull down assay is underway.

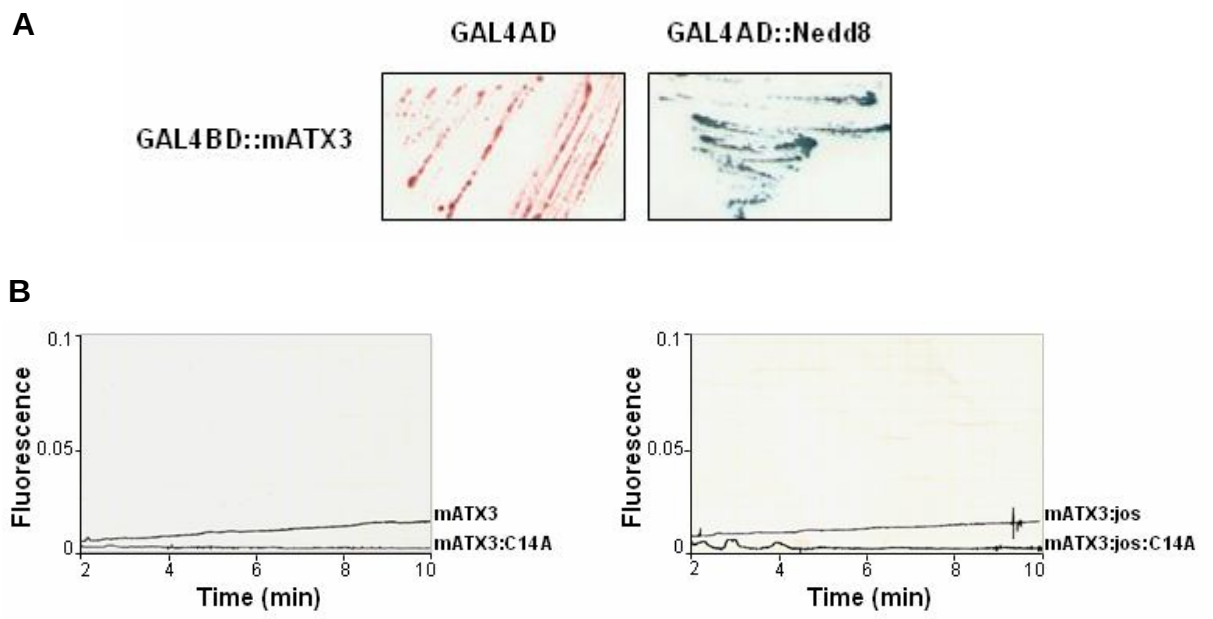

Figure 4.2.2. Mouse ataxin-3 (mATX3) interacts with Nedd8 conserves the deneddylase activity observed for the human ataxin-3. A) The mATX3/ Nedd8 interaction was verified by yeast two-hybrid co-transformation. The interaction between the GAL4BD::mATX3 and the fusion GAL4AD::Nedd8 protein is shown by the blue colony streaks of the yeast cells co-transformed with both bait and prey plasmids, and plated in SD-WLH90mM3-AT. The positive signal of GAL4 reporter expression is the blue colour of the colonies after the β-gal activity assay. The empty GAL4AD expression vector pGAD424 (negative control) was co-transformed with the pGBT9Mjd plasmid (expressing GAL4BD::mATX3) in Y190 cells, and streaks of these transformants were included in each testing plate to further be performed the β-gal colony-lift activity assay. B) Fluorimetric assay showing that mATX3 is able to hydrolyse NEDD8-AMC substrates by its josephin domain (mATX3:jos) carrying a functional catalytic cysteine 14, since both mutated mATX3:C14A and mATX3:jos:C14A can not cleave NEDD8-AMC substrates.

Mouse ataxin-3 possesses one josephin domain, containing the four essential residues Q9, C14, H119 and N134 for the catalytic pocket, and three ubiquitin interacting motifs (UIMs), as well as the hATX3-v1 (Chapter 2). This high conservation suggests conserved functional roles for mATX3. To test the conservation of the deneddylation activity of mATX3, we have expressed a series of His-tagged mATX3 recombinant proteins (mATX3, mATX3:C14A, mATX3:jos, and mATX3:jos:C14A) in *E. coli*, purified by ionic change chromatography, and additionally by gel filtration chromatography in order to isolate the monomeric species. We have performed fluorimetric assays using as substrate NEDD8-AMC and as enzymes mATX3, mATX3:jos, or the corresponding proteins with the catalytic cysteine 14 mutated for an alanine (mATX3:C14A and mATX3:jos:C14A). Both the entire

protein and the josephin domain alone were able to cleave the NEDD8 moiety from the AMC molecule, while the respective mutated C14A proteins were not (Figure 4.2.2B), showing that mATX3 conserves the ability to hydrolyse NEDD8 substrates.

Mouse ataxin-3 interacts with the C-terminal of Cul1 independently of its neddylation state

As described in Chapter 4.1, in the y2h mouse libraries screenings for mATX3 interactors, Cul1 was found to be one of them. More precisely, a prey clone encoding the last 62 amino acids of Cul1 (aa714-776) was isolated for three times in two different y2h screenings corresponding to the 11-day mouse embryo and mouse testis libraries. The fact that this clone was isolated more than once and from different libraries strengthened the hypothesis of the potential interaction between mATX3 and Cul1. In fact, as shown in Chapter 4.1, we have confirmed this direct interaction of mATX3 with the C-terminal of Cul1[aa714-776] by y2h co-transformation and mating assays. Here, we have cloned the entire coding sequence of mouse Cul1 into the pGAD vector, expressing the fusion protein GAL4AD::Cul1, and confirmed by y2h co-transformation assays that interacts with mATX3 (Figure 4.2.3).

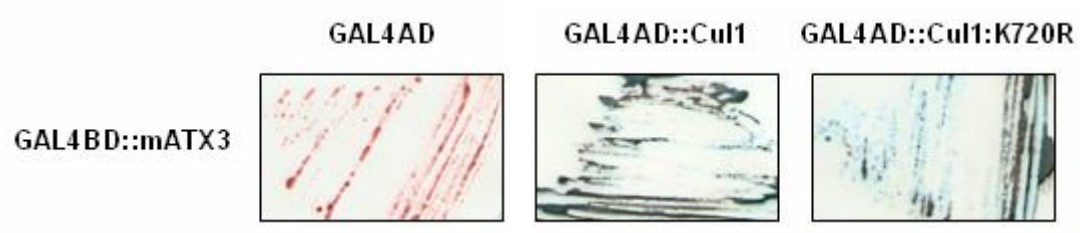

Figure 4.2.3. Mouse ataxin-3 (mATX3) interacts with Cul1 independently of its neddylation state. The mATX3/ Cul1 and mATX3/ Cul1:K720R interactions were verified by yeast two-hybrid co-transformation. The interactions between the GAL4BD::mATX3 and the fusion GAL4AD::Cul1 or GAL4AD::Cul1:K720R proteins are shown by the blue colony streaks of the yeast cells co-transformed with both bait and prey plasmids, and plated in SD-WLH90mM3-AT. The positive signal of GAL4 reporter expression is the blue colour of the colonies after the β-gal activity assay. The empty GAL4AD expression vector pGAD424 (negative control) was co-transformed with the pGBT9Mjd plasmid (expressing GAL4BD::mATX3) in Y190 cells, and streaks of these transformants were included in each testing plate to further be performed the β-gal colony-lift activity assay.

As the interaction region of Cul1 with mATX3 was the C-terminal including the neddylation lysine residue at position 720, and mATX3 interacts with Nedd8 and presents

deneddylase activity, the interaction of mATX3 with Cul1 may potentially be dependent of its neddylation state. To test this hypothesis we have mutated the lysine residue for an arginine (K720R) and evaluated the interaction of the fusion proteins GAL4AD::Cul1:K720R and GAL4BD::mATX3. In yeast co-transformation assays, mATX3 seemed to interact with the mutated Cul1 at the neddylation site (Figure 4.2.3). Confirmation of the neddylation state of Cul1 in yeast should be performed in the future by immunoblotting. Further confirmation of the interaction of mATX3 with Cul1[aa714-776], and Cul1 using a GST-pull down assay is ongoing.

These results suggest that mATX3 interacts with the C-terminal of Cul1 including the neddylation site, but that the neddylation state of Cul1 is not important for this interaction.

4.2.5. DISCUSSION

Ataxin-3 is an evolutionary highly conserved protein that, as we have previously reported, presents 86% and 38% of homology in mouse and *C. elegans* species (Costa et al. 2004; Rodrigues et al. 2007). Recently, our group has shown that both human and *C. elegans* ATX3 interact with the human Ub-like protein NEDD8, and that human ATX3 presents deneddylase activity trough its josephin domain (Ferro et al. 2007).

Here, we have shown that this ATX3/ NEDD8 interaction is also conserved in mouse. We have verified by y2h assays that mATX3 also interacts with mouse Nedd8, which was in accordance to the abovementioned results (Ferro et al. 2007). Nevertheless, this interaction should be further confirmed using other technique, namely GST pull-down assay that is already ongoing. In our previous report, we have shown that mATX3 was a ubiquitous expressed protein since the earliest embryonic developmental stage studied (E11.5), and presenting a highly expression in all types of muscle (Costa et al. 2004). In a similar way, Kamitani and co-authors (Kamitani et al. 1997) showed that the highest mouse Nedd8 mRNA expression levels were at embryonic day E11, and that in human adult tissues NEDD8 was mostly restricted to the heart and skeletal muscle. Thus, the expression patterns of both mATX3 and NEDD8 proteins seem to be compatible either during embryonic development and adulthood, in a tissue-specific manner, which is consistent with the biological of their interaction.

Similarly to what was shown for ATX3 (Ferro et al. 2007), and using the same *in vitro* assays, we have confirmed that the recombinant mATX3 presents deneddylase activity against the fluorogenic NEDD8-AMC substrate, and that this functional activity is undertaken by the josephin domain and dependent of the cysteine residue at position 14.

NEDD8 is an Ub-like protein crucial for the activity of cullin-containing ubiquitin E3 ligases (Hori et al. 1999; Kamura et al. 1999). Interestingly, in this study we found that Cul1 was also a mATX3 interactor in a y2h library screening for mATX3 partners. We have confirmed this interaction by direct y2h assays and found that the interaction region of Cul1 with mATX3 was the C-terminal corresponding to the last 62 amino acid residues [aa714-776]. Given that this region also comprised the neddylation lysine residue at position 720, we have mutated this residue for an arginine and found that in yeast mATX3 maintain its interaction with this mutated Cul1, suggesting that Cul1/ mATX3 interaction is not dependent of the Cul1 neddylation state, i.e. that mATX3 binding to Cul1 is not via Nedd8. However, this result should be further confirmed in a mammalian cellular system. GST pull-down assays are presently ongoing to confirm the Cul1/ mATX3 interaction. Moreover, it will be interesting to verify if Cul1 is a target of mATX3 deneddylase activity, and for that we are currently determining the neddylation state of Cul1 in mATX3 knockdown cells.

In fact, the C-terminal region of Cul1 is also the binding site of Rbx1 for the formation of the core of CRLs and taking on the E2 ligase (Skowyra et al. 1997), which may suggest that mAT3 could alternatively be interfering with this interaction and consequently regulating E2 ligase recruitment.

In addition, in chapter 4.1 we have confirmed the interaction of mATX3 with Lrrc40, a leucine-rich repeat (LRR) protein also found in the y2h screening for mATX3 interactors. Lrrc40 is a protein of yet unknown function, but given that it contains a LRR domain we may speculate that this protein could function as a F-box protein, recruiting specific substrate for the SCF complex.

The conservation of the interaction of mATX3 with Nedd8 and this new Cul1/ mATX3 interaction support the hypothesis of a possible physiological role of ATX3 in the modulation of the UPS activity (Ferro et al. 2007; Rodrigues et al. 2007). Here, we have shown the direct involvement of mATX3 with the SCF complex by its interaction with Cul1. This result is in agreement with the previous report of the transcriptomic analysis of *atx-3* knockout *C. elegans* strains that revealed a down-regulation of several genes encoding SCF complex subunits (*skr-8*, *skr-10*, *skr-13*, and *pes-2*) (Rodrigues et al. 2007), and also with the *C. elegans* genetic interactome that identified several genes encoding UPS-related and components of SCF-like complexes as genetic interactors of atx-3 in this nematode (Zhong and Sternberg 2006).

In this study we have confirmed that mATX3 interacts with mouse Nedd8 using yeast two hybrid (y2h) assays, and that it also presents deneddylase activity *in vitro*, through its josephin domain. This indicates that this protein interaction and functional activity is evolutionary conserved and of great relevance. Furthermore, we have identified Cul1 as an interactor of mATX3 in an y2h screening for mATX3 partners. Cul1 was found to interact with

mATX3 through its C-terminal region, more precisely the last 62 residues. This Cul1 region comprised the neddylation site at lysine 720 that when mutated for an arginine showed to continue to interact with mATX3 in y2h assays. Therefore, the interaction of mATX3 with Cul1 may be independent of its neddylation state. ATX3 may be potentially regulating or making part of the SCF complex by interacting with Cul1 and Nedd8.

More precisely, in this study we suggest a possible regulation of the SCF complex by mATX3 trough its interaction with Cul1 and Nedd8. Several hypotheses may be raised for this potential activity (Figure 4.2.4): (1) mATX3 may deneddylate Cul1 in order to regulate it's activity and/ stability; (2) mATX3 may compete with either Nedd8 or TIP120A for the neddylation binding site in order to regulate Cul1 activity and/ stability; (3) mATX3 may be interfering with the Rbx1/ Cul1 interaction modulating the formation of the integral core, or the E2 ligase recruitment to the complex; (4) mATX3, given that it may also potentially interact with some F-box proteins, might be a link between the F-box and Cul1; (5) since auto-ubiquitination of E3 Ub-ligases is a common phenomenon, mATX3 might be deubiquitinating Cul1; or (6) mATX3 might be interacting with Cul1 for the recognition of its substrate. Further studies should be performed to test these hypotheses in order to clarify the role of ATX3 in the SCF complex and its physiological relevance.

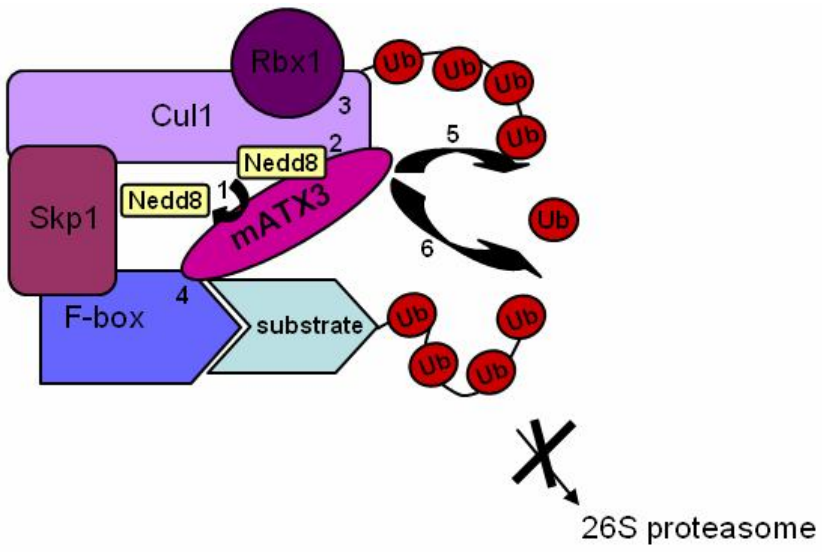

Figure 4.2.4. Schematic representation of the possible hypotheses for the regulation of the SCF complex by mATX3: (1) deneddylase activity; (2) competition for the binding site of Nedd8 at Cul1; (3) interference with the Rbx1/Cul1 interaction; (4) establishment of a link between Cul1 and specific F-box proteins; (5) desubiquitination of Cul1; or (6) recognition of the substrate via Cul1 interaction.

Chapter 4.3

Ataxin-3 and microtubules: a role in mitosis?

4.3.1. SUMMARY

Our previous evidences that mATX3 was highly expressed in muscle, in cilia and in flagellum of spermatozoids led us to search for a possible role of mATX3 in the cytoskeleton. We hypothesised that mATX3 might be implicated in the regulation of microtubule dynamics.

In this study, we have confirmed the interaction of mATX3 with α-tubulin and verified for the first time that mATX3 associates with microtubules preferentially during mitosis, co-localising with the centrosomes, mitotic spindle, and midbody. Interestingly, searching for conserved protein domains of mATX3, we found a potential structural maintenance chromosome (SMC) domain presenting a 47% of homology with cytoplasmic dynein heavy chain 1 (Dyhc). SMCs are important players in chromosome segregation. This potential SMC domain comprises residues between 187 and 304, starting immediately after the josephin domain and spanning by the region containing the UIM1, UIM2, and polyQ domains.

Additionally, we described the mATX3 interaction with Twa1, a member of the CTLH complex, and Kif2c, both implicated in microtubule dynamics and chromosome segregation. These results led us to hypothesise that mATX3 might be involved in these cellular processes. However, further work will be necessary to explore this hypothesis.

4.3.2. INTRODUCTION

All eukaryotic cells have a very well organised cytoskeleton that gives them their shape, capacity to move, ability to arrange and transport the organelles, and to divide. Three types of protein filaments are the major components of the cytoskeleton: actin filaments, intermediate filaments, and microtubules.

The assembly of microtubules is undertaken by polymerisation of heterodimeric subunits of α- and β-tubulin. Microtubules contain a fast-growing end terminated by a β–tubulin subunit (plus end) and a slow-growing end (minus end) (Howard and Hyman 2003), and are dynamically unstable structures, transiting between the states of growing or shrinking (Walker et al. 1988). A transition from shrinkage to growth is denominated “rescue”, and a transition from growth to shrinkage is called “catastrophe” (Walker et al. 1988). In animal cells, microtubules are nucleated at the centrosomes (Job et al. 2003), growing out from the γ-tubulin rings with their plus ends throughout the cytoplasm. Among many functions of microtubules, these filaments play an important role during cell division.

When a eukaryotic cell starts to divide, a striking reorganisation of cellular components occurs: the cell rounds, chromosomes condense, the nuclear envelope breaks

down, and the large amounts of stable microtubules that exist in interphase become very short and dynamic before the assembly of the mitotic spindle. Mitosis (M phase) comprises several stages: prophase, prometaphase, metaphase, anaphase and telophase.

Upon entry into mitosis, in prophase, replicated interphase chromosomes are compacted within the nucleus to facilitate their segregation, and a proteinaceous structure (kinetochore) starts to be built at their centromeric region, to connect with spindle microtubules. After the nuclear envelope breakdown, kinetochores start to interact both laterally and in an ends-on-manner with spindle microtubules – prometaphase. In metaphase, all chromosomes are bi-oriented, with sister kinetochores specifically connected to microtubules that are extended from opposite spindle poles. Once chromosomes become bi-oriented, the machinery that separates sister chromatids is activated and the separated chromatids move to opposite spindle poles – anaphase. Subsequently, during telophase, sister chromatids decondense, the nuclear envelope is restored, and a contractile actomyosin ring is formed. The ring creates an invaginated furrow that defines the cleavage plane in plasma membrane, and gives rise to another structure, the midbody, composed by the remaining of the two sets of polar microtubules and dense matrix material. Finally, during cytokinesis the cell is bisected into two daughter cells with exact copies of the duplicated genome.

It is known that the stability of the plus ends of microtubules, nucleating from centrosomes, is highly variable during the cell cycle and assembly of a mitotic spindle. Although the regulation of microtubule dynamics is still poorly understood, several microtubule-associated proteins (MAPs) have been characterised and associated to this process (Cassimeris and Spittle 2001). XMAP215 and adenomatous polyposis coli (APC)/EB1 complex are known microtubule stabilisers, whereas the mitotic centromere-associated kinesin (MCAK) is a destabiliser (Tournebize et al. 2000; Tirnauer et al. 2002), MCAK, or Kif2c, is a member of a family of kinesin-like proteins (the kinesin-13 subfamily) known as “catastrophe kinesins” given their capacity to induce catastrophes (Wordeman 2005). MCAK couples ATP hydrolysis to the removal of GTP-dimers from both ends of microtubules (Hunter et al. 2003). This protein is found in mammalian mitotic centromeres from late prophase to late telophase (Wordeman and Mitchison 1995), and is thought to be implicated in chromosome segregation and in the correction of improper kinetochore-microtubule interactions (Maney et al. 1998; Kline-Smith et al. 2004). The activity of this catastrophe kinesin was shown to be inhibited during interphase, when microtubules are stable, by its interaction with other MAPs (XMAP215, EB1, APC, and CLIP170); in mitosis, MCAK was shown to be free, acting as a strong microtubule destabiliser leading to the depolymerisation (Niethammer et al. 2007). Furthermore, the activity of MACK is also inhibited by Aurora-B kinase phosphorylation (Lan et al. 2004).

Interestingly, the annotated MCAK-like protein in the protozoan parasite *Leishmania major* was shown to localise essentially to its single flagellum and to be involved in its length control (Blaineau et al. 2007). This MCAK-like protein was highly abundant during G2+M phase (localised to the mitotic spindle and spindle poles), and present at very low levels after mitosis, its levels being potentially regulated by the UPS (Dubessay et al. 2006).

In fact, the M phase of cell cycle progresses by the periodic activation and inactivation of regulatory proteins by phosphorylation and dephosphorylation (Nigg 2001), and by their selective degradation by the UPS at critical moments (Peters 2002). In addition to the putative involvement of the UPS in the degradation of MCAK, other MAPs implicated in microtubule dynamics were also shown to be regulated by this system. APC seems to be down-regulated by the UPS in a process facilitated by axin (Choi et al. 2004), and EB1 is protected from UPS degradation by the COP9 signalosome (CSN)-mediated phosphorylation (Peth et al. 2007). Moreover, some DUBs seem to be associated to microtubules and/or involved in the regulation of their dynamics. The cylindromatosis gene (*CYLD*) encodes a DUB that removes K^{63}-linked ubiquitin chains from upstream signaling components of the NF-kB pathway (Brummelkamp et al. 2003; Kovalenko et al. 2003; Trompouki et al. 2003). This DUB, detected in microtubules in interphase and in the midbody during telophase, is required for the entry into mitosis, the protein kinase Plk1 being its potential target (Stegmeier et al. 2007). The ubiquitin specific protease USP11 is a DUB that deubiquitinates RanBPM (Ideguchi et al. 2002), a Ran-binding protein with centrosomal localisation that plays a critical role in microtubule nucleation (Nakamura et al. 1998). RanBPM contains a domain called LisH-CTLH that is detected in proteins implicated in microtubule dynamics, cell migration, nucleokinesis and chromosome segregation (Emes and Ponting 2001). It associates with other LisH-CTLH-containing proteins (Twa1, muskelin, p44CTLH, p48EMLP) and with two armadillo-repeat proteins ARMC8α and ARMC8β, forming a large protein complex denominated CTLH complex (Kobayashi et al. 2007). In fact, RanBPM interacts with β2 integrin LFA-1 (Denti et al. 2004), supporting the hypothesis for a role of the CTLH complex in cell migration.

The fact that ATX3 was shown to immunoprecipitate with tubulin (Zhong and Pittman 2006) and that mATX3 is highly expressed in all types of muscle, in ciliated cells and in the flagellum of spermatozoids (Costa et al. 2004), suggested a possible role for this protein in the cytoskeleton. Furthermore, given that mATX3 presents DUB (Chapter 2) and deneddylase activities (Chapter 4.2), potentially acting in the UPS, led us to hypothesise that ATX3 may be involved in the regulation of microtubule dynamics.

4.3.3. MATERIALS AND METHODS

Antibodies

The primary antibodies used were: rabbit anti-hATX3 serum (kindly provided by H. Paulson), mouse anti-α-tubulin (Santa Cruz Biotechnology), mouse anti-γ-tubulin (Santa Cruz Biotechnology), and sheep anti-hMCAK (kindly provided by L. Wordeman, Washington University).

The peroxidase-conjugated secondary antibodies used for immunoblotting were: goat anti-mouse (Santa Cruz Biotechnology), and anti-rabbit (Santa Cruz Biotechnology). For double immunofluorescence assays, Alexa Fluor (AF) secondary antibodies (Molecular Probes) were used: AF 488 goat anti-rabbit, AF 568 goat anti-mouse, and AF 568 goat anti-sheep.

3T3 cell culture

Mouse 3T3-Swiss albino fibroblasts were obtained from the American Type Cell Collection (CCL-92). Cells were cultured in Dulbecco's modified Eagle's (DMEM) (Gibco BRL), 10% calf bovine serum (CBS) and 1% penicillin/streptomycin, in a 5% CO_2 humidified chamber at 37ºC.

Cell suspension correspondent to a 150 mL flask was centrifuged, washed twice with PBS and whole protein extracts from 3T3 cells were prepared by pellet resuspension in 300 μL of hypotonic buffer (50 mM Tris-HCl pH 7.8, 10 % glycerol, 10 mM EDTA, 5 mM KCl, COMPLETE). After 10 min incubation on ice, cells were disrupted by sonication.

Co-immunoprecipitation

IgG Sepharose™ 6 Fast flow beads (GE Healthcare) (50 μL) were incubated overnight at 4ºC in the presence of 40 μg of either anti-ATX3 serum or anti-α-tubulin antibodies, in a final volume of 300 μL of PBS/ protease inhibitors (COMPLETE, Roche Diagnostics). Beads were washed three times to remove the antibody excess. For antibody crosslinking to the IgG beads, these were washed twice in 0.2 M triethanolamine (TEA) pH 9.0, and then incubated in the same buffer containing 20 mM dimethylpimelimidate (DMP) dihydrochloride (Sigma) for 1h at room temperature. The beads were then incubated in 1 % Triton-X100/ TEA during 10 min at 4ºC, and washed three times in PBS-Tween20 buffer (PBS-T). For the immunoprecipitation, crosslinked beads were incubated with 100 μg of 3T3

cell whole extract during 3h at 4ºC. After six washes with PBS-T, the immunoprecipitated product was eluted in 65 μL of Laemmli sample buffer.

Immunoblotting

The immunoprecipitated products were resolved in a 10% SDS-PAGE polyacrylamide gel and then transferred to a nitrocellulose membrane (Hybond-C, GE Healthcare). Membranes were incubated, overnight at 4ºC, with primary antibodies: anti-ATX3 serum (1:5000) or anti-α-tubulin (1:10000). Detection of the immunocomplexes was performed using the peroxidase-conjugated secondary antibodies anti-rabbit (1:10000) or anti-mouse (1:10000), and a SuperSignal West Pico Chemiluminescent Substrate (Pierce). The signal was registered in ECL-films (Hyperfilm, GE Healthcare).

Immunofluorescence staining

For immunofluorescence labelling, 3T3 cells were seeded in coverslips. After 24 hours cells were washed briefly with PBS and fixed with either 2 % paraformaldehyde (PFA)/ PBS (20 min), or with methanol/ EGTA 2mM (2 min at -20ºC). All the following procedures were undertaken using Tris-buffered saline (TBS) in methanol fixation, or PBS in PFA fixation. After fixation, cells were permeabilised in 0.5 % Triton-X-100 (5 min). Then cells were blocked in 10 % FBS (1 h), and incubated with the anti-ATX3 serum (1:500) in combination with other primary antibody (all diluted in 5 % FBS), overnight at 4 ºC. Alexa Fluor (AF) secondary antibodies used were AF 488 goat anti-rabbit, AF 568 goat anti-mouse, and AF 568 goat anti-sheep, diluted 1:1000 in 5 % FBS. Finally, coverslips were stained with 4',6-Diamidino-2-phenylindole dihydrochloride (DAPI, Sigma) diluted 1:2000 in PBS during 5 min, and mounted with Vectashield (Vector Laboratories).

Imaging

Most images were acquired as Z-stacks with 0.2-0.3 μm spacing using a x60 1.42 NA on a Olympus FluoView FV1000 confocal microscope. Maximal intensity projections of the entire Z-stack are shown.

Bioinformatics

In order to find common protein domains between mATX3 (Accession number

NP_083981) and other proteins, we have used the program BLAST (blastp algorithm) to search a mouse non-redundant protein sequence database. Protein alignments were performed using the CLC combined workbench 3.5.1 software.

4.3.4. RESULTS

Mouse ataxin-3 immunoprecipitates with α-tubulin

In order to determine whether mATX3 was associated with microtubules, we have used Swiss 3T3 cells that, given their large size and flat morphology, have a sparse microtubular network at their periphery allowing easy visualisation. First, we assessed whether mATX3 and α-tubulin co-immunoprecipitated. A protein extract from the 3T3 fibroblasts was incubated in the presence of the anti-ATX3 or the anti-α-tubulin antibodies previously covalently couplet to protein G sepharose beads. Proteins bound to the respective antibodies, were then eluted in a denaturing buffer that allowed the disruption of the protein/protein complexes. The anti-mATX3 immunoprecipitate (containing mATX3 and its interacting proteins) was evaluated by immunoblotting for the presence of α-tubulin; and the anti-α-tubulin immunoprecipitate (including α-tubulin and its associated proteins) was analysed for the existence of mATX3 (Figure 4.3.1). In fact, mATX3 was found to be co-immunoprecipitated with α–tubulin and vice-versa (Figure 4.3.1). 10% of the 3T3 whole extract (WE) was used in the immunoblots to detect the presence of the corresponding proteins (Figure 4.3.1). Positive controls were included in each immunoblot. These controls corresponded to the loading of the immunoprecipitates carried out with the same antibody that was used in the membrane incubation (Figure 4.3.1). When

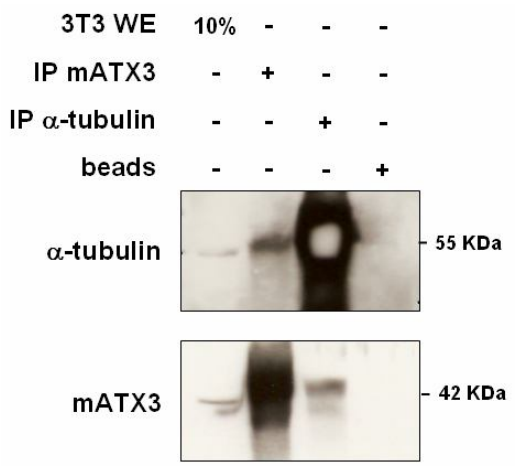

Figure 4.3.1. Co-immunoprecipitation of mATX3 and α-tubulin. 3T3 cell whole extract (WE) was incubated with either anti-ATX3 or anti-α-tubulin antibodies covalently bounded to protein G beads. The immunoprecipitated (IP) material was analysed by immunoblotting with anti-ATX3 or anti-α-tubulin antibodies. Anti-ATX3 antibody co-immunoprecipitated mATX3 and α-tubulin from the cellular protein extract. Reciprocally, anti-α-tubulin antibody immunoprecipitated α-tubulin and mATX3. Neither mATX3 nor α-tubulin were immunoprecipitated from beads without crosslinked antibodies (lane 4).

the antibodies were excluded from the beads (negative control) no proteins were bound (Figure 4.3.1). This result suggests that mATX3 might be a microtubule associated protein (MAP) or otherwise interact with a MAP.

3T3 cells were then fixed with paraformaldehyde and double stained for mATX3 and α-tubulin. In interphasic cells, mATX3 was dispersed mainly in the cytoplasm being mainly localised in the perinuclear region, presenting a partial co-localisation with microtubules in this particular region (Figure 4.3.2).

After exposure to nocodazole during 16 hours, microtubules were disrupted and mATX3 maintained mostly its perinuclear localisation, co-localising with some fragments of microtubules that persisted after the drug treatment (Figure 4.3.3).

In order to verify if mATX3 was localised to the centrosomes we have performed double immunofluorescence assays in 3T3 cells for mATX3 and γ-tubulin, a centrosomal protein. During interphase, mATX3 did not co-localise with γ-tubulin at the centrosome, but showed to be highly expressed around this microtubule organizing center, possibly associating with astral microtubules (Figure 4.3.4).

Double immunofluorescence staining for mATX3 and α-tubulin revealed that mATX3 is highly expressed during mitosis, independently of the mitotic stage (Figure 4.3.5). Furthermore, mATX3 seems to accumulate mainly at regions of higher microtubule density as the poles and midbody (Figure 4.3.5).

During mitosis mATX3 co-localises with spindle structures

In order to evaluate the sub-cellular distribution pattern of mATX3 during the M-phase we analysed the immunofluorescent stainings of mATX3 and α-tubulin in all the mitotic stages: prophase, prometaphase, metaphase, anaphase, and telophase (Figure 4.3.6). We observed that mATX3 is widely distributed in the cytoplasm, co-localising however with microtubules (labelled for α-tubulin) particularly at high microtubule density areas such as the poles and midbody (Figure 4.3.6). This expression pattern may suggest a role for mATX3 in mitosis, probably associated with the regulation of microtubule dynamics, or regulation of microtubule associated proteins crucial for the mitosis process.

mATX3 contains a Smc protein domain

In order to find conserved protein domains in mATX3, we have used the NCBI/BLAST program (blastp algorithm) to search a mouse non-redundant protein sequence database, using the mATX3 sequence as query. This analysis revealed that the josephin domain was

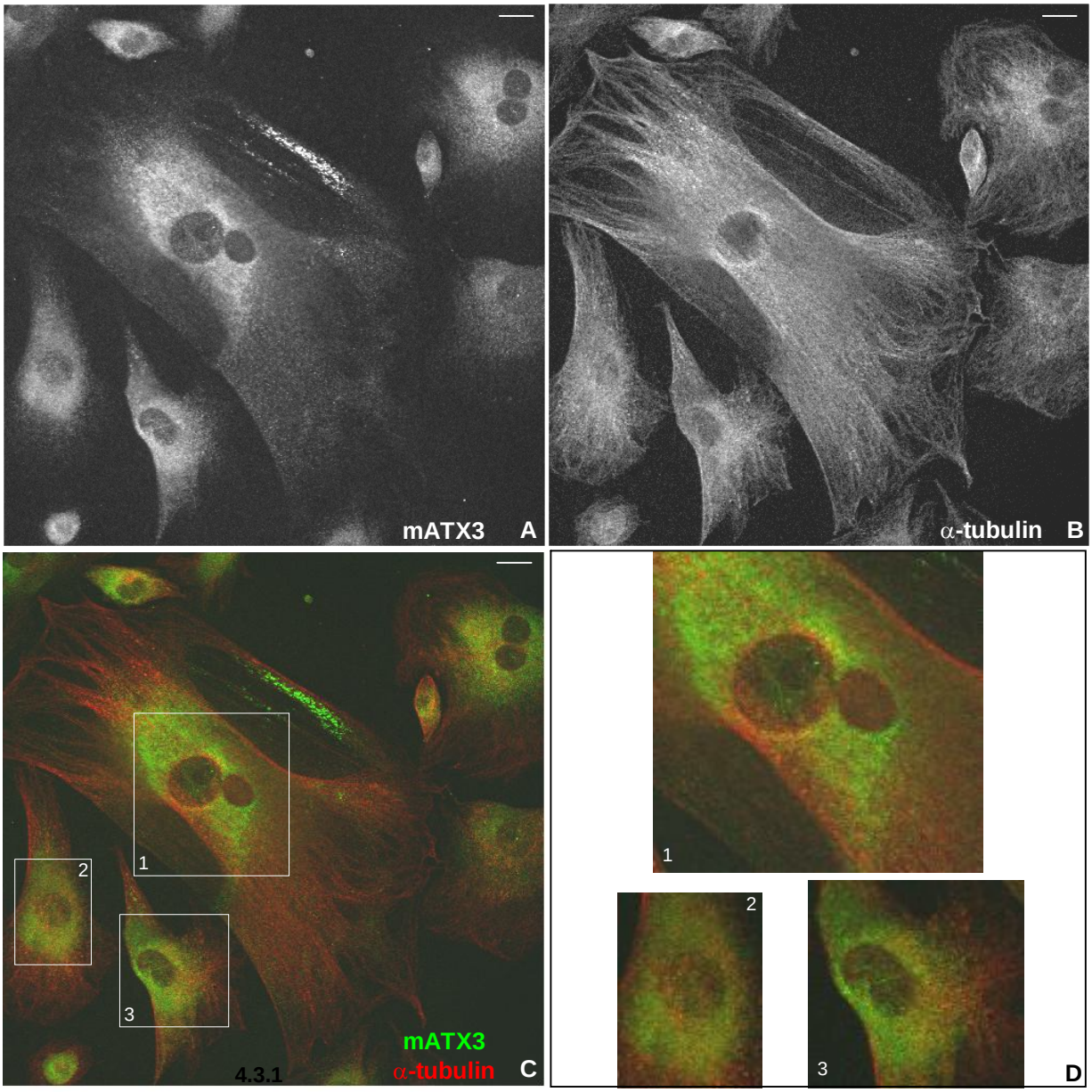

Figure 4.3.2. Mouse ataxin-3 co-localises partially with microtubules during interphase. Confocal optical z-series images of double immunofluorescence stainings for (A) mATX3 (green) and (B) α-tubulin (red) of 3T3 cells. Merged staining is represented in (C). In interphasic 3T3 cells, mATX3 seems to be mainly perinuclear where it overlaps with the denser part of the microtubular network, as evidenced in the higher magnifications of regions 1, 2, and 3 in (D). Scale bars represent 10 μm.

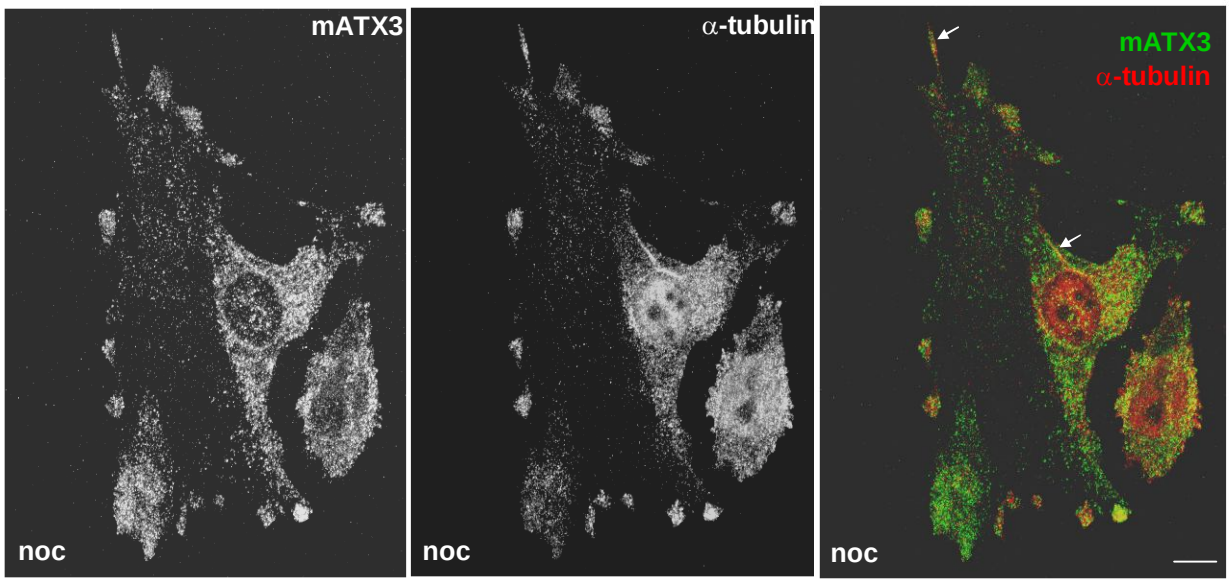

Figure 4.3.3. mATX3 immunolocalisation upon disruption of microtubules during interphase. Confocal optical z-series images of 3T3 cells double immunostained for mATX3 (green) and α-tubulin (red). After incubation with nocodazole, microtubules were disrupted and tubulin acquired a patchy and diffuse distribution. The white arrows indicate fragments of microtubules to which mATX3 remained associated. *noc*, nocodazole. Scale bars represent 10 μm.

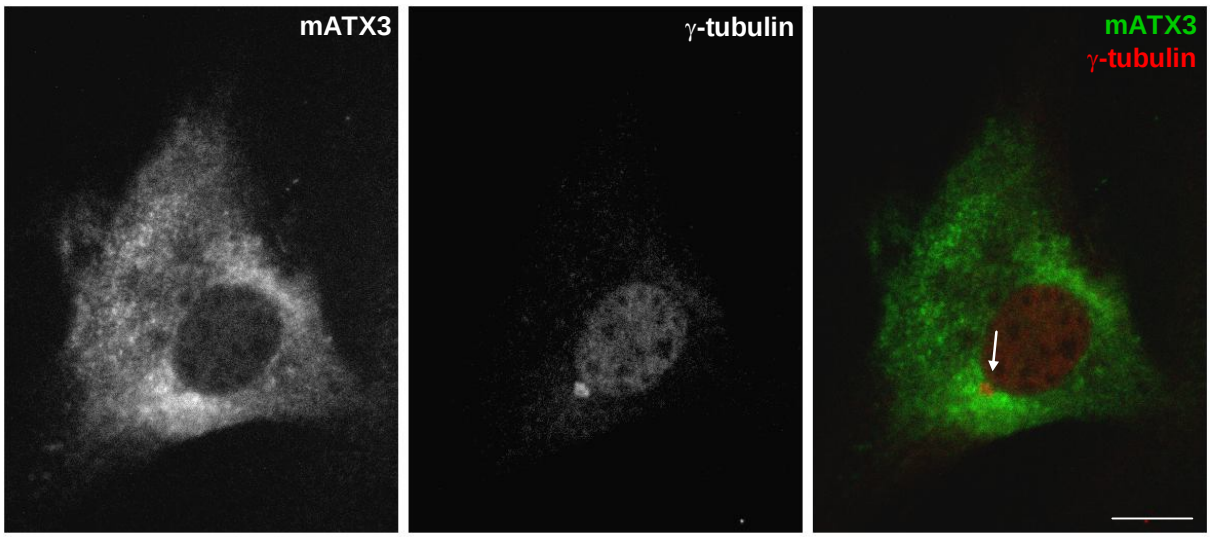

Figure 4.3.4. Mouse ataxin-3 does not localise at the centrosome in interphase 3T3 cells. Confocal optical z-series images of double immunofluorescence staining for mATX3 (green) and γ-tubulin (red) of 3T3 cells. The white arrow indicates the centrosome. Scale bar represent 10 μm.

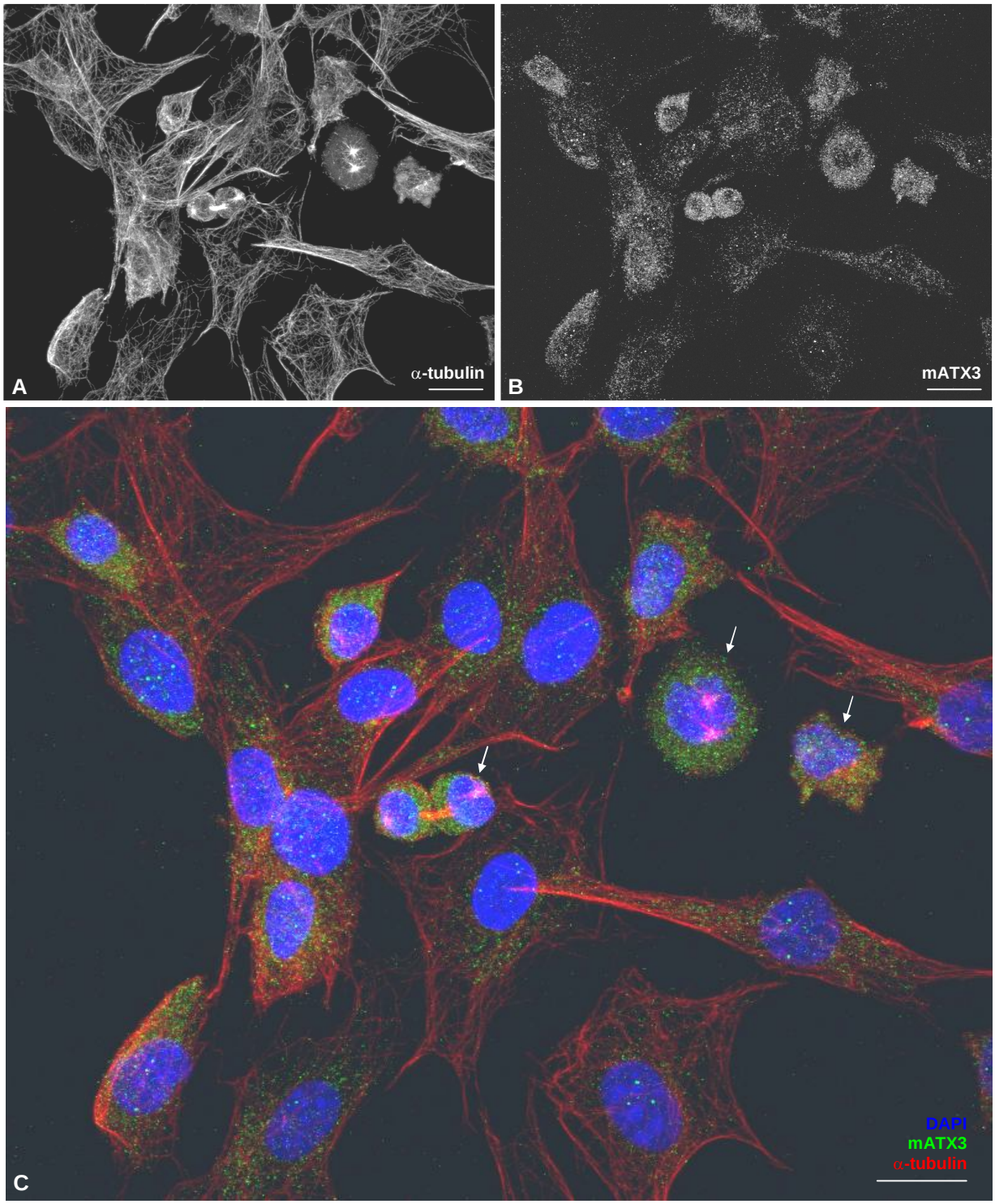

Figure 4.3.5. Mouse ataxin-3 seems to be highly expressed during mitosis. Confocal optical z-series images of double immunofluorescence staining for mATX3 (green) and α-tubulin (red) of 3T3 cells. Microtubules are labelled for α-tubulin (A). mATX3 staining is shown (B). DNA was labelled with DAPI (blue) as shown in the merge (C). The white arrows indicate mitotic cells. Scale bar represent 20 μm.

present in three other mouse proteins named Josd1 (Accession number Q9DBJ6), Josd2 (Accession number Q9CR30), and Josd3 (Accession number EDL01225.1). Several other small regions of mATX3 aligned with other protein domains. Interestingly, mATX3 aligned with the cytoplasmic dynein heavy chain 1 (Dyhc): the region of mATX3 comprising the residues 187-304 presented 47% of homology, and 21% of identity with Dyhc[aa3180-3285] (Figure 4.3.7A), and started immediately after the josephin domain comprising the first two UIM domains (UIM1 and UIM2), and the polyQ repeat (Figure 4.3.7B). In relation to Dyhc, the alignment region corresponded to a conserved structural maintenance of chromosome (Smc) protein domain. This domain is present in chromosome segregation ATPases, important for cell division and chromosome partitioning (Smc, COG1196). The Smc domain is also present in other motor proteins namely in the classical type II myosins (Accession number BAA1961), and in the ubiquitous kinesin heavy chain (UKHC, Accession number Q61768). This result again raises the intriguing possibility that mATX3 might be a MAP with properties similar to those of motor proteins, particularly proteins involved in chromosome segregation during cell division.

mATX3 interacts with Twa1, a member of the CTLH complex

One of the prey proteins isolated in the y2h library screenings for mATX3 interactors described in Chapter 4.1 was Twa1, a RanBPM interacting protein that is a member of the CTLH complex. Several evidences suggest an involvement of the CTLH complex in microtubule dynamics, nucleokinesis, chromosome segregation, cell migration and cell adhesion. Twa1 was isolated five times in one screening of an 11-day mouse embryo y2h library. We have further confirmed this mATX3/ Twa1 interaction by y2h co-transformation and mating assays (Chapter 4.1). However, this interaction must still be confirmed by other techniques namely GST pull-down, using the plasmids described in Chapter 4.1, co-immunoprecipitation, and co-localisation. Mouse Twa1 (mTwa1) is 99.56% identical to the human TWA1 (hTwa1) differing only in one residue (Figure 4.3.8). Its characteristic LisH and CTLH motifs are localised in the N-terminal of the protein (Figure 4.3.8). Interestingly, the interaction region of mTwa1 with mATX3 did not overlap with the abovementioned domains, corresponding to the last 66 C-terminal amino acids [aa163-228] (Figure 4.3.8), which could suggest non-exclusive binding of mATX3 and RanBPM to Twa1, potentially for regulation of microtubule nucleation.

mATX3 may interact with Kif2c

The mouse homologue of MCAK (Kif2c) was another of the proteins isolated in the

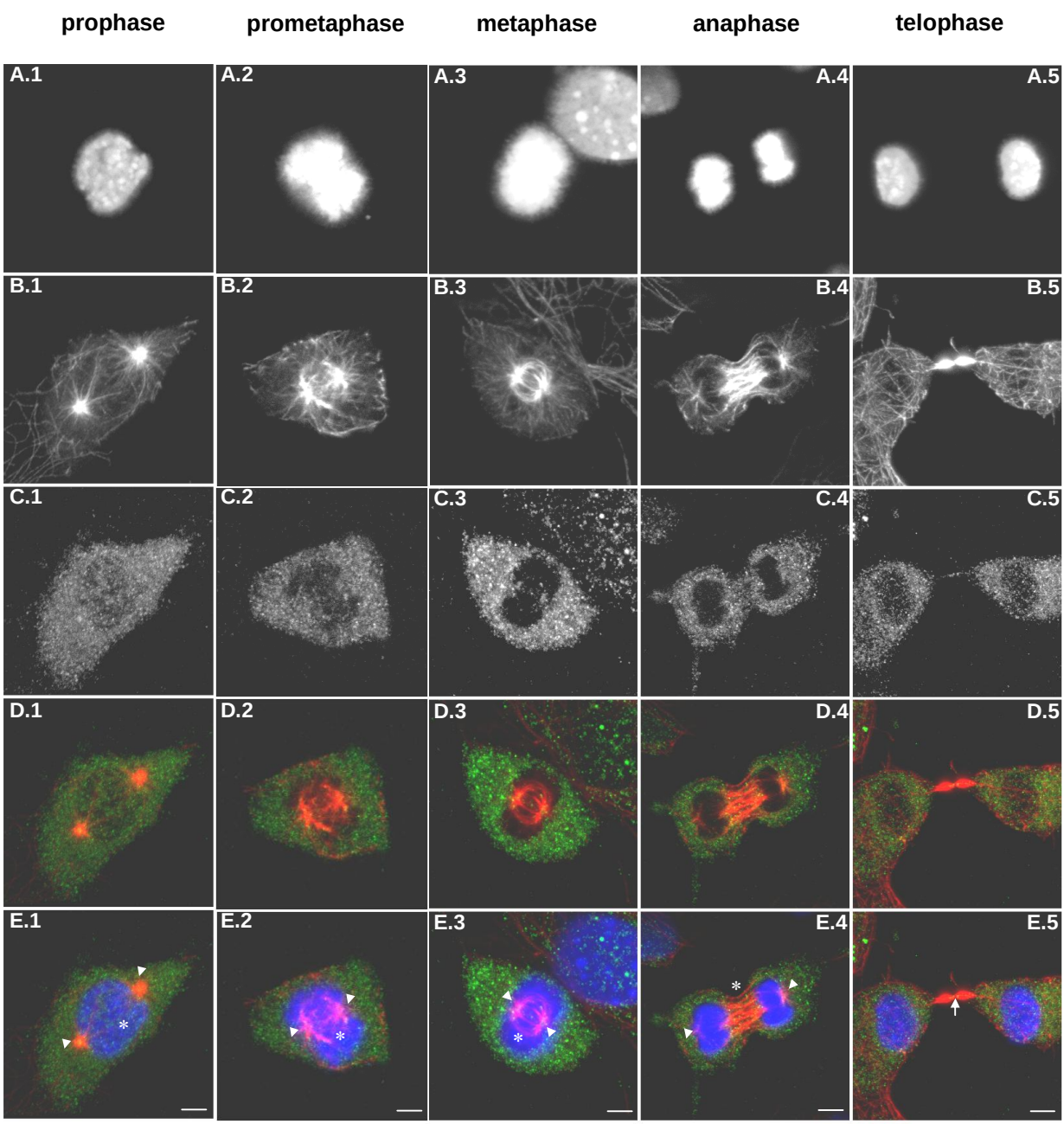

Figure 4.3.6. Mouse ataxin-3 co-localises with microtubules during mitosis. Confocal optical z-series images of double immunofluorescence staining for α-tubulin (red, B) and mATX3 (green, C) of 3T3 cells fixed with methanol; DNA was labelled with DAPi (blue, A). Merged stainings are shown in D and E. In all the mitotic stages (1-5) mATX3 seems to be associated with microtubules. Arrowheads indicate the centrosomes, asterisk the mitotic spindle and arrow the midbody. Scale bar represent 5 μm.

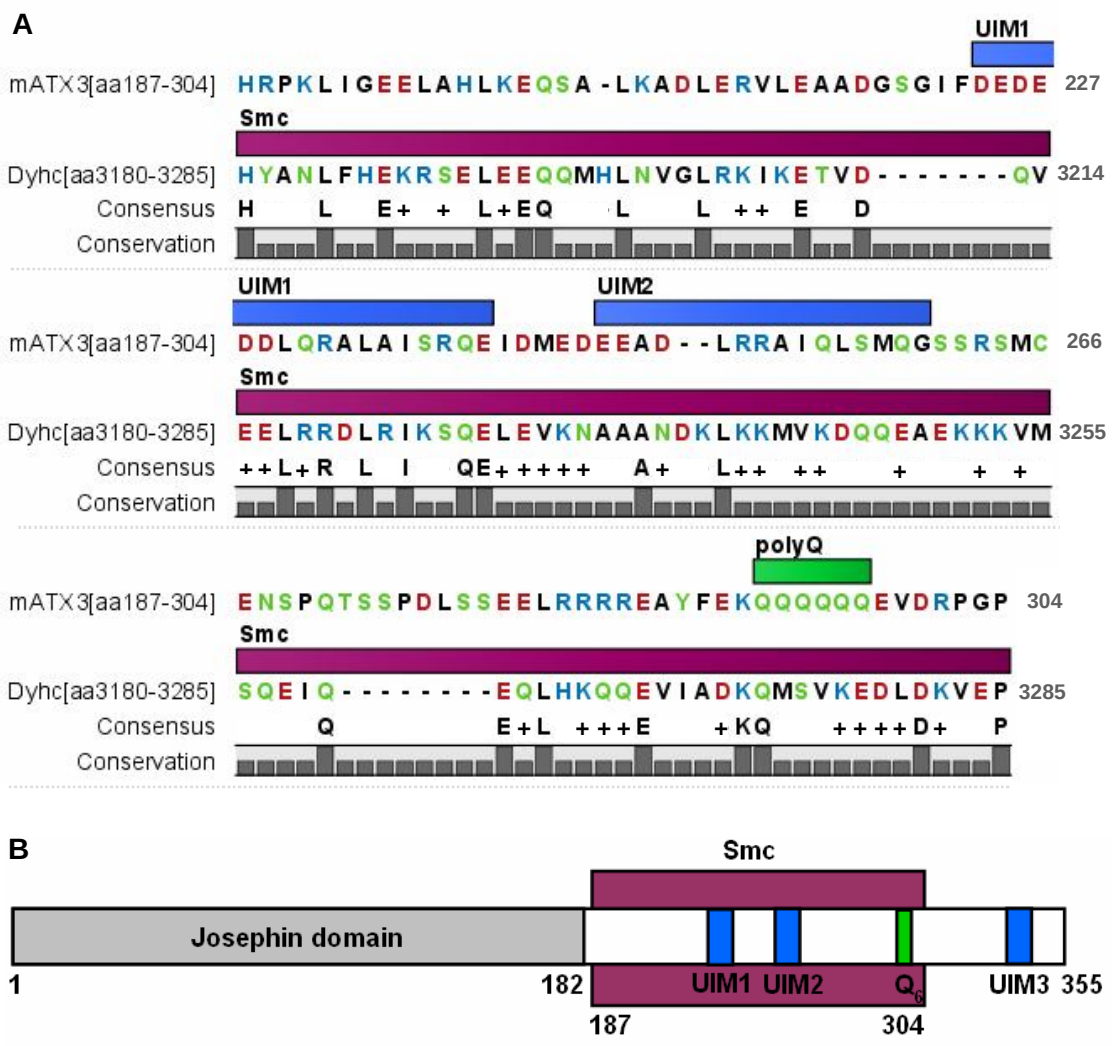

Figure 4.3.7. Mouse ataxin-3 contains a putative Smc domain. A) Alignment of the mATX3 (Accession number NP_083981) with Dyhc (Accession number Q9JHU4). The UIM1 and UIM2 domains and the polyQ repeat are represented over the mATX3 sequence (blue and green, respectively), as well as the Smc domain in Dyhc sequence (purple). The identical residues between the two sequences are represented by their respective symbols and the residues presenting similar chemical properties are symbolised by (+). Residues gaps are showed as (-). B) Schematic representation of the known mATX3 domains and the relative position of the potential Smc domain [aa187-304]. The alignment was adapted from the one performed using the CLC combined workbench 3.5.1 software.

y2h library screenings for mATX3 interactors, described in Chapter 4.1. A Kif2c cDNA fusion clone was found once in the screening of the mouse testis y2h library. The mATX3/ Kif2c interaction must still be confirmed by y2h and GST pull-down assays using the plasmids described in Chapter 4.1. The interaction region of Kif2c with mATX3 was found to be the last C-terminal 77 residues [aa645-721], which does not overlap with the kinesin motor

Figure 4.3.8. Mouse ataxin-3 interacts with the C-terminal of Twa1. Alignment of the mouse Twa1 (mTwa1, Accession number NP_083883) and human TWA1 (hTwa1, Accession number NP_060366) sequences. The LisH and CTLH motifs, as well as the interaction region with mATX3 are indicated by coloured boxes over the sequence alignment. The alignment was adapted from the one performed using the CLC combined workbench 3.5.1 software.

domain. In order to assess mATX3/ Kif2c interaction *in vivo*, we have performed immunofluorescence double staining for mATX3 and Kif2c in 3T3 cells fixed with paraformaldehyde (Figure 4.3.9). In this preliminary study, we have verified that mATX3 and Kif2c co-localised in high density microtubule spindle regions such as the poles and midbody (Figure 4.3.9 and data not shown). Nevertheless, further co-localisation should be performed in the future covering all the mitotic stages.

4.3.5. DISCUSSION

The characterisation of the expression pattern of mATX3 revealed that this protein is highly expressed in all types of muscles, in cilia and spermatozoid flagella (Costa et al. 2004). This finding together with the fact that ATX3 was shown to immunoprecipitate with tubulin (Zhong and Pittman 2006) led us to search for a potential role of mATX3 in the cytoskeleton, namely in microtubules.

We have shown that the endogenous proteins mATX3 and α-tubulin co-immunoprecipitated from whole protein extracts of 3T3 cells, suggesting that these two

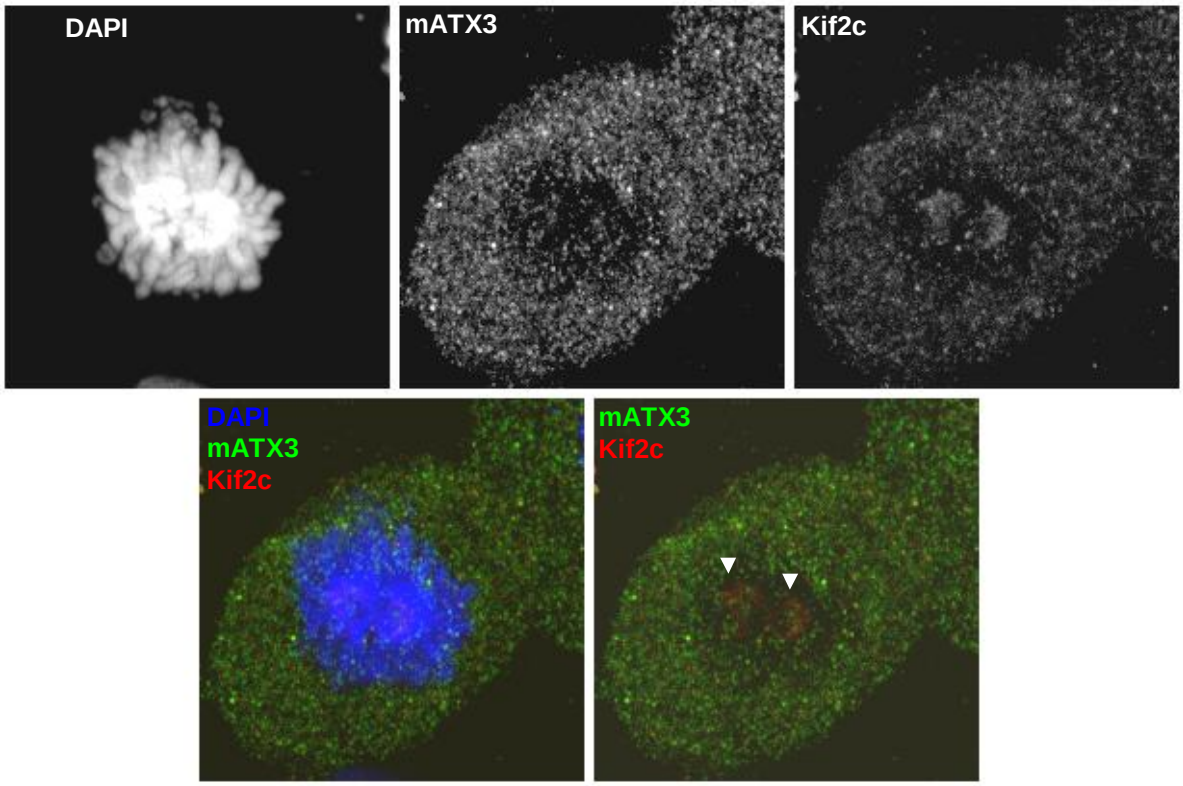

Figure 4.3.9. Mouse ataxin-3 co-localises partially with Kif2c in the spindle region of prometaphase cells. Confocal optical z-series images of double immunofluorescence staining for Kif2c (red), and mATX3 (green) of 3T3 cells. DNA was labelled with DAPI (blue). mATX3 seems to be localised at the kinetochores labelled by Kif2c. Kinetochores are pointed by arrowheads.

proteins interact with each other or that mATX3 might be a MAP. To study the potential association of mATX3 with microtubules, we have chosen the fibroblast 3T3 line since these cells have a large size and a flat morphology that allows a good visualisation of their microtubular network at the periphery.

Double immunofluorescence assays for mATX3 and α-tubulin were performed to determine their co-localization. In interphasic cells, mATX3 showed a widely distributed pattern with a higher expression in the perinuclear region, co-localising only partially with microtubules. Moreover, mATX3 did not co-localise with γ-tubulin at the centrosome, suggesting that mATX3 did not interact with tubulins in general, but specifically with the structural components of microtubules, in this case α-tubulin. If confirmed to be a MAP, ATX3 could participate in one or more microtubule associated cellular processes: transport, structure maintenance, cell division, among others. In fact, mAT3 was also shown in Chapter 4.1 to interact with the adaptin Ap3b1, a subunit of the AP-3 complex that is involved in

vesicle transport (Yang et al. 2000). A perinuclear localisation and (a more obvious) association with microtubules was also observed for huntingtin, another polyQ-containing protein (Hoffner et al. 2002). In the case of huntingtin, both normal and expanded polyQ proteins bound to microtubules with the same affinity suggesting that the expansion did not alter this association (Hoffner et al. 2002). It will be interesting to compare the affinity of normal and expanded ATX3 to microtubules in the future.

Interestingly, we found an accumulation of mATX3 around the microtubule organising centers both in interphase and mitosis. In addition, we observed mATX3 to be highly expressed during mitosis, and to co-localise particularly with regions of high microtubule density such as the poles and midbody. Therefore, whether through its DUB or deneddylase activities, or through any other yet unknown function, mATX3 may be related to microtubules, namely microtubule dynamics, which is a very important process during mitosis (Walker et al. 1988).

Furthermore, searching for conserved protein domains between mATX3 and other proteins we have found that the region comprised by residues 187-304 showed homology with a region of Dyhc corresponding to a domain highly conserved in SMCs. SMC proteins are highly evolutionary conserved and regulate the structural and functional organisation of chromosomes from bacteria to humans (Hirano 2006). These proteins have crucial roles in chromosome segregation (during meiosis and mitosis), chromosome-wide gene regulation and recombinational repair (Hirano 2006). Furthermore, the analysis of conserved domains, at the NCBI URL, revealed that not only dynein, but classical myosins and kinesins also carry a Smc domain. The existence of a putative Smc domain in mATX3, similarly to other microtubule motor proteins, further suggests a possible role of mATX3 in mitosis. In addition, very recently it was shown that some SMC proteins are neddylation targets by Nedd8 binding, which lead us to speculate that SMCs could be substrates of the mATX3 deneddylase activity.

Additionally, in the y2h library screenings for mATX3 interactors we have found, and confirmed, that Twa1 was one of the molecular partners of mATX3 (Chapter 4.1). Twa1 (Two hybrid Associated protein 1), a LisH-CTLH-containing protein, was found in an y2h library screening for RanBPM interactors (Adams et al. 1998). Proteins containing LisH-CTLH motifs are implicated in microtubule dynamics, cell migration, nucleokinesis, and chromosome segregation (Emes and Ponting 2001). Recently, it was shown that Twa1 in conjunction with RanBPM and other proteins (muskelin, p44CTLH, p48EMLP, ARMC8α, and ARMC8β), comprised a complex named CTLH that most probably might be involved in the abovementioned processes (Kobayashi et al. 2007). In addition, RanBPM, that plays an important role in microtubule nucleation, is known to be regulated by the UPS and was also

shown to be a target of the DUB USP11 (Ideguchi et al. 2002). These evidences suggest that mATX3 might also regulate the CTLH complex through interaction with Twa1.

Of great interest was also the finding of Ki2c as a potential interactor of mATX3 (Chapter 4.1). Kif2c is a well known microtubule destabiliser (Tirnauer et al. 2002), very important during cell division, being also implicated in chromosome segregation and in the correction of improper kinetochore-microtubule interactions. Here we have shown that mATX3 co-localised partially with Kif2c in the mitotic spindle, although further studies should be performed to confirm this interaction. Since Kif2c seems to be regulated by the UPS (Peters 2002), we may speculate that it could also be a substrate of the mATX3 DUB activity, which in turn could be regulating its levels during mitosis.

In conclusion, here we provided the first evidences that mATX3 might associate with microtubules during mitosis. We have also found a potential Smc domain in mATX3, and described the interaction of this protein with a member of the CTLH complex (Twa1), and potentially also with Kif2c, both involved in microtubule dynamics and chromosome segregation. We raise the hypothesis that mATX3 might be involved in these cellular events. Further work will be required to explore this hypothesis. The interactions of mATX3 with Twa1 and Kif2c should be confirmed. The knockdown of mATX3 in 3T3 cells by siRNA, for instances, would allow: (1) to observe the effect of the absence of mATX3 in microtubule assembly using immunofluorescence analysis; (2) to determine if Twa1 and Kif2c are substrates of the mATX3 DUB activity for UPS degradation, measuring their protein levels by immunoblotting; (3) to verify the localisation of Twa1 and Kif2c by immunofluorescence in order to test the hypothesis that mATX3 might be important for their localisation.

Chapter 4.4

Ataxin-3 in sarcomeres

4.4.1. SUMMARY

Mouse ataxin-3 is highly expressed in all types of muscles since the embryonic developmental stages. At the subcellular level, mATX3 is widely distributed throughout the skeletal muscle. Here we aimed to determine in which sarcomeric bands (A or I) mATX3 was preferentially expressed, and to test the potential interaction of mATX3 with some sarcomeric proteins.

Our results show that mATX3 is equally distributed by the sarcomeric thin (I) and thick (A) bands. The selected group of sarcomeric proteins to test for mATX3 interaction comprised the proteins: Tnni1, Tnni2, Acta1, and Myh2. All these proteins were shown to interact directly with mATX3 in y2h assays, suggesting that ATX3 may have an important role in the regulation of the sarcomeric structure, or in the muscle cell contraction. Further experiments should be performed in order to clarify whether these proteins are targets of mATX3 DUB activity.

4.4.2. INTRODUCTION

Striated muscle function is highly dependent on specific interactions and alignment of complex cytoskeleton networks. The basic contractile units of myofibrils are the sarcomeres, which consist in highly regular arrays of the contractile proteins myosin and actin, and of other regulatory proteins (Trinick 1994; Gautel et al. 1999; Sanger et al. 2000). In sarcomeres contraction is driven by the thin actin-containing filaments that are anchored in the Z-lines and are prolonged toward the centre of the sarcomere, the M-line, the point where they interact with the thick myosin-containing filaments (Figure 4.4.1). The sarcomeres contain a third filament system composed by individual giant molecules of titin that span half of a sarcomere, with their N-termini overlapping in the Z-lines and their C-termini overlapping in the M-lines (Obermann et al. 1996; Mues et al. 1998) (Figure 4.4.1). Other cytoskeleton arrays, such as intermediate filaments and microtubules, play important role in the sarcomeric arrangement, but their function in muscle morphogenesis is poorly understood.

In mammals there are six actin isoforms that are expressed in a tissue-specific way. Two sarcomeric actins, α-skeletal (ACTA1) and α-cardiac actin, are co-expressed in the striated muscles (Vandekerckhove et al. 1986). Muscle contraction is driven by the interaction between myosin and actin, and the energy required is provided by the hydrolysis of ATP carried out by myosin during this process.

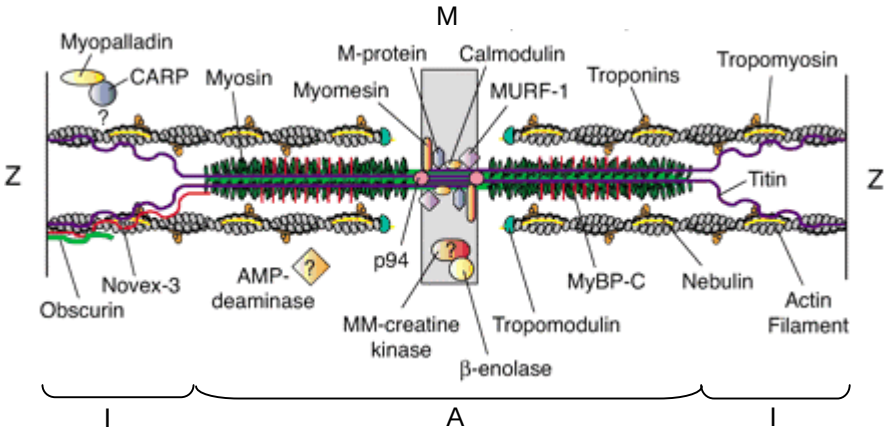

Figure 4.4.1. Schematic representation of a sarcomere showing its protein components. A, A-band; I, I-band; M, M-line; Z, Z-line (*Adapted from Ingraham P, 2006*).

Myosins are actin-based motors that play essential functions in several cellular processes (Berg et al. 2001). The myofibrillar myosins of striated muscles belong to the class II (Berg et al. 2001) and are heterohexamers consisting of two myosin heavy chains (MyHC) and two pairs of myosin light chains (MyLC). In mammalian species, nine MyHC isoforms are known, three of them being expressed in adult fast skeletal fibers: MYH2, MYH1, and MYH4.

In vertebrates, sarcomere contraction is controlled by the troponin complex and by tropomyosin that constitute the Ca^{2+}-sensitive core. The troponin complex is located in the thin filament and is composed of three members: troponin I (TnnI), troponin C (TnnC), and troponin T (TnnT). In the skeletal muscle, two TnnI isoforms, slow-TnnI1 and fast-TnnI2, are expressed in slow and fast myofibers, respectively (Koppe et al. 1989).

Other examples of sarcomeric components are the muscle-specific RING finger proteins (MURFs) that are expressed in both the cardiac and skeletal muscle. There are three known MURFs: MURF-1, MURF-2, and MURF-3 (Centner et al. 2001). MURF-1 is localised exclusively in the M-line interacting also with titin, MURF-3 localises in microtubules, and MURF-2 colocalises with both the other MURFs linking potentially their functions (McElhinny et al. 2002; Pizon et al. 2002; McElhinny et al. 2004; Witt et al. 2005).

Skeletal muscle is a very adjustable tissue, responding effectively to altered mechanical or metabolic conditions. These adaptations can lead to gain (hypertrophy) or loss (atrophy) of muscle mass. Muscle wasting, or atrophy, results of an imbalance between protein synthesis and degradation that leads to a loss of myofibrillar proteins. The UPS was shown to play an important role in the regulation of proteolysis in these conditions, as well as

in the normal maintenance of the muscle structure (Attaix et al. 2005). Particularly, in muscle wasting models, several UPS components were shown to be upregulated at the mRNA level. These included ubiquitin, E2 ligases, proteasome subunits (20S and 19S), deubiquitinating enzymes and E3 ligases (Price 2003; Attaix et al. 2005; Combaret et al. 2005; Wing 2005). However, the corresponding UPS proteins were not significantly altered in muscle wasting. This might be explained by a potential compensation of the increased synthesis of these proteins by an accelerated turnover under the observed conditions (Nury et al. 2007). Interestingly, the *Mjd* gene, encoding mATX3 that possess DUB activity *in vitro* (Chapter 2), was also upregulated in the skeletal muscle of starved mice (Chapter 3).

The myofibrillar components are the major proteins in muscle, and although monomeric actin, myosin, troponin, and tropomyosin can be degraded by the UPS, this does not occur in intact myofibers since specific protein interactions between these proteins protect them from degradation by this system (Solomon and Goldberg 1996). Therefore, myofibers must be firstly dissociated by non-UPS proteases such as calpains (Bartoli and Richard 2005), caspase 3 (Du et al. 2004), and cathepsin L (Deval et al. 2001).

Although, in general, the substrates of the UPS are poorly characterised, some protein targets are known. Specifically, two E3 ubiquitin ligases, SCF^{MAFbx} and MURF-1, that were upregulated in most muscle wasting models, interact with and possibly mediate the ubiquitination of several myofibrillar proteins (Li et al. 2004; Witt et al. 2005). SCF^{MAFbx} mediates the degradation of calcineurin A (Li et al. 2004) and of MyoD (Tintignac et al. 2005). MURF-1 and MURF-2 interact with eight myofibrillar proteins (titin, nebulin, the nebulin-related protein NRAP, TnnI, TnnT, myosin light chain 2 (MLC-2), myotilin, and T-cap), TnnI and MLC-2 being potential targets of MURF-1 mediated ubiquitination (Witt et al. 2005). Interestingly, in *C. elegans* it was shown that myosin assembly in muscle thick-filament formation is mediated by the molecular chaperone UNC-45 (Landsverk et al. 2007). UNC-45 protein levels are in turn regulated by the E3 ubiquitin ligase complex CDC-48(p97)/UFD2/CHN-1(CHIP) linking UNC-45 to functional muscle formation (Janiesch et al. 2007). In addition, the DUB USP25 was shown to interact with the sarcomeric proteins α-actin 1 (ACTA1), filamin C (FLNC), and myosin binding protein C1 (MyBPC1), MyBPC1 being a potential substrate of USP25 (Bosch-Comas et al. 2006).

The fact that mATX3 is highly expressed in muscle (Costa MC et al. 2004), that it seems to be widely distributed trough the skeletal muscle sarcomeres and it presents DUB activity (Chapter 2), and that human ATX3 interacts with the E3 ubiquitin ligases VCP/p97, UBE4B (UFD2), and CHIP (Hirabayashi M et al. 2001; Matsumoto M et al. 2004; Jana NR et al. 2005) which seem to be involved in myosin assembly (Janiesch et al. 2007), led us to test the hypothesis of interaction of mATX3 with a group of sarcomeric proteins: Tnni1, Tnni2, Acta1, myosin heavy polypeptide 2 (Myh2).

4.4.3. MATERIALS AND METHODS

Ultrastructural analysis and immunogold electron microscopy

Six adult male C57Bl/6 mice with 12-13 weeks of age were anesthetised and perfused transcardially with PBS followed by a fixative solution (4% paraformaldehyde in PBS, pH 7,3) during 15 min. Quadricep fragments were fixed 4% glutaraldehyde in 0,2M sodium cacodilate buffer (pH 7,3) overnight (at 4 ºC), postfixed in 1% osmium tetroxhyde in 0,2M sodium cacodilate buffer (pH 7,3) overnight, dehydrated through a graded ethanol series followed by an incubation in propylene oxide (10 min), and embedded in Epon 812 resin at 60 ºC, during 24 hours. Ultrathin sections (~60 nm) were made from the tissue fragments and mounted in nickel grids. For immunogold labelling of endogenous mouse ataxin-3, sections on grids were exposed to a saturated aqueous solution of sodium metaperiodate for 30 min, washed in PBS (10 min), incubated in 1% bovine serum albumin (BSA)/ PBS during 30 min, incubated with the antibody anti-humanATX3 (anti-hATX3) antiserum diluted 1:30 in 1% BSA/ PBS during 3 hours at 37ºC, and 1 hour at room temperature, washed 4 times in 1%BSA/ PBS, floated in 10 nm gold labelled goat anti-rabbit IgG(H+L) (RPN421V, Amersham Biosciences) diluted 1:15 in 1%BSA/ PBS for 45 min at room temperature, and washed 4 times in 1% BSA/PBS and a last one in distilled water. Sections were stained with uranyl acetate (5 min) and then with lead citrate (4 min). For negative controls, reactions with the primary antibody preadsorbed with the recombinant His tagged mATX3 protein, and without the primary antibody were used. Ultrathin immunogold labelled sections were visualised in transmission electron microscopes (EM10C and EM902A, Zeiss).

Yeast strains and culture medium

The *Saccharomyces cerevisiae* strains used in the yeast two-hybrid system assays (GAL4 2H-2) were Y190 and Y187 (Harper et al. 1993).

The genotype of the Y190 strain is *MATa*, *ura3-52*, *his3-200*, *ade2-101*, *lys2-801*, *trp1-901*, *leu2-3*, *112*, *gal4Δ*, *gal80Δ*, *cyh^{r}2*, *MEL1*, *LYS2::GAL1$_{UAS}$-HIS3$_{TATA}$-HIS3*, *URA3::GAL1$_{UAS}$- GAL1$_{TATA}$-lacZ*. This strain contains two reporter genes (*HIS3* and *lacZ*), each regulated by a different GAL4-dependent promoter to reduce the incidence of background. The *HIS3* reporter is under the control of the *GAL1$_{UAS}$*, and a minimal promoter containing both *HIS3* TATA boxes, TR (regulated) and TC (constitutive). The *lacZ* reporter is regulated by the intact *GAL1* promoter, including the *GAL1$_{UAS}$* and the *GAL1* minimal

promoter.The genotype of the Y187 strain is *MAT*α, *ura3-52*, *his3-200*, *ade2-101*, *trp1-901*, *leu2-3*, *112*, *gal4*Δ, *met*$^-$, *gal80*Δ, *MEL1*, *URA3::GAL1*$_{UAS}$- *GAL1*$_{TATA}$-*lacZ*. This yeast strain possesses only the *lacZ* reporter gene above described.

Complete medium (YPAD) and selection medium (SD) used for yeast growth and manipulation were prepared as described in the Yeast Protocols Handbook (Clontech). The base of SD (SD-WLH) was prepared with all amino acids except tryptophan (W), leucine (L) and histidine (H). These nutrients were added separately depending on the necessary selection medium. The background expression of IGP dehydratase (*HIS3* product), in the Y190 yeast strain, was controlled by including 90 mM of 3-AT (Sigma) in the medium.

Yeast two-hybrid constructs

The bait plasmid used in the co-transformation and mating assays was pGBT9Mjd. This construct, expressing the GAL4BD::mATX3 fusion protein (GAL4BD N-terminal to the full-length of mATX3) (Chapter 4.1) has a *TRP1* gene that allows auxotrophic yeasts to grow in media lacking tryptophan (SD-W).

Total RNA was isolated from adult C57Bl/6 mouse skeletal muscle, using Trizol reagent (Invitrogen Life Technologies). Total RNA (2.5 μg) was used to perform reverse transcription using the SuperScript^{TM} First-Strand Synthesis System for RT-PCR (Invitrogen Life Technologies) with an oligo(dT) primer. The coding sequences encoding the entire Tnni1, Tnni2, and Acta1, or the partial fragment of Myh2[aa88-773] were amplified in frame by RT-PCR using the pair of primers including the 5' (attB1) and 3' (attB2) attB site-specific recombination sequences (Gateway Cloning System) attB1Tnni1/ attB2Tnni1 (625 bp), attB1Tnni2/ attB2Tnni2 (610 bp), attB1Acta1/ attB2Acta1 (1195 bp) or attB1Myh2[88]/ attB2Myh2[773] (2119 bp) (Appendix 1, Table A.2), and 1 μL of total cDNA from mouse skeletal muscle or of the plasmid pCMV-SPORT6-Myh2 (Open Biosystems) in the specific case of Myh2.

For PCR products smaller than 700 bp, PCRs were performed using the enzyme Taq DNA Polymerase (Fermentas) under the following conditions: one cycle of 5 min at 95°C, followed by 35 cycles of one min at 95°C, one min at 55°C, one min at 72°C, and ending with 5 min at 72°C. To amplify PCR products higher than 700 bp the enzyme BIO-X-ACT-LONG (Bioline) was used in the conditions: one cycle of 5 min at 95°C, followed by 35 cycles of one min at 95°C, one min at 55°C, three min at 68°C, and ending with 15 min at 68°C.

The RT-PCR products were purified from 1% agarose gels using the GFX^{TM} PCR DNA and Gel Band Purification Kit (Amersham Pharmacia Biotech) or the QIAQuick Gel

Extraction kit (Qiagen) and cloned in the pDONR207 vector using the Gateway Cloning System (Invitrogen Life Technologies), using the manufacturer instructions.

The y2h prey constructs were obtained by recombination of a Gateway version of the pGAD424 vector (provided by RZPD) with the corresponding pDONR207Tnni1, pDONR207Tnni2, pDONR207Acta1, and pDONR207Myh2[aa88-773] plasmids, using the Gateway Cloning System (Invitrogen Life Technologies). Prey coding sequences were introduced in the pGAD424 vector in frame with the GAL4AD coding sequence. These y2h prey constructs pGADTnni1, pGADTnni2, pGADActa1, and pGADMyh2[a88-773] (Table 4.4.1) have a *LEU2* gene that allows auxotrophic yeasts to grow in media lacking leucine.

Each construct was confirmed by automated sequencing using primers GAL4AD-F and GAL4AD-R, and in the case of pGADMyh2[88-773] with primers Myh2(1), and Myh2(2) (Appendix 1, Table A.1) to verify the correct in frame cloning, and tested for their toxicity in yeast and for self-activation of the two reporter genes, *HIS3* and *lacZ*.

GST::prey expressing constructs

Recombinant glutathione-S-transferase (GST)-tag prey protein expression plasmids were obtained by recombination of the corresponding pDONR207 plasmids with the pDEST15 vector using the Gateway Cloning System (Invitrogen) in order to obtain the constructs pDEST15Tnni1, pDEST15Tnni2, pDEST15Acta1, and pDEST15Myh2[aa88-773] (Table 4.4.1).

Table 4.4.1. GAL4AD::prey and GST::prey expressing constructs

candidate protein	vector	fusion protein
Tnni1	pGADTnni1	GAL4AD::Tnni1
	pDEST15Tnni1	GST::Tnni1
Tnni2	pGADTnni2	GAL4AD::Tnni2
	pDEST15Tnni2	GST::Tnni2
Acta1	pGADActa1	GAL4AD::Acta1
	pDEST15Acta1	GST::Acta1
Myh2[aa88-773]	pGADMyh2[aa88-773]	GAL4AD::Myh2[88-773]
	pDEST15Myh2[aa88-773]	GST::Myh2[88-773]

Yeast transformation

All yeast transformations were performed using the high efficiency lithium acetate

method (Gietz et al. 1995). Y190 and Y187 strains without plasmids were grown in YPAD medium overnight at 30ºC, at 200 rpm, while pretransformed strains were grown in the appropriate SD medium to keep selective pressure of the plasmid. Overnight cultures were diluted in the respective medium to a cell density of 0.3 at 600 nm, and then incubated at 30ºC, at 200 rpm, until reached at an optical density (OD) of 0.6 at 600 nm. Cells were harvested by centrifugation at 1800 rpm for 5 min, first washed with sterile water and then with fresh made 100 mM LiAc. The following components were added to yeast pellets by order: 240 μL PEG (50% w/v), 36 μL 1M LiAc, 25 μL denatured salmon sperm DNA (2mg/mg), and 50 μL plasmid (1 μg) diluted in sterile water. Each tube was vortexed vigorously until the cell pellet was completely ressuspended, and then cells were incubated at 30 ºC during 30 min. Yeast cells where subsequently heat-shocked at 42ºC for 20 min. Finally, cells were centrifuged one min at 3000 rpm, and ressuspended in 1 mL of YPAD. A volume of 20 μL of the transformed yeast culture was plated onto the appropriated selective medium, and plates were incubated at 30ºC during five days.

Yeast mating

Yeast mating assays were performed using a previously described method (Bendixen et al. 1994). Briefly, one fresh yeast colony from each of the two mating types was used to inoculate 500 μL of YPAD, vortexed, and then incubated overnight at 30ºC, at 200 rpm. In the day after, 20 μL of the mating culture were spread in SD-WLH to select diploids, and in SD-WLH 30 mM 3-AT plates to select diploids with a positive two-hybrid interaction, after an incubation period of five days at 30ºC.

β-Galactosidase (β-gal) colony-lift filter assay

The β-galactosidase expression test was performed by colony-lift filter assay (Breeden and Nasmyth 1985). The assay was either performed directly on fresh plates with single colonies or with dots of yeast transformants grown on the specific selective medium supplemented with 90 mM or 30 mM of 3-AT, for co-transformation or mating assays, respectively. A nylon membrane (Hybond-N, GE Healthcare) was placed over the surface of the plate containing the yeast cells to be assayed. When the membrane was uniformly wet, it was lifted and submerged in liquid nitrogen for 10 seconds to allow cell permeabilisation. After that, the membrane was thawed at room temperature and placed, with colony side up, on a Petri dish containing a filter paper pre-soaked in Z buffer (16.1 mg/mL $Na_2HPO_4.7H_2O$, 5.5 mg/mL $NaH_2PO_4.H_2O$, 0.75 mg/mL KCl, 0.246 mg/mL Mg_2SO_4, pH 7.0), supplemented

with 1 mg/mL X-Gal (5-bromo-4-chloro-3indolyl-β-D-galactopyranoside) and 38.6 mM β-ME (β-mercaptoethanol). Filters were incubated 1-12 hours at 30ºC, and then analysed for the presence of blue colonies (*lacZ* positive transformants)

Statistical analysis

The immunogold particles corresponding to mATX3 were counted in one sarcomeric band A and I in 20 photographs of different randomly chosen regions of skeletal muscle ultrathin slices per mouse, using the Stereo Investigator 4.34 software. The number of immunogold dots/ band area was compared between both bands A and I using the t-test, which was calculated using the SPSS version 14.0 package. A significant value of $P< 0.05$ was considered.

4.4.4. RESULTS

Mouse ataxin-3 is widely distributed by the sarcomeric myosin and actin-rich bands

We have previously characterised the subcellular localisation of mATX3 in the skeletal muscle using immunoelectron microscopy (Chapter 2) and verified that mATX3 was widely distributed through all the cellular structures and also in sarcomeres. In order to evaluate if mATX3 was preferentially associated with myosin or actin-rich bands in the sarcomeres, we have counted the number of immunogold particles corresponding to mATX3 in one band A (myosin-rich) and one band I (actin-rich) in 20 photographs of different regions of skeletal muscle sarcomeres per mouse (n=6) (Figure 4.4.1A). No differences in the number of immunogold dots/ band area between the bands A and I were found (Figure 4.4.1B). This result suggests that mATX3 might be equally associated with both myosin and actin-rich bands.

mATX3 interacts with four sarcomeric proteins: Tnni1, Tnni2, Acta1, and Myh2

Given that mATX3 was shown to be widely distributed through the sarcomere, we have tested the direct interaction of mATX3 with four sarcomeric proteins: Tnni1, Tnni2, α-skeletal actin 1 (Acta1), and myosin heavy chain polypeptide 2 (Myh2). For that, we have cloned the entire cDNA coding sequence of mouse Tnni1, Tnni2 and Acta1, and a partial

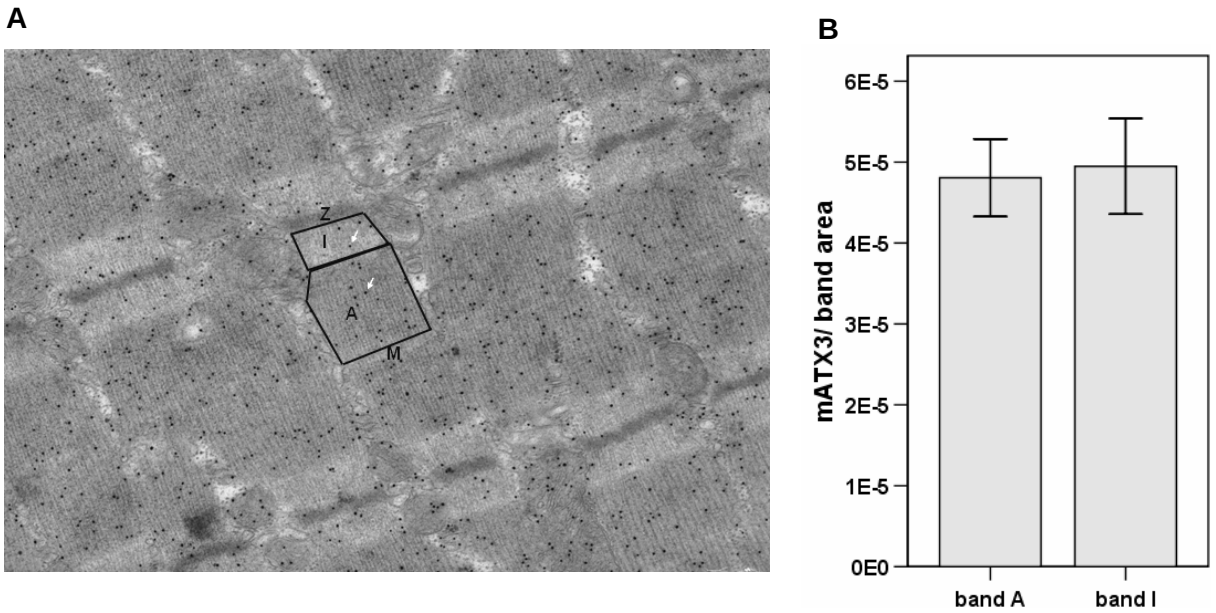

Figure 4.4.1. Mouse ataxin-3 is widely distributed by the sarcomeric bands. A) Immunoelectron microscopy photograph corresponding to the immunogold labelling of mAtX3 (black dots pointed by white arrows) in the sarcomeres showing the limits of bands A and I used in the countings. B) Counting of the immunogold dots per band area in bands A and I. The results correspond to the mean of the counting in 20 photographs per mouse (n=6) ± SEM (error bars).

region of Myh2 [aa88-773] into the pGAD vector. These y2h plasmids expressed the fusion proteins GAL4AD::Tnni1, GAL4AD::Tnni2, GAL4AD::Acta1, and GAL4AD::Myh2[aa88-773] that were found to interact with GAL4BB::mATX3 in y2h co-transformation and mating assays (Figure 4.4.2 A,B). In particular, the myosin fragment chosen to test for interaction with mATX3 corresponded to the myosin motor domain present in all type II myosins. These proteins mediate cortical contraction in cell motility, and are the motors in smooth and skeletal muscle. Additional confirmation of these mATX3 interactions by GST-pull down assays is underway.

4.4.5. DISCUSSION

In spite of the long-known involvement of the UPS in the maintenance of the striated muscle structure or in muscular wasting and atrophy, only a small group of muscular UPS substrates are currently known. Since we have previously observed that mATX3 was widely distributed through the skeletal muscle fibers (Chapter 2), here we decided to quantify the distribution of mATX3 in the sarcomeric A and I–bands by immunoelectron microscopy, and

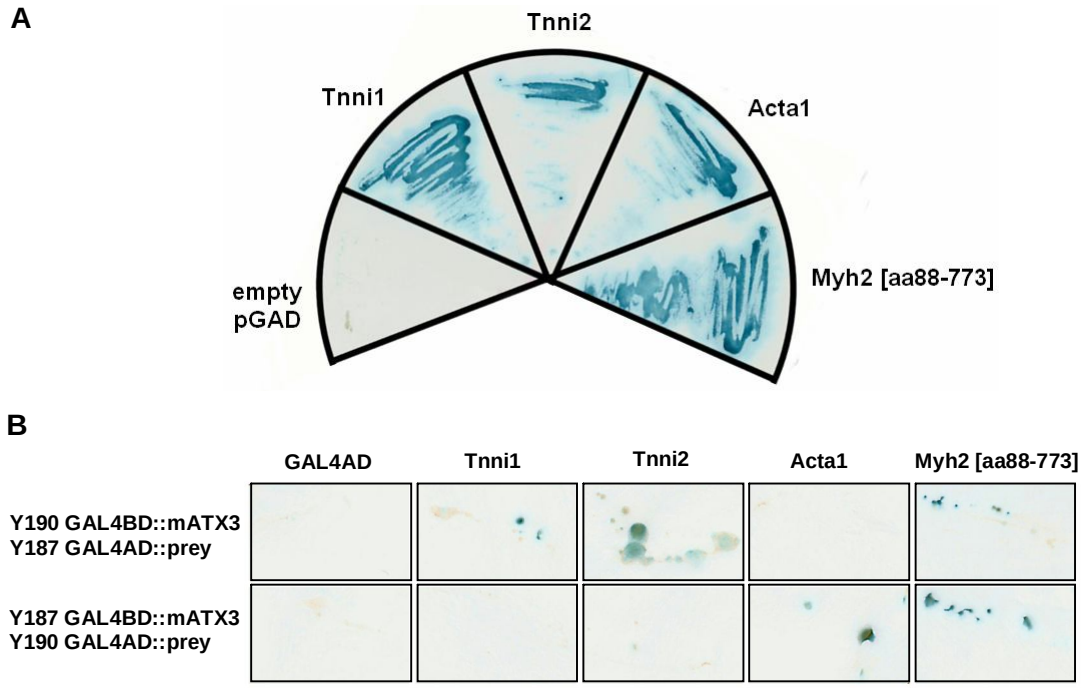

Figure 4.4.2. Mouse ataxin-3 interacts with the sarcomeric proteins Tnni1, Tnni2, Acta1, and Myh2. A) The interaction between the GAL4BD::mATX3 and each fusion GAL4AD::prey protein is shown by the blue colony streaks of the yeast cells co-transformed with both bait and prey plasmids, and plated in SD-WLH90mM3-AT. B) The protein interactions with mATX3 were additionally confirmed by yeast two-hybrid mating. The interaction between the GAL4BD::mATX3 and each fusion GAL4AD::prey protein is shown by the blue colonies of diploid cells, and plated in SD-WLH30mM3-AT. The positive signal of GAL4 reporter expression is the blue colour of the colonies after the β-gal activity assay. The empty GAL4AD expression vectors pGAD424 (GAL4AD, negative control) was co-transformed with the pGBT9Mjd plasmid (expressing GAL4BD::mATX3) or used in the mating assays, and streaks of these transformants were included in each testing plate to further be performed the β-gal colony-lift activity assay.

verified that this protein was equally distributed by these bands. This result indicates that mATX3 is present in both actin and myosin-rich bands and might be potentially associated to both of these myofibrillar proteins. Although some UPS components are known to present specific sarcomere localisation patterns, such as MURF-1 that is localised specifically in the M-line, other UPS proteins like MURF-2 present a ubiquitous distribution pattern, similar to that presented by mATX3 (McElhinny et al. 2002; Pizon et al. 2002 ; McElhinny et al. 2004).

DUBs play an important role in the UPS, however, similarly to the UPS as a whole, very few of their specific physiological substrates are known. Particularly in the sarcomeres, only USP25 and some of its potential substrates are better understood. In this study we have selected a group of sarcomeric proteins to test their interaction with mATX3. Interestingly, all

the proteins tested Tnni1, Tnni2, Acta1 and Myh2 were shown to interact with mATX3 in y2h assays. Further confirmation of these interactions is undergoing using GST-pull down assays. All these proteins have been shown to be degraded, in their monomeric state, by the UPS (Solomon and Goldberg 1996), so one could speculate that ATX3 could, as a DUB, play a role in the modulation of their degradation or maintenance. However, in order to test if these proteins are substrates of mATX3, the levels of these sarcomeric interactors should be evaluated in mATX3 knockdown and/or overexpression cellular extracts (ongoing work).

All these proteins that interact with mATX3 are structural components of sarcomeres (Acta1) or are essential players in muscle cell contraction (Tnni1, Tnni2, and Myh2). Among actin isoforms, Acta1 is the most prominent actin isoform expressed in differentiated adult skeletal muscle. As actins are highly conserved proteins, we can not exclude that mATX3 may also interact with other actins. In order to evaluate this, protein interaction assays should be performed using different actin isoforms, allowing for differences in the recognition and binding. Ataxin-3 is the second DUB known to interact with Acta1, since USP25 was also shown to be its partner (Bosch-Comas et al. 2006). Nevertheless, Acta1 did not prove to be a direct target of the DUB activity of USP25 (Bosch-Comas et al. 2006).

Interestingly, mATX3 also interacted with both the slow and fast-troponins I, Tnni1 and Tnni2, suggesting that mATX3 might be exerting its role in both slow and fast muscle fibers (Koppe et al. 1989). Furthermore, these interactions might suggest that mATX3 may act in the regulation of sarcomeric contraction since troponins I, in conjunction with tropomyosin, are the Ca^{2+}- sensitive centre that control contraction.

The interaction of mATX3 with the motor domain of Myh2 (aa 88-773) may further contribute to the hypothesis that mATX3 might be involved in muscle contraction. Myh2 is one of the three myosin class II isoforms expressed in fast adult skeletal fibers (Berg et al. 2001). Myosin II mediates cortical contraction in cell motility, and its catalytic (head) domain is a molecular motor, which utilizes ATP hydrolysis to generate directed movement toward the plus end along actin filaments (Berg et al. 2001). Myosins are actin-dependent molecular motors that play important roles not only in muscle contraction, but also in cell motility, and organelle transport.

Other hypothesis for the cellular relevance of this mATX3/myosin interaction might be that mATX3 could be a member of, or act in parallel with, the CDC-48(p97)/UFD2/CHN-1(CHIP) E3 ubiquitin ligase complex that in *C. elegans* regulates the levels of UNC45 (Janiesch et al. 2007), which in turn is the chaperone responsible for myosin assembly (Landsverk et al. 2007). This hypothesis is strengthened by the fact that human ATX3 interacts with all the members of the abovementioned E3 ubiquitin ligase complex (Hirabayashi M et al. 2001; Matsumoto M et al. 2004; Jana NR et al. 2005). In future

investigations, it will also be interesting to test the protein interaction of mATX3 with the homologue of UNC45 in the mouse.

Interestingly, very recently, in a proteomic study of neddylated (NEDD8-binding) proteins, several myosins (including Myh2) and actins (not Acta1, but for example alpha-cardiac actin) were shown to be neddylated (Jones et al. 2008). These evidences suggest that Myh2 and perhaps also Acta1 might be a substrate of deneddylation of mATX3.

In conclusion, here we added further potential knowledge to the functional role of UPS in skeletal muscle by the identification of four novel interactors of the DUB and deneddylase mATX3: Tnni1, Tnni2, Acta1, and Myh2. This opens the possibility that mATX3 might have a role in the regulation of the degradation levels of sarcomeric structural components, and/or of muscle cell contraction. Further experiments are required to confirm these interactions and to clarify if these novel molecular partners are substrates of mATX3.

Chapter 5

Role of ataxin-3 in muscle development

Chapter partially based on the manuscript in preparation:

Costa MC, Bajanca F, Rodrigues A-J, Tomé RJ, Macedo-Ribeiro S, Logarinho E, Maciel P. *Ataxin-3: a deubiquitinating role in myogenic differentiation through UPS regulation of α5 integrin subunit.*

5.1. SUMMARY

During myogenesis several transcription factors and numerous other proteins participating in the regulation of protein synthesis, degradation and assembly, are rapidly degraded by the UPS. Given a potential role of mATX3 in the UPS, and the previously observed high expression of this protein in muscle since early embryogenesis, we aimed to define its physiological role in muscle differentiation.

In fact, we have observed a high expression of mTX3 in the early myotome of E9.5 mouse embryos using immunofluorescence assays. In order to verify the role of mATX3 during muscle differentiation, we have knocked down mATX3 (using siRNA approaches) in C2C12 undifferentiated cells and determined the phenotypic and molecular effects of the absence of this protein upon induction of muscle differentiation. We have observed that the mATX3-depleted cells were misaligned, showed morphological changes (more round cells), continued to proliferate upon differentiation, and seemed to have a delay in muscle differentiation. The possible contribution to this phenotype of a deletion of other Josephin domain-containing proteins was excluded by measuring their corresponding transcript levels by quantitative real-time PCR.

Interestingly, we have observed a down-regulation of the α5 and α7 integrin subunit levels in cells lacking mATX3, by immunoblotting quantification and by immunofluorescence. The analysis of the expression curves of these proteins during the differentiation of the cells lacking mATX3 revealed that the α5 integrin subunit, in particular, showed a similar expression curve to that of mATX3. This, plus the fact that the α5 integrin subunit is known to be degraded by the UPS, and the interaction of this protein with mATX3 evidenced here by GST pull-down, suggested to us that this integrin subunit may be a substrate of the DUB activity of mATX3, which may be acting in its rescue from proteasomal degradation.

In order to further define the molecular effects of the absence of mATX3 in C2C12 cells, we have determined the proteomic profile of these cells before and after differentiation. The evaluation of this data suggest that mATX3 is involved in the regulation of the levels of intracellular, cell-surface and extracellular proteins involved in cytoskeleton assembly, cell cycle, protein synthesis/degradation and transcription repression. Furthermore, this experiment confirmed the effect of mATX3 depletion upon several molecules related to the integrin signaling pathway.

5.2. INTRODUCTION

Skeletal muscle in vertebrates originates from paraxial mesoderm that segment into somites on each side of the neural tube and notochord. The ventral part of the somite, the sclerotome, will give rise to the cartilage and bones of the vertebral column and ribs, while the dorsal region of the somite, the dermomyotome, will contribute to the dermis of the back , the myotome and limb myogenic precursor cells (MPCs) (Buckingham et al. 2003) (Figure 5.1). The dermomyotome can be divided into epaxial (adjacent to the neural tube and notochord) and hypaxial (ventral to notochord) parts. In mice, around the embryonic day E9.5 (Sporle 2001), MPCs from the hypaxial dermomyotome migrate and will form the limb muscles, whereas other MPCs from the dermomyotome delaminate and will originate the myotome under it and above the sclerotome (Gros et al. 2004). The myotome is a complex embryonic transitory structure that gives rise to all trunk skeletal muscles (Sporle 2001).

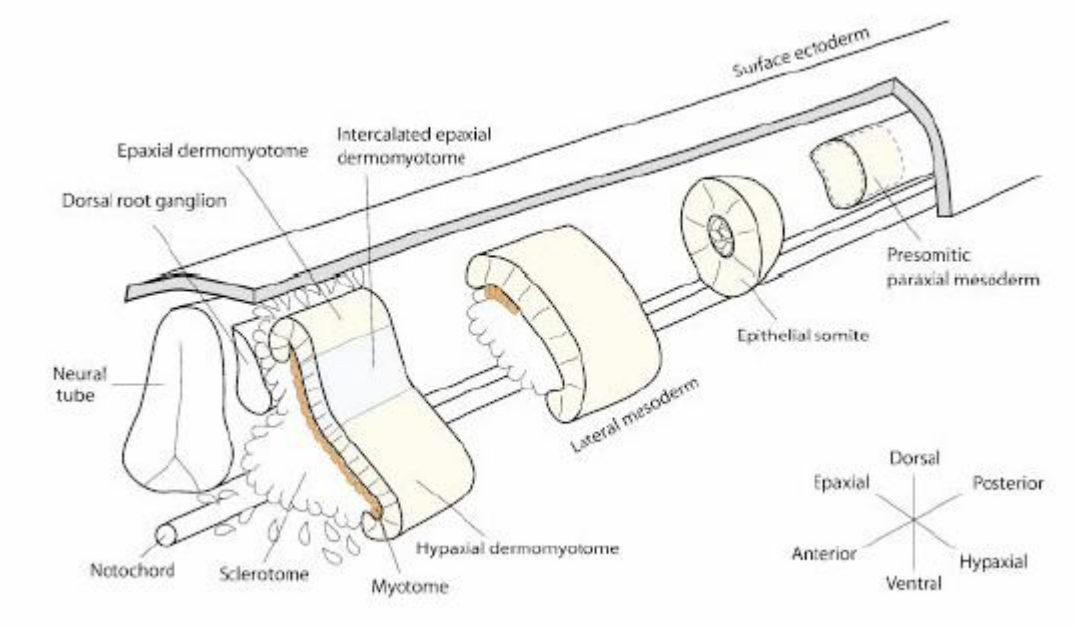

Figure 5.1. Schematic representation of somitogenesis (a*dapted from Buckingham et al 2003*).

The development of trunk skeletal muscles starts in the myotome, where MPCs differentiate into myocytes, which will fuse and originate multinucleated myotubes that mature into myogenic fibers. This process is known as myogenesis. For myogenic fibers become functional, myotendinous junctions and innervation are essential. Myogenesis is strictly regulated by two families of transcription factors: the myogenic regulatory factors (MRFs), and the myocyte enhancer-binding factor 2 (MEF2).

The myogenic regulatory factors (MRFs) are responsible for triggering the process of myogenesis. These belong to the basic helix-loop-helix (bHLH) family of transcription factors (Berkes and Tapscott 2005), and consist of Myf5, MyoD, MRF4 and myogenin. MRFs usually heterodimerise with ubiquitous E-proteins, encoded by the E2A gene (E12 or E47), and bind to the consensus sequence CANNTG (E-box) in the promoters of several muscle-specific genes (Molkentin and Olson 1996; Sabourin and Rudnicki 2000; Tapscott 2005). The MRFs act in combination with the myogenic enhancer-binding factor 2 (MEF2) transcription factor family to activate many muscle-specific genes (Molkentin et al. 1995). The MEF2 transcription factors consist of MEF2A, 2B, 2C, and 2D that are identical in its N-terminal which contains a MADS (MCM1, Agamous, Deficiens and Serum response factor) domain, by which they bind to the DNA sequence CTA$(A/T)_4$TAG/A (McKinsey et al. 2002).

Muscle stem cells, also called muscle satellite cells (MSCs), start to be formed at the late stages of vertebrate embryo development (Morgan and Partridge 2003). In the adult, these MSCs are quiescent and located between the basal lamina and the plasma membrane of the myofibers. In response to muscle injury and exercise, they become activated to differentiate into myoblasts, and are able to fuse with each other or existing myofibers. The C2C12 immortalised cell line consists of cells derived from mouse MSCs and represent an excellent model to study myogenic differentiation (Yaffe and Saxel 1977).

For a successful myogenesis, is not only necessary that transcription is regulated in the right way by MRFs and MEF2, but also that other processes such as intracellular signalling, cell migration, cell-cell interaction, cell connection with the extracellular matrix (ECM) occur properly. Therefore, through myogenesis it is crucial to regulate the synthesis, degradation, assembly, and maintenance of many proteins in each specific phase of this event. It is of our knowledge that a large number of transcription factors and many other molecules participating in the aforementioned processes are rapidly degraded by the ubiquitin-proteasome system (UPS), namely MyoD (Kim J and Hoppe T 2006), Myf5 (Lindon et al. 2000), myogenin (Shiraishi et al. 2007), Pax3 (Boutet et al. 2007), Id proteins (Bounpheng et al. 1999), and β-catenin (Matsuzawa and Reed 2001; Wu et al. 2003).

The reversal of ubiquitination catalysed by deubiquitinating (DUB) enzymes is equally important in several cellular processes. DUBs are needed for (1) generation of free ubiquitin (Ub) from its precursors, (2) editing or rescue of ubiquitin conjugates, (3) recycling of Ub from the branched polyUb chains of the ubiquitin-protein conjugates targeted for degradation, or (4) disassembly of unanchored ubiquitin oligomers (Amerik and Hochstrasser 2004; Nijman et al. 2005). So far, only two DUBs, UBP45 and UBP69, were verified as regulators of myogenesis event but their specific role is still unknown (Park et al. 2002). Thus, it remains to unveil in each way the cleavage of ubiquitin from proteins by DUBs contributes to muscle development.

Ataxin-3 (ATX3) is a recently discovered DUB, that given its different structure in relation to the previous classes of DUBs, gave rise, in conjunction with other homologue proteins, to a new subclass of DUBs (Nijman et al. 2005). DUB activity is conferred by its N-terminal josephin domain, a globular structure containing the four essential residues Q9, C14, H119 and N134, that are responsible for its cysteine protease activity (Chow et al. 2004; Mao et al. 2005; Nicastro et al. 2005).

Several evidences suggest that ATX3 may have a role in the UPS, since this protein: (1) binds and hydrolyses K^{48}- linked multiubiquitin chains *in vitro* (Burnett et al. 2003; Doss-Pepe et al. 2003; Chai et al. 2004; Berke et al. 2005); (2) interacts with ubiquitin (Ub) and with neural precursor cell expressed developmentally down-regulated gene 8 (NEDD8), which is a ubiquitin-like (UBL) protein that regulates activity of E3 ligases (Ferro A et al. 2007); and (3) associates with the proteasome interacting with p45 (an ATPase subunit of the 19S proteasome subunit) (Wang et al. 2007), and with VCP/p97 (an AAA ATPase important for the shuttling of many polyubiquitinated proteins to the proteasome) (Wang et al. 2006; Zhong and Pittman 2006).

ATX3 is a highly conserved protein throughout evolution. We have previously observed that its mouse homologue protein (mATX3) conserved its ubiquitous expression pattern, and was expressed during embryonic development since the earliest embryonic day (E) studied (E11.5) (Costa et al. 2004). Furthermore, we have verified that mATX3 is highly expressed in muscle cells since the embryonic development until adult age, and that the mouse MJD homologue gene (*Mjd*) promoter was activated to a great extent in muscle differentiated P19 cells (Costa et al. 2004). Until now, from our knowledge, no other functions for ATX3 are known, as well as, no substrates of its DUB enzyme or physiological role(s).

In this study we aimed to define the role of mATX3 in muscle differentiation. We have determined that mATX3 is highly expressed in the early myotome of E9.5 mouse embryos, and using C2C12 cells, we performed mATX3 knockdown experiments and observed its phenotypic and molecular effects. We verified that mATX3 is important in the control of cellular proliferation, cell-cell alignment and interaction, and therefore for acceleration of differentiation. This mATX3 role may occur particularly through direct regulation of α5 integrin, preventing its degradation by the UPS; and in general, as determined by proteomics, by regulating the levels of several cell-surface and extracellular matrix proteins important for myogenesis.

5.3. MATERIALS AND METHODS

Constructs

Glutathione-S-transferase (GST)-tag mATX3 (GST::mATX3) expression plasmid (pDEST15Mjd) was obtained by recombination of the pDONR207Mjd with the pDEST15 vector using the Gateway Cloning System (Invitrogen). The pGEX-5X-1 vector (GE Healthcare) was used for the expression of recombinant GST.

The pEGFP:Mjd plasmid was generated by subcloning a *BamHI*-digested PCR product into the *BamHI* restriction site of he pEGFP-C1 vector (Clontech). This PCR product was obtained by introducing the *BamHI* restriction sites, in frame at both 5' and 3' of the *Mjd* cDNA coding region, using the pair of primers 5'MjdBamHI/ 3'MjdBamHI (Appendix 1), the pDONR207Mjd plasmid as template, and the Expand High Fidelity System (Roche) under the conditions: 5 min at 95ºC, followed by 35 cycles of 1min at 95ºC, 1min at 55ºC, 1min at 72ºC, and ending with 5 min at 72ºC. All constructs were confirmed by automated sequencing.

Antibodies

The primary antibodies used were: rabbit anti-ATX3 antiserum (kindly provided by H. Paulson), monoclonal antibody for ubiquitinylated proteins (clone FK2, Biomol International LP), mouse anti-MHC (clone F59, DSHB), mouse anti-slow MHC (clone 1A, provided by J. Harris), mouse anti-myogenin (clone F5D, DSHB), rabbit anti-MyoD (provided by J. Harris) rabbit anti-α5 integrin subunit (Chemicon) , goat anți-α5 integrin subunit (Santa Cruz Biotechnology), rat anti-α7integrin subunit (provided by A. Sutherland), mouse anti-α-tubulin (clone AA4.3, DSHB), and goat anti-GST (GE Healthcare).

The peroxidase-conjugated secondary antibodies used for immunoblotting were: goat anti-mouse (Santa Cruz Biotechnology), goat anti-rabbit (Santa Cruz Biotechnology), goat anti-rat (Serotec), and donkey anti-goat (Santa Cruz Biotechnology). For double immunofluorescence assays, the Alexa Fluor (AF) secondary antibodies (Molecular Probes) used were the following: AF 488 goat anti-rabbit, AF 568 goat anti-mouse, AF 594 goat anti-rat, AF 594 goat anti-rabbit, and AF488 donkey anti-rabbit.

RNA interference

Dicer small interference RNA (d-siRNA) was prepared using the Block-iT^{TM} RNAi

Topo transcription kit (Invitrogen) for topo-mediated generation of templates and production of double-stranded RNA (dsRNA), and the Block-It^{TM} Dicer RNAi kit (Invitrogen) for the generation, purification of Mjd-specific d-siRNA, using the manufacturer's conditions. Briefly, we started to generate by PCR an *Mjd* cDNA fragment, consisting in the first (5'-3') 646 bp, using primers mmMJD106/ mmMJD10, the pMjd1 plasmid as template, and the Platinum Taq DNA Polymerase High Fidelity; this PCR product was processed using the abovementioned kits to produce the *Mjd* d-siRNA.

C2C12 culture and transfection

Mouse C2C12 myoblasts were cultured in growth medium (GM) corresponding to Dulbecco's modified Eagle's (DMEM) Glutamax (Gibco BRL), 20% fetal bovine serum (FBS) and 1% penicillin/streptomycin, in a 5% CO_2 humidified chamber at 37ºC. To induce myogenic differentiation, C2C12 cells at 80-100% confluence in GM where washed with phosphate-buffered saline (PBS) and grown in differentiation medium (DM) consisting of DMEM glutamax, 2% horse serum and 1% penicillin/streptomycin, that was changed every day.

Mjd siRNA and mATX3 overexpression experiments were undertaken by transfection of 1x10^5 C2C12 myoblasts per well (6-well plates) with either 300 ng of *Mjd* siRNA and 2 μL of Lipofectamine 2000 (Invitrogen), or 2 μg of pEGFP:Mjd and 5 μL of Lipofectamine 2000 in antibiotic-free medium (Opti-MEM, Life Technologies) for 6 hours, after which the medium was changed for GM. Mock transfections were also performed in the same way but without siRNA, as well as transfections with the empty pEGFP-C1 vector (Clontech). Three independent experiments were performed. In terms of C2C12 differentiation, the day of transfection was named Day -2 of differentiation. Two days after, the GM was changed for DM (Day 0), that was changed every day and cellular extracts were collected from Days -2, 0, 1, 2, 3, and 5 of differentiation.

Protein synthesis inhibition

C2C12 cells were transfected with pEGFP:Mjd or pEGP-C1 plasmids as abovementioned. Forty eight hours after transfection, the medium was changed for DM. After 24 hours, cells were treated with cycloheximide (Merck) at 50 μg/mL during 15, 30, 60, 90, or 120 min. Whole protein extracts were prepared from each experiment that was performed in triplicate.

Preparation of whole cellular and tissue extracts

For total protein extraction, C2C12 cells from the differentiation days – Day -2, Day 0, Day 1, Day 2, Day 3 and Day 5 – were washed briefly with PBS and collected in 500 μL of cell lysis buffer (1 % Nonidet P-40, Complete (Roche Diagnostics) in PBS). Total protein extract from a mouse E15,5 embryo was collected after homogenisation in 1 mL of tissue lysis buffer (0,25% Triton X-100, Complete (Roche Diagnostics) in PBS), sonication, and centrifugation. The total protein amount was quantified using the Bradford reagent (Sigma Aldrich) and appropriate dilutions were stored at -20 ºC.

For total RNA extraction, cells from the differentiation Day 0 and Day 1 were washed with PBS and after centrifugation the cell pellet was stored at -80 ºC. Total RNA was purified using the Versagene kit (Gentra Systems) according to the manufacturer instructions.

Recombinant protein expression and purification

The recombinant GST::mATX3 protein was expressed in *Escherichia coli* BL21SI cells (Invitrogen Life Technologies). Cells were grown at 37ºC in LB/ON (without NaCl) medium containing 100 mg/l of ampicillin and 0.2% (w/v) of glucose until a cell density of 0.6 at 600 nm, the moment when the recombinant protein expression was induced by the addition of NaCl to a final concentration of 0.3 M and culture was further grown for 3 hours at 30ºC. The recombinant GST protein was expressed in the same way, but the induction of expression was done by the addition of 1 mM isopropyl-β-D-thiogalactopyranoside (IPTG).

Cells were harvested, ressuspended in the buffer (phosphate-buffered saline (PBS), 200 μg/mL lysozime, 1% Triton X-100,1mM phenylmethylsulphonyl fluoride (PMSF), protease inhibitors (Complete, Roche), and stored at -20ºC. After defrosting, the cell suspension was incubated with agitation at 4 ºC, during 1 hour, sonicated, and after centrifugation the supernatant was collected. The soluble recombinant proteins were purified using glutathione-sepharose^{TM} 4B beads (GE Healthcare) according to manufacturer's instructions, being eluted in three fractions of 10 mM reduced glutathione in 50 mM Tris-Cl pH 8.0.

The eluted fractions considered appropriate were dialysed using a dialysis membrane with a cut-off of 14 KDa (Medicell) placed in PBS, overnight, at 4ºC. We added protease inhibitors (Complete, Roche Diagnostics) and PMSF to the dialysed proteins, and quantified the protein amount using the Bradford reagent (Sigma Aldrich).

GST pull-down

For GST pull-down assay, the purified GST or GST-tagged proteins (2 μg) were incubated rotating with 40 μL of glutathione-sepharose™ 4B beads (GE Healthcare), in a final volume of PBS/ protease inhibitors, during 1 hour, at 4 ºC. Whole E15.5 embryo proteins extract (150 μg) was added and incubated for 2 hours, at 4 ºC, in a rotator. Beads were washed four times with PBS and bound proteins were eluted in 65 μL of Laemmli sample buffer, at 95 ºC, for 5 min.

Immunoblotting

Total proteins from the several C2C12 differentiation days (20 μg) were resolved in a 10% SDS-PAGE polyacrylamide gel and then transferred to a nitrocellulose membrane (Hybond-C, GE Healthcare). Membranes were incubated, overnight at 4ºC, with primary antibodies: anti-ATX3 antiserum (1:5000), anti-myogenin (1:50), anti-MyoD (1:1000), rabbit anti- α5 integrin subunit (1:5000), or anti-α7 integrin subunit (1:2000). All membranes were incubated with anti-α-tubulin (1:500) for loading control.

For the GST pull-down assays, bound proteins were resolved in an 8% SDS-PAGE polyacrylamide gel and transferred in the abovementioned way. Blots were incubated with anti-GST (1:7,500) or rabbit anti- α5 integrin subunit (1:5000) overnight at 4ºC.

Detection of the immunocomplexes was performed using the peroxidase-conjugated secondary antibodies anti-mouse (1:10000), anti-rabbit (1:10000), anti-rat (1:10000), or anti-goat (1:30000), and a SuperSignal West Pico Chemiluminescent Substrate (Pierce). The immunocomplexes signal was registered in ECL-films (Hyperfilm, GE Healthcare), and after that quantified using the software Quantity One 4.6.3 (Bio-Rad).

Quantitative real-time RT-PCR

C2C12 total RNA (2 μg) from differentiation Day 0 and Day 1 (mock, and *Mjd* siRNA transfections) was reverse transcribed using the SuperScript First-Strand Synthesis System for RT_PCR (Invitrogen) with an oligo(dT) primer. Gene amount was assessed by quantitative real-time RT-PCR, using the QuantiTec SYBR Green PCR kit (Qiagen), 2 μL of total cDNA, and 500 nM of each primer. The pair of primers used to amplify the genes *Itga5*, *Itga7*, *Myog*, *Myod1*, *Mjd*, *Josd1*, *Josd2*, *Josd3* and *Hprt* was respectively: Itga5(1)/ Itga5(2) (148 bp), Itga7(1)/ Itga7(2) (151 bp), Myogenin(1)/ Myogenin(2) (140 bp), Myod1(3)/ Myod1(4) (152 bp), mmMJD14/ mmMJD21 (138 bp), Josd1(1)/ Josd1(2) (116 bp), Josd2(1)/

Josd2(2) (147 bp), Josd3(1)/Josd3(2) (141 bp), and Hprt(3)/ Hprt(4) (249 bp) (Appendix 1). The reactions were carried out in a real-time cycler LightCycler (Roche) using standard cyclic conditions indicated in the abovementioned kit.

Proteomics

iTRAQ labeling and trypsin digestion

Total protein extracts were obtained from C2C12 cells from differentiation Day 0 and Day 1 (mock, and *Mjd* siRNA transfections). After quantification, 100 μg of total proteins from each condition was precipitated using six volumes of cold acetone to remove interfering substances. The samples were incubated at -20ºC for 1 hour and then centrifuged at maximum speed at 4ºC. Protein pellet was ressuspended in 40 μl of 500 mM triethyl ammonium bicarbonate with 1% SDS, vortexed, and briefly sonicated until fully dissolved. The proteins were reduced using 2 μl of 50 mM tris-(2-carboxyethyl) phosphine for 1 hour at 60ºC, and cysteines were blocked with 200 mM methyl methane thiosulfonate (MMTS) for 10 minutes at room temperature. Ten micrograms of Sequencing Grade Modified Trypsin (Promega) diluted in water was added to each sample and incubated overnight at 37ºC. The iTRAQ reagents (Applied Biosystems) were reconstituted in 70% ethanol, transferred to the respective sample and allowed to incubate for one hour. Reagent 114 was added to the Day 0 mock, 115 to Day 0 *Mjd* siRNA, 116 to Day 1 mock and 117 to Day 1 *Mjd* siRNA; and the labelled peptides were then combined and evaporated to dryness in a SpeedVac. Each sample was re-dissolved in 50 μl of 0,1 % trifluoroacetic acid (TFA) and desalted using C_{18} empore disks.

Isoelectric focusing

Desalted samples were applied on a 13 cm IPG strip, pH 3-10 (GE Healthcare), rehydrated for 12 hours and then focused in a IPGphor using the following parameters: hold at 500V 1h, linear gradient from 500-1000V 15 minutes, hold at 1000V 1h, linear gradient from 1000V-8000V 30 minutes, hold at 8000V 2 hours. The strips were cut into 12 fractions and focused peptides were extracted from the gel using a TFA gradient. The sample were evaporated and desalted as mentioned above. Peptides were dissolved in 1 % HCOOH just before LC-ESI-MS/MS analyses.

LC-ESI-MS/MS analyses

Around 6-8 μg of peptides from each fraction were analyzed using a nanoflow LC (Famos, Switchos, and Ultimate^{Plus}; LC Packings - Dionex Corporation, Sunnyvale, CA, USA) coupled to a QSTAR Pulsar i ESI-hybrid Q-TOF tandem mass spectrometer (Applied Biosystems/MDS Sciex, Toronto, Canada). Peptides were concentrated and desalted on a

precolumn (0.3 x 5 mm C_{18} PepMap100, LC Packings), and eluted at 200 nl/min by increasing concentration of acetonitrile onto a self-packed C_{18} reverse phase column (75 μm x 15 cm, Magic 5 μm 100 Å C_{18}, Michrom BioResources Inc.) A linear 90 min gradient from 98 % solvent A (97.8% water, 2% acetonitrile, and 0.2% formic acid) to 35% solvent B (95% acetonitrile, 4.8% water, and 0.2% formic acid) was used. Data from LC-MS/MS runs were converted to peak list files with the Analyst QS software (version 1.1).

Data analysis and protein identification

MS/MS spectra generated was analyzed using Protein Pilot (version 2.0, Applied Biosystems / MDS Sciex) search engine running over a *Mus musculus* database downloaded from NCBI. The default search settings used for quantitative analysis and protein identification were: trypsin cleavage with fixed MMTS modification of cysteine, iTRAQ labelling and variable methionine oxidation. We have considered only protein identifications with >95% statistical confidence in Protein Pilot. The quantification of the identified proteins was reported using the 114 (Day 0 mock) and 116 (Day 1 mock) tags as the controls with bias correction. For data analysis, a P-value< 0.05 was considered for 115/114 and 117/116 comparisons, and the expression ratio cut-off used was of 20%, i.e were considered the ratio values smaller than 0.8 and higher than 1.2. Data analysis and molecular network pathways were created using the trial version of the Ingenuity Pathways Analysis Inc. 5.0 software, which in turn uses all the information known for a specific gene/protein including the one from their homologues in other species.

Embryo collection and histology

For embryonic expression studies, the day of detection of a vaginal plug was designated as embryonic day (E) 0.5. Pregnant C57Bl/6 (Harlan Interfauna Iberica, SA) females were sacrificed by CO_2 inhalation, and embryos from E9.5, E11.5, E14.5, E15.5 and E18.5 stages were collected in cold PBS. The embryos were fixed, in a rotator at 4 ºC, using the following solutions: (1) 0.2 % para-formaldehyde (PFA), 4 % sucrose, 100 mM sodium phosphate, 120 μM $CaCl_2$ (pH 7.4) overnight; (2) the previous solution without PFA overnight; (3) 15 % sucrose, 120 mM phosphate buffer (pH 7.2) overnight. Then, they were incubated in 7.5 % gelatin, 15 % sucrose, 120 mM phosphate buffer (pH 7.2), during 1 hour at 37 ºC with agitation, slowly frozen in this solution (in isopentane/ dry ice), and stored at –80 ºC. Embryos were cryosectioned in a Leica CM1900 cryostat into 15 μm- thick sagital slices, which were collected on Super Frost slides and stored at -20 ºC.

Embryos and C2C12 immunofluorescence staining

Slides containing the embryo slices from the several collected stages were placed in a humified chamber and the tissues were permeabilised in 0.2 % Triton-X-100/ PBS during 20 min, blocked in 10 % goat serum, 1 % bovine serum albumin (BSA)/ PBS during 30 min. For double staining analysis, the slices were then incubated with the rabbit anti-ATX3 antiserum (1:500) in conjunction with another primary antibody (all diluted in 1 % BSA/ PBS) overnight at 4 ºC. Primary antibodies used were mouse anti-fast MHC (1:20), mouse anti-slow MHC (1:100), mouse anti-myogenin (1:20), and rat anti-α7integrin subunit (1:100).

For immunofluorescence labelling, C2C12 cells were transfected after being seeded in coverslips. At the differentiation days 0, 1, 3, and 5, cells were washed briefly with PBS and fixed with 1 % PFA/ PBS, through 10 min, and permeabilised in 0.5 % Triton-X-100/ PBS (5 min). After blocking in 2 % BSA/ PBS (30 min), coverslips were incubated with the anti-ATX3 antiserum (1:500) in combination with other primary antibody (all diluted in 2 % BSA/ PBS) overnight at 4 ºC.

Subsequently, slices and coverslips were washed with PBS and incubated for one hour with the two corresponding Alexa Fluor (AF) secondary antibodies, diluted 1:1000 in 1 % BSA/ PBS: AF 488 goat anti-rabbit, AF 568 goat anti-mouse, and AF 594 goat anti-rat. After that, slices were stained with 4',6-Diamidino-2-phenylindole dihydrochloride (DAPI, Sigma) diluted 1:2000 in PBS during 5 min, and mounted with Vectashield (Vector Laboratories).

Imaging

Embryo sections and C2C12 coverslips processed for immunofluorescence were photographed in an OLYMPUS IX 81 confocal microscope using the software OLYMPUS Fluoview1000 (FV viewer v.1.6.a). Optical z-series for both embryos and C2C12 cells were obtained. C2C12 cells were photographed with a SONY digital camera coupled to a phase contrast Axiovert 200 Zeiss microscope, during differentiation after mock and *Mjd* siRNA transfections.

Statistical analysis

For immunoblots, corresponding to three independent experiments, relative mean band density for each analysed protein, was compared between two groups of experiments using the t-test, which was calculated using the SPSS version 14.0 package. The same

approach was used to analyse real-time PCR data. A significant $P< 0.05$ value was considered.

5.4. RESULTS

Ataxin-3 is highly expressed in the early myotome and colocalises with myogenic fibers

In order to characterise the expression pattern of mATX3 in the developing muscle, we have performed double immunofluorescence labelling for mATX3 and myogenic markers in mouse embryo sections at the following stages: E9.5, formation of the primary myotome; E11.5, onset of the primary myogenesis; E14.5, end of the primary myogenesis; and E18.5, late foetal stage.

Mouse ATX3 is broadly expressed and although it was detected in the dermomyotome, which gives rise to the myotome, and throughout the whole extent of the myotome, it is surprisingly up-regulated at E9.5 in elongated myosin-positive cells (Figure 5.2B). This specificity for myosin-positive cells is also evident in the developing cardiac muscle (Figure 5.2A). In the differentiated myotomal cells mATX3 is found along the myocyte protrusions, preferentially at the tips (Figure 5.2B), being detected in myogenin-positive but also negative cells (Figure 5.2C).

At the beginning of the primary myogenesis (E11.5), mATX3 continues to colocalise with myosin-expressing cells and with myogenin-positive cells in the myotome (Figure 5.2D,E). Furthermore, by the end of primary myogenesis, in E14.5 embryos, mATX3 is also colocalising with myosin-positive (primary) myogenic fibers of abdominal muscles (Figure 5.2F).

Additionally, as shown in Figure 5.3 in the double immunofluorescence assays, mATX3 shows a fiber-like labelling pattern in the hindlimb muscles of E18.5 embryos. We could also verify that mATX3 makes part of the fast contracting muscle (fast myosin-positive fibers), but also of other types of fibers, as could be seen in Figure 5.3A. Furthermore, mATX3 colocalises with either primary myogenic fibers (slow myosin-positive), or with secondary myogenic fibers (slow myosin-negative) (Figure 5.3B).

The expression pattern of mATX3 suggests that this protein is present in all stages of myogenesis, with increasing immunoreactivity in the early stages and highly correlated with the presence of myosin, indicative of cytoskeletal modifications and therefore, is likely to be important in the muscle development process.

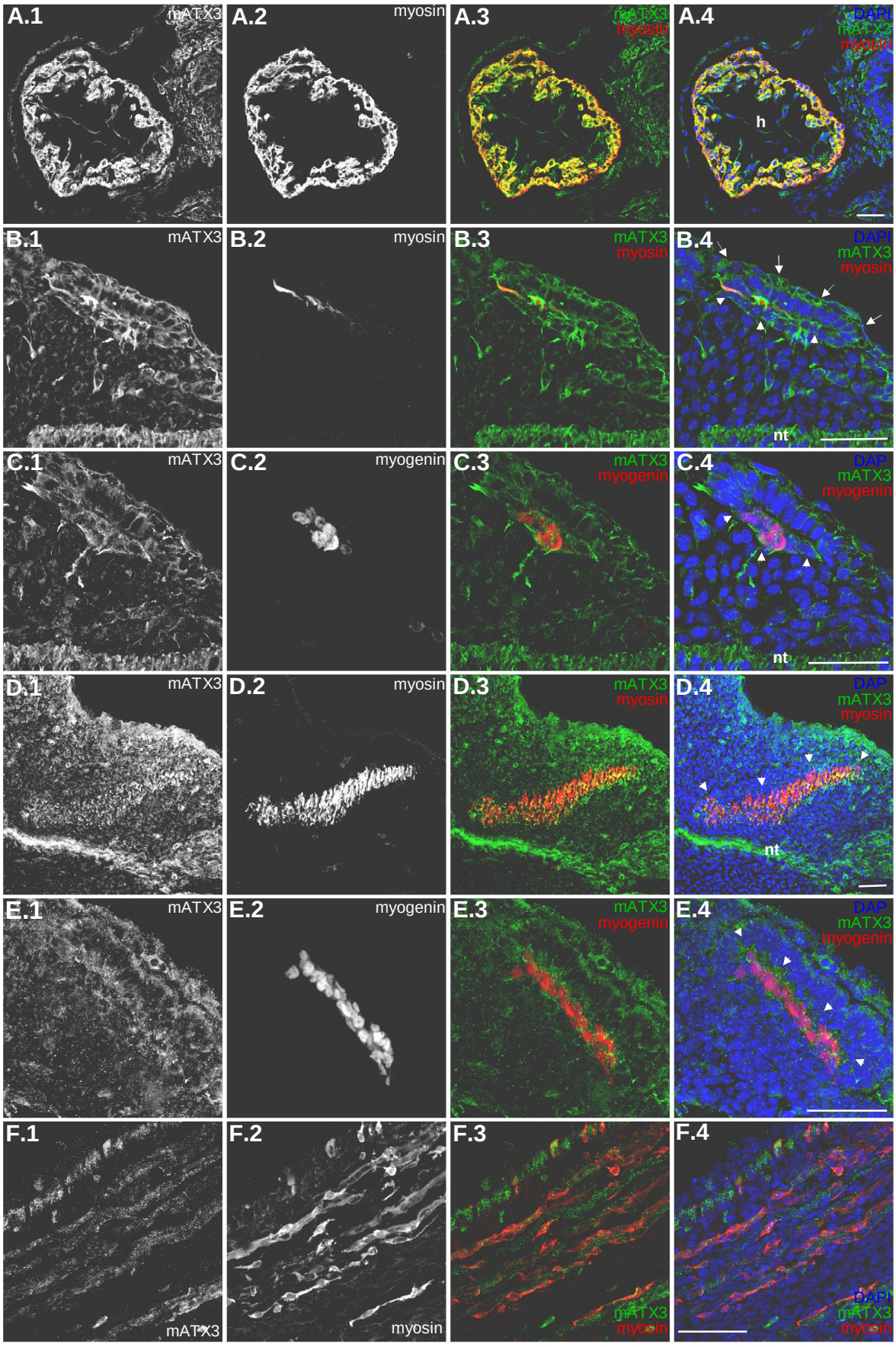

Figure 5.2. (see legend in the next page)

Figure 5.2. Mouse ataxin-3 is highly expressed in the early myotome. Confocal optical z-series micrographs from sagittal sections of mouse embryos at (A, B, C) embryonic day 9.5 (E9.5), (D, E) E11.5, and (F) E14,5. (A) mATX3 (green) is highly expressed in heart (h), in myosin-positive cells (red). (B) In E9.5 embryo, mATX3 (green) is widely expressed but in a higher extent in neural tube (nt), in the dermomyotome (arrows), and much strongly in the early myotome (arrowheads) in either myosin-positive (red) or myosin-negative cells. (C) E9.5 embryo showing that mATX3 (green) colocalises with myogenin-positive cells (red) in the myotome (arrowheads). (D) The myotome (arrowheads) in E11.5 embryos shows a high staining for mATX3 (green) in myosin-positive cells (red), and (E) in myogenin-positive cells (red). (F) E14.5 shows a fiber-like labelling pattern of mATX3 (green) in an intercostal muscle, colocalising with myosin-positive fibers (red). DNA was stained with DAPI (blue). (1) mATX3 staining, (2) myosin (MHC) or myogenin labelling, (3) overlay of mATX3 and myogenic marker, and (4) triple overlay of mATX3, myogenic marker, and DAPI. Scale bars represent 80 μm.

Ataxin-3 is necessary for myogenic differentiation of C2C12 cells

To study the involvement of mATX3 in the myogenic differentiation process we have used C2C12 myoblast cells, that are able to differentiate into myotubes upon change of the normal growth medium (GM) for a serum-limited differentiation medium (DM). Pilot experiments (not shown) indicated that C2C12 cells express mATX3 and the expression profile of mATX3 during C2C12 differentiation myoblasts into young myotubes was determined (Day 0-Day 5). Controls for siRNA experiments (mock) followed a similar pattern, characterised by levels of mATX3 slightly rising upon the changing of GM for DM at Day 0, which were maintained during the differentiation process (Figure 5.4A,B). The increase of mATX3 during myogenic differentiation was consistent with the hypothesis that this protein may be implicated in this mechanism.

To further define the potential role of mATX3 in C2C12 differentiation, small interference RNA (siRNA)-mediated knockdown experiments were carried out. C2C12 myoblasts were transfected at Day -2 with dicer siRNA for the *Mjd* transcript and the cells were maintained in GM. Two days after transfection (Day 0), when the smallest amount of mATX3 was observed in *Mjd* siRNA-transfected C2C12 cells (Figure 5.4A,B), differentiation was induced by changing to DM medium every day, for five days. The same procedure was performed for the control “mock” experiments. We have collected total protein extracts from the differentiation days: Day -2, Day 0, Day 1, Day 2, Day 3, and Day 5; and studied the expression profile of mATX3 by immunoblotting. The proportion of expression of the *Mjd* transcript in knockdown cells (*Mjd* siRNA) was of 18%, 32%, 55%, 63% and 59% in relation to the normal levels (mock) for Days 0, 1, 2, 3, and 5, respectively (Figure 5.4A,B).

As shown in Figure 5.5, during the C2C12 differentiation process (since Day 0 to Day 5), the *Mjd* knockdown cells were phenotypically different from mock-transfected cells: they

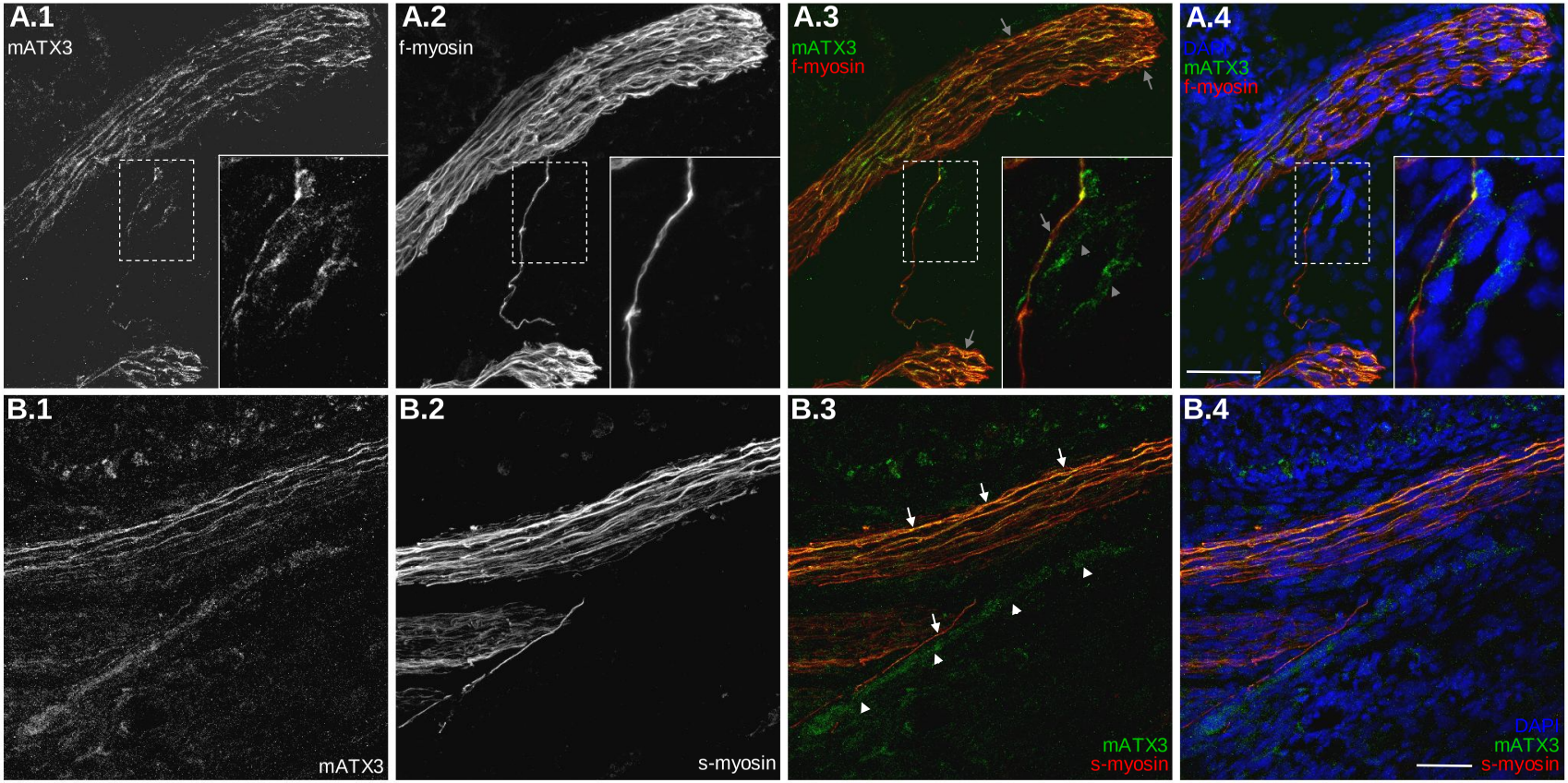

Figure 5.3. Ataxin-3 colocalises with several types of myogenic fibers. Confocal optical z-series images of hindlimb muscles from E18.5 mouse embryos. (A) Double staining (3) for mATX3 (green) and fast-myosin (f-myosin, in red) showing that mATX3 is expressed in fast-contracting fibers (grey arrows) and in other type of fibers (grey arrowheads); a higher magnification corresponding to the dashed rectangle is represented by the inset in the right inferior corner showing that the fiber-like pattern of mATX3 is not exclusively of f-myosin. (B) Double immunofluorescence (3) for mATX3 (green) and slow-myosin (s-myosin, in red) evidences that mATX3 colocalises with both primary myogenic fibers (slow myosin-positive, blank arrows), and secondary myogenic fibers (slow myosin-negative, blank arrowheads). DNA was stained with DAPI (blue) that could be seen in the triple overlay (4). Scale bars represent 80 μm.

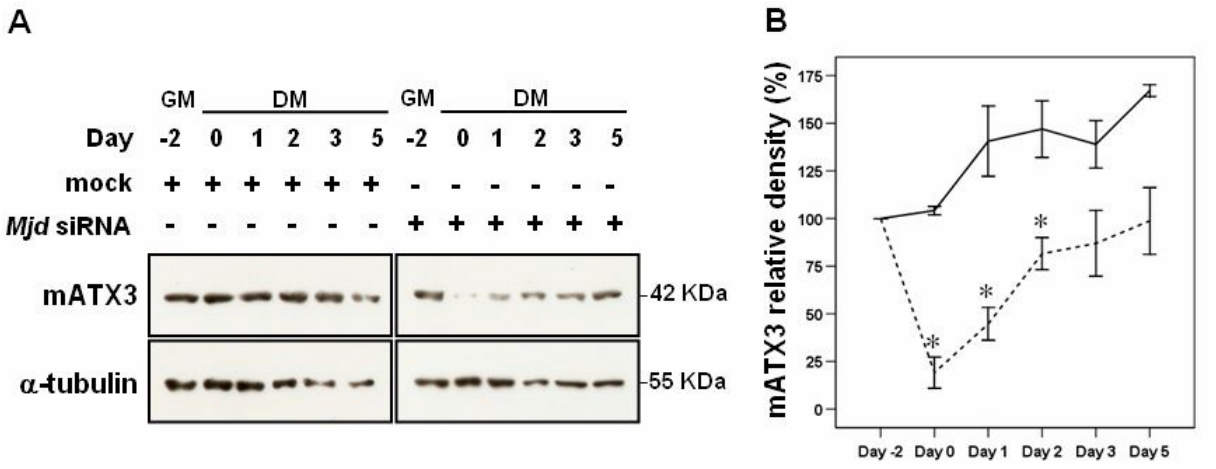

Figure 5.4. Expression profile of mATX3 during C2C12 differentiation and when is knockdown using *Mjd* siRNA. (A) The amounts of ataxin-3 were determined by immunoblotting. Whole cell extracts of undifferentiated (Day -2) and differentiated cells (Day 0 to Day 5) were analysed for mATX3 and α-tubulin in mock and *Mjd* siRNA transfected cells. Cells were transfected at Day -2 and maintained in growth medium (GM) for 48 hours (Day 0), when the medium was changed for differentiation medium (DM). (B) Relative band density of mATX3 in each day and for each transfection condition. The results were normalised for α-tubulin and correspond to the average of three independent transfections ± SEM (error bars). ∗, statistical significance.

appeared rounder, with very thin cell extensions; seemed to be completely misaligned and unable to fuse with each other; and appeared to continue to proliferate, which is a process that normally stops when differentiation begins at Day 0. This phenotype suggests that mATX3 is important for the myogenic differentiation of C2C12 cells.

Furthermore, although at Day 5 the *Mjd* siRNA cells seem to present the same amount of myosin, the myosin-containing filaments seem to be more condensed, with a fragmented aspect and not elongated (Figure 5.6), which suggest that mATX3 might be important for the proper arrangement of the myosin filaments.

In summary, the behaviour of C2C12 cells when mATX3 is knocked-down to low levels prior to the beginning of myogenic differentiation suggests that this protein is required during the differentiation process.

The *Mjd* siRNA does not affect the levels of the genes that encode other josephin-domain containing proteins (*Josd1*, *Josd2* and *Josd3*)

To knockdown mATX3 we have used *Mjd* dicer siRNA that consist in a mixture of oligonucleotides that interfere in principle specifically with the *Mjd* mRNA. However, these

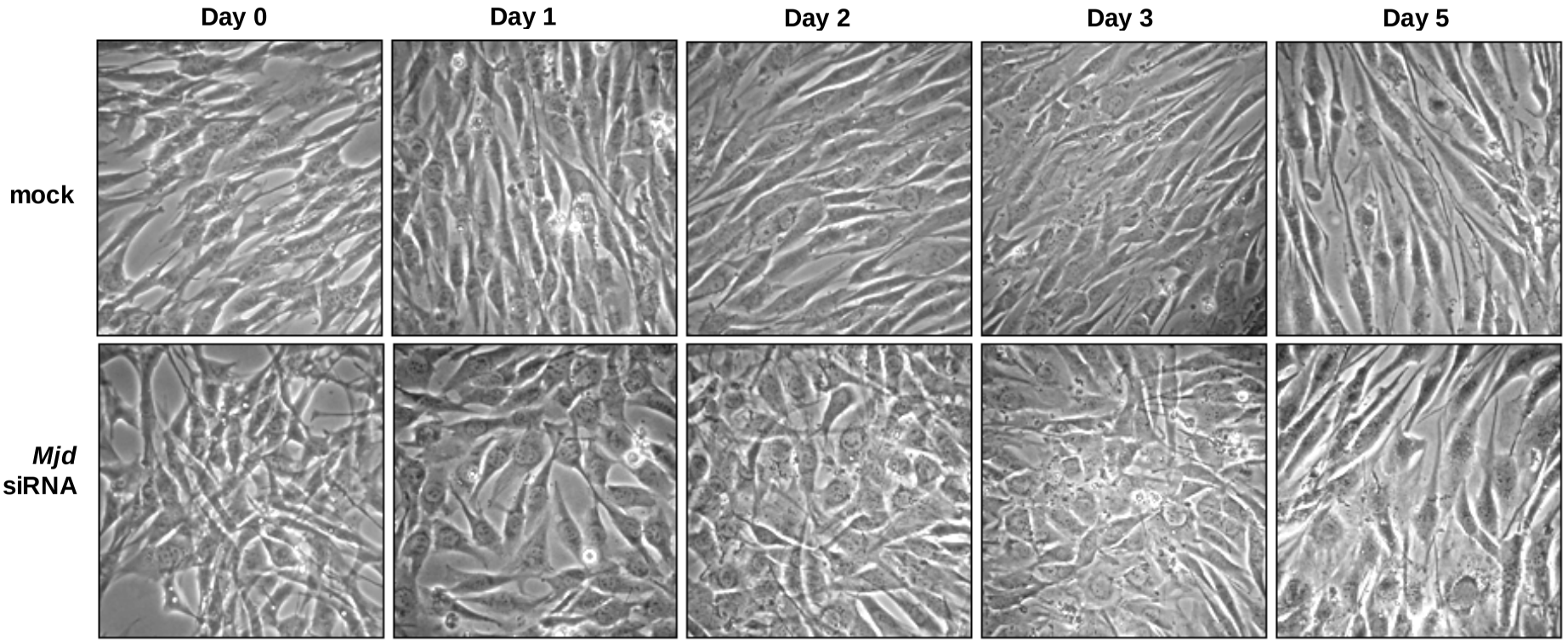

Figure 5.5. Phenotype of the *Mjd* siRNA C2C12 cells during differentiation. Mock and *Mjd* siRNA transfections were performed at Day -2 and maintained in growth medium (GM) for 48 hours (Day 0), when the medium was changed for differentiation medium (DM) and changed every day until Day 5. The photographs indicate that the *Mjd* siRNA transfected cells look like to be misaligned and continue to proliferate, as could be seen from Day 0 to Day 3.

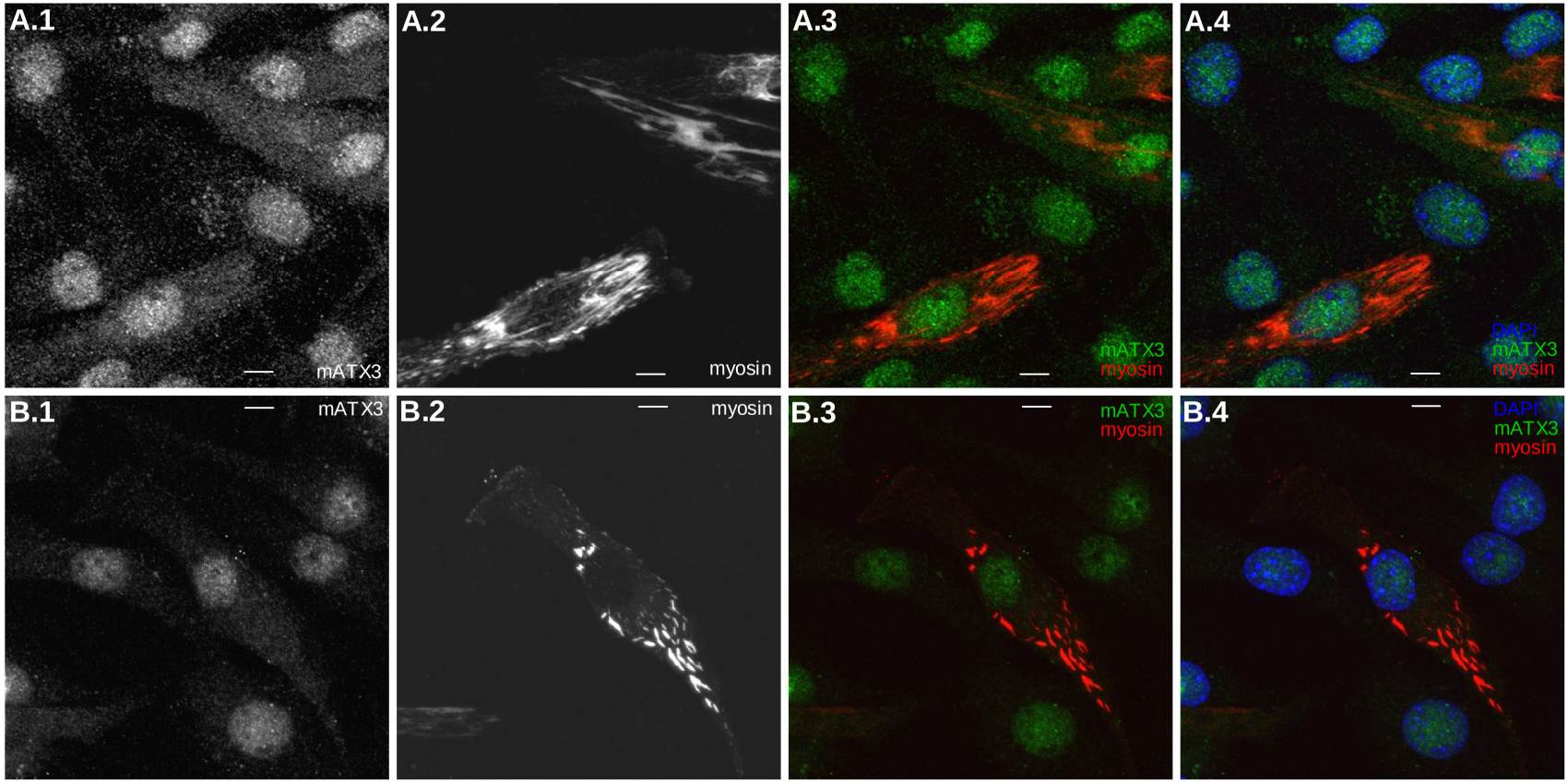

Figure 5.6. Ataxin-3 is important for the appropriate arrangement of the myosin filaments. Confocal optical z-series images of double immunofluorescence staining for mATX3 (green) and myosin (red) of C2C12 differentiated cells at Day 5. (A) The mock transfected cells show a normal and continuous myosin string arrangement. (B) The myosin fibers of *Mjd* siRNA transfected cells seem to be fragmented. DNA was stained with DAPI (blue) that could be seen in the triple overlay (4). Scale bars represent 10 μm.

oligonucleotides may also interfere with other similar mRNAs. In order to confirm if the observed phenotype in C2C12 cells transfected with *Mjd* siRNA was specifically given to the absence of mATX3, we have analysed the levels of expression of the genes encoding the other josephin-domain proteins (*Josd1*, *Josd2*, and *Josd3*) by quantitative real-time PCR. No significant differences were found for these genes between mock and *Mjd* siRNA transfected C2C12 cells at Day 0 and Day 1 of differentiation (Figure 5.7). However, a trend for a higher expression of *Josd3* could be observed in mATX3 knockdown cells at Day 0, suggestive of a possible compensation of the mATX3 absence. These results suggest that among the genes encoding josephin-domain containing proteins, the *Mjd* siRNA interfered exclusively with the *Mjd* mRNA.

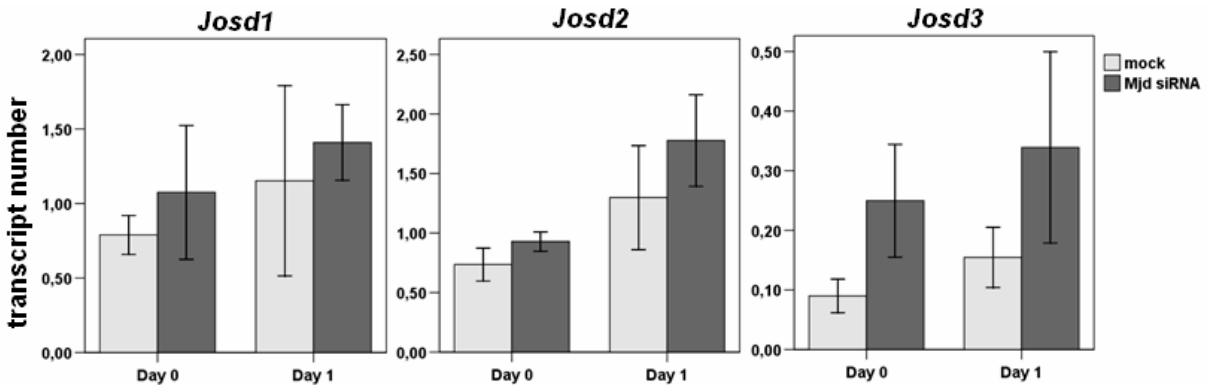

Figure 5.7. The transcript levels of the genes encoding other josephin-domain containing proteins *Josd1*, *Josd2* and *Josd3*, for mock and *Mjd* siRNA transfected C2C12 cells at Day 0 and Day 1 of differentiation, were measured by quantitative real-time RT-PCR, and showed to be similar. The results were normalised for the *Hprt* gene and correspond to the mean of three independent transfections ± SEM (error bars).

The levels of myogenin and MyoD are not altered in mATX3 knockdown differentiating C2C12 cells

To verify if the mATX3 knockdown cellular phenotype was due to a global alteration of the myogenic program, we have analysed, by immunoblotting, whether the expression of the myogenic regulatory factors MyoD and myogenin was affected at the protein level. No differences were observed between siRNA transfected and control (mock) differentiated cells (Figure 5.8A and 5.8B), suggesting that mATX3 is not affecting the levels of these two transcription factors, essential for myogenic differentiation.

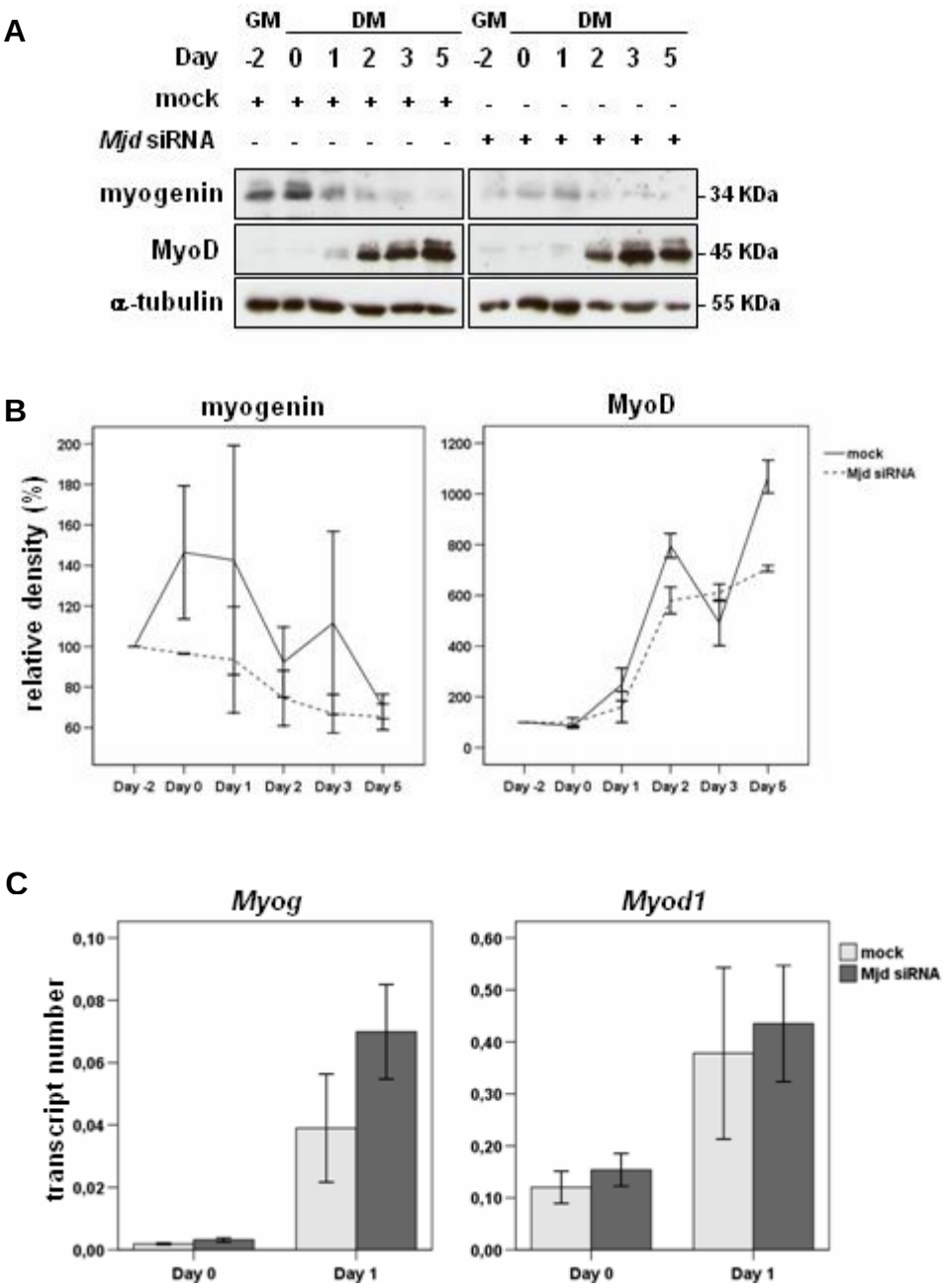

Figure 5.8. The myogenic factors myogenin and MyoD are not targets of mATX3. (A) The amounts of myogenin and MyoD were determined by immunoblotting. Whole cell extracts of undifferentiated (Day -2) and differentiated cells (Day 0 to Day 5) were analysed for myogenin, MyoD and α-tubulin in mock and *Mjd* siRNA transfected cells. Cells were transfected at Day -2 and maintained in growth medium (GM) for 48 hours (Day 0), when the medium was changed for differentiation medium (DM). (B) Relative band density of myogenin and MyoD in each day and for each transfection condition. The results were normalised for α-tubulin and correspond to the average of three independent transfections ± SEM (error bars). (C) The transcript levels of *Myog* and *Myod1* for mock and *Mjd* siRNA transfected C2C12 cells at Day 0 and Day 1 of differentiation were measured by real-time RT-PCR, and showed to be similar. The results were normalised for the *Hprt* gene and correspond to the mean of three independent transfections ± SEM (error bars).

In order to confirm if, at the mRNA level, the expression of these myogenic factors was not altered, we have extracted total RNA from mock and *Mjd* siRNA transfected Day 0 and Day 1 differentiated cells (the days of the higher knockdown proportion of the *Mjd* transcript), and performed quantitative real-time RT-PCR for the genes encoding myogenin (*Myog*) and MyoD (*Myod1*). No significant differences between normal and knockdown cells were observed for both *Myog* and *Myod1* genes (Figure 5.8C). Taken together, these results suggest that the cellular alterations seen in *Mjd* siRNA cells did not result from a change of the expression of the myogenic factors, myogenin and MyoD.

Ataxin-3 regulates α5 and α7 integrin subunit levels during myogenic differentiation

Many developmental events, such as cell proliferation and differentiation, depend on integrin-mediated cell adhesion and signalling. Integrins act as a link between the extracellular matrix and the cytoskeleton, activating signalling cascades and regulating cell behaviour. During the muscle differentiation process, integrins play fundamental roles and are the subject of a strict regulation, presenting highly specific expression patterns for each discrete phase of myogenesis (Bajanca et al. 2004).

Since the *Mjd* knockdown cells showed characteristics of differentiation delay, with continuous proliferation, we analysed by immunoblotting the expression pattern of the α5 integrin subunit, known to be upregulated upon C2C12 differentiation (Tomczak et al. 2004) and the *in vivo* expression pattern of which also correlates with mATX3 expression pattern in the mouse embryo (Bajanca et al. 2004). In addition, we analysed the α7 integrin subunit as this integrin was suggested to be a marker for pluripotent satellite cells (Ozeki et al. 2006), from which the C2C12 cells were derived.

Usually, during differentiation of C2C12 cells, α5 integrin increases in the first days (Tomczak et al. 2004), and α7 integrin subunits increase in the late stages (Song et al. 1993), as we could confirm in mock transfection experiments (Figure 5.9A,B). Comparing the *Mjd* siRNA with the mock transfected cells we observed a decrease in the expression level of both these integrins (Figure 5.9A,B).

Interestingly, α5 integrin showed a similar protein expression pattern to that of mATX3, both in normal and mATX3 knockdown C2C12 differentiating cells (Figure 5.4 and 5.9). In the low-expression mATX3 cells (siRNA), the levels of α5 integrin start to diminish since the differentiation start day (Day0), in which an expression level of 71% of the normal amounts (mock) was observed, which further decreased to 35% in Day 1, returning to 45%, and 73% in Days 2, and 3, respectively; a statistically non significant decrease was still found

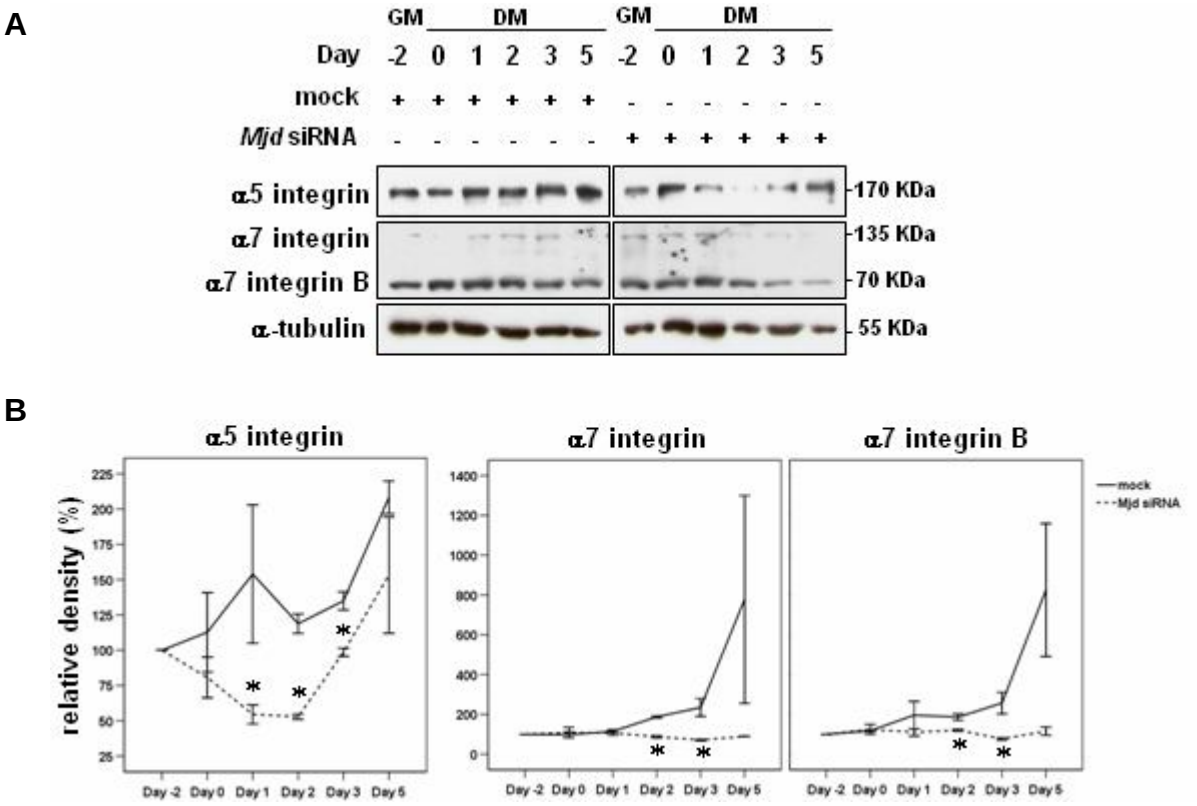

Figure 5.9. Ataxin-3 regulates the protein levels of α5 and α7 integrin subunits. (A) The amounts of α5 and α7 integrin subunits were determined by immunoblotting. Whole cell extracts of undifferentiated (Day -2) and differentiated cells (Day 0 to Day 5) were analysed for α5 integrin, α7 integrin and α-tubulin in mock and *Mjd* siRNA transfected cells. Cells were transfected at Day -2 and maintained in growth medium (GM) for 48 hours (Day 0), when the medium was changed for differentiation medium (DM). (B) Relative band density of α5 integrin, α7 integrin and α7 integrin isoform B in each day and for each transfection condition. The results were normalised for α-tubulin and correspond to the average of three independent transfections ± SEM (error bars). ∗, statistical significance ($p<0.05$).

in Day 5 (74%) (Figure 5.9A,B). The reduced levels of both mATX3 and α5-integrin in C2C12 *Mjd* siRNA transfected cells, compared to normal cells, were also confirmed by double immunofluorescence for these two proteins, as can be seen for Days 0, 1, 3 and 5, in Figure 5.10.

Although α7 integrin increases during myogenic differentiation, this increase was only observed from Day 2, and this protein showed a different expression profile than that of mATX3 (Figure 5.4). Very interestingly, in reduced-mATX3 cells (siRNA) we have verified that both α7 integrin and its isoform B levels remain low relative to undifferentiated C2C12 cells until Day 3. This was shown by a decrease of the quantity of α7 integrin and α7 integrin B in Days 2, 3 and 5 to: 47%, 65%; 30%, 30%; and 12, 14% of the normal levels,

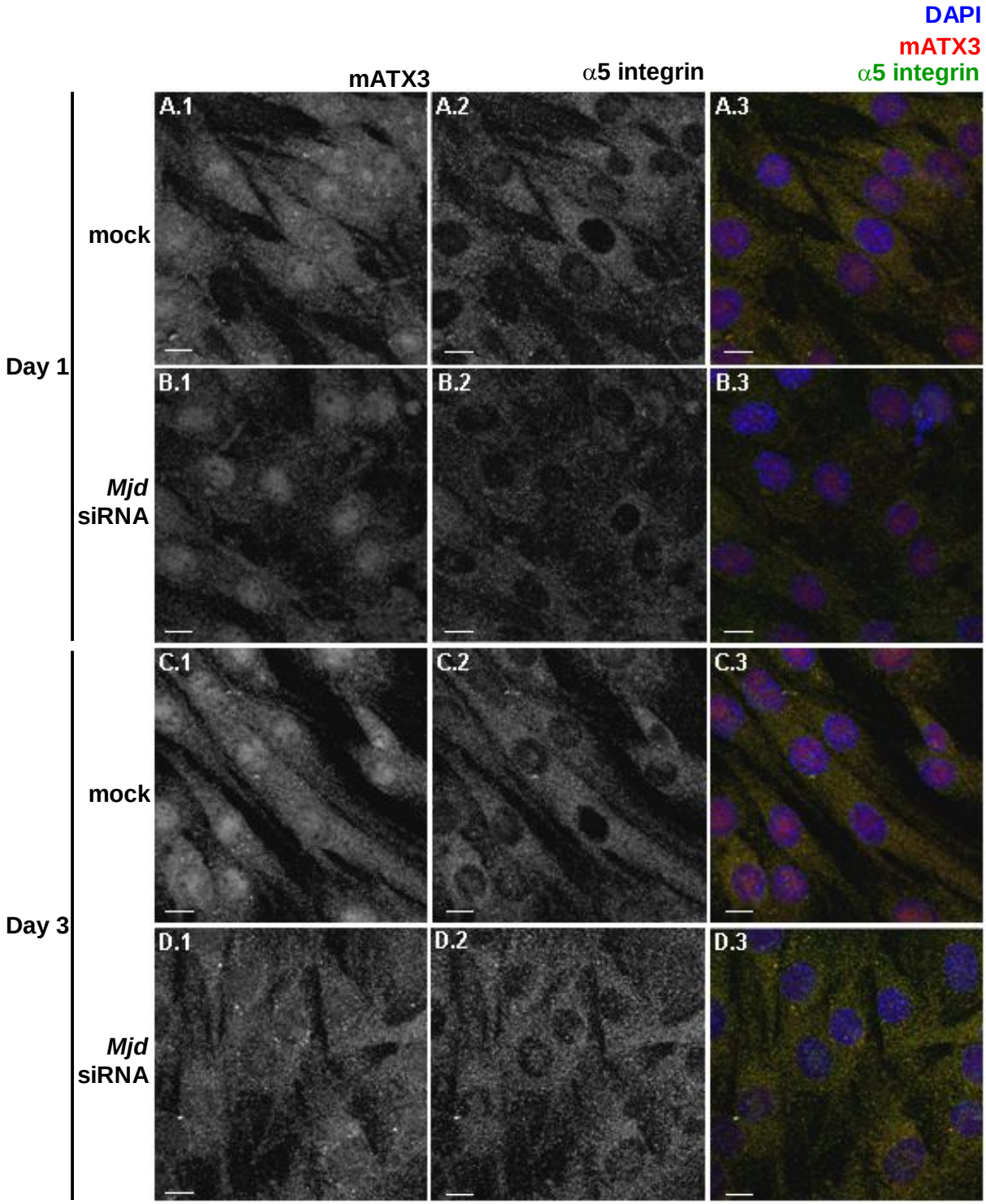

Figure 5.10. α5 integrin is down-regulated in mATX3 knockdown cells. Confocal optical z-series images of double immunofluorescence staining for mATX3 (red) and α5 integrin (green) of C2C12 differentiated cells at Day 1 (A,B) and Day 3 (C,D). At Day 1, mATX3 knockdown cells seem to be misaligned presenting reduced levels of mATX3 and α5 integrin (B), compared with mock transfected cells (A). At Day 3, the *Mjd* siRNA transfected cells still present lower amounts of mATX3 and α5 integrin (D) in comparison with the mock transfected cells (C). DNA was stained with DAPI (blue) that could be seen in the triple overlay (3). Scale bars represent 10 μm.

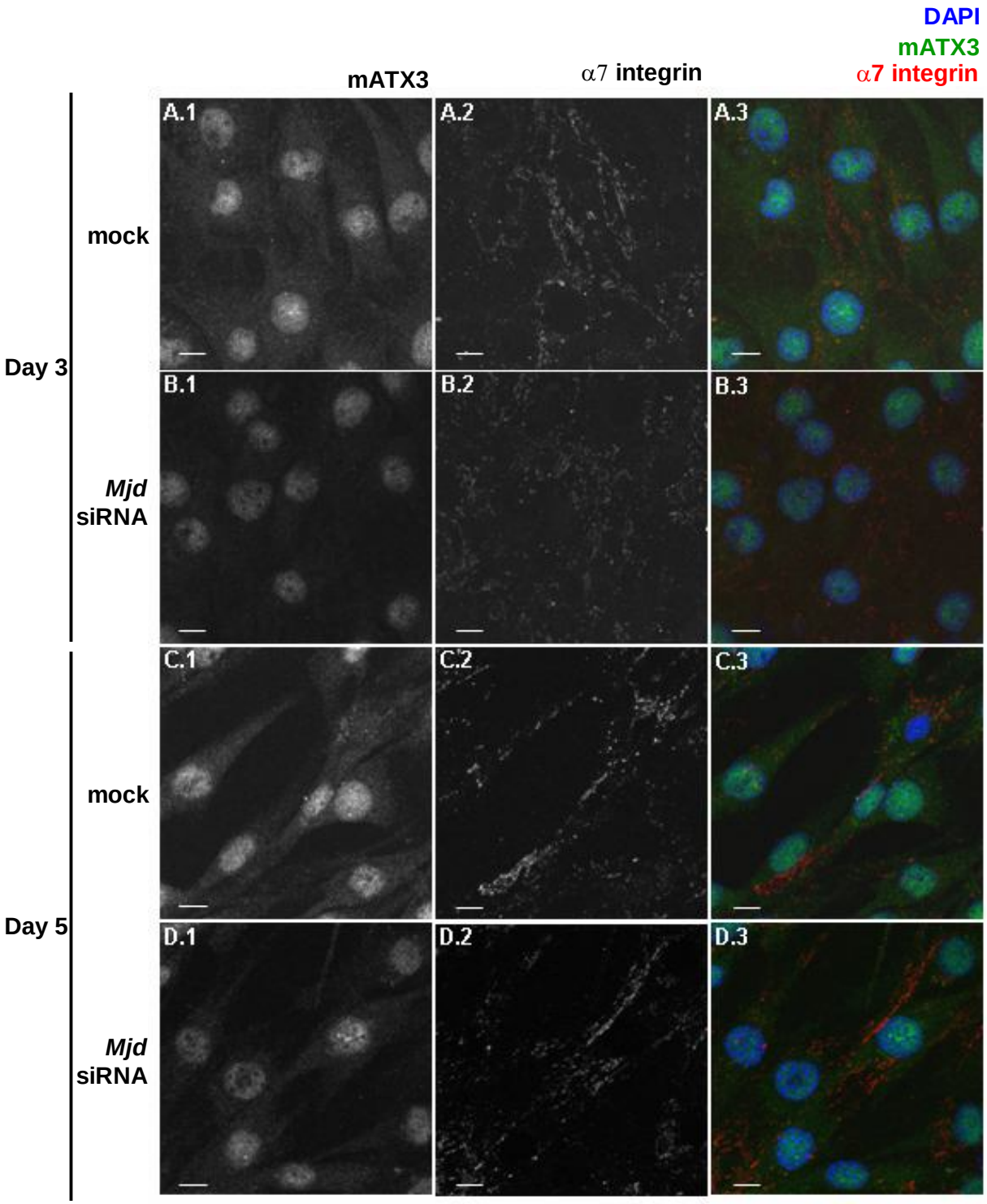

Figure 5.11. α7 integrin is down-regulated in mATX3 knockdown cells. Confocal optical z-series images of double immunofluorescence staining for mATX3 (green) and α7 integrin (red) of C2C12 differentiated cells at Day 3 (A,B) and Day 5 (C,D). At Day 3, mATX3 knockdown cells show reduced levels of mATX3 and α7 integrin (B), compared with mock transfected cells (A). At Day 5, the *Mjd* siRNA transfected cells still present lower amounts of mATX3 and α7 integrin (D) in comparison with the mock transfected cells (C). DNA was stained with DAPI (blue) that could be seen in the triple overlay (3). Scale bars represent 10 μm.

respectively (Figure 5.9A,B). Double immunofluorescence assays for mATX3 and α7 integrin confirmed the decrease of the amount of the α7 integrin subunit in Day 3 differentiated *Mjd* siRNA transfected cells (Figure 5.11). At Day 5, mATX3 knockdown cells revealed a more diffused pattern of α7 integrin staining (Figure 5.11). In these immunofluorescence assays, we could also confirm the misalignment and the increasingly round form of mATX3 knockdown cells at all the studied differentiation days (Figures 5.10 and 5.11).

In order to define whether mATX3 is affecting the expression of α5 and α7 integrin subunits at the mRNA or protein levels, we have extracted total RNA from mock and *Mjd* siRNA-transfected differentiated cells at Day 0 and Day 1 (the days of stronger knockdown of the *Mjd* transcript), and performed quantitative real-time RT-PCR to determine the amounts of the mRNAs encoding α5 integrin (*Itga5*), and α7 integrin (*Itga7*). No significant differences between normal and knockdown cells, during this period, were observed for both *Itga5* and *Itga7* genes at the mRNA level (Figure 5.12), suggesting that mATX3 is important for the maintenance the corresponding protein levels. If anything, there was a trend towards an increase of the mRNA levels, perhaps as an attempt to compensate for reduced protein levels.

The expression patterns of α5 and α7 integrin subunits in *Mjd* siRNA-transfected cells relative to mATX3 levels suggest to us that the α5 integrin subunit might be directly regulated by mATX3 whether the effect on α7 integrin subunit is probably indirect, since the levels of the latter do not recover with the progressive recovery of mATX3 levels.

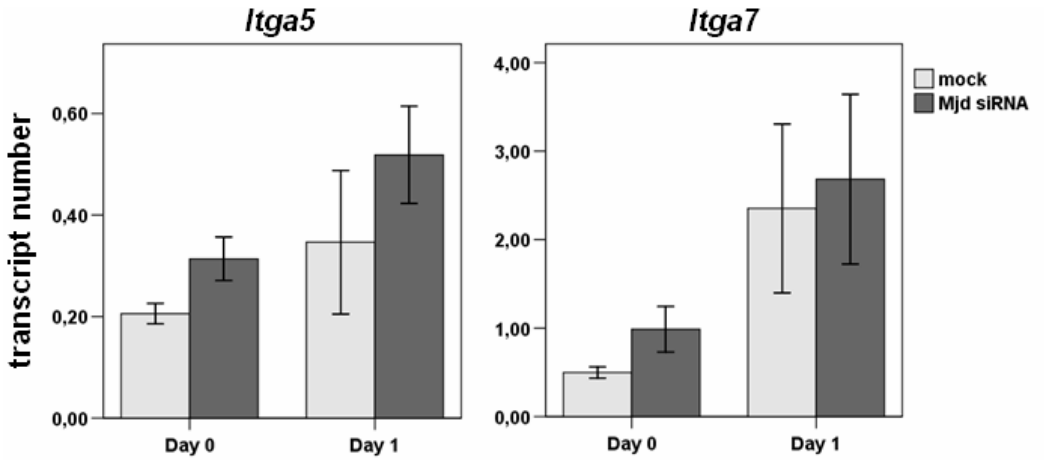

Figure 5.12. Ataxin-3 is not regulating the amounts of α5 and α7 integrin subunits at the gene expression level. Mock and *Mjd* siRNA transfected C2C12 cells at Day 0 and Day 1 of differentiation, show identical transcript levels of *Itga5* and *Itga7* that were measured by real-time RT-PCR. The results were normalised for the *Hprt* gene and correspond to the mean of three independent transfections ± SEM (error bars).

Ataxin-3 interacts directly with α5 integrin subunit

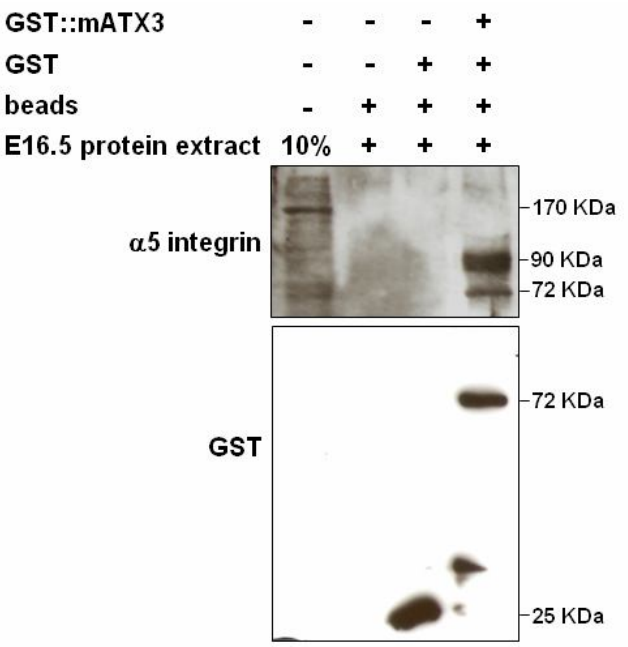

Figure 5.13. The GST pull-down assay shows direct interaction of mATX3 and α5 integrin. Purified recombinant GST::mATX3 protein was incubated with a whole protein extract from an E16.5 mouse embryo. The upstream immunoblotting correspond to the incubation with the anti-α5 integrin antibody, and the downstream blot refers to its incubation with the anti-GST antibody after stripping of the membrane. Lane 1 corresponds to 10% of the input showing α5 integrin as its main form with 170 KDa and also many other bands potentially corresponding to cleaved forms of this apparent unstable protein. Lane 4 shows that GST-mATX3 is able to pull-down α5 integrin in its 90 and 72 KDa forms probably corresponding to cleaved products produced during the assay. The recombinant GST protein did not show binding, as well as the glutathione-sepharose beads (*beads*) used in this assay.

Since the expression profile of α5 integrin was identical to that one of mATX3 either in mock or *Mjd* siRNA transfected C2C12 differentiating cells, the *Itga5* gene levels were not altered in the mATX3 knockdown cells, and knowing that mATX3 is able to deubiquitinate a protein, we hypothesised that mATX3 could be acting, as a DUB, directly in the recovery of α5 integrin from degradation. To test the association of mATX3 with α5 integrin we performed GST pull-down assays. Using GST::mATX3 and total protein extracts from a E16.5 mouse embryo, we were able to pull down α5 integrin (Figure 5.13), thus confirming that the interaction between these two proteins occurs in the conditions of the embryo milieu.

Ataxin-3 represses proteolysis of α5 integrin

The α5 integrin subunit levels are known to be regulated by the UPS system (Kaabeche et al. 2005). We have studied the expression levels of endogenous α5 integrin upon protein synthesis blocking by cycloheximide in GFP::mATX3 overexpressing C2C12 cells. We observed that mATX3 overexpression increased the amounts of α5 integrin subunit, its half-life being prolonged (Figure 5.14).

This result suggests that the α5 integrin subunit is stabilised by mATX3.

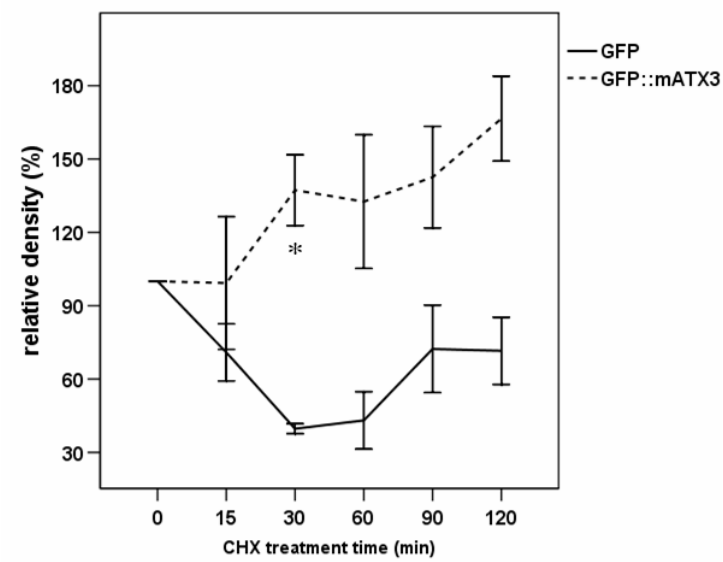

Figure 5.14. Stabilisation of the α5 integrin subunit by ataxin-3. The effect of the mATX3 overexpression in the half-life of α5 integrin is shown. C2C12 cells were transfected with the pEGFP:Mjd plasmid or with the pEGFP-C1 empty plasmids and the levels of endogenous α5 integrin were measured by immunoblotting. The graph represents the relative amounts of α5 integrin in mATX3 overexpressing cells (GF::mATX3) and in control cells (GFP) at various cycloheximide treatment times. The results were normalised for α-tubulin and correspond to the average of three independent transfections ± SEM (error bars). ∗, statistical significance ($p<0.05$).

Proteomic profile of C2C12 cells knock-down for mATX3 by siRNA at Day 0 and Day 1 of differentiation

The above mentioned results pointed out that ataxin-3 may be important in the myogenesis process by regulating the levels of some proteins potentially through the UPS. In order to verify the type(s) of proteins mATX3 is regulating during this process, we have performed a large-scale proteomic analysis of C2C12 cells knock-down for mATX3 by *Mjd* siRNA before (Day 0) and after differentiation (Day 1).

Two independent samples of total proteins from C2C12 cells of differentiation Day 0 and Day 1 (mock and *Mjd* siRNA transfections) were labelled using the iTRAQ labelling system, separated by isoelectric focusing, and analysed by LC-ESI-MS/ MS. The average number of proteins detected per sample was of 1634 proteins. We defined the proteins with altered expression levels as the ones presenting fold changes higher then or equal to 20% of the normal levels (1.2< fold change< 0.8) considering a statistical significant p-value< 0.05.

At Day 0, when the levels of mATX3 were reduced to 18% in *Mjd* siRNA transfected cells, a total of 110 proteins showed to be altered (Table 5.1). Among these proteins, 66 were identified in sample1 (exp1) and 50 in sample2 (exp2). Six proteins were detected in

Table 5.1. Proteins that showed to be altered upon the *Mjd* siRNA in undifferentiated C2C12 cells (Day 0) and in 24 hours differentiated C2C12 cells (Day 1) in each of the two independent experiments performed.

Name	Description	Fold change *Mjd* siRNA/ mock Day 0		Fold change *Mjd* siRNA/ mock Day 1	
		exp 1	exp 2	exp 1	exp 2
AARS	alanyl-tRNA synthetase		1.803	-1.453	-2.696
ACACA	acetyl-Coenzyme A carboxylase alpha		1.470		-1.730
ACOT7	acyl-CoA thioesterase 7			1.264	
ADSS	adenylosuccinate synthase			1.306	
AHNAK	AHNAK nucleoprotein		1.321		-1.439
AHSA1	activator of heat shock 90kDa protein ATPase homolog 1 (yeast)	-1.621			
ALDH1L2	aldehyde dehydrogenase 1 family, member L2				1.312
ANXA2	annexin A2				1.277
ANXA6	annexin A6		1.210		
ANXA7	annexin A7				1.349
AP1B1	adaptor-related protein complex 1, beta 1 subunit		-1.470		1.632
AP2S1	adaptor-related protein complex 2, sigma 1 subunit	-1.406			
ARHGDIA *	Rho GDP dissociation inhibitor (GDI) alpha	1.401			
ARPC2	actin related protein 2/3 complex, subunit 2, 34kDa	-1.303			
ARPC3	actin related protein 2/3 complex, subunit 3, 21kDa	1.362		1.359	
BANF1	barrier to autointegration factor 1		2.233		-2.886
BTF3	basic transcription factor 3	1.391			
CACYBP	calcyclin binding protein		-1.330		
CALU	calumenin	1.316			
CAPN2	calpain 2, (m/II) large subunit				1.300
CCT3	chaperonin containing TCP1, subunit 3 (gamma)	-1.251			
CCT8	chaperonin containing TCP1, subunit 8 (theta)	-1.261		-1.276	
CDC42	cell division cycle 42 (GTP binding protein, 25kDa)		1.372		-1.655
CFL2	cofilin 2 (muscle)				1.664
CHORDC1	cysteine and histidine-rich domain (CHORD)-containing 1				1.304
CKAP4	cytoskeleton-associated protein 4			1.327	
COPB1	coatomer protein complex, subunit beta 1	-1.289			
CPNE3	copine III				-1.423
CRYAB	crystallin, alpha B				-1.332
CSE1L	chromosome segregation 1-like (yeast)		1.264	-1.361	
CSRP1	cysteine and glycine-rich protein 1	1.234			
CTPS	CTP synthase				-1.758
CTSB	cathepsin B		1.440		
DBI	diazepam binding inhibitor (GABA receptor modulator, acyl-Coenzyme A binding protein)	1.387			
DCTN1	dynactin 1 (p150, glued homolog, Drosophila)			-1.807	
DDX3X	DEAD (Asp-Glu-Ala-Asp) box polypeptide 3, X-linked	-1.447			
DDX6	DEAD (Asp-Glu-Ala-Asp) box polypeptide 6			1.264	
DIABLO	diablo homolog (Drosophila)			-1.636	

Table 5.1. (continued)

Name	Description	Fold change *Mjd* siRNA/ mock Day 0		Fold change *Mjd* siRNA/ mock Day 1	
		exp 1	exp 2	exp 1	exp 2
DKFZP564J0863	DKFZP564J0863 protein			-1.431	
DNPEP	aspartyl aminopeptidase				1.232
DPYSL3	dihydropyrimidinase-like 3	1.284			
DUT	dUTP pyrophosphatase		-1.254		
DYNLL1	dynein, light chain, LC8-type 1	2.611			
EEF2	eukaryotic translation elongation factor 2		-1.371		1.244
EG382844	predicted gene, EG382844		-1.605		1.370
EG633683	predicted gene, EG633683		-1.261		
EHD1	EH-domain containing 1	1.201			
EIF2S1	eukaryotic translation initiation factor 2, subunit 1 alpha, 35kDa			-1.386	
EIF2S3	eukaryotic translation initiation factor 2, subunit 3 gamma, 52kDa			1.311	
EIF3EIP	eukaryotic translation initiation factor 3, subunit E interacting protein				-1.886
EIF4G1	eukaryotic translation initiation factor 4 gamma, 1		-1.393		
ESD	esterase D/formylglutathione hydrolase			-1.324	
FASN	fatty acid synthase		1.223	-1.438	-1.287
FER1L3	fer-1-like 3, myoferlin (*C. elegans*)	1.302		1.315	
FHL1	four and a half LIM domains 1	1.287			
FKBP4	FK506 binding protein 4, 59kDa	-1.506			
FSCN1	fascin homolog 1, actin-bundling protein (*S. purpuratus*)		1.224		
GANAB	glucosidase, alpha; neutral AB				-1.642
GART	phosphoribosylaminoimidazole synthetase		-1.310		1.267
GDI2	GDP dissociation inhibitor 2	-1.272			
GLS	glutaminase			-2,198	
GNAI2	guanine nucleotide binding protein (G protein), alpha inhibiting activity polypeptide 2			-1.330	
GNAS	GNAS complex locus		-1,341		
GNB2L1	guanine nucleotide binding protein (G protein), beta polypeptide 2-like 1	-1.346			
GOLPH3	golgi phosphoprotein 3 (coat-protein)			1.289	
GSTA4	glutathione S-transferase A4	1.264	1.309		
GSTA5	glutathione S-transferase A5	1.540			1.333
GSTP1	glutathione S-transferase pi	1.303			
HIST1H3I	histone cluster 1, H3i		-1.477		
HMGB2	high-mobility group box 2		3.087		-1.933
HPRT1	hypoxanthine phosphoribosyltransferase 1	1.476	1.328		
HSP90B1	heat shock protein 90kDa beta (Grp94), member 1				-1.273
HSPA9	heat shock 70kDa protein 9 (mortalin)	1.218	-1.277		1.291
HSPD1	heat shock 60kDa protein 1 (chaperonin)		-1.361		
KIF5B	kinesin family member 5B				-1.349
LDB3	LIM domain binding 3	1.574			

Table 5.1. (continued)

Name	Description	Fold change *Mjd* siRNA/ mock Day 0		Fold change *Mjd* siRNA/ mock Day 1	
		exp 1	exp 2	exp 1	exp 2
LGALS3	lectin, galactoside-binding, soluble, 3	1.463		1,308	
LONP1	lon peptidase 1, mitochondrial			-1.255	
LRP1	low density lipoprotein-related protein 1 (alpha-2-macroglobulin receptor)				-1.322
LRRC59	leucine rich repeat containing 59	1.272		1.201	
MAGOH	mago-nashi homolog, proliferation-associated (Drosophila)		-1.551		1.485
MCM7	minichromosome maintenance complex component 7		-1.527		1.797
MDH2	malate dehydrogenase 2, NAD (mitochondrial)	1.225			
MIF	macrophage migration inhibitory factor (glycosylation-inhibiting factor)	1.223			
MRPS22	mitochondrial ribosomal protein S22			1.339	
MTHFD1	methylenetetrahydrofolate dehydrogenase (NADP+ dependent) 1			1.563	
NAP1L4	nucleosome assembly protein 1-like 4				-1.309
NCAPD2	non-SMC condensin I complex, subunit D2	-1.276			
NCBP1	nuclear cap binding protein subunit 1, 80kDa			-2.036	
NCL	nucleolin		-1.342		
NME1	non-metastatic cells 1, protein (NM23A)	1.314	2.235	1.276	-1.964
NRD1	nardilysin (N-arginine dibasic convertase)			-1.399	
OGDH	oxoglutarate (alpha-ketoglutarate) dehydrogenase (lipoamide)		1.835		
OLA1	Obg-like ATPase 1	1.262			
OXCT1	3-oxoacid CoA transferase 1			-1.475	
PCMT1 *	protein-L-isoaspartate (D-aspartate) O-methyltransferase				-1.312
PDHA1	pyruvate dehydrogenase (lipoamide) alpha 1		1.572		
PDIA6	protein disulfide isomerase family A, member 6				1.339
PDLIM1	PDZ and LIM domain 1 (elfin)		-1.607		1.548
PGAM1	phosphoglycerate mutase 1 (brain)	1.774			
PGD	phosphogluconate dehydrogenase				-1.502
PGLS	6-phosphogluconolactonase	1.336			
PHB	prohibitin			1.335	
PLEC1	plectin 1, intermediate filament binding protein 500kDa	-1.300			
PLS3	plastin 3 (T isoform)				1.295
PPIA	peptidylprolyl isomerase A (cyclophilin A)	1.304			
PPP2R1A	protein phosphatase 2 (formerly 2A), regulatory subunit A , alpha isoform				1.343
PREP	prolyl endopeptidase		1.236		
PRSS1	protease, serine, 1 (trypsin 1)			-2.140	
PSAP	prosaposin	-1.629			
PSMA3	proteasome (prosome, macropain) subunit, alpha type, 3	-1.355	-1.525	-1.596	
PSMA6	proteasome (prosome, macropain) subunit, alpha type, 6	-1.545		-1.721	
PSMB2	proteasome (prosome, macropain) subunit, beta type, 2		2.266		-2.474
PSMB7	proteasome (prosome, macropain) subunit, beta type, 7		-2.217		

Table 5.1. (continued)

Name	Description	Fold change *Mjd* siRNA/ mock Day 0		Fold change *Mjd* siRNA/ mock Day 1	
		exp 1	exp 2	exp 1	exp 2
RARS	arginyl-tRNA synthetase				1.368
RPL10	ribosomal protein L10		-1.255		
RPL11	ribosomal protein L11	-1.280			
RPL18A	ribosomal protein L18a	-1.428			
RPL26	ribosomal protein L26	1.206		1.215	
RPL32	ribosomal protein L32	-1.520			
RPL38	ribosomal protein L38	1.331		1.805	1.541
RPLP2	ribosomal protein, large, P2				-1.477
RPS24	ribosomal protein S24	-1.266			1.289
RPS3A	ribosomal protein S3A				1.200
RPS8	ribosomal protein S8	-1.424			
RRBP1	ribosome binding protein 1 homolog 180kDa (dog)			-1.620	
S100A10	S100 calcium binding protein A10	1.360			
S100A11	S100 calcium binding protein A11 (calgizzarin)	1.559		1.460	
S100A4	S100 calcium binding protein A4		-1.587		
S100A6	S100 calcium binding protein A6	1.219			
SCYE1	small inducible cytokine subfamily E, member 1 (endothelial monocyte-activating)	1.220			
SEC31A	SEC31 homolog A (*S. cerevisiae*)	-1.319		-1.324	
SHMT2	serine hydroxymethyltransferase 2 (mitochondrial)	-1.276			
SLC2A1	solute carrier family 2 (facilitated glucose transporter), member 1		1.246		
SNRPE	small nuclear ribonucleoprotein polypeptide E	-1.284		-1.328	
SOAT1	sterol O-acyltransferase (acyl-Coenzyme A: cholesterol acyltransferase) 1	-2.555		-2.130	
STRAP	serine/ threonine kinase receptor associated protein			1.370	
SUB1	SUB1 homolog (*S. cerevisiae*)	-1.328			
SURF4	surfeit 4	-1.612			
TARS	threonyl-tRNA synthetase	-1.346			
TFRC	transferrin receptor (p90, CD71)			-1.373	
TLN1	talin 1				1.213
TNPO1	transportin 1		1.491		-1.399
TOR1B	torsin family 1, member B (torsin B)	1.252			
TPM2	tropomyosin 2 (beta)			1.717	
TPP2	tripeptidyl peptidase II	-1.265			
TPT1	tumor protein, translationally-controlled 1			-1.443	
TUBA4A	tubulin, alpha 4a			-1.267	
TXN	thioredoxin				-1.300
TXNDC5	thioredoxin domain containing 5	1.337	1.219		
TXNRD1	thioredoxin reductase 1				1.240
UBE1	ubiquitin-activating enzyme E1				1.234
USP11	ubiquitin specific peptidase 11			-1.298	

Table 5.1. (continued)

Name	Description	Fold change *Mjd* siRNA/ mock Day 0		Fold change *Mjd* siRNA/ mock Day 1	
		exp 1	exp 2	exp 1	exp 2
VCP	valosin-containing protein				1.238
VIM	vimentin		-1,263		
VPS35	vacuolar protein sorting 35 homolog (S. cerevisiae)			-1,613	
WBP11	WW domain binding protein 11		-1,549		
WDR61	WD repeat domain 61			1,677	
XPO1	exportin 1 (CRM1 homolog, yeast)	-1,517		-1,290	
XPO5	exportin 5			-1,646	
YWHAE	tyrosine 3-monooxygenase/tryptophan 5-monooxygenase activation protein, epsilon polypeptide		1,476		

(∗) ATX3 interactor

both samples: Gsta4, Hprt1, Nme1, Psma3, Txndc5, and Hspa9. Hspa9 showed opposite trends of change in the two samples, and thus was eliminated from the subsequent analysis.

Knock-down of mATX3 in C2C12 cells differentiated during 24 hours (32% of mATX3) caused an alteration of the expression levels of 103 proteins (Table 5.1). A total of 51 and 56 proteins were detected in sample 1 (exp1) and sample 2 (exp2), respectively. Four proteins showed to be the same in both samples: Fasn, Aars, Rpl38, and Nme1. Nme1 showed contradictory fold changes in the two samples and was removed from the analysis.

Interestingly, two ATX3 interactors were shown to be altered in mATX3 depleted cells. ARHGDIA, a Rho GTP dissociation inhibitor, a known ATX3 interactor, was upregulated in undifferentiated cells (Day 0). The other interactor that showed decreased expression levels in 24 hours differentiated cells was Pcmt1, a newly found mATX3 partner identified in this work that is a RNA-binding protein presenting methyltransferase activity and interacts with CREBBP and p300 (Chapter 4.1).

A total of 35 proteins presented expression changes in mATX3 depleted cells at both days of differentiation (Day 0 and Day 1): Aars, Acaca, Ahnak, Ap1b1, Arpc3, Banf1, Cct8, Cdc42, Cse1l, Eef2, EG382844, Fasn, Gart, Fer1l3, Gsta5, Hmgb2, Hspa9, Lgals3, Lrrc59, Mgoh, Mcm7, Nme1, Pdlim1, Psma3, Psma6, Psmb2, Rpl26, Rpl38, Rps24, S100A11, Sec31a, Snrpe, Soat1, Tnpo1, and Xpo1. In general and independently of the differentiation cellular state, mATX3 seem to be implicated in protein synthesis and degradation processes, given that several of these proteins were proteasomal and ribosomal components.

To better understand the biological significance of the overall changes in protein levels, proteins were functionally grouped in networks using the Ingenuity Pathways Analysis software.

In undifferentiated C2C12 cells (Day 0) six functional networks were found to be affected in the absence of mATX3 related to: (A) cellular movement, cancer, gastrointestinal disease; (B) drug metabolism, metabolic disease; (C) protein synthesis, viral function, cancer; (D) skeletal and muscular system development and function, tissue morphology, cancer; (E) cellular development, embryonic development, cellular assembly and organisation; and (F) lipid metabolism, small molecule biochemistry, gene expression (Table 5.2).

The reduced levels of mATX3, 24 hours after differentiation of C2C12 cells (Day 1), resulted in a dysregulation of the levels of proteins involved in the following networks: (G) lipid metabolism, nucleic acid metabolism, small molecule biochemistry; (H) protein synthesis, cell death, cancer; (I) lipid metabolism, small molecule biochemistry, protein synthesis; (J) cellular movement, cell death, cancer; (K) cancer, cell cycle, gastrointestinal disease; and (L) molecular transport, protein trafficking, RNA trafficking (Table 5.3).

Ataxin-3 seems to be important in the regulation of the levels of several proteins directly implicated or related with the integrin signaling pathway

To analyse the effect of the decreased levels of mATX3 in both undifferentiated (Day 0) and differentiated C2C12 cells in the integrin signaling pathway we have overlaid the altered proteins in these days with this canonical pathway using the above mentioned software (Figure 5.15).

At Day 0, the decreased levels of mATX3 lead to the alteration of the levels of three proteins involved in one of the signal transduction cascades stimulated by integrin/ extracellular matrix (ECM) interactions that lead to cytoskeleton rearrangements contributing to cell motility. These proteins were two subunits of the actin related protein 2/3 (Arp2/3) complex, Arpc2 and Arpc3; and the GTPase Cdc42, which in turn activates the Arp2/3 complex (Figure 5.15). Arpc3 and Cdc42 showed to be upregulated (1.362 and 1.372, respectively), and Arpc2 down-regulated (-1.303). This suggests that the actin filament organisation may be deregulated in undifferentiated cells with decreased levels of mATX3, which may lead to alterations in cytoskeleton and cell motility.

At Day 1, knockdown of mATX3 caused changes in proteins implicated in two signal transduction cascades stimulated by integrins triggering cytoskeleton rearrangements or ERK/MAPK-mediated transcription (Figure 5.15). Interestingly, the levels of Arpc3 and Cdc42, which were altered at Day 0, were also changed at Day1 (Figure 5.15). Though Arpc3 also increased at Day1 (1.359), Cdc42 levels showed the opposite trend (-1.655). In addition, talin1 (Tln1) was increased (1.213) (Figure 5.15). Tln1 is a cytoskeleton protein that

Table 5.2. Functional networks of the proteins that showed to be altered upon *Mjd* siRNA in C2C12 undifferentiated cells (Day 0).

Network	Name	Fold change *Mjd* siRNA/mock
	EIF4G1	-1.393
	EEF2	-1.371
	HSPD1	-1.361
	CACYBP	-1.330
	ARPC2	-1.303
	PLEC1	-1.300
	VIM	-1,263
	SCYE1	1.220
Cellular movement	MIF	1.223
	FSCN1	1.224
Cancer	MDH2	1.225
Gastrointestinal disease	SLC2A1	1.246
	ARPC3	1.362
	CDC42	1.372
	DBI	1.387
	ARHGDIA*	1.401
	LGALS3	1.463
	ACACA	1.470
	YWHAE	1.476
	PGAM1	1.774
	NME1♦	1.775
	PDLIM1	-1.607
	FKBP4	-1.506
	DDX3X	-1.447
	GNB2L1	-1.346
	NCL	-1.342
	SUB1	-1.328
	SEC31A	-1.319
	NCAPD2	-1.276
Drug metabolism	CCT8	-1.261
	CCT3	-1.251
Metabolic disease	GNAS	-1,341
	FASN	1.223
	FHL1	1.287
	GSTA4♦	1.287
	GSTP1	1.303
	PPIA	1.304
	BTF3	1.391
	TNPO1	1.491
	GSTA5	1.540
	LDB3	1.574

Network	Name	Fold change *Mjd* siRNA/mock
	AHSA1	-1.621
	MAGOH	-1.551
	RPL32	-1.520
	AP2S1	-1.406
	GART	-1.310
	SHMT2	-1.276
Protein Synthesis	TPP2	-1.265
	RPL10	-1.255
Viral Function	RPL26	1.206
Cancer	S100A6	1.219
	PREP	1.236
	PPIA	1.304
	RPL38	1.331
	S100A10	1.360
	HPRT1♦	1.402
	CTSB	1.440
	PSMB7	-2.217
	PSAP	-1.629
	PSMA6	-1.545
	MCM7	-1.527
Skeletal and muscular system development and function	AP1B1	-1.470
	PSMA3♦	-1.440
	SNRPE	-1.284
	GDI2	-1.272
Tissue morphology	CSE1L	1.264
Cancer	FER1L3	1.302
	BANF1	2.233
	PSMB2	2.266
	DYNLL1	2.611
	HMGB2	3.087

Table 5.2. (continued)

Network	Name	Fold change *Mjd* siRNA/mock
	SURF4	-1.612
	S100A4	-1.587
	RPL18A	-1.428
	RPS8	-1.424
Cellular development	COPB1	-1.289
	RPL11	-1.280
Embryonic development	RPS24	-1.266
	EHD1	1.201
Cellular assembly and organization	S100A6	1.219
	CSRP1	1.234
	TXNDC5♦	1.278
	AHNAK	1.321
	NME1♦	1.775
	SOAT1	-2.555
	XPO1	-1.517
	DUT	-1.254
	ANXA6	1.210
Lipid metabolism	MIF	1.223
	DPYSL3	1.284
Small Molecule biochemistry	CALU	1.316
	CTSB	1.440
Gene expression	S100A11	1.559
	PDHA1	1.572
	AARS	1.803
	OGDH	1.835

(∗) ATX3 interactor, (♦) common to exp 1 and 2

Table 5.3. Functional networks of the proteins that showed to be altered upon *Mjd* siRNA in C2C12 differentiated cells (Day 1).

Network	Name	Fold change *Mjd* siRNA/mock
	ACACA	-1.730
	CDC42	-1.655
	EIF2S1	-1.386
	TFRC	-1.373
	FASN♦	-1.363
	KIF5B	-1.349
	CRYAB	-1.332
	LRP1	-1.322
	TXN	-1.300
Lipid metabolism	HSP90B1	-1.273
	TLN1	1.213
Nucleic acid metabolism	VCP	1.238
	TXNRD1	1.240
Small molecule biochemistry	EEF2	1.244
	HSPA9	1.291
	CAPN2	1.300
	LGALS3	1.308
	PPP2R1A	1.343
	ANXA7	1.349
	STRAP	1.370
	PDLIM1	1.548
	MCM7	1.797
	AARS♦	-2.075
	EIF3EIP	-1.886
	CTPS	-1.758
	RRBP1	-1.620
	RPLP2	-1.477
	CSE1L	-1.361
Protein synthesis	SNRPE	-1.328
	SEC31A	-1.324
Cancer	RPS3A	1.200
Cell death	ANXA2	1.277
	GOLPH3	1.289
	CKAP4	1.327
	PDIA6	1.339
	RARS	1.368
	WDR61	1.677

Table 5.3. Functional networks of the proteins that showed to be altered upon *Mjd* siRNA in C2C12 differentiated cells (Day 1)

Network	Name	Fold change *Mjd* siRNA/mock
	BANF1	-2.886
	GLS	-2.198
	SOAT1	-2.130
	PGD	-1.502
Lipid metabolism	ESD	-1.324
	CCT8	-1.276
Small molecule biochemistry	RPL26	1.215
	ACOT7	1.264
Protein synthesis	DDX6	1.264
	GART	1.267
	CAPN2	1.300
	MTHFD1	1.563
	RPL38♦	1.673
	VPS35	-1.613
	OXCT1	-1.475
	GNAI2	-1.330
	NAP1L4	-1.309
Cellular movement	TUBA4A	-1.267
	LONP1	-1.255
Cancer	UBE1	1.234
Cell death	ADSS	1.306
	FER1L3	1.315
	ARPC3	1.359
	AP1B1	1.632
	CFL2	1.664
	PSMB2	-2.474
	DCTN1	-1.807
	PSMA6	-1.721
	DIABLO	-1.636
Cancer	PSMA3	-1.596
Cell cycle	TPT1	-1.443
	AHNAK	-1.439
Gastrointestinal disease	NRD1	-1.399
	USP11	-1.298
	RPS24	1.289
	EIF2S3	1.311
	GSTA5	1.333
	NCBP1	-2.036
	HMGB2	-1.933
Molecular transport	XPO5	-1.646
	TNPO1	-1.399
Protein trafficking	PCMT1∗	-1.312
	XPO1	-1.290
RNA trafficking	S100A11	1.460
	MAGOH	1.485
	TPM2	1.717

(∗) ATX3 interactor, (♦) common to exp 1 and 2

is co-distributed with integrins in the cell surface membrane in order to assist in the attachment of adherent cells to ECM, participating in actin filament assembly, and in spreading and migration of several types of cells. Furthermore, calpain 2 (Capn2), a large subunit of calpain activated by the ERK/MAPK pathway (Leloup et al. 2007), was increased (1.300) in Day 1 cells depleted of mATX3 (Figure 5.15). These results indicate that during myogenic differentiation, namely at Day 1, the decreased levels of mATX3 may be responsible for a deregulation of the cytoskeleton assembly and of the ERK/MAPK-mediated transcription an effect that may be directly related to the integrin signaling pathway.

In order to determine which proteins, deregulated in the presence of low levels of mATX3 before differentiation, were related with the integrin signaling pathway we have

Day 0

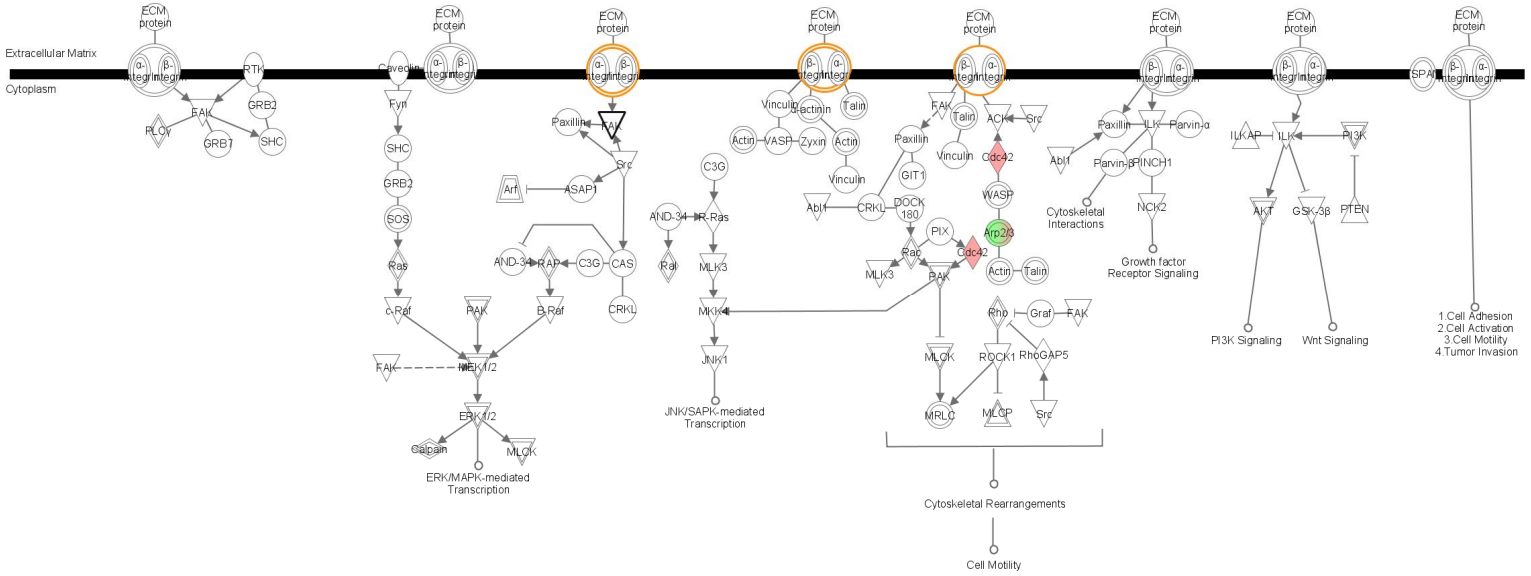

Day 1

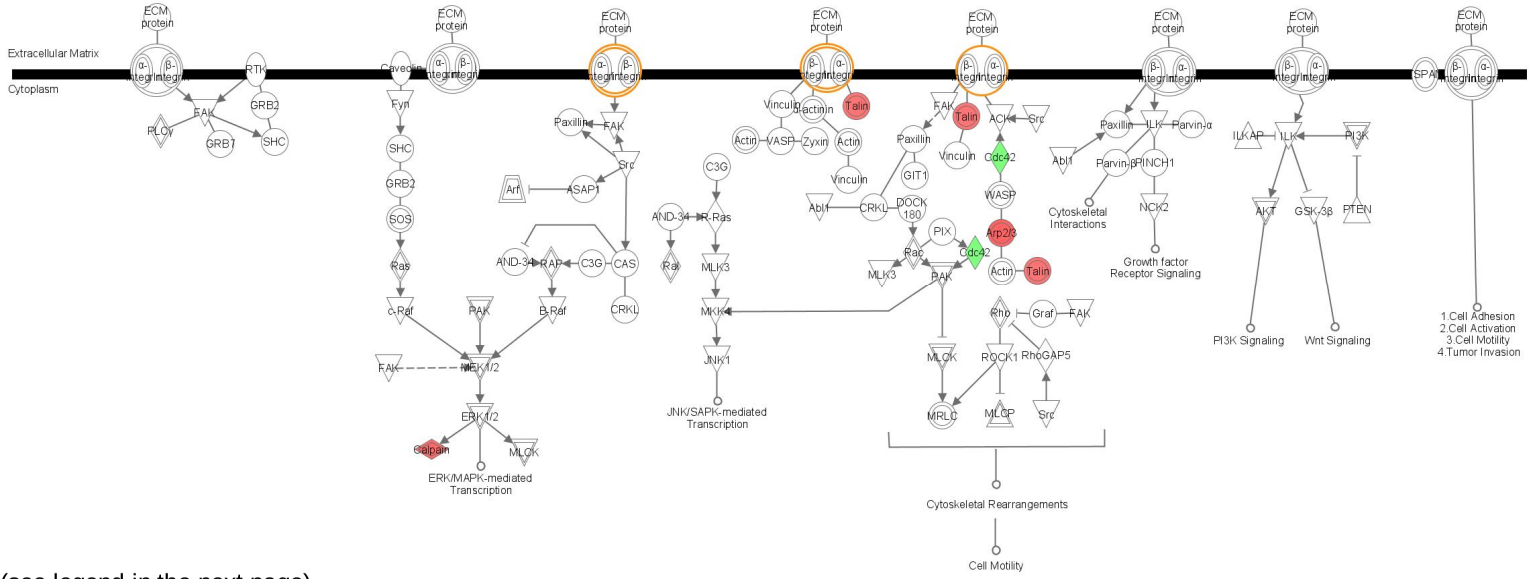

Figure 5.15. (see legend in the next page)

Figure 5.15. Schematic representations of the overlay of the proteins that showed to be altered in undifferentiated (Day 0), or in differentiated (Day 1) C2C12 cells with depleted levels of mATX3 with the integrin signaling pathway. Schemes were adapted from Ingenuity Pathways Analysis Inc.

---

overlaid the Day 0 corresponding functional networks with this canonical pathway. We have verified that three of the networks were related to the integrin signaling pathway – networks A (Figure 5.16), B (Figure 5.17), and C (Figure 5.18).

The analysis of the network A (comprising Arpc2, Arpc3 and Cdc42) revealed that three upregulated proteins (Arhgdia, Nme1, and Pgam1) were related to Cdc42, a member of a signal transduction cascade stimulated by integrin/ECM interactions that showed to be increased in mATX3 knockdown cells as abovementioned (Figure 5.16). Interestingly, ARHGDIA was recently shown to interact with ATX3 (Shen et al. 2006). Two structural increased in mATX3 knockdown cells as abovementioned (Figure 5.16). Interestingly, ARHGDIA was shown to interact with ATX3 (Shen et al. 2006). Two structural components of the cytoskeleton, plectin 1 (Plec1) and vimentin (VIM), were down-regulated (-1.300 and -1.263, respectively). Galectin 3 (Lgals3), a β-galactoside binding protein involved in cell growth and cell adhesion that also binds to some integrin subunits, was shown to be increased (1.463). The macrophage migration inhibition factor (MIF), which activates cell proliferation and in a complex with Jab1 may have a role in integrin signaling cascades, was upregulated in mATX3 depleted cells (1.223).

Evaluating network B, no proteins directly involved integrin signaling cascades were changed. However, two GTPases showing decreased levels were related to actin: Gnas, and Gnb2l1 that are implicated in cell growth and migration (Figure 5.17).

Similarly to network B, none of the members of integrin triggered cascades were altered in network C. Nevertheless, a protein showing diminished expression was related to Arf, one member of these cascades. This protein was the adaptor-related protein complex 2 sigma 1 subunit (Ap2s1), a component of a clathrin-associated adaptor complex Ap2 involved in endocytosis, which in turn depends of Arf for its recruitment for endosome membranes (Figure 5.18).

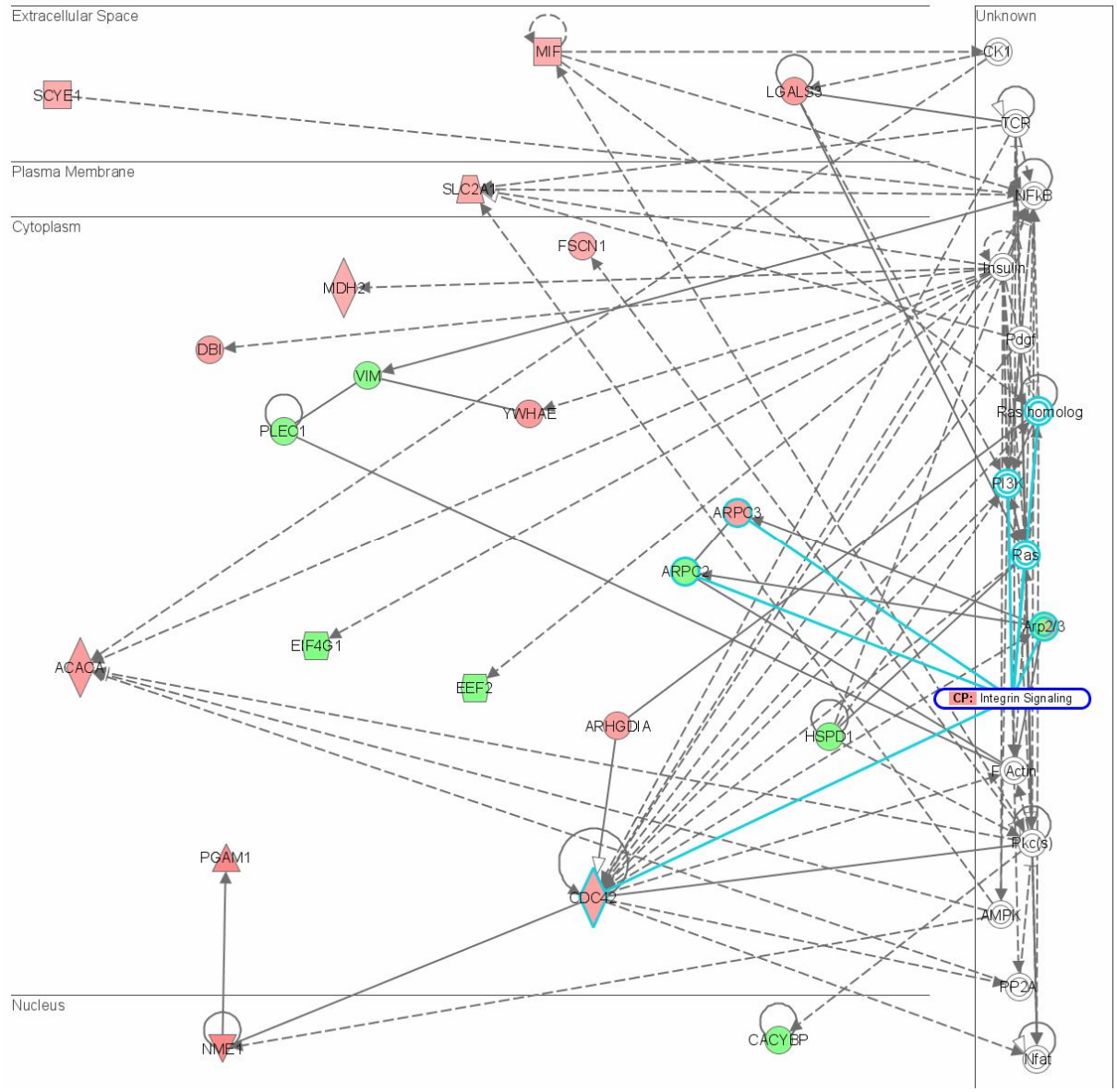

Figure 5.16. Scheme of the overlay of the functional network (A) of the proteins that showed altered expression levels in mATX3 depleted cells with the integrin signaling pathway. The biological mechanisms involved in this network of interacting proteins are: (1) cellular movement; (2) cancer; and (3) gastrointestinal disease. Upregulated proteins are highlighted in red and down-regulated proteins in green. Proteins directly involved in integrin triggered signaling cascades are delimited by a blue line. Lines correspond to binding only, full-line arrows indicate direct interactions and “action on” the pointed protein, and dashed arrows represent indirect interactions. For full-name of the proteins see Table 5.1. Network analysis was performed using the Ingenuity Pathways Analysis Inc. 5.0 software.

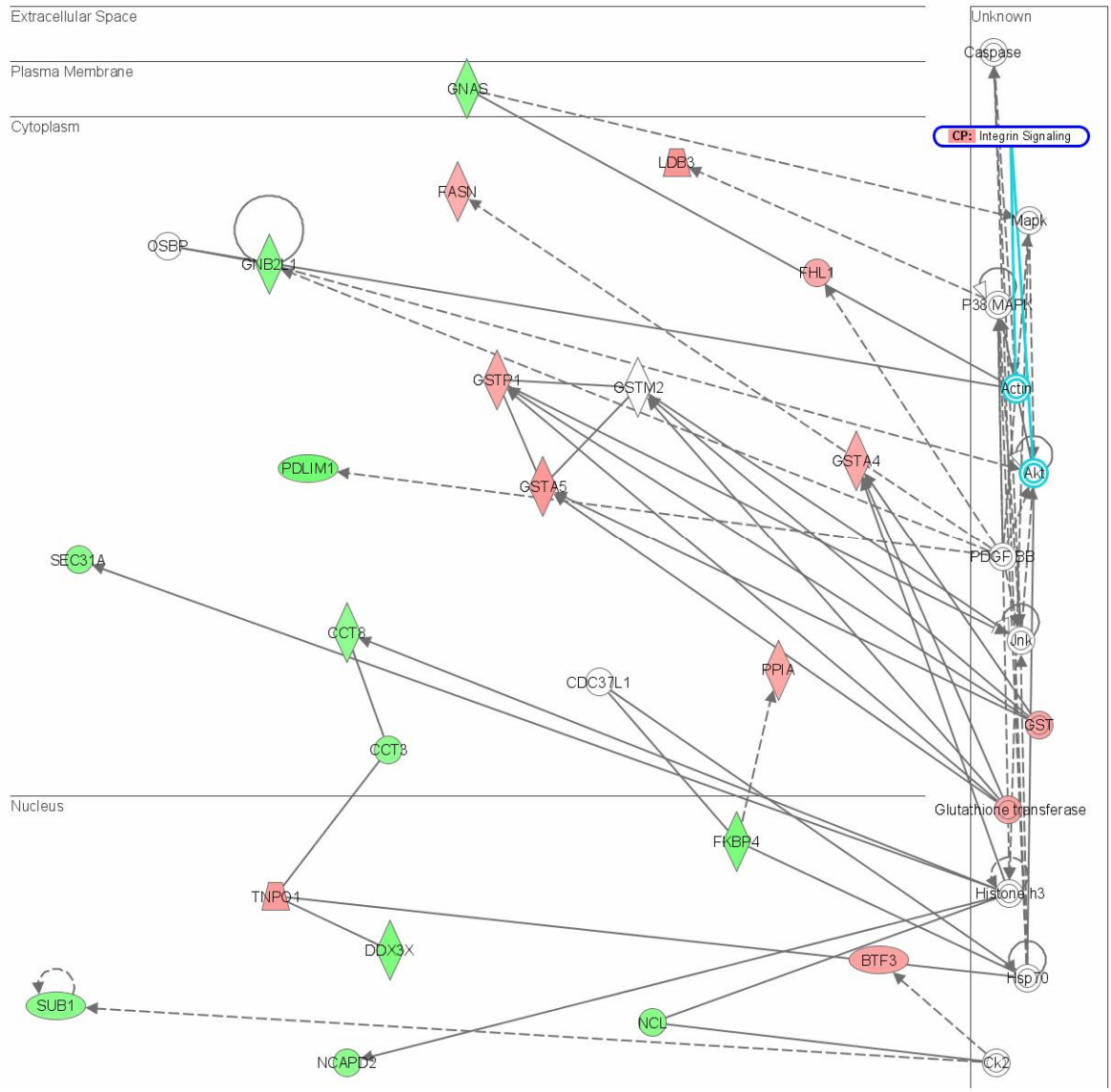

Figure 5.17. Scheme of the overlay of the functional network (B) of the proteins that showed altered expression levels in mATX3 depleted cells with the integrin signaling pathway. The biological mechanisms involved in this network of interacting proteins are: (1) drug metabolism; and (2) metabolic disease. Upregulated proteins are highlighted in red and down-regulated proteins in green. Proteins directly involved in integrin triggered signaling cascades are delimited by a blue line. Lines correspond to binding only, full-line arrows indicate direct interactions and "action on" the pointed protein, and dashed arrows represent indirect interactions. For full-name of the proteins see Table 5.1. Network analysis was performed using the Ingenuity Pathways Analysis Inc. 5.0 software.

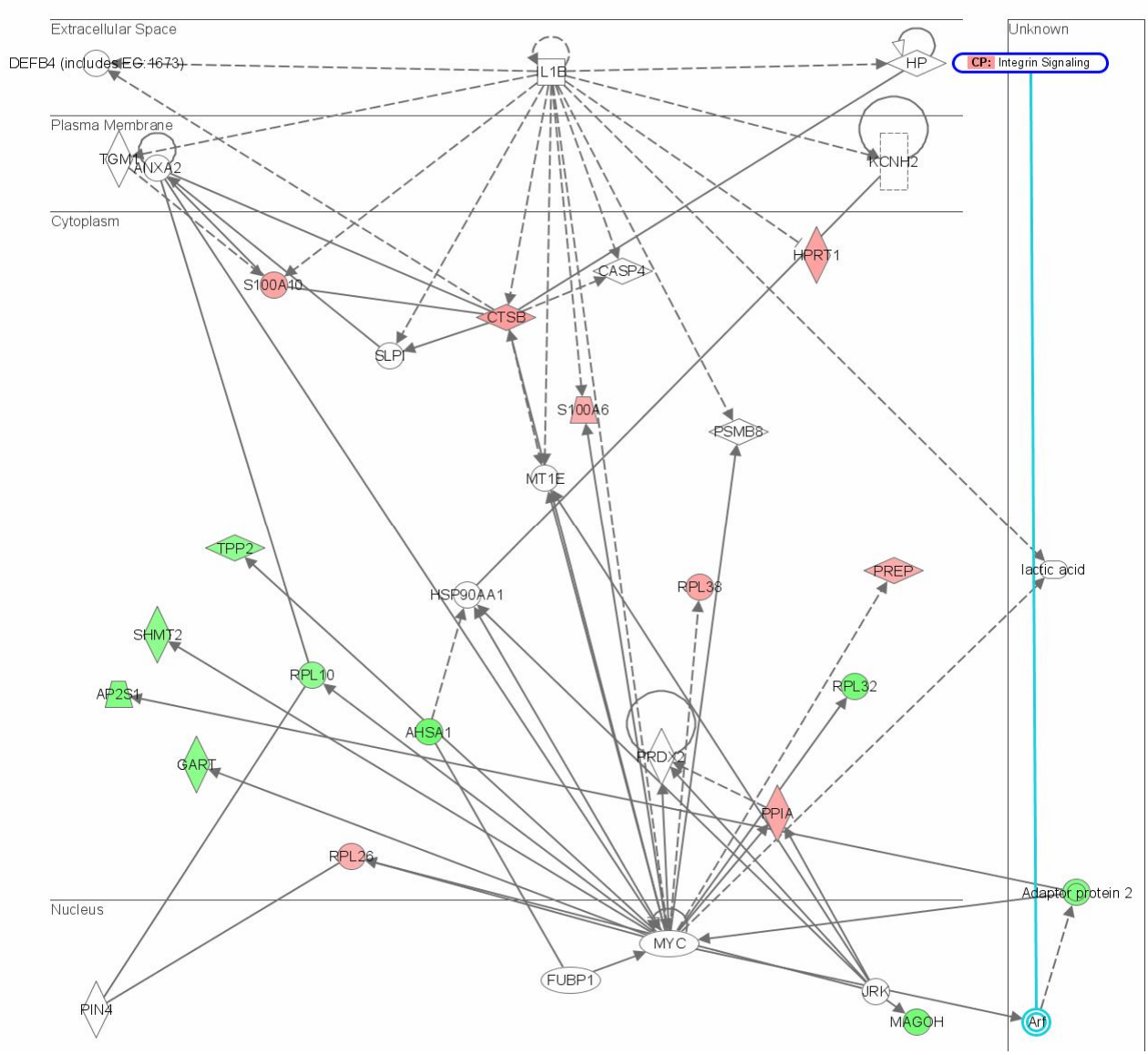

Figure 5.18. Scheme of the overlay of the functional network (C) of the proteins that showed altered expression levels in mATX3 depleted cells with the integrin signaling pathway. The biological mechanisms involved in this network of interacting proteins are: (1) protein synthesis; (2) cancer; and (3) viral function. Upregulated proteins are highlighted in red and down-regulated proteins in green. Proteins directly involved in integrin triggered signaling cascades are delimited by a blue line. Lines correspond to binding only, full-line arrows indicate direct interactions and "action on" the pointed protein, and dashed arrows represent indirect interactions. For full-name of the proteins see Table 5.1. Network analysis was performed using the Ingenuity Pathways Analysis Inc. 5.0 software.

5.5. DISCUSSION

Myogenesis is one of the most studied systems of cell differentiation. The muscle, in particular the striated muscle, is well known for its unique structure consisting of a very well organised cytoskeleton that enables its characteristic contractile function. However, the formation and maintenance of these “rigid” structures, as well as the entire event of myogenic differentiation from MPCs into the final myofibers are very dynamic processes that require a high coordination between the synthesis, degradation and assembly of key proteins. Degradation of muscle proteins occurs through several mechanisms but more importantly by the UPS. The fast regulation of protein levels by the UPS, in precise moments, is crucial for muscle development (Kim and Hoppe 2006). Several key factors in myogenesis are known to be regulated by the UPS, namely myogenic transcription factors, such as MyoD and Myogenin, and membrane proteins, like β-catenin and integrins.

As shown in chapter 2, mATX3, as the human and *C.elegans* protein, has DUB activity. However, the cellular and physiological role(s) of this enzymatic activity are not known, and it is possible that it is involved in facilitating or avoiding substrate degradation through the UPS.

Here, we studied the role of mATX3 in muscle development, given the potential function of mATX3 in the UPS, and our previous observations of high mATX3 expression during muscle development, and of *Mjd* gene activation in muscle-differentiated P19 cells (Costa et al. 2004). Similarly, other mouse DUBs, such as Usp22 (Lee et al. 2006), and Usp2-45 and Usp2-69 (Gousseva and Baker 2003) are expressed during mouse embryonic development indicating that these proteins could be involved in specific processes in different types of cells, especially those that are differentiating. We demonstrated that, at the E9.5 stage, mATX3 is highly expressed in the heart and in the skeletal muscle precursor structures, the dermomyotome and the early myotome. The mATX3 labelling pattern was more pronounced in the myotome in differentiated myogenin-positive and especially in myosin-positive cells. This profile was maintained in E11.5 embryos, and at the E14.5 developmental stage, we verified that mATX3 shows a striking fiber-like pattern. Moreover, in E18.5 hindlimbs we have observed that mATX3 is expressed in both primary and secondary myogenic fibers, fast-contracting or non fast-contracting. These results indicate that mATX3 may be involved in all stages of muscle development, playing an important role in this process. Indeed, mATX3 levels showed to increase in differentiating C2C12 cells.

We studied the involvement of mATX3, particularly, in the early stages of myogenic differentiation, by knocking down mATX3 expression in C2C12 cells, using *Mjd* siRNA transfection, and verified that, indeed, mATX3 appeared to regulate skeletal muscle differentiation. The cells with reduced expression of mATX3 seemed to continue to proliferate

and presented a delay in myogenic differentiation given to potential defects in cell-cell recognition or alignment.

Analysis of the whole protein and RNA extracts showed that the cellular phenotype verified in mATX3 knockdown cells is not due to alterations of the amounts of MyoD and myogenin, at protein or mRNA expression level, which suggests that mATX3 is acting downstream of these transcription factors. Given the apparent failure of *Mjd* siRNA cells to differentiate properly in the absence of mATX3, we decided to investigate, in these cells, the levels of two downstream targets that are involved in cell adhesion and myogenesis: α5 and α7 integrin subunits.

Integrins are heterodimeric, transmembrane cell surface receptors, composed by a α and a β subunit, which mediate cell-cell and cell-matrix interactions (Luo et al. 2007). Until now, 18 α and 8 β chains were identified, and these combine in a specific manner to form at least 24 dimers. The extracellular domains of integrin receptors bind ECM ligands, but they can also associate laterally with other proteins at the cell surface (Miranti and Brugge 2002). Integrin cytoplasmic domains form multi-molecular complexes with cell signaling proteins, and with adaptor proteins that connect to the cytoskeleton (Hynes, 2002). Clustering of integrins, following their binding with the matrix, provides a bi-directional crosstalk between inside-out and outside-in signaling. As consequence of cell-matrix adhesions, several proteins are recruited to the adhesion complexes activating signaling cascades that control cytoskeletal organisation, gene regulation, and diverse cellular processes and functions (Figure 5.19) (Berrier and Yamada 2007).

Matrix adhesions associate with actin filaments, and bidirectional interactions mediated by the actomyosin contraction and the clustering of integrins bound to the ECM provide in combination an increase of cell contractility, also known as endogenous tension. On the other hand, endogenous tension is transmitted through integrins to the ECM and increases matrix rigidity, named exogenous tension, by changing its composition (Berrier and Yamada 2007). This dynamic formation and disassembly of cell-matrix adhesions is crucial to cell migration, cell polarity, proliferation, differentiation, survival, protein synthesis and gene regulation during development (Figure 13).

There are several types of adhesion structures: focal complexes, focal adhesions, fibrillar adhesions, and three-dimensional (3D)-matrix adhesions. The ability of integrins to localise to adhesion structures is, in general, a feature of all integrin receptors. However, certain integrins concentrate in specific types of cell-adhesion structures (Berrier and Yamada 2007). As a consequence, different sets of proteins are recruited depending of the integrin receptor. For instance, focal adhesions are rich in αVβ3, fibrillar adhesions in α5β1,

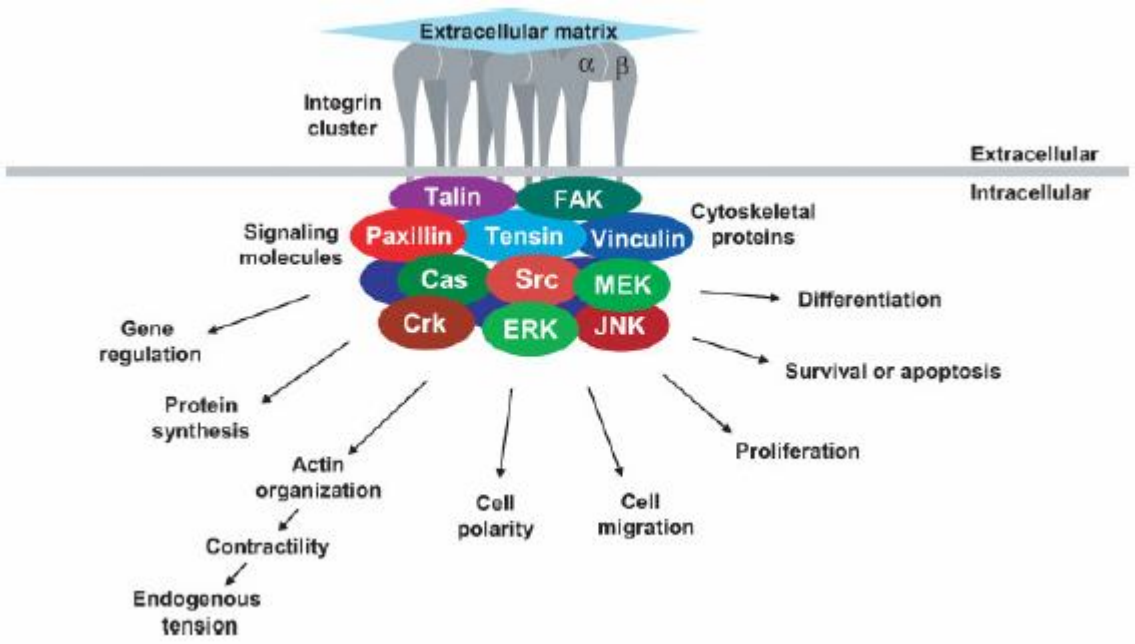

Figure 5.19. General model of cell-matrix adhesions and their downstream regulation. Cell-extracellular matrix adhesions containing clusters of integrins recruit cytoplasmic proteins, which in cooperation with other cellular receptors control diverse cellular processes. *(Berrier and Yamada 2007)*

and 3D-matrix adhesions primarily in α5β1, and in αVβ3 at the periphery (Cukierman et al. 2001). The cell-matrix interactions are coordinated with local actin polymerisation and F-actin organisation. Actin and nucleators of its polymerisation, such as Arp2/3 complex have different spatial localisation in cells in two-dimensional (2D) and 3D matrices (Pollard 2007). Therefore, dynamics in the exogenous tension within 3D matrices may influence the cellular distribution of actin and the Arp2/3 complex. On the other hand, an increase in the endogenous tension induces a conformational change in cell-associated fibronectin (an ECM molecule) that triggers its assembly in matrix (Mao and Schwarzbauer 2005). Thus, adjustments in either endogenous or exogenous tension regulate matrix assembly, and inside the cell, the cytoskeleton and signaling pathways.

In vitro studies in avian and rodent species showed that α4β1, αVβ1, α5β1, α6β1, and α7β1 integrins are the major players in skeletal muscle development (Mayer 2003).

α5β1 is the classical fibronectin receptor, whereas α6β1 and α7β1 are laminin receptors. α5β1 is ubiquitously expressed and is up-regulated in the first stages of differentiation of C2C12 cells into myotubes, which suggests a function in the cell-cycle withdrawal phase (Tomczak et al. 2004). Chimeric α5-/- mice display muscular dystrophy

(Taverna et al. 1998), pointing the human *ITGA5* as a good candidate gene to screen for mutations in patients with muscular dystrophies.

α7β1 expression is mainly restricted to skeletal and cardiac muscle, and is strongly up-regulated upon myoblast fusion, being important for cell migration (Mielenz et al. 2001). α7β1 is the major, if not the exclusive, integrin receptor found in adult skeletal muscle being enriched in myotendinous junctions (MTJ) (Bao et al. 1993), localised at the neuromuscular junctions (NMJ) together with α3 and αV integrins (Martin et al. 1996), and present in MSCs (Ozeki et al. 2006). The α7 integrin subunit is very diverse due to the occurrence of alternative mRNA splice variants for both the extracellular and cytoplasmic domains. For the cytoplasmic domains, in humans and mice, there are the A and B variants, the α7B being expressed in proliferating myoblasts and α7A isoform induced only upon terminal differentiation (Collo et al. 1993; Ziober et al. 1993). The α7A variant appear to be muscle–specific, whereas the α7B isoform is ubiquitously expressed as it has been detected in smooth muscle, neuronal, and in a variety of other tissues (Collo et al. 1993; Velling et al. 1996; Yao et al. 1997; Werner et al. 2000). Mutations in the *ITGA7* gene, the gene encoding the α7 integrin subunit, lead to congenital myopathy in humans (Hayashi et al. 1998). The knockout mice for α7 integrin subunit are viable, showing that this molecule is not essential for myogenesis, but develop a mild but progressive muscular dystrophy soon after birth (Mayer et al. 1997).

The mATX3 knockdown C2C12 cells, with an apparent defect in differentiation, presented a decrease in the protein levels of both α5 and α7 integrin subunits, which suggests that ATX3 is important in the regulation of the levels of these two molecules in the context of muscular differentiation. We have defined that mATX3 acting at the protein level, since we verified that when lowest levels of mATX3 are detected upon Mjd siRNA transfection, the *Itga5* and *Itga7* mRNA amounts were not different from the mock transfected cells. The fact that in the knockdown cells, the decreased levels of α7 integrin subunit remained at the same level during differentiation, and that this protein did not increase when the amount of mATX3 was restored, implies that mATX3 could have an indirect effect but long-lasting over the α7 integrin subunit. The role of mATX3 in this case could be to regulate the degradation of other proteins that control the up-regulation of α7 integrin, in particular at Day 2; it is possible that when mATX3 it is not present at this specific moment, the levels of these proteins could not be restored soon enough. Further experiments should be performed in order to define the protein(s) that mATX3 is having a direct effect upon and that are responsible for regulating the expression of α7 integrin subunit.

In contrast, the expression pattern of α5 integrin subunit was identical to that of mATX3 either in mock or *Mjd* siRNA transfected C2C12 differentiating cells, which means that when mATX3 levels decrease, α5 integrin subunit levels also decrease, and when mATX3 level is restored, the amount of α5 integrin subunit is also restored. Interestingly, as mATX3, α5 integrin is ubiquitously expressed and has the same expression pattern in the myotome of E9.5 and E11.5 mouse embryos (Bajanca et al. 2004; Cachaco et al. 2005). In addition, in C2C12 cells, mATX3 and α5-integrin subunit seem to colocalise. As a DUB, one could speculate that mATX3 could "recover" molecules of α5 integrin that were otherwise targeted for degradation by the UPS. Indeed, the E3 ubiquitin ligase Cbl is known to mediate the ubiquitination of α5 integrin, which is then sent for degradation in the proteasome (Kaabeche et al. 2005). Given this set of evidences, we have hypothesised that mATX3 could be acting, as a DUB, directly in the recovery of α5 integrin from degradation by the proteasome. The fact that mATX3 interacts with this integrin subunit, as shown by GST pull-down, is consistent with this possibility. Furthermore we also have shown that the overexpression of mATX3 stabilised the α5 integrin subunit. The activity of deubiquitination of α5 integrin by mATX3 could explain that, in its absence, the levels of ubiquitination of α5 integrin increase and the protein is degraded by the proteasome, which leads to an alteration in the composition of the cell surface molecules and consequently to an impairment of cell-cell and cell-matrix interactions and consequently to a maintenance of proliferation and differentiation delay.

The proteomic profile of mATX3 depleted undifferentiated and differentiated C2C12 cells revealed an involvement of mATX3 in several cellular pathways namely in protein synthesis and degradation, given that several proteasomal and ribosomal protein levels were shown to be altered. In relation to the integrin signaling transduction cascades, two of their members implicated in the actin cytoskeleton assembly and organisation presented altered expression levels in both mATX3 knockdown undifferentiated and differentiated cells. These proteins were Cdc42 and Arpc3 (a subunit of the Arp2/3 complex). Cdc42, a Rho-GTPase activates Arp2/3-mediated actin polymerisation (Noren and Pasquale 2004). In mATX3 depleted undifferentiated cells, one of the core subunits of the Arp2/3 complex (Arpc2) was down-regulated which eventually lead to an inappropriate assembly of this nucleation complex. This may suggest a dysregulation of the assembly of the Arp2/3 complex, potentially by a decrease of the integrin core signaling, specifically of the α5 and α7 integrin subunit-containing receptors. Interestingly, the other Arp2/3 lateral subunit, Arpc3, as well as Cdc42, were upregulated. We may speculate that this upregulation can be a result of the signaling by other types of integrin receptors in an attempt to overcome the dysregulation of the actin cytoskeleton, or that the higher levels of Arpc3 correspond to its free form. In

addition, the transmembrane Gnas complex, involved in signal transduction that binds to actin (Cote et al. 1997) showed to be down-regulated.

In conformity, two other cytoskeleton proteins, components of intermediate filaments, were shown to be down-regulated: plectin1 (Plec1) and vimentin (Vim). Interestingly, $\alpha 6\beta 4$ integrin binds to Plec1 preventing its binding to F-actin but not interfering with intermediate filament binding (Geerts et al. 1999). In addition, vimentin also binds to plectin 1 in intermediate filaments (Spurny et al. 2007). These alterations suggest that the cytoskeleton structures in general may be deregulated in the absence of mATX3, which may explain the altered morphologic features of mATX3 depleted cells.

Endocytosis may also be compromised, since Ap2s1, a subunit of the clathrin-associated adaptor complex Ap2, presented decreased levels in mATX3-depleted conditions. This dysregulation may also be a consequence of integrin signaling transduction impairment since Ap2s1 is incorporated in endosome membranes by Arf, a member of these cascades (Martin 1998).

In fact, Cdc42 seemed to be a central altered protein since is regulated or regulates many of the proteins altered in the knockdown condition. Cdc42 upregulation in undifferentiated *Mjd* siRNA transfected cells may also be explained by the higher levels of ARHGDIA, a Rho GDP dissociation inhibitor that is also an ATX3 interactor and in turn increases the translocation of Cdc42 (Sun and Barbieri 2004). Galectin-3 (Lgals3) is an extracellular protein that showed increased levels. This protein forms a complex on the cell surface with $\alpha 3\beta 1$ integrin and NG2 proteoglycan potentiating cell migration and morphogenesis (Fukushi et al. 2004). The upregulation of Lgals3 is consistent with the high levels of Cdc42 since the former is responsible for its activation via Cspg4 (Eisenmann et al. 1999). We may suggest that the increase of Lgals3 may be an attempt to trigger other integrin receptors in order to overcome the $\alpha 5$ and $\alpha 7$ integrin down-regulation at the cell surface.

In differentiated mATX3 cells, several aspects also suggest a dysregulation of the cytoskeleton structure. Cdc42 showed to be down-regulated, and talin (Tln1) and calpain2 were upregulated. Tln1 and calpain2 are members of integrin signaling transduction pathways and directly linked with the cytoskeleton. Their upregulation may impair the cytoskeleton, which could explain the morphologic abnormalities in mATX3 depleted cells.

In summary, here, we were able to demonstrate that mATX3 is important for myogenesis by regulating cell surface proteins and the cytoskeleton. Our previous results showed that mATX3 is able to deubiquitinate K^{48} and K^{63}-linked polyubiquitinated chains (Chapter 2). We found the first cellular substrate described until now, of deubiquitination activity by ATX3. The recovery of $\alpha 5$ integrin from UPS degradation by ATX3 seems to be

crucial for the correct cell-cell interaction and alignment for future cell fusion and myogenesis. However, the recently reported mATX3 knockout mouse (Schmitt et al. 2007), was not described to display any apparent muscle malformation, which could suggest that the phenotype presented by the *Mjd* siRNA C2C12 cells (an isolated system) during particular phases of myogenesis, could be overcome in the mouse embryo, probably by other proteins such as the other mouse josephins, or by other physiological processes in the embryo. The absence of an obvious muscle phenotypes commonly verified in knockouts of very important factors for muscle development, as for MRFS Myf5 and MyoD (Braun et al. 1992; Rudnicki et al. 1992). Nevertheless, more specific muscle structure/ function studies should be performed in this recently available mATX3 knockout mouse to confirm the absence of a muscular phenotype, namely during the earliest phases of myogenesis in the embryo. In addition, ATX3 is here described as the first DUB with an identified substrate in muscle developing cells, which may be of great importance as being a target of study for the development of therapeutic strategies for diseases caused by integrin or other cell-adhesion protein defects, as some muscular dystrophies (Hayashi et al. 1998).

We could speculate that these results may also have implications for our understanding of the function of ataxin-3 in other tissues, or even of its involvement in MJD pathogenesis. Thus, in MJD patients, and supposing some loss of the function of ataxin-3, defects in the levels of α5 and α7 integrin subunits may lead to an impairment of myogenesis either during development or in adult MSCs, that differentiate and give rise to new muscle fibers upon muscle injury, eventually causing or worsening the muscle atrophy seen in some (type III) MJD patients (Nakano et al. 1972; Coutinho and Andrade C 1978). Furthermore, α5 integrin, as a critical regulator of the actin cytoskeleton, is known to be very important in the regulation of spine morphogenesis and synapse formation in hippocampal neurons, playing a fundamental role in synaptic plasticity (Webb et al. 2007). It is possible that in neurons, the role of ataxin-3may be linked to this.

In neurons, and probably in many other cell types, ATX3 could be acting at a basal level, in the regulation of cell surface proteins and cytoskeleton. Since an impairment of synaptic transmission was reported in MJD transgenic worms (Khan et al. 2006), it will be interesting to test in MJD transgenic worms and/or mice the expression of cell surface proteins, in particular of α5 integrin, and of other key cytoskeleton components known to be relevant in spine and synapse formation.

Chapter 6

General Discussion and Future Perspective

6.1. GENERAL DISCUSSION

Although polyQ diseases were extensively investigated during the last 15 years, since the cloning of the first causative genes, no treatment is yet available for any of them. Many studies have been performed, aiming at defining the pathogenic effect of polyQ expanded proteins in the disease context, and a gain-of-function was proposed for these mutant proteins. This means that aberrant proteins can, rather than losing their normal function, acquire novel functions, for instance by establishing new protein interactions (Orr and Zoghbi 2007). According to this model, the normal function of the polyQ proteins may not be directly related to the disease process. Very recently, another model emerged proposing that a gain-of-function of the expanded polyQ protein occurs in combination with a partial loss-of-function of the normal protein (Leavitt et al. 2006; Thomas et al. 2006; Lim et al. 2008).

One of the possible therapeutic strategies for polyQ diseases could be the silencing of the corresponding causative gene by the use of RNAi or other approaches (Paulson 2006). However, for this kind of therapeutic, it is crucial to know the normal biological and physiological function(s) of each polyQ protein, in order to predict the effect of their absence in the organism. In general, the knowledge of a protein function in a certain physiological context is also of great importance, in the sense that it may provide a potential target for therapies of other (related or unrelated) disorders. Many studies have thus been carried out, in order to get some insight into the normal function of polyQ proteins. One of the possible ways of doing this is to study the function of the homologue proteins in model organisms of easy manipulation. In this work, our goal was to study the normal function of ataxin-3 using the mouse as a model.

6.1.1. The “exploratory” phase

When we started this work, little was known about the function of ATX3 and, in particular, nothing was known regarding its homologue in the mouse. Thus, we performed an extensive descriptive study of the mouse *Mjd* gene and of its encoded protein, mATX3.

Cloning and determination of the genomic structure of the *Mjd* gene revealed a similar organisation to that of its human counterpart (Ichikawa et al. 2001; Costa et al. 2004). In addition, the promoter regions of the mouse and human genes were shown to comprise several conserved transcription factor binding sites, suggesting a common functionality for these promoters (Costa et al. 2004). Similarly to what has been seen for other mouse homologues of polyQ-containing proteins (Barnes et al. 1994; Lin et al. 1994; Banfi et al.

1996; Nechiporuk et al. 1998; Strom et al. 2002), mATX3 is highly conserved and reveals a similar expression pattern to that of the human protein (Paulson et al. 1997; Costa et al. 2004).

Interestingly, and although mATX3 is ubiquitously expressed, we found it to be highly expressed in muscle cells since the first stages of embryonic development, consistently with the preferential activation of the *Mjd* gene in muscle differentiated cells, potentially directed by MyoD and other muscle-specific transcription factors (Costa et al. 2004). This evidence pointed for a potential physiological function of mATX3 in muscle. Overall, all cells possessing a very well organised cytoskeleton, namely muscle cells, ciliated cells and spermatozoids, including their cilia and flagella, presented a high expression of mATX3, suggesting that this protein may also have a function associated to the cytoskeleton (Costa et al. 2004).

Here, we have also shown that mATX3 conserves the two biochemical functions until now attributed to human ATX3, DUB (Chapter 2) and deneddylase (Chapter 4.2) activities, suggesting the orthology of the mouse *Mjd* gene (Burnett et al. 2003; Doss-Pepe et al. 2003; Chai et al. 2004; Berke et al. 2005; Ferro et al. 2007).

Additionally, we described an exploratory investigation for new mATX3 protein interactors using the y2h system. Among the first 81 potential mATX3 interactors initially isolated from the y2h library screens, direct interaction with mATX3 was confirmed for 18 proteins by y2h assays (Chapter 4.1). These protein interactors have different subcellular localisations, being distributed through several cellular compartments, what is in agreement with the widely distributed subcellular pattern of mATX3 (Chapter 2).

The novel mATX3 partners identified brought additional insights into the previous hypotheses proposing the involvement of ATX3 in transcription regulation, and in protein degradation pathways. However, new hypotheses were also raised here for potential roles of ATX3 in protein synthesis and in cell-cycle processes.

Since mATX3 presents DUB and/or deneddylase activities, we may speculate that these interactors could be its potential substrates. Alternatively, mATX3 may act through its participation in protein complexes, the function of which it may affect. These possibilities need to be further explored for the newly identified interactors of mATX3.

In this work, we have confirmed that mATX3 presents DUB activity against K48-linked polyubiquitin chains *in vitro* (Chapters 2), as do the human (Burnett et al. 2003; Doss-Pepe et al. 2003; Chai et al. 2004; Berke et al. 2005; Ferro et al. 2007) and *C. elegans* proteins (Rodrigues et al. 2007). The deubiquitination of K48-linked polyubiquitin tagged proteins by ATX3 suggests an involvement of this protein in the UPS at different levels. If mATX3 is acting either in the rescue of proteins targeted for proteasomal degradation, or in the recycling of ubiquitin from ubiquitin-conjugates upon entering in the proteasome, functionality

of the interactor as a substrate of mATX3 DUB activity can be evaluated by: (1) measuring the interactor protein levels in cell extracts lacking mATX3 - down-regulated levels would mean that the interactor is a substrate of mATX3, which may be rescuing it from proteasomal degradation, whereas upregulated levels would mean that mATX3 promotes it's degradation, for instance by acting in the recovery of the ubiquitin moieties from the protein, or by adjusting the length of polyUb chains to a proper size for the entry in the proteasome; or (2) evaluating the ubiquitination pattern of (i) the endogenous interactor, in immunoprecipitates from extracts of cells transfected with a vector expressing a tagged ubiquitin and lacking mATX3, or (ii) a recombinant interactor (performed using commercial kits *in vitro*), in the presence or the absence of the recombinant mATX3 – in these experiments, if the ubiquitination pattern is increased in the absence of mATX3, the interactor might be a substrate of mATX3.

Several evidences are suggestive of an involvement of ATX3 in the UPS. Here, we have described a new interaction of mATX3 with Cul1, leading to a potential regulation of the SCF complex activity, an E3 ubiquitin ligase, responsible for the ubiquitination of several proteins (Chapter 4.2). In addition, ATX3 interacts with some other UPS E3 and E4 enzymes, namely parkin (Tsai et al. 2003), CHIP (Jana et al. 2005), PCAF (Li et al. 2002), and UBE4B (Matsumoto et al. 2004); and was shown to be involved in the retro-translocation of polyUb substrates from the endoplasmic reticulum to the 26S proteasome through its binding to VCP, HHR23B, and some components of the Derlin-VIMP complex (Hirabayashi et al. 2001; Kobayashi et al. 2002; Doss-Pepe et al. 2003; Boeddrich et al. 2006; Wang et al. 2006; Zhong and Pittman 2006).

Additionally, we were able to demonstrate that mATX3 is able to hydrolyse, *in vitro*, K63-linked polyubiquitin chains and monoubiquitinated substrates (Chapter 2). These types of post-translational modifications play important roles in subcellular localisation, endocytosis, intracellular trafficking, DNA repair and translation (Glickman and Ciechanover 2002; Woelk et al. 2007). The ability of a mATX3 interactor to be a substrate of the mATX3 DUB activity against K63-linked polyubiquitin chains can be evaluated by comparison of its subcellular localisation patterns in cells expressing mATX3 with that in cells lacking mATX3. If the absence of mATX3 leads to any alteration in the subcellular localisation of a protein, and in its levels of K63-linked polyUb modification, this might be a mATX3 substrate. Similarly, the capability of a protein to be a substrate of the mATX3 deneddylase activity can be assessed by analysing its neddylation pattern in extracts of cells knocked down for mATX3.

However, protein binding partners can interact with mATX3 in a way other than an enzyme-substrate interaction, probably through other potential functional domains, yet unexplored. According to this possibility, is the existence of a putative ATX3 isoform lacking

the cysteine 14 residue, crucial for its DUB activity (Ichikawa et al. 2001), suggesting that ATX3 may have additional domains of functional relevance. We have found a putative Smc domain, immediately after the josephin domain, comprising the more conserved C-terminal region between human variants and homologues, including the first two UIMs and the polyQ tract (Chapter 4.3). Nonetheless, the functionality of this domain (involved for instance in the binding of mATX3 to chromatin, or in the interaction with other proteins) must be yet analysed, by testing for instance the effect of mATX3 carrying a mutation in the potential Smc domain in the cellular context, in particular in cells that are originally mATX3 depleted.

Although the existence of novel mATX3 domains should be explored in the future, the enzymatic activities of mATX3, already demonstrated *in vitro*, may explain the high variability of roles that mATX3 can play, as well as its wide tissue and subcellular localisation pattern.

6.1.2. What is ataxin-3 doing in muscle?

Several pieces of evidences from our work pointed for important potential function(s) of mATX3 in the muscle, which led us to raise and explore some hypotheses for the involvement of this protein in: (1) the response to stress; (2) structure maintenance; and/or (3) development of the muscle. Although we have begun to explore the role of mATX3 in the response to stress and/or structure maintenance of skeletal muscle, further studies should be performed in the future. The third possibility has been analysed in more depth and our results do confirm a role for ataxin-3 in muscle development, as discussed below.

Ataxin-3 might be involved in the response to stress of skeletal muscle

Our first evidence from the bioinformatic analysis of the *Mjd* promoter, revealing several putative binding regions for muscle-specific transcription factors and for FOXOs (Chapter 3) (Santos 2005), led us to explore a potential role of mATX3 in the stress response in skeletal muscle. We have studied the expression levels of *Foxos* and *Mjd* transcripts in the skeletal muscle of mice subjected to starvation or to short-term cold exposure. The response to starvation has been better studied then the response to cold exposure. Currently, it is known that, in the skeletal muscle, starvation leads to both an increase of protein degradation and a decrease of protein synthesis (Sandri et al. 2004; Stitt et al. 2004), and that cold exposure leads to a decrease in protein synthesis (Samuels et al. 1996).

The UPS plays an important role in starvation conditions, controlling muscle mass by a tight regulation of protein degradation, in order to produce free amino acids to be used for gluconeogenesis (Sandri et al. 2004; Stitt et al. 2004). The response to starvation is in part controlled by the insulin signaling pathway, and involves Foxo transcription factors whereas for the response to cold exposure this is unknown. Thus, it was very interesting to see that *Foxo1* and *Mjd* expression levels were simultaneously upregulated in the skeletal muscle of mice subjected to either starvation or cold exposure (Chapter 3) (Furuyama et al. 2003). This result suggests that mATX3 might act in connection with the UPS to facilitate the degradation of proteins by the proteasome.

On the other hand, the molecular effect common to both of these stress conditions (starvation and cold) is, as mentioned above, the decrease of protein synthesis (Samuels et al. 1996; Sandri et al. 2004; Stitt et al. 2004), which in conjunction to some novel protein interactors found here (Chapter 4.1), raises a different potential implication of mATX3 in this pathway. Given that, in skeletal muscle, Foxo1 induces the expression of 4E-BP1 (Southgate et al. 2007), which is the inhibitory protein of eIF4E, and that this latter translation initiation factor is a putative mATX3 interactor, we might hypothesise that ATX3 is upregulated in stress conditions, acting synergistically with Foxo1, in order to inhibit the translation process, possibly by regulating the levels of eIF4E through UPS degradation, or by making part of an inhibition complex, together with eIF4E and possibly with 4E-BP1 (Figure 6.1).

This would be in accordance with a general role of ATX3 in the inhibition of protein synthesis at several levels by: (1) the regulation of Foxo1 levels, potentially through the UPS by a putative direct interaction (Figure 6.1); (2) the regulation of Foxo1 activity by blocking its acetylation through the CBP/p300 complex (Li et al. 2002) (Figure 6.1); (3) the potential regulation of eIF4E levels, substrate of mATX3 DUB activity (Figure 6.1); (4) taking part in the inhibition complex of eIF4E (Figure 6.1); (5) interacting with ribosomal proteins Rpl6 and Rps9, possibly regulating of their stability through neddylation, acting as a deneddylase, since recently several ribosomal proteins, including Rpl6, were shown to be neddylated[1] (Xirodimas et al. 2008); and (6) repressing the RNA polymerase III multisubunit complex (responsible for the production of tRNAs and small structural RNAs) through its interaction with Brf1 and potentially with Rbbp4, acting as a deneddylase - given that this protein was also found to be neddylated[1] (Jones et al. 2008) (see Figure 4.1.9, Chapter 4.1).

These hypotheses should be better explored in the future, in order to clarify the role of mATX3 in the skeletal muscle upon stress.

[1]although the functional consequences of this post-translation modification are not yet known

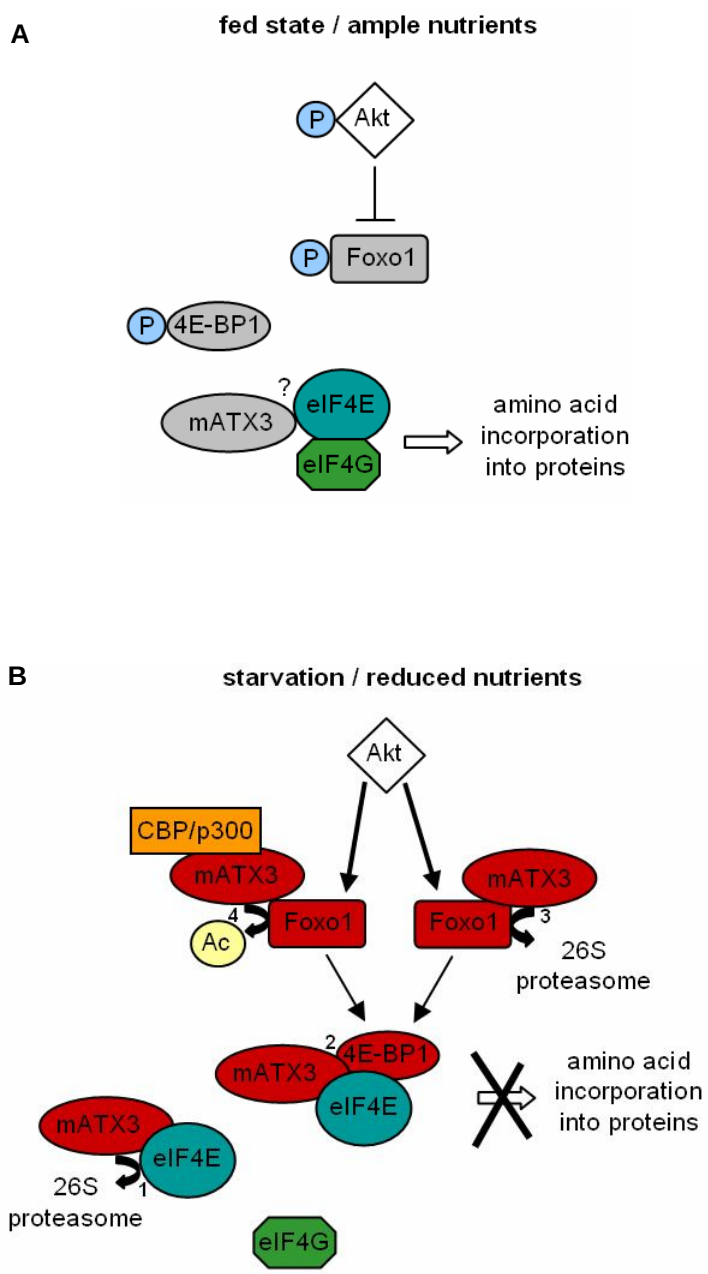

Figure 6.1. Potential involvement of mATX3 in protein synthesis regulation in the skeletal muscle. A) In the fed state, Foxo1 and 4E-BP1 (the inhibitory protein of eIF4E) are phosphorylated, the translation initiation complex eIF4E/eIF4G complex is formed and amino acids are incorporated into proteins. We showed that mATX3 potentially interacts with eIF4E. B) In starvation, Foxo1 is upregulated and, in turn, upregulates 4E-BP1 and potentially mATX3 (upregulated proteins are indicated in red) leading to the disruption of the eIF4E/eIF4G complex and to the inhibition of protein synthesis. The upregulated mATX3 can be acting: (1) in the regulation of the levels of eIF4E through the UPS degradation; (2) as a component of the inhibition complex interacting with eIF4E and possibly with 4E-BP1; (3) in the regulation of Foxo1 levels through the UPS by a putative direct interaction; and (4) the regulation of Foxo1activity through modulation of its acetylation, by blocking the acetylation of Foxo1 through the CBP/p300 complex.

Ataxin-3 might be involved in structural maintenance of the skeletal muscle

Skeletal muscle is a very adjustable tissue upon altered mechanic or metabolic conditions. The UPS plays an important role in the regulation of proteolysis in these conditions, as well as in the normal maintenance of muscle structure (Attaix et al. 2005). The skeletal muscle myofibrillar components, such as actin, myosin, troponin, and tropomyosin can be degraded by the UPS (Solomon and Goldberg 1996), but only after dissociation of myofibres by non-UPS proteases (Deval et al. 2001; Du et al. 2004; Bartoli and Richard 2005). Taking into account a possible role of mATX3 in the UPS, we have verified that mATX3 interacts with the structural sarcomeric components Tnni1, Tnni2, Acta1 and Myh2 (Chapter 4.4).

Thus, ATX3 might be acting, in skeletal muscle, at the protein degradation level by controlling: (1) the levels of the sarcomeric proteins Tnni1, Tnni2, Acta1, and/or Myh2, through the UPS, acting as a DUB; (2) myosin assembly, either as a member of the CDC-48(p97)/UFD2/CHN-1(CHIP) E3 ubiquitin ligase complex that regulates the levels of UNC45 (Hirabayashi et al. 2001; Matsumoto et al. 2004; Jana et al. 2005; Janiesch et al. 2007; Landsverk et al. 2007), or interacting with both myosin and UNC45; or (3) the stability of Myh2 and Acta1, through the potential regulation of their neddylation state, as a recently reported proteomic study on neddylated proteins showed that Myh2 is one of these proteins, together with alpha cardiac actin (opening the possibility that Acta1 might also be neddylated)[1] (Jones et al. 2008).

Nevertheless, all these hypotheses should be further studied in the future, in order to define the physiological relevance of ATX3 in the regulation of sarcomeric structure in the skeletal muscle.

Ataxin-3 plays a role in muscle development

In this work, we have found a high expression of mATX3, at the E9.5 stage, in the heart and in the skeletal muscle precursor structures, the dermomyotome and the early myotome (Chapter 5). As seen above, being a DUB, mATX3 may play a role in the UPS, which in turn is known to be extremely important in the tight regulation of protein levels at precise moments of myogenesis. All these evidences led us to further study the involvement of ATX3 in this process.

To perform this study, we have knocked down mATX3, using siRNA, in undifferentiated C2C12 cells and evaluated the effect of its absence during the differentiation

[1] although the functional consequences of this post-translation modification are not yet known

process. Here, we showed the first phenotype ever described related to the absence of mATX3: cells with reduced expression of mATX3 apparently retain a proliferative state upon differentiation induction, delaying the myogenic differentiation response, and later show misalignment behaviour (Chapter 5). Among all the Josephin domain-containing proteins in mouse that could have a similar role of mATX3, we have confirmed that this phenotypic effect was exclusive to the absence of mATX3 (Chapter 5).

The misalignment phenotype observed in C2C12 cells lacking mATX3 led us to hypothesise the occurrence of an impairment of cell-matrix adhesions, known to induce signaling cascades that regulate cytoskeleton organisation, gene expression, protein synthesis and several other cellular processes important for cell proliferation, migration and differentiation (Berrier and Yamada 2007). In fact, these cells presented a decrease in the protein levels of two integrin subunits important in cell adhesion and in myogenesis, the α5 and α7 integrin subunits (Chapter 5).

The fact that the decreased levels of α7 integrin subunit remained low during differentiation, even when the amount of mATX3 was restored, suggested that mATX3 might have an indirect effect over the α7 integrin subunit, probably affecting (in an irreversible manner) the degradation of other proteins that control up-regulation of the α7 integrin subunit.

The expression patterns of α5 integrin subunit and mATX3 are very similar, in the myotome of E9.5 and E11.5 mouse embryos and in C2C12 cells mATX3, and the cytoplasmic domain of α5 integrin subunit seem to colocalise (Bajanca et al. 2004; Cachaco et al. 2005) (Chapter 5). Here, we have showed that: (1) mATX3 interacts directly with the α5 integrin subunit; (2) overexpression of mATX3 stabilises the α5 integrin subunit; and (3) in the mATX3-depleted cells, when the mATX3 levels decrease, levels of α5 integrin subunit also decrease, and when mATX3 level is restored, the amount of this integrin subunit is also restored. This evidence, and the fact that the α5 integrin subunit is degraded by the UPS (Kaabeche et al. 2005), led us to suggest that the α5 integrin subunit could be the first described substrate of mATX3 DUB activity, which could be rescuing this protein from proteasomal degradation.

In agreement, the proteomic profile of mATX3-depleted C2C12 cells revealed altered protein levels of members of the integrin signaling cascades, namely Cdc42 and subunits of the Arp2/3 complex, which are directly related to actin cytoskeleton rearrangements. Moreover, other cytoskeleton-related proteins were also deregulated, suggesting a general cytoskeleton disorganisation that might further explain the morphologic abnormalities in mATX3-depleted cells, probably due to the decreased levels of α5 and α7 integrin subunits, originating an impairment of the integrin core signaling. In fact, some of these cytoskeleton-

related proteins were down-regulated, such as the structural components plectin1 and vimentin, and the GTPases Gnas and Gnb2l1, related to actin polymerisation (suggested as directly responsible for the incorrect assembly of both actin and intermediate filaments); and others were upregulated, such as the case of talin1, co-distributed with integrins in the cell surface (possibly as an attempt to compensate the cytoskeleton impairment), ARHGDIA, an ATX3 interactor, which decreases actin polymerisation (Leffers et al. 1993), and other extra-cellular proteins such as galectin 3 and MIF, in a possible attempt to trigger other integrin receptors, in order to overcome the down-regulation of α5 and α7 integrin subunits at the cell surface.

The observation that the mATX3 knocked down cells continue to proliferate in the presence of the differentiation medium may suggest that mATX3 is acting in the regulation of cell proliferation by: (1) a downstream effect of the deregulation of the integrin signaling pathway; (2) another direct effect of its protein interactions; (3) playing a role in the modulation of cell-cycle regulators through the UPS; and/or (4) acting in the protein synthesis process.

In fact, some of our data led us to hypothesise that mATX3 could be regulating microtubule dynamics during mitosis, either directly through its interaction with tubulin, or indirectly through a potential interaction with Kif2c, and Twa1 (Chapter 4.3), two proteins playing important roles in chromosome segregation; also mATX3 might regulate both transcription or chromosome segregation binding to chromatin through its putative Smc domain. Alternatively, mATX3 could be acting through the regulation of the SCF complex (Chapter 4.2), which, in turn, is implicated in the ubiquitination of several proteins of the cell cycle, among others.

Additionally, the proteomic study indicated that the levels of calpain 2 were upregulated in differentiated mATX3-depleted C2C12 cells, which could also be related to the altered integrin-mediated signaling, as transcription of this protein is activated by the ERK/MAPK pathway (Leloup et al. 2007) that, in turn, is activated by integrins. Interestingly, Brf1, a mATX3 interactor, is phosphorylated by ERK and promotes the RNAPIII-mediated transcription of biosynthetic RNAs (Felton-Edkins et al. 2003). Our abovementioned hypothesis pointed to a potential role of mATX3 as a repressor of this type of transcription, which is also crucial for protein synthesis. In the case of depleted levels of mATX3, we could speculate that Brf1 can be phosphorylated by the ERK/MAPK and promote the RNAPIII-mediated transcription, leading to an increase of protein synthesis, which could explain the fact that mATX3-depleted cells continue to proliferate even in the presence of differentiation-inducing conditions, whereas cells usually stop to proliferate.

The role of ATX3 in muscle differentiation seems to be crucial for the withdrawal of cellular proliferation and probably for the correct cell-cell interactions and cell alignment,

which are essential mechanisms for future cell differentiation. The physiological implication of mATX3 in myogenesis described here, in integrin signaling transduction, might indicate that this protein, acting as a DUB and/or deneddylase, could have downstream effects of this pathway namely in cytoskeleton assembly, transcription repression, protein synthesis/degradation, and cell cycle. However, the involvement of mATX3 in the latter cellular mechanisms must be further studied in the future.

6.1.3. Effects of the absence of ataxin-3 in cells versus organisms

Although poorly studied, the mATX3 knockout mouse, recently reported, does not display any apparent phenotype (Schmitt et al. 2007). Similarly, the *atx3* knockout in *C. elegans* does not present any obvious alterations (Rodrigues et al. 2007). In particular, no muscle malformations were observed in these two knockout models (Rodrigues et al. 2007; Schmitt et al. 2007), which could suggest that the phenotype presented by the *Mjd* siRNA C2C12 cells (an isolated system) during particular phases of myogenesis, can be overcome in the embryo, probably by other proteins such as the other Josephin-domain containing proteins, or by other physiological processes. Although in a study knocking down human ATX3 no indications about the cellular phenotype were reported (Miller et al. 2003), this should be better analysed in the future. More detailed studies of the muscle of ataxin-3 knockout animals should be performed as they may reveal yet undiscovered subtle anomalies. In fact, as the *Mjd* knockout mouse, knockout mice for the majority of the myogenic factors are viable and recover muscle development as is the case of the MRFs, Myf5 and MyoD (Braun et al. 1992; Rudnicki et al. 1992).

6.1.4. Relevance of the novel findings

New insights about the functioning of DUBs

As described in Chapter 1, the post-translational modification of proteins by Ub or UBL proteins is an important regulatory mechanism in Cell Biology. The reverse process, the removal of the Ub or UBL moieties, is carried out by DUBs. Although these enzymes play crucial roles in the cellular context, their mechanisms of regulation and substrate specificity are poorly understood.

During this work, we added new knowledge about the function of the mouse homologue of one specific DUB, ataxin-3, and identified targets for its activity. As the human ATX3 (Burnett et al. 2003; Donaldson et al. 2003; Ferro et al. 2007), mATX3 was shown here to display protease activity towards K48-linked polyUb chains and the UBL NEDD8, *in vitro*. This lack of specificity towards the modification signal is a feature common to other DUBs (Groisman et al. 2003; Nijman et al. 2005). Additionally, and to increase this variability, there is also the possibility that ATX3 to displays protease activity towards SUMO1, given its interaction with this UBL protein (Shen et al. 2006).

The specificity of a DUB is most probably given by the combined recognition of a target protein and the type of the attached moiety (Ub or UBL). In the case of Ub, this specificity is increased taking into account the different types of polyUb branches. The evidence provided here, that mATX3 is also able to hydrolyse K63-linked polyUb chains, and monoubiquitinated substrates *in vitro* (Chapter 2), increases the diversity of possible modified target proteins and the cellular pathways upon which mATX3 may impact. Moreover, since the presence of UIMs may contribute to the polyUb chain selectivity (Raasi et al. 2005), the fact that human ATX3 variants can comprise two or three UIMs (Goto et al. 1997; Ichikawa et al. 2001) could be important for this DUB, to select the type of polyUb chain. Future studies of target specificity of mATX3 should take into account the different isoforms and possible post-translational modifications that may define affinity of this protein for different substrates. It should also be highlighted that these enzymatic activity studies, if undertaken *in vitro*, may not reflect what really occurs *in vivo*, given a potential lack of crucial post-translational modifications of mATX3 and/or co-factors. Given this, the high number of potential interactors from different classes of proteins found here (Chapter 4.1), and the hydrolase activity of ATX3 towards a high variability of post-translationally modified proteins, we suggest that this ubiquitously expressed DUB may play important roles in different cellular processes, namely acting in the UPS, subcellular localisation regulation, endocytosis, and protein trafficking.

However, the fact that the knockout animals for the homologue proteins do not present any apparent phenotype (Rodrigues et al. 2007; Schmitt et al. 2007), is suggestive of ATX3 as having very specific protein targets, rather than define the overall level of protein degradation.

Here, we provided important insights about the potential function of ATX3 in the UPS. In addition to its DUB and deneddylase activities, we have identified a possible regulation of the SCF complex, an E3 Ub-ligase, by mATX3 through its interaction with Cul1 or Nedd8 (Chapter 4.2), which could be of relevance, since this complex regulates the ubiquitination and consequent proteasomal degradation of several proteins, involved in different cellular processes. Since the UPS is involved both in the control of the “normal” levels of specific

proteins at different time points or cell types, and in the degradation of denatured or misfolded proteins in case of altered cell function or disease situations, the characterisation of the role of mATX3 is very significant for the general knowledge on the UPS function. In this way, ATX3 might prove to be a potential therapeutic target for one of the many diseases in which the UPS plays an important role, namely cardiac dysfunction, cancer, cataract formation, viral infections, autoimmune diseases, cachexia, and neurodegenerative disorders (Dahlmann 2007).

Importantly, we have identified the first DUB substrate of mATX3, the α5 integrin subunit. mATX3 appears to act in the rescue of this protein from proteasomal degradation, a process that is crucial for muscle differentiation. This knowledge may be of relevance for the development of therapeutic strategies for diseases caused by defects in integrin or other cell-adhesion protein, that occur in some muscular dystrophies (Hayashi et al. 1998). Given that α5 integrin subunit is also ubiquitously expressed, this functional enzyme-substrate activity of mATX3 may have importance in other tissues, not explored in this work (see below).

Potential combination of gain and loss of function in polyQ diseases

The first model proposed as the general process underlying these disorders, was based on a gain-of-function of the expanded polyQ protein (Orr and Zoghbi 2007). However, more recently an alternative model emerged, proposing a combinatorial pathogenic mechanism, in which the gain-of-function of an expanded polyQ protein overlaps with a partial loss-of-function of the normal protein (Leavitt et al. 2006; Thomas et al. 2006; Lim et al. 2008).

Given that the UPS has been shown to be impaired in polyQ diseases (Holmberg et al. 2004), namely in MJD (Chai et al. 1999), the recently reported evidence that the cellular turnover of the expanded ATX3 protein is regulated by its DUB catalytic activity (Todi et al. 2007) and the additional evidence provided here for the involvement of the normal ATX3 in the UPS, support the alternative model, in which some loss-of-function of the normal protein could also contribute to the pathogenesis in MJD.

Several reports have been proposing that the normal polyQ-containing protein have a protective effect on the cellular abnormalities caused by the mutant protein. Studies of spinal and bulbar muscular atrophy (SBMA) mouse models, revealed that the animals resultant from the crossing of a transgenic mouse model (expressing an expanded androgen receptor (AR) carrying 100 glutamines) with the AR knockout mouse presented a worse phenotype than the original AR100 transgenic mice (Thomas et al. 2006). Additional indications of a loss-of-function contributing to Huntington disease (HD) pathogenesis came from the fact

that conditional targeting of the mouse *Hdh* gene lead to neurodegeneration of basal ganglia (an affected region in HD patients), supporting the hypothesis that decreased the levels of full-length wildtype huntingtin sensitizes neurons to cell death (Dragatsis et al. 2000). In fact, increased levels of full-length wildtype huntingtin were shown to be neuroprotective against NMDA-mediated excitotoxicity (Leavitt et al. 2006).

Currently, studies in some polyQ diseases support the combinatory pathogenic model of gain and loss of function. In fact, indications from studies in HD models revealed a loss of huntingtin normal function to induce the expression of brain-derived neurotrophic factor (BDNF) in the HD pathogenesis context (Strand et al. 2007). The recent study in SCA1 revealed that the polyQ expansion in ATXN1 promotes the formation of a new protein complex containing RBM17, contributing to SCA1 neuropathology by a gain-of-function mechanism; and concomitantly, it attenuates the formation and function of another complex comprising ATXN1 and capicua, thus contributing to SCA1 by means of a partial loss-of-function (Lim et al. 2008).

In this line of thought, the study of the molecular and physiological function of the normal ATX3 is also important for the understanding of the pathogenic mechanism of polyQ diseases. In this way, for example, the identification of ATX3-protein interactions may be an important contribution for the understanding of the pathogenic mechanism in MJD; this is also in agreement with the proposed gain- plus loss-of-function model, given that protein interactions can either be “lost” or “gained” in the disease context. The functional study of ATX3 interactions, and its involvement in the suggested pathways, can thus give important insights for the general knowledge of the pathogenic mechanisms, but it can also help to explain the selectivity observed in MJD neurodegeneration, which might be correlated to the expression patterns of the different components of the affected complexes.

The normal DUB activity of mATX3 in the rescue of α5 integrin subunit from proteasomal degradation, here described, and shown to be physiological relevant in muscle development, can also be important for the understanding of the function of ataxin-3 in other tissues, or even of its involvement in MJD pathogenesis. Interestingly, the α5 integrin subunit, as a critical regulator of the actin cytoskeleton, is known to be implicated in the regulation of spine morphogenesis and synapse formation, playing a fundamental role in synaptic plasticity (Webb et al. 2007). According to this evidence, we may speculate that ataxin-3 has a similar role in neurons, and that a potential deregulation of this function might contribute for MJD pathogenesis.

6.2. FUTURE PERSPECTIVES

The exploratory studies performed in this work opened several new hypotheses regarding ATX3 function. Among these hypotheses, we have already begun to exploring a few and obtained some preliminary results that should be completed in the near future.

Concerning the newly identified molecular partners of mATX3 the next steps should be: (1) to confirm all the interactions using GST pull-down, and co-localisation assays; (2) to analyse the mATX3 interactors as substrates of its DUB or deneddylase enzymatic activities; (3) to study the conservation of the interactions and the respective enzymatic activities in human; (4) to evaluate the effect of the polyQ expansion of ATX3 in its protein interactions; (5) to test the possibility of mATX3 being a member of the CDC-48(p97)/UFD2/CHN-1(CHIP) E3 ubiquitin ligase complex, important for the regulation of myosin assembly; and (6) to study the potential regulation of the SCF complex by mATX3 through its interactions with Cul1 and Nedd8.

Regarding the regulation of *Mjd* expression by Foxo transcription factors it will be necessary: (1) to study the binding and consequent functional regulation of the *Mjd* promoter by Foxos, using chromatin immunoprecipitation, and evaluating the endogenous *Mjd* expression in cells overexpressing Foxos; and (2) to evaluate the expression levels of *Foxos* and *Mjd* genes in specific brain regions of stressed mice.

The involvement of mATX3 in cell cycle may be clarified through: (1) the functional study of its interactions with Kif2c and Twa1, and their possible effect in microtubule dynamics; and (2) the exploitation of the potential existence of a Smc domain in mATX3, and of its putative importance for the mATX3 role in cell cycle.

In relation to the proteomic analysis performed in the C2C12 mATX3-depleted cells, the protein level alterations, specifically those corresponding to proteins directly involved in the integrin signaling pathway, associated to the cytoskeleton and to cell-cycle should be confirmed by immunoblotting, and it should be investigated which of the deregulated proteins are direct targets of the enzymatic activity of mATX3.

In general, interesting themes of study for the normal function of ATX3 might be the functional analysis of this protein in the following pathways: transcription regulation, protein synthesis and degradation, cytoskeleton assembly, integrin signaling transduction, and cell-cycle. The study of these same pathways, in the expanded ATX3 cellular context, should also be of great importance, in order to analyse the possible model of a combination of a gain-of-function and a loss-of-function, as the pathogenic mechanism in MJD.

Appendixes

Appendix 1

Primers used in the experimental work

Table A.1. Primers used in this work, and their different applications

Name	Sequence 5'→ 3'	Orientation	Application
Afx(1)	GTGAGCAGAGCCTCTAGAGACTG	reverse	quantitative real-time RT-PCR
Afx(2)	CACGCTCAGTGAAGATCTAGAGC	forward	quantitative real-time RT-PCR
Brf1(1)	GCTCATCTGCTGGAGTTTG	forward	sequencing
Cul1(1)	CTGATTAGTGGAGTTGTAC	forward	sequencing
Cul1(2)	GCTGCTCTTGATAAGGCTTG	forward	sequencing
Fkhr(1)	GCTCATGCTGGATTGGCCGTATG	reverse	quantitative real-time RT-PCR
Fkhr(2)	GCCAAGATGGCGTCTACGCTG	forward	quantitative real-time RT-PCR
Fkhrl1(1)	CGTCGCTGTGGCTGAGTGAGTC	reverse	quantitative real-time RT-PCR
Fkhrl1(2)	CGCCATCGCAGCCATCGCCTC	forward	quantitative real-time RT-PCR
GAL4AD-F	TACCACTACAATGGAT	forward	sequencing
GAL4AD-R	GAGATGGTGCACGATG	reverse	sequencing
GAL4BD-F	GAAAAACCGAAGTGCGCCAAGTG	forward	sequencing
GAL4BD-R	CCACTTCTGTCAGATGTGC	reverse	sequencing
Hprt(1)	GTAATGATCAGTCAACGGGGA	forward	quantitative real-time RT-PCR
Hprt(2)	GACACAAACGTGATTCAAATTCCT	reverse	quantitative real-time RT-PCR
Hprt(3)	GCTGGTGAAAAGGACCTCT	forward	quantitative real-time RT-PCR
Hprt(4)	CACAGGACTAGAACACCTGC	reverse	quantitative real-time RT-PCR
Itga5(1)	GGACGGAGTCAGTGTGCTG	forward	quantitative real-time RT-PCR
Itga5(2)	GAATCCGGGAGCCTTTGCTG	reverse	quantitative real-time RT-PCR
Itga7(1)	GAGCTGGCTGCTGGTGGGCG	forward	quantitative real-time RT-PCR
Itga7(2)	CTCCTTCTGCACGTTAGCTC	reverse	quantitative real-time RT-PCR
Josd1(1)	AAGATGCCAGAGTGGATTGG	forward	quantitative real-time RT-PCR
Josd1(2)	TGATGGGCTTCCACTTCTTC	reverse	quantitative real-time RT-PCR
Josd2(1)	CGGCAACTATGATGTCAACG	forward	quantitative real-time RT-PCR
Josd2(2)	AGCGACACAGGAGAGGGTAG	reverse	quantitative real-time RT-PCR
Josd3(1)	GAGACGGGAAAGGAGGAGTC	forward	quantitative real-time RT-PCR
Josd3(2)	TTGTTGAGAGCATGGACAGC	reverse	quantitative real-time RT-PCR
Kif2c(1)	GGATCTGTGTCTGTGTCAG	forward	sequencing
Lrcc40(1)	CATGGAATCACTGGAATTGC	forward	sequencing
mmMJD1	GAGGGGCTGCTCCGCGCCGGGGCCGT	forward	cDNA cloning; probe synthesis; sequencing
mmMJD2	TCTGCTTTCAAGTTGTCTTTAGCAG	reverse	cDNA cloning; sequencing
mmMJD3	GTAAACCAGTGTTCTTTATAATTGCA	reverse	probe synthesis; sequencing
mmMJD4	ACGGCCCCGGCGCGGAGCAGCCCCTC	reverse	sequencing
mmMJD5	TAGACCGACCTGGACCCCTTTCATAT	forward	sequencing
mmMJD6	AGCTCCACAGGGCTAAAATACTCTC	reverse	sequencing
mmMJD7	CTCTATTCAAGTTATAAGCAATGCT	forward	sequencing
mmMJD8	CAAAGTAGGCTTCTCGTCTCCT	reverse	sequencing
mmMJD9	TGATGAAGATGAGGATGATTTACAG	forward	sequencing
mmMJD10	TGCTTCTAAGACGCGCTCCAGGTCT	reverse	d-siRNA production; sequencing
mmMJD11	TTGAATTCTCTGTTGACGGGTCCAG	forward	sequencing
mmMJD12	CATGCATTTAGATCCTTTGA	forward	sequencing
mmMJD13	GCAGTAAGAGGAACATGCAG	reverse	sequencing

Name	Sequence 5'→ 3'	Orientation	Application
mmMJD14	CGAAAGATCCTTTATATGCA	forward	quantitative real-time RT-PCR; sequencing
mmMJD15	GACACCCCCACTAAATCCAT	reverse	sequencing
mmMJD16	GGAGAGTATTTTAGCCCTGT	forward	sequencing
mmMJD17	GGATGACAGCGGCTTTTTCT	forward	sequencing
mmMJD18	AGAAAAAGCCGCTGTCATCC	reverse	sequencing
mmMJD19	AACGCCCACACTCACTTTCTC	reverse	sequencing
mmMJD20	CCTTTCTCCTCATCTTTAT	reverse	sequencing
mmMJD21	TGAGCCAAGAATAGTGCGAG	reverse	quantitative real-time RT-PCR; sequencing
mmMJD22	GTTGTTAAGGGTGATCTGCCA	forward	sequencing
mmMJD23	CTGTTGGACCTTGATCATCT	reverse	sequencing
mmMJD24	AGTGCTGAGAACACTCAAAG	forward	sequencing
mmMJD25	TCCAGGTCGGTCTACCTCCTG	reverse	sequencing
mmMJD26	TAGTTCCAGAAGTATGTGTGA	forward	sequencing
mmMJD27	GTCTGTGTAGGCATCTGTGA	forward	sequencing
mmMJD28	CTCTGTGTCTCCAGACTGA	forward	sequencing
mmMJD29	CTTGGACTTGAAGATTTTCC	reverse	sequencing
mmMJD30	GCCTGCCTCTGCCTCCCGAG	forward	sequencing
mmMJD31	GACCACACTTCTGTGTGAA	reverse	sequencing
mmMJD32	TGTATGTAGCGTTGGTCACC	forward	sequencing
mmMJD33	GCCATCTCCTGAAGGAGGAAG	reverse	sequencing
mmMJD34	GCAGAGTGGCATATGCTTGT	reverse	sequencing
mmMJD35	CTAACCTGTCCTCTGGCA	forward	sequencing
mmMJD36	TCTGTCCTTCTGTAGCCTAG	forward	sequencing
mmMJD37	ACCCTCTGACCTCAGGTCAG	forward	sequencing
mmMJD39	CACAAGTTCAGGAGGACGTA	forward	sequencing
mmMJD40	ATACACTTGACACTAAATC	reverse	sequencing
mmMJD41	TTGAGTGGCTCGCGCAGGG	reverse	sequencing
mmMJD42	AGCACATCATGACCTATC	reverse	sequencing
mmMJD43	CTGAGGTATTCAGGCAGTGAC	forward	sequencing
mmMJD44	AGAAGCCACTGGAAAACACC	reverse	sequencing
mmMJD45	AGGAGCATTGACTCATAGTG	forward	sequencing
mmMJD46	GCAGTAAGAGGAACTGCAG	reverse	sequencing
mmMJD47	TCAGCTTGCTATCATCAGG	forward	sequencing
mmMJD48	GTTACATAACAGAAACCAAG	reverse	sequencing
mmMJD49	CTAGTACATCTCTACTATC	forward	sequencing
mmMJD50	GTTACATAGGAGGACCCTG	reverse	sequencing
mmMJD51	TCACTGGGGAACAATACTTG	reverse	sequencing
mmMJD52	ACTTTGATGAGGGACTGG	reverse	sequencing
mmMJD53	CCTGGAAGTCAGTCTTC	reverse	sequencing
mmMJD54	GACTCCAGAGAGCACCTG	reverse	sequencing
mmMJD55	GTTGGTAACTCGAGACTCAG	reverse	sequencing
mmMJD56	GTGTATACTGTTGACCACAG	forward	sequencing
mmMJD57	GTAGCACAGCTACTATAAG	reverse	sequencing

Name	Sequence 5'→ 3'	Orientation	Application
mmMJD58	CCTATATATGTTATGTCAT	forward	sequencing
mmMJD59	CACTTTGTAGACCAAGCTGC	forward	sequencing
mmMJD60	GTTGAAGGAGGATAAAGG	reverse	sequencing
mmMJD61	TCCATAGTAGATAATTGAAC	forward	sequencing
mmMJD62	CAAGATCCTCGTCAATTGTAC	forward	sequencing
mmMJD63	GCACTATGACATGGCTACAAG	reverse	sequencing
mmMJD64	CAAGTCTGGGATTAAAGGT	reverse	sequencing
mmMJD65	GAGTCTGACAGAGAGCTAG	reverse	sequencing
mmMJD66	AGAGGATGGAGAGCTAAGC	reverse	sequencing
mmMJD67	TGTGAGACAGTGTTATCTAC	forward	sequencing
mmMJD68	GGATTCACAGACAGTTGTG	forward	sequencing
mmMJD69	CCATAAATGACATAGAAGTC	reverse	sequencing
mmMJD70	GAGATGAAGTCCATCATG	forward	sequencing
mmMJD71	CTCGGACAACCATGTTTC	forward	sequencing
mmMJD72	CTGAAGTAGATATAGCATAC	reverse	sequencing
mmMJD73	GTTACTGTTTGTGTGTATG	reverse	sequencing
mmMJD74	GATGCTGGGACAACCTG	reverse	sequencing
mmMJD75	GCTCCATGTGTACTCTTG	forward	sequencing
mmMJD76	GCCACGTGGGTGTGAGGAATTG	forward	sequencing
mmMJD77	CATATGCAGACATGAGTGC	reverse	sequencing
mmMJD78	CATGAAGGTTCTGGGGATTAAGC	forward	sequencing
mmMJD79	CAACCTGGAGACTTCATTGC	forward	sequencing
mmMJD80	CATCTTCTGAGCCTAGCAC	reverse	sequencing
mmMJD81	GCATGCCACTGTGTACTACG	forward	sequencing
mmMJD82	GTCAAATTCTACTCGAAG	forward	sequencing
mmMJD83	CTTCGAGTAGAATTTGAC	reverse	sequencing
mmMJD84	GCTGGTGACCAGGAGCTCAG	forward	sequencing
mmMJD85	GCGTGCGCCACCACCG	forward	sequencing
mmMJD86	GCTCCACAGAGGGAGGTTG	reverse	sequencing
mmMJD87	GTAGTGCTGTAGTGAGTG	forward	sequencing
mmMJD88	GCTAGCTAGAGCTACTTATTG	forward	sequencing
mmMJD90	GCAGGTAGTAAGTGTAGGAAG	forward	sequencing
mmMJD91	GATTCTGTGCACTCTACCCAAG	forward	sequencing
mmMJD92	GAAGCCGGGCGCGGTGGCG	forward	sequencing
mmMJD93	CTGAGGACAGCTACAGTAAC	forward	sequencing
mmMJD94	CAGTCACCTGGAAGGAGCC	reverse	sequencing
mmMJD95	CAACCTCAGAGGTGCCCTAAC	reverse	sequencing
mmMJD96	CGTGTAAGGTCAGCCCTTC	forward	sequencing
mmMJD97	CATGGCTGGTGTGAAGAC	reverse	sequencing
mmMJD98	CGAAGGTCCTGAGTTC	forward	sequencing
mmMJD99	GCCCACAAGTAAGGCCACTG	forward	sequencing
mmMJD100	GATGGTACCACCCACAATG	forward	sequencing
mmMJD101	GTGAATCCTCTGCAAGAG	forward	sequencing

Name	Sequence 5'→ 3'	Orientation	Application
mmMJD102	GATTAAAGGTGTGCCTCCAG	reverse	sequencing
mmMJD103	CCTGCACAAGAACAATTC	forward	sequencing
mmMJD104	GAACTTGGCCCTTTGGAG	forward	sequencing
mmMJD105	CGCTTCCTATGCTCATTGC	forward	sequencing
mmMJD106	CATGGAGTCCATTTTCCACGA	forward	d-siRNA production; sequencing
mmMJD107	CGGGGCCGTTGGCTCCAGAC	forward	sequencing
Myh2(1)	GACATCGAGACCTATCTG	forward	sequencing
Myh2(2)	GCTCATCGAGAAGCCGATG	forward	sequencing
Myod1(3)	CTGATGGCATGATGGATTAC	forward	quantitative real-time RT-PCR
Myod1(4)	CTCCACTATGCTGGACAGGC	reverse	quantitative real-time RT-PCR
Myogenin(1)	GTGAATGCAACTCCCACAG	forward	quantitative real-time RT-PCR
Myogenin(2)	GTCCACGATGGACGTAAG	reverse	quantitative real-time RT-PCR
Tsga10ip(1)	GAATTCTGAAGAGGCTGAG	forward	sequencing

Table A.2. Primers used for insertion of 5' and 3' attB site-specific recombination sequences (Gateway Cloning System, Invitrogen Life Technologies)

Name	Sequence 5'→ 3'	Orientation
attB1Acta1	**GGGGACAAGTTTGTACAAAAAAGCAGGCT**ATATGTGCGACGAAGACGAG	forward
attB2Acta1	**GGGGACCACTTTGTACAAGAAAGCTGGGT**CCTAGAAGCATTTGCGGTG	reverse
attB1Ap3b1	**GGGGACAAGTTTGTACAAAAAAGCAGGCT**ATATGTCTAGCAACAGTTTCG	forward
attB2Ap3b1[138]	**GGGGACCACTTTGTACAAGAAAGCTGGGT**CTTAAACTCTCAAGGCACTTG	reverse
attB1Atp5j	**GGGGACAAGTTTGTACAAAAAAGCAGGCT**ATATGGTTCTGCAGAGGATCT	forward
attB2Atp5j	**GGGGACCACTTTGTACAAGAAAGCTGGGT**CTCAGGACTGGGGTTTGTCG	reverse
attB1Bcl7c	**GGGGACAAGTTTGTACAAAAAAGCAGGCT**ATATGGCCGGCCGGACCGTG	forward
attB2Bcl7c	**GGGGACCACTTTGTACAAGAAAGCTGGGT**CTCAGGGGTCAGGGGCATT	reverse
attB1Brf1	**GGGGACAAGTTTGTACAAAAAAGCAGGCT**ATATGACGGGCCGCGTCTG	forward
attB2Brf1	**GGGGACCACTTTGTACAAGAAAGCTGGGT**CTCAGTAGCCATCATCTTCA	reverse
attB1Ccdc113	**GGGGACAAGTTTGTACAAAAAAGCAGGCT**ATATGTCTGAGGAAGACTCG	forward
attB2Ccdc113	**GGGGACCACTTTGTACAAGAAAGCTGGGT**CCTATTTCCCAGGGGGCCG	reverse
attB1Cul1	**GGGGACAAGTTTGTACAAAAAAGCAGGCT**ATATGTCATCAAACAGGAG	forward
attB1Cul1[714]	**GGGGACAAGTTTGTACAAAAAAGCAGGCT**ATGCCATCGTGAGAATCATG	forward
attB2Cul1	**GGGGACCACTTTGTACAAGAAAGCTGGGT**CTTAAGCCAAGTAACTGTAG	reverse
attB1Eef1b2	**GGGGACAAGTTTGTACAAAAAAGCAGGCT**ATATGGGATTCGGAGACCTG	forward
attB2Eef1b2	**GGGGACCACTTTGTACAAGAAAGCTGGGT**CTTAAATCTTGTTAAAAGCAG	reverse
attB1Eif4e	**GGGGACAAGTTTGTACAAAAAAGCAGGCT**ATATGGCGACTGTGGAACCG	forward
attB2Eif4e	**GGGGACCACTTTGTACAAGAAAGCTGGGT**CTTAAACAACAAACCTATT	reverse
attB1Etfb	**GGGGACAAGTTTGTACAAAAAAGCAGGCT**ATATGGCGGAGCTGCGCGCG	forward
attB2Etfb	**GGGGACCACTTTGTACAAGAAAGCTGGGT**CTCAGATCCGCCCCACCT	reverse
attB1Gtf2e2	**GGGGACAAGTTTGTACAAAAAAGCAGGCT**ATATGGATCCAAGCCTATTG	forward
attB2Gtf2e2	**GGGGACCACTTTGTACAAGAAAGCTGGGT**CCTATTTGCCCGGGGTAATG	reverse
attB1Lrcc40	**GGGGACAAGTTTGTACAAAAAAGCAGGCT**ATATGTCGCGCCAGCTGAGAG	forward
attB2Lrcc40	**GGGGACCACTTTGTACAAGAAAGCTGGGT**CTCAGGCAGGGATTCGATCT	reverse

Name	Sequence 5'→ 3'	Orientation
attB1Mjd	**GGGGACAAGTTTGTACAAAAAAGCAGGCT**GGATGGAGTCCATCTTCCACGAG	forward
attB2Mjd	**GGGGACCACTTTGTACAAGAAAGCTGGGT**CTTACTTCTTTCGCTCTGCTT	reverse
attB1Mjd:UlMs	**GGGGACAAGTTTGTACAAAAAAGCAGGCT**ATATGGCTGATGGGTCGGGCA	forward
attB2Mjd:Jos	**GGGGACCACTTTGTACAAGAAAGCTGGGT**CTTATGCTTCTAAGACGCGCT	reverse
attB1Myh2[88]	**GGGGACAAGTTTGTACAAAAAAGCAGGCT**ATATCGAGGACATGGCCATG	forward
attB2Myh2[773]	**GGGGACCACTTTGTACAAGAAAGCTGGGT**CTCATTTGAAAAAGACCTTGG	reverse
attB1Myod1	**GGGGACAAGTTTGTACAAAAAAGCAGGCT**ATATGGAGCTTCTATCGCCGCCACTCCG	forward
attB2Myod1	**GGGGACCACTTTGTCCAAGAAAGCTGGGT**CTCAAAGCACCTGATAAATCGCATTG	reverse
attB1Nedd8	**GGGGACAAGTTTGTACAAAAAAGCAGGCT**ATATGCTAATTAAAGTGAAGA	forward
attB2Nedd8	**GGGGACCACTTTGTACAAGAAAGCTGGGT**CTCACTGCCCAAGACCACCT	reverse
attB1Pcmt1	**GGGGACAAGTTTGTACAAAAAAGCAGGCT**ATATGGCCTGGAAATCCGGCG	forward
attB2Pcmt1	**GGGGACCACTTTGTACAAGAAAGCTGGGT**CTCACTTCCACCTGGACCACT	reverse
attB1Rpl6	**GGGGACAAGTTTGTACAAAAAAGCAGGCT**ATATGGCGGGTGAAAAAGCG	forward
attB2Rpl6	**GGGGACCACTTTGTACAAGAAAGCTGGGT**CTTAGAAGACCAGTTTGTGAG	reverse
attB1Rps9	**GGGGACAAGTTTGTACAAAAAAGCAGGCT**ATATGCCGGTCGCCAGAAG	forward
attB2Rps9	**GGGGACCACTTTGTACAAGAAAGCTGGGT**CTTAATCCTCTTCCTCATCAT	reverse
attB1Spatc1	**GGGGACAAGTTTGTACAAAAAAGCAGGCT**ATATGTCTCTACTTACAAGT	forward
attB2Spatc1	**GGGGACCACTTTGTACAAGAAAGCTGGGT**CTTACCAGATGAACATAGG	reverse
attB1Thg1l	**GGGGACAAGTTTGTACAAAAAAGCAGGCT**ATATGTGGGCTTTCCGCACAG	forward
attB2Thg1l	**GGGGACCACTTTGTACAAGAAAGCTGGGT**CTCAGTTCTCTTCCGCCAG	reverse
attB1Tnni1	**GGGGACAAGTTTGTACAAAAAAGCAGGCT**ATATGCCGGAAGTTGAGAGG	forward
attB2Tnni1	**GGGGACCACTTTGTACAAGAAAGCTGGGT**CCTACTGGGAGGTCGGGGA	reverse
attB1Tnni2	**GGGGACAAGTTTGTACAAAAAAGCAGGCT**ATATGGGAGATGAGGAGAAG	forward
attB2Tnni2	**GGGGACCACTTTGTACAAGAAAGCTGGGT**CTTAGGACTCAGACTCGAACA	reverse
attB1Tsga10ip	**GGGGACAAGTTTGTACAAAAAAGCAGGCT**ATATGCTAAACACTGACCAA	forward
attB2Tsga10ip	**GGGGACCACTTTGTACAAGAAAGCTGGGT**CTTAATTTTTCTCTCGGGG	reverse
attB1Twa1	**GGGGACAAGTTTGTACAAAAAAGCAGGCT**ATATGAGTTATGCAGAAAAG	forward
attB2Twa1	**GGGGACCACTTTGTACAAGAAAGCTGGGT**CCTACTTGGGCTCCTCAAT	reverse

attB sequences are represented in bold letters

Table A.3. Primers used for insertion of endonuclease restriction sites

Name	Sequence 5'→ 3'	Orientation
5'MjdBamHI	GCCT**GGATCC**ATGGAGTCCATCTTCCACGAG	forward
3'MjdBamHI	GCCT**GGATCC**TTACTTCTTTCGCTCTGCTTT	reverse
PMjd-BglIIR	GCAC**AGATCT**GTTTATTTGTCTGGAG	reverse
PMjd-237KpnIF	CGAG**GGTACC**ACAGCAGGCGGCGCC	forward
PMjd-358KpnIF	GCAC**GGTACC**AGAAGGTGGAGATGG	forward
PMjd-559KpnIF	GGCT**GGTACC**GTATAATATTACAAAAG	forward
PMjd-928KpnIF	CGAG**GGTACC**CAGGGTCCTCCTATGTAAC	forward
PMjd-1173KpnIF	GGCT**GGTACC**CCAGTCCCTCATCAAAGT	forward

Table A.4. Forward primers used for site-directed mutagenesis

Name	Sequence 5'→ 3'	Type of mutation
Mjd-mutC14A	GAAACAAAAAGGCTCACTT**GC**TGCTCAGCATTGCCTGAA	point
Cul1-K720R	CCATCGTGAGAATCATG**CG**AATGAGGAAGGTCCTGAAAC	point

Appendix 2

Publication

Costa MC, Gomes-da-Silva J, Miranda CJ, Sequeiros J, Santos MM, Maciel P (2004) *Genomic structure, promoter activity, and developmental expression of the mouse homologue gene of the Machado-Joseph disease (MJD) gene*. Genomics 84:361-373

Available online at www.sciencedirect.com

SCIENCE DIRECT®

Genomics 84 (2004) 361–373

GENOMICS

www.elsevier.com/locate/ygeno

Genomic structure, promoter activity, and developmental expression of the mouse homologue of the Machado–Joseph disease (*MJD*) gene☆

Maria do Carmo Costa,[a,b] Joana Gomes-da-Silva,[c] Carlos J. Miranda,[a,d] Jorge Sequeiros,[a,e] Manuela M. Santos,[a,d] and Patrícia Maciel[a,b,e,*]

[a] *UnIGENe, Institute for Molecular and Cell Biology, University of Porto, 4150-180 Porto, Portugal*
[b] *Life and Health Sciences Research Institute, Health Sciences School, University of Minho, 4710-057 Braga, Portugal*
[c] *Neurobehavior Unit, Institute for Molecular and Cell Biology, University of Porto, 4150-180 Porto, Portugal*
[d] *Department of Medicine, CHUM, Hôpital Notre-Dame, H2L 4M1 Montreal, QC, Canada*
[e] *Department of Populations Studies, ICBAS, University of Porto, 4050-097 Porto, Portugal*

Received 14 August 2003; accepted 20 February 2004
Available online 21 April 2004

Abstract

Machado–Joseph disease (MJD) is a neurodegenerative disorder, caused by the expansion of the $(CAG)_n$ tract in the *MJD* gene. This encodes the protein ataxin-3, of unknown function. The mouse *Mjd* gene has a structure similar to that of its human counterpart and it also contains a TATA-less promoter. Its 5′ flanking region contains conserved putative binding regions for transcription factors Sp1, USF, Arnt, Max, E47, and MyoD. Upon differentiation of P19 cells, the *Mjd* gene promoter is preferentially activated in endodermal and mesodermal derivatives, including cardiac and skeletal myocytes; and less so in neuronal precursors. Mouse ataxin-3 is ubiquitously expressed during embryonic development and in the adult, with strong expression in regions of the CNS affected in MJD. It is particularly abundant in all types of muscle and in ciliated epithelial cells, suggesting that it may be associated with the cytoskeleton and may have an important function in cell structure and/or motility.

Keywords: Ataxin-3; Polyglutamine; Spinocerebellar ataxia; Triplet repeat; Muscle; Myocytes; MyoD; E47; Max; Arnt

Machado–Joseph disease (MJD), also known as spinocerebellar ataxia type 3 (SCA3), is a neurodegenerative disorder of late onset and the most common dominant spinocerebellar ataxia worldwide (30% among all forms) [1]. Patients present with cerebellar ataxia and progressive external ophthalmoplegia, associated in a variable degree with pyramidal signs, extrapyramidal signs (dystonia or rigidity), amyotrophy, and peripheral neuropathy [2]. Pathologically, MJD is characterized by neuronal loss in the spinocerebellar, dentate, pontine, and vestibular nuclei, the substantia nigra, the locus coeruleus, the palidoluysian complex, the motor cranial nerve and medulla anterior horn nuclei, and the dorsal root ganglia [2–4].

The MJD causative gene was mapped to chromosome 14q32.1 in 1993 [5] and cloned in 1994 [6], but its structure has only recently been elucidated [7]. Alternative splicing of *MJD* results in the production of different isoforms of ataxin-3 [8], which are expressed in various tissues and have been detected both in the nucleus and in the cytoplasm [7,9–11]. MJD is one of the CAG repeat/polyglutamine disorders, which includes Huntington disease (HD), spinal and bulbar muscular atrophy, dentatorubropallidoluysian atrophy (DRPLA), and other spinocerebellar ataxias, such as SCA1, 2, 6, 7, 12, and 17. Each is characterized by selective neuronal cell death in specific regions of the brain, and their causative genes do not show homology with each other, except for the polyglutamine segment itself. The minimal poly(Q) length to cause disease is variable among these disorders. The CAG repeat tract in *MJD* contains 10–51 triplets in healthy individuals and 55–87 in patients [12,13].

Mutant ataxin-3, like other pathogenic proteins carrying expanded poly(Q) stretches, appears to undergo a conformational change and aggregate in cells forming inclusion

☆ Supplementary data for this article may be found on ScienceDirect.

* Corresponding author. Life and Health Sciences Research Institute, Health Sciences School, University of Minho, Campus de Gualtar, 4710-057 Braga, Portugal. Fax: +351-253604831.
E-mail address: pmaciel@ecsaude.uminho.pt (P. Maciel).

0888-7543/$ - see front matter © 2004 Elsevier Inc. All rights reserved.
doi:10.1016/j.ygeno.2004.02.012

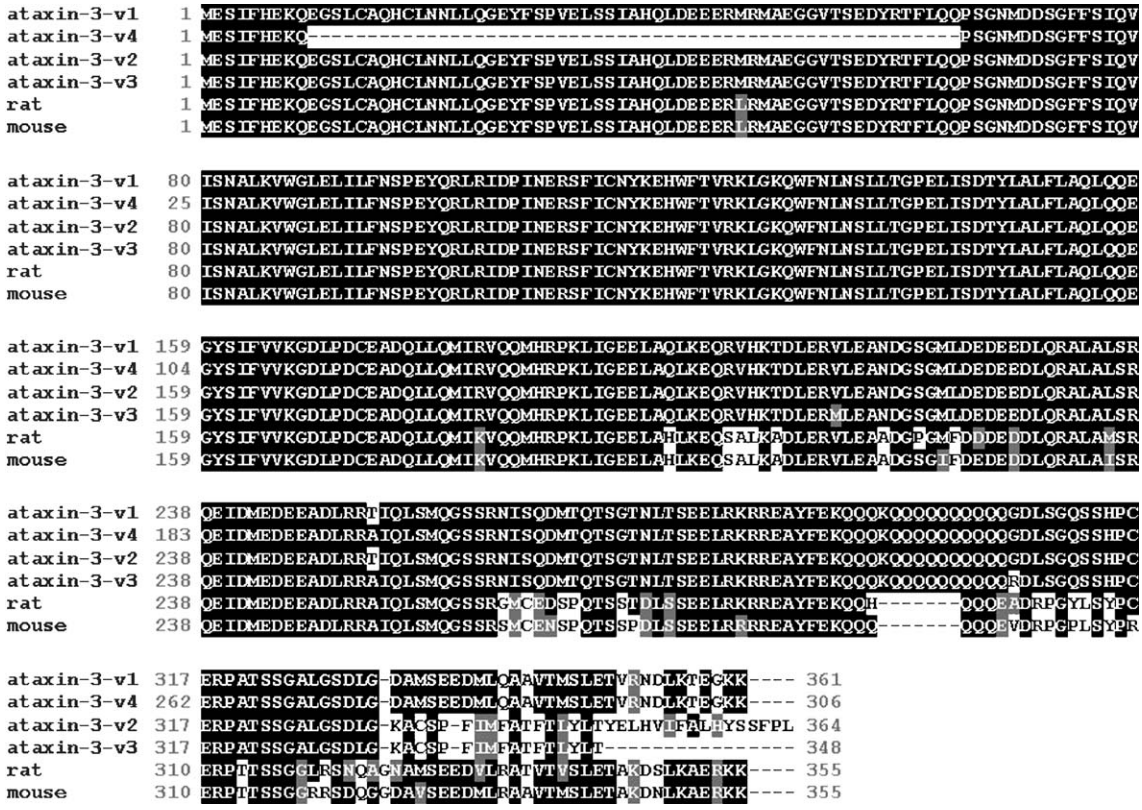

Fig. 1. Multiple sequence analysis of mouse and rat ataxin-3 homologues and human ataxin-3 variants (CLUSTAL W). Aligned residues that are identical or similar are shaded with a black or gray background, respectively.

bodies [12]. Ubiquitinated neuronal intranuclear inclusions (NIIs) have been observed in the brains of patients [14], cultured cells [15], and transgenic mouse models [16,17]. The observation that NIIs sequestrate transcriptional activators/coactivators suggests that an interference with gene transcription might be underlying the polyglutamine patho-

Table 1
Exon–intron boundaries of the mouse *Mjd* gene

Exon/intron	Length (bp)		Acceptor site	Donor site
	Exon	Intron		
Exon 1	67			CCACGAGAAA/gtgagtgtgg
Intron 1		10098		
Exon 2	165		gaaacactag/CAAGAAGGCT	ATTTTTACAG/gtactgattt
Intron 2		226		
Exon 3	45		aattgaacag/CAGCCTTCTG	CTCTATTCAA/gtaagtagtc
Intron 3		2084		
Exon 4	86		cttttgacag/GTTATAAGCA	TTGATCCTAT/gtaagatttt
Intron 4		367		
Exon 5	67		tttcttctag/AAACGAAAGA	AGGCAAGCAG/gtaatatatc
Intron 5		3198		
Exon 6	88		tttttcctag/TGGTTTAACT	CAGCAAGAAG/gtaaataaga
Intron 6		4648		
Exon 7	133		ctctttttag/GTTATTCTAT	AAGAGCAGAG/gtaaaactac
Intron 7		3192		
Exon 8	167		tgttgtttag/TGCCCTCAAA	AGTATGCAAG/gtttggacat
Intron 8		1183		
Exon 9	97		ttgtttttag/GTAGTTCCAG	ACTTTGAAAA/gtaaagtagt
Intron 9		6386		
Exon 10	98		aatgtttcag/GCAACAGCAG	AGCGACCAAG/gtttgctttc
Intron 10		3279		
Exon 11	97		tctttcccag/GAGGCGACGC	

genic mechanism [18]. It is not clear, however, if these NIIs are the cause or a consequence of the pathogenic mechanism. The potential conformational change and protein misfolding may be of importance to pathogenesis, since increased expression of chaperones can diminish the poly(Q) toxicity [19,20], while inhibition of the proteasome pathway enhances cell death [21,22]. Another hypothesis for the mechanism of neurodegeneration is the possibility of amyloid formation, as in Alzheimer disease and other neurodegenerative disorders, but with a different subcellular location [23]. Infrared spectroscopy measurements have shown that ataxin-3, containing an expanded poly(Q) tract, also forms fibrils in vitro presenting a higher content of β

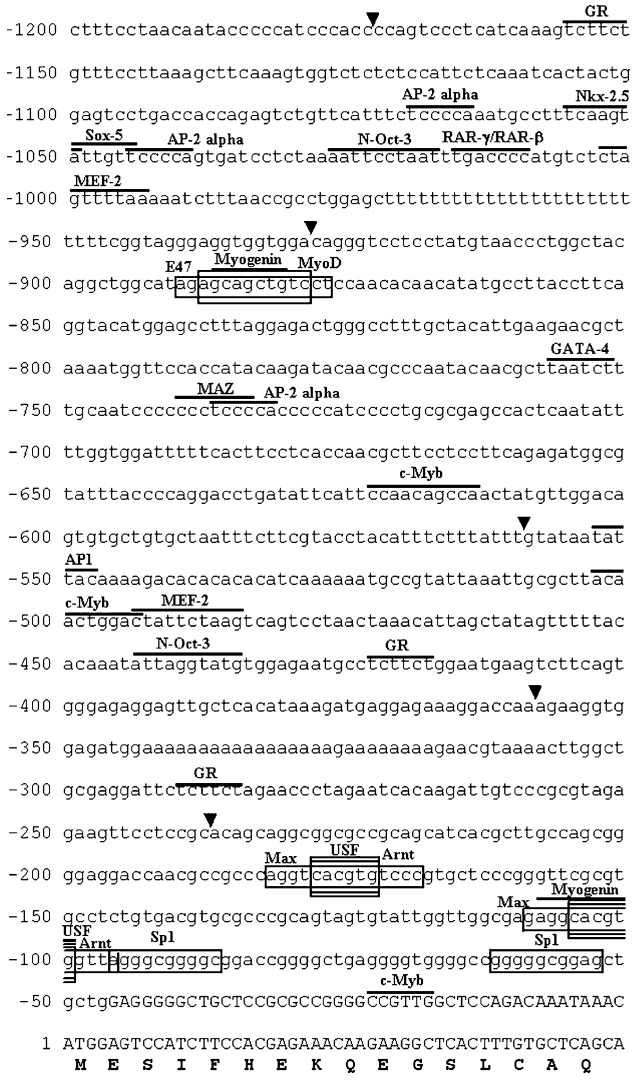

Fig. 2. Nucleotide sequence of the 5′ flanking region of the mouse *Mjd* gene. The translation start site is numbered as +1. Uppercase letters represent exon sequences and untranscribed sequences are represented by lowercase letters. The coding region of the first exon is shown as codon triplets. For the detection of promoter activity, an arrowhead indicates the start point of each construct. Consensus binding sequences of the conserved transcription factor binding sites are boxed; other potential transcription factor binding sites are indicated by a line.

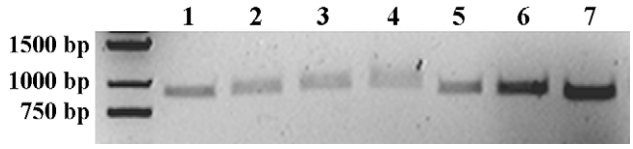

Fig. 3. Binding of MyoD to the *Mjd* gene promoter. EMSAs were performed with 2.5 (lane 2), 5 (lane 3), or 15 μg (lane 4) of purified recombinant MyoD incubated with the −928 bp fragment of the promoter. For the competition assay 2.5 μg of purified recombinant MyoD was incubated with 2 (lane 6) or 4 μg (lane 7) of competitor double-stranded oligonucleotides followed by the addition of the −928 bp fragment. Lanes 1 and 5 correspond to the −928 bp fragment of the promoter.

sheets [24]. There is evidence that polyglutamine aggregates exhibit most of the features of amyloid [25].

The first transgenic mouse models of MJD were generated with truncated and full-length human MJD1a cDNAs (containing 79 CAGs) under the control of the L7 promoter, which specifically directs their expression in Purkinje cells [16]. Recently, YAC transgenic mouse models for MJD were also generated [17]. These mice, carrying the full-

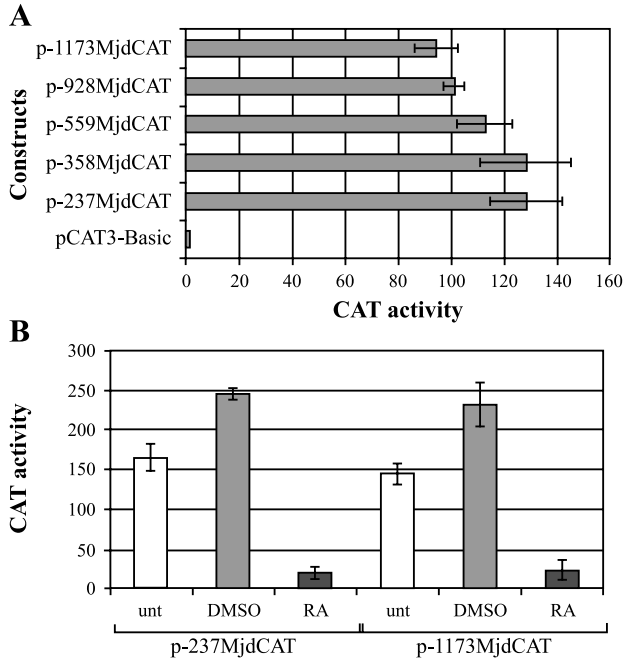

Fig. 4. Functional analysis of the mouse *Mjd* gene promoter. (A) A series of constructs containing different sizes of the 5′ flanking region of the *Mjd* gene was transfected into P19 cells. CAT activity is represented in arbitrary units, normalized for β-galactosidase activity and for total protein amount. (B) Activation of the mouse *Mjd* promoter during RA- or DMSO-induced differentiation of P19 cells. Undifferentiated P19 were incubated with medium or with DMSO- or RA-supplemented medium, on bacterial-grade petri dishes, for 3 days, then dissociated, transfected with p-237MjdCAT and p-1173MjdCAT constructs, and further grown on tissue culture plates. Cells were harvested at day 3 after replating (day 6 after induction of differentiation). Data are expressed as the fold increase in CAT activity compared with transfections using empty CAT plasmid, pCAT3-Basic. The results are the averages of three independent transfections ± SEM (error bars).

length human *MJD* gene with expanded CAG repeats and its own regulatory elements, showed a mild and slowly progressive cerebellar deficit, cell loss in the dentate and pontine nuclei, as well as in other regions of the cerebellum, and peripheral nerve demyelination.

The function of ataxin-3 remains unknown. Recent studies suggest that ataxin-3 protein interacts with DNA-repair proteins HHR23A and HHR23B [26] and with the major histone acetyltransferases CBP, p300, and PCAF [27]. A recent computational structure-based sequence alignment study revealed that ataxin-3 has homology to ENTH and VHS domain proteins, which are involved in membrane trafficking and regulatory adaptor functions [28].

Several protein sequences highly homologous to human ataxin-3 have been described in rat [29] and chicken [30] and found in databases for mouse, *Fugu, Drosophila, Caenorhabditis elegans*, and *Arabidopsis thaliana* [28], suggesting that this protein is highly conserved throughout evolution and has functional relevance. To gain insight into the function of ataxin-3, we isolated and characterized the mouse *Mjd* gene. We cloned mouse *Mjd*, determined its genomic structure, characterized (spatially and functionally) the promoter region using the P19 cell model, and analyzed the expression pattern of mouse ataxin-3 during embryonic development and in the adult, using immunohistochemistry and immunoblotting techniques. Our results indicate that mouse ataxin-3 is ubiquitously expressed and is developmentally regulated, with high expression in muscle and ciliated epithelial cells, as well as in regions of the central nervous system (CNS) affected in MJD.

Results

Cloning of full-length cDNA and analysis of mouse Mjd gene organization

Using one of the cDNA sequences of human *MJD* (pMJD1a), we searched for homologous sequences in GenBank and found one mouse cDNA (Accession No. AK008675) with 1097 bp. A full-length mouse cDNA clone with 1100 bp (pMjd1) was obtained by RT-PCR from cerebral cortex total RNA and verified by sequencing. Analysis of the nucleotide sequence revealed 88, 84, 81, 80, and 68% identity with the human MJD1-1, MJD5-1, MJD1a, MJD2-1, and H2 cDNA sequences, respectively, and 92% identity with the rat homologue cDNA. The pMjd1 cDNA contains a coding region of 1065 bp, predicted to encode a 355-amino-acid protein—mouse ataxin-3.

A multiple sequence alignment, using CLUSTAL W, of mouse ataxin-3 with rat ataxin-3 and human ataxin-3-v1, ataxin-3-v2, ataxin-3-v3 [28], and ataxin-3-v4 (see Materials and methods) showed a 94, 86, 80, 82, and 83% identity, respectively, at the amino acid level (Fig. 1). This indicates that the obtained sequence is in fact the mouse homologue to human ataxin-3.

A probe of 400 bp (nucleotides 1 to 400 of the cDNA), obtained by PCR, was used to screen a BAC Mouse II library. One positive BAC clone was identified and sequenced. Comparisons of the mouse cDNA clone sequence with the BAC clone sequence enabled us to determine the exon/intron structure of the mouse *Mjd* gene (Table 1). This gene of

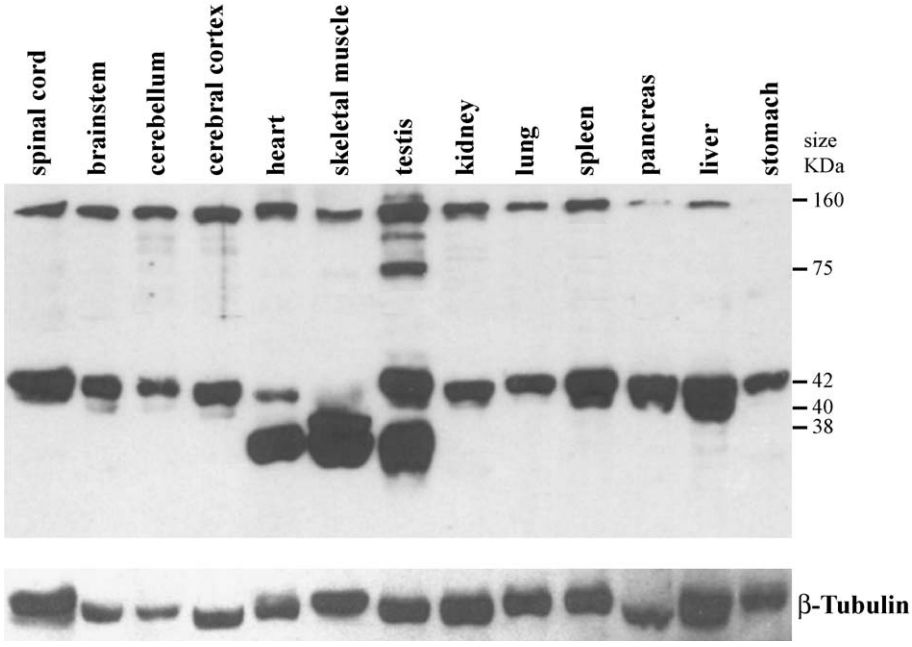

Fig. 5. Mouse ataxin-3 expression in wild-type C57Bl/6 mouse tissues. Protein extracts were resolved on 10% SDS–polyacrylamide gels. Immunoblotting reveals immunoreactive bands of 42 and 160 kDa present in all tissues analyzed. Heart, skeletal muscle, and testis presented another, lower molecular mass of 38 kDa, while skeletal muscle presented an additional band of 40 kDa.

approximately 36 kb, localized on chromosome 12, is very similar to its human counterpart, in both number and sizes of exons and introns. *Mjd* is composed of 11 exons and 10 introns, carrying a $(CAG)_6$ repeat on exon 10 (Table 1). Thus, the genomic structure of mouse *Mjd* is highly homologous to that of human *MJD,* which is localized on chromosome 12, in a region syntenic to the human chromosome 14.

Sequence analysis of the 5′ flanking region

Analysis of the 5′ flanking region of *Mjd* revealed that its promoter consists of a sequence lacking TATA boxes or CCAAT boxes, similar to the human counterpart (Fig. 2). The G+C-rich region extends from −307 to −8 bp (GC content, 68%). Analysis of the 1173-bp region upstream of

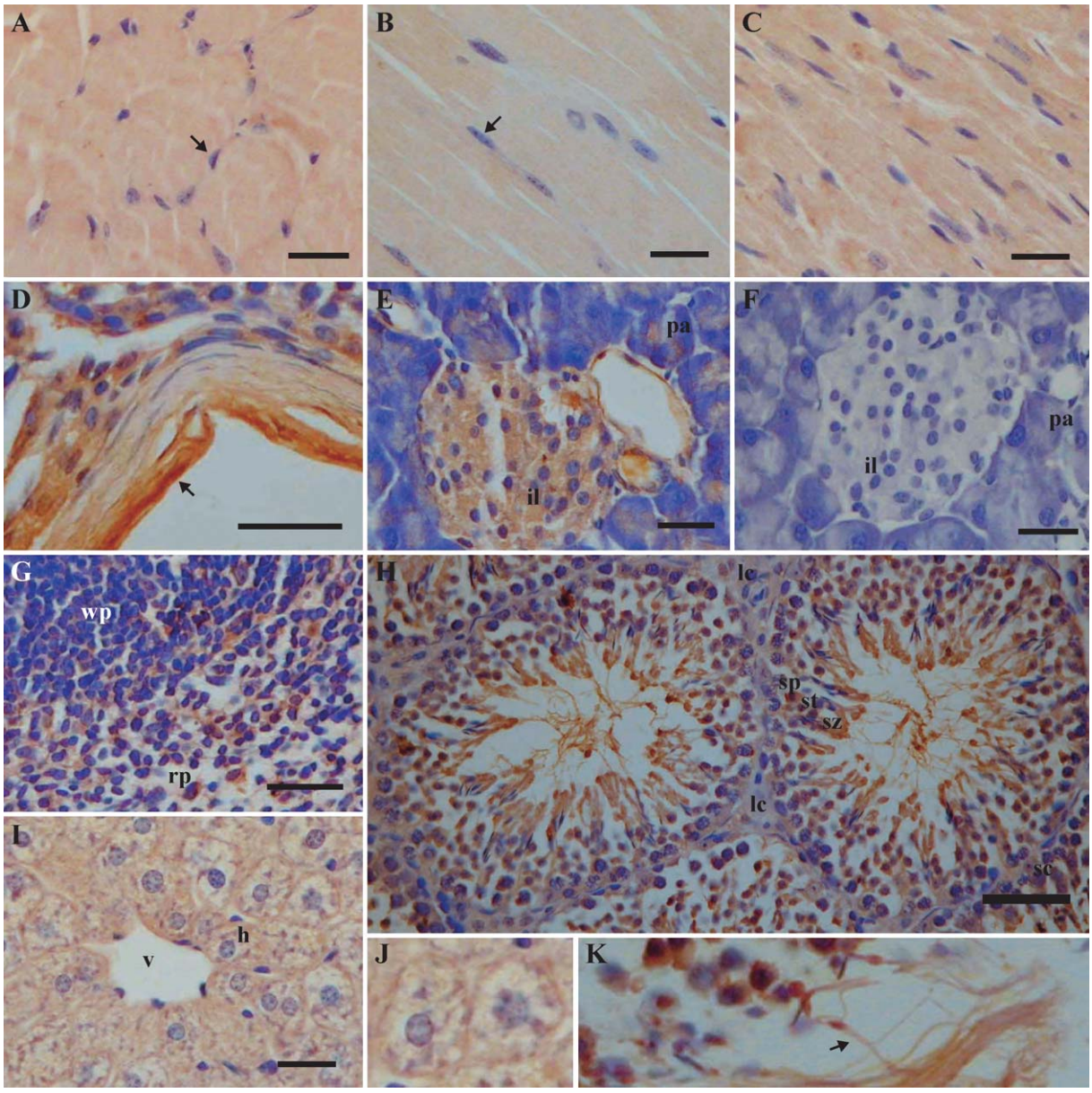

Fig. 6. Mouse ataxin-3 immunoreactivity in adult mouse tissues. Bright-field micrographs of (A) transversal and (B) longitudinal sections of skeletal muscle, (C) cardiac muscle, (D) smooth muscle, (E) pancreas, (F) control for staining, without the primary antibody, in pancreas section, (G) spleen, (H) testis, and (I) liver. (A–D) High immunoreactivity was found in all types of muscles analyzed. (E) In the pancreas, staining was ubiquitous and could be clearly observed in the islets of Langerhans, though it was also present in the exocrine component. (G) In the spleen, labeling was found in both the white and the red pulp. (H) In the testis, the protein was also widely distributed, both within and outside the seminiferous tubules; in the tubules, it was found on spermatogonia, spermatocytes, spermatids, and spermatozoa and appeared to be absent on Sertoli cells; high reactivity was also found in the surrounding tunica propria (D). (I) In the liver, mouse ataxin-3 immunoreactivity was widely distributed throughout the section. (J) High magnification of two hepatocytes evidencing the more intense perimembrane staining, and (K) high magnification of spermatozoa. The arrows point to, in (A, B), a nucleus of muscular cell, showing no anti-mouse ataxin-3 immunoreactivity; in (D), the smooth muscle layer in the tunica propria of the testis; and in (K), the flagellum of a spermatozoon. The black bar on the lower right corner is equivalent to 50 μm. h, hepatocyte; il, islet of Langerhans; lc, Leydig cells; pa, pancreatic acinar cells; rp, red pulp; sc, Sertoli cell; sp, spermatocytes; st, spermatids; sz, spermatozoa; v, venule; wp, white pulp.

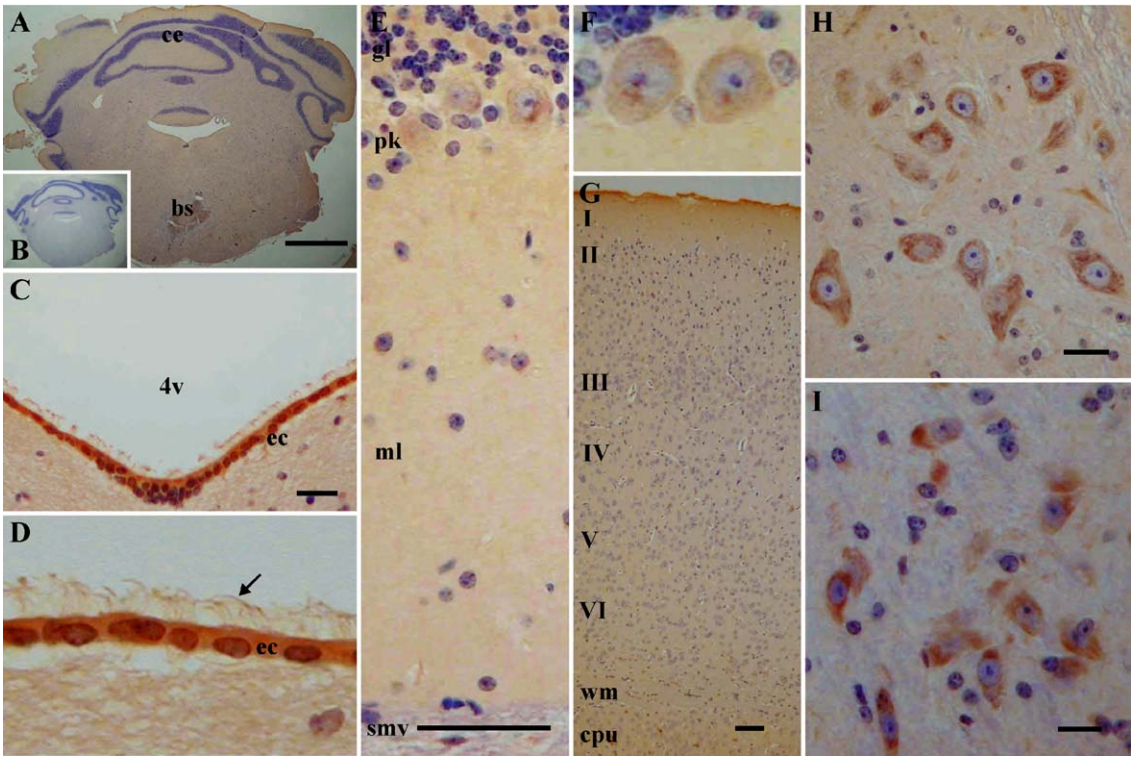
A
ce
bs
B
C
4v
ec
D
ec
E
gl
pk
ml
smv
F
G
I
II
III
IV
V
VI
wm
cpu
H
I

Fig. 7.

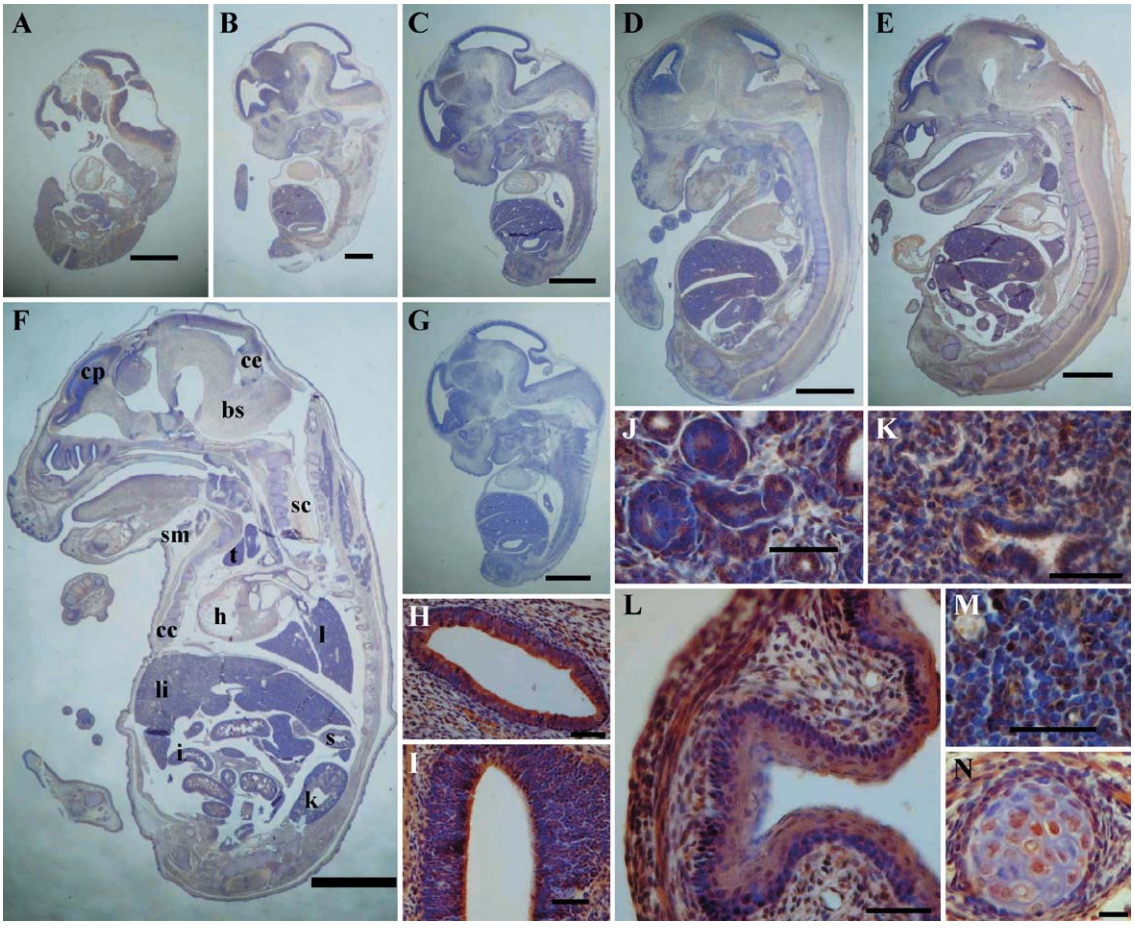
A
B
C
D
E
F
cp
cc
bs
sc
sm
t
h
cc
l
li
i
s
k
G
H
I
J
K
L
M
N

Fig. 8.

the start codon of both mouse and human genes for conservation of putative transcription factor binding regions using the TRES/TRANSFAC program revealed the presence of putative Sp1, upstream stimulatory factor (USF), aryl hydrocarbon receptor nuclear translocator (Arnt), Myc-associated factor X (Max), E47 and MyoD regulatory element binding sites, and also GC box elements in the gene promoters of both species (see supplementary data). Potential transcription factor binding sites for GATA-4, Nkx-2.5, myogenin, myocyte-specific enhancer factor-2 (MEF-2), c-Myb, activating enhancer-binding protein-2α (AP-2α), retinoic acid receptor-γ/retinoid X receptor-β (RAR-γ/RXR-β), N-Oct-3, SRY-related HMG-box-5 (Sox-5), glucocorticoid receptor (GR), activating protein-1 (AP1), and Myc-associated zinc-finger protein (MAZ) were also found in the 5′ flanking region of mouse *Mjd* (see supplementary data). These data suggest that the *Mjd* gene may be developmentally regulated.

Binding of MyoD to the Mjd promoter

To confirm the binding of the transcription factor MyoD, whose target region is conserved in mouse and human, we expressed and purified a recombinant mouse MyoD-His tag protein and analyzed its binding to the −928 bp fragment of the 5′ flanking region of the *Mjd* gene by electrophoretic mobility-shift assay (EMSA). We analyzed the binding of various quantities of the recombinant protein (2.5, 5, and 15 μg) to the DNA and verified that the binding, as revealed by gel retardation assay, increased proportionally with the amount of protein added (Fig. 3). To verify that the binding of the recombinant protein to the −928 bp fragment was specific, we performed a competition assay using two different quantities of oligonucleotides corresponding to the MyoD binding region of the *Mjd* gene promoter (localized at position −888 bp) and verified that in the presence of these oligonucleotides the binding of the recombinant protein to the promoter fragment decreased proportionally to the amount of competing oligonucleotides (Fig. 3). This result suggests that the *Mjd* gene promoter is indeed regulated by MyoD, which is a transcriptional activator of muscle-specific genes.

Promoter activity of the 5′ flanking region

To characterize the regions regulating the transcription activity of the mouse *Mjd* gene, we constructed a series of plasmids containing different lengths of the 5′ flanking region of *Mjd* fused to the promoterless *CAT* gene in pCAT3-Basic (Promega): p-237MjdCAT, p-358MjdCAT, p-559Mjd CAT, p-928MjdCAT, and p-1173Mjd CAT. Transient transfection assays were performed using undifferentiated mouse embryonic carcinoma P19 cells. CAT activity was normalized for transfection efficiency, with reference to the β-galactosidase activity derived from the cotransfected internal control plasmid. As shown in Fig. 4A, we observed minimal activity of the promoter with the p-1173MjdCAT construct and maximal activity with either p-237MjdCAT or p-358MjdCAT plasmid, which presented a 94- and a 128-fold increase over the empty pCAT3-Basic plasmid, respectively. The fragments with 237 and 358 bp presented a 1.4-fold increase over the 1173-bp segment of the 5′ flanking region of the gene. We observed a decrease in the promoter activity for the fragments larger than −358 bp, which suggests the existence of repressor-binding sequences in these regions.

These results suggest that the −237 bp region of the cloned 5′ region of the *Mjd* gene is sufficient to direct maximal transcription in P19 cells.

Activation of the mouse Mjd gene promoter during differentiation of P19 cells

We next examined the behavior of the isolated promoter sequence in terms of transcriptional activation during the differentiation of P19 cells onto three different types of cells: neuronal precursors, cardiac/skeletal myocytes, and

Fig. 7. Ataxin-3 is ubiquitously expressed in the central nervous system of the adult mouse. (A, B) Low-magnification photomicrographs of a coronal section of the cerebellum and brain stem (approximate level 5.68 mm anterior to bregma) [46]. (A) Mouse ataxin-3 immunoreactivity and (B) control of staining, without the primary antibody. Mouse ataxin-3 staining is prominent in ependymal cells, as evidenced (C) in the cells in the fourth ventricle and at high magnification in (D), also showing the labeled cilia. (E) Low magnification of the anti-ataxin-3 labeling, in the different layers of the cerebellum, evidencing the cytoplasmic labeling in the Purkinje cells, also shown in higher magnification in (F). (G) Low magnification of immunoreactivity in cerebral cortex layers. (H) High magnification of the neuronal immunolabeling in the brain stem and (I) in the substantia nigra. The arrow points to, in (D), the labeled cilia of the ependymal cells. The black bar on the lower right corner is equivalent in (A) to 1 mm, in (G) to 200 μm, and in (C, E, H, I) to 50 μm. I–VI, cortical layers I–VI; 4v, fourth ventricle; bs, brain stem; ce, cerebellum; cpu, caudate putamen; ec, ependymal cells; gl, granule cell layer; ml, molecular cell layer; pk, Purkinje cells; smv, superior medullary velum; wm, white matter.

Fig. 8. Ataxin-3 immunoreactivity during mouse embryonic development. Sagittal micrographs of mouse embryos at (A) embryonic day 11.5 (E11.5), (B) E12.5, (C) E13.5, (D) E14.5, (E) E15.5, and (F) E16.5. (F) At E16.5, the developing cardiac, skeletal, and smooth muscle were visibly labeled for mouse ataxin-3; immunoreactivity was also found in the respiratory and digestive tracts, especially marking the nonkeratinizing stratified squamous epithelia of the oral cavity and nasopharynx and the intestinal villi, in the apical portion of enterocytes, as well as in the adrenal glands, the pancreas, and the salivary glands (sublingual and submaxillary). (G) Control for staining, without the primary antibody, in a sagittal section of an E13.5 mouse embryo. (H–N) High-magnification images of E16.5 embryo. The black bar in the lower right corner is equivalent in (A, B) to 1 mm, in (C–G) to 2 mm, and in (H–N) to 50 μm. Intense ataxin-3 staining is evidenced (H) in the cochlear and (I) in the olfactory epithelia. Ataxin-3 is marked in the developing (J) kidney, (K) lung, (L) stomach, (M) thymus (both in the medulla and in the cortex), and (N) ossification areas (the periosteum was stained, as well as the cytoplasm of osteoprogenitor cells, whereas larger and more cuboidal osteoblasts appeared to exhibit no staining). bs, brain stem; cc, costal cartilage; ce, cerebellar primordium; cp, cortical plate; h, heart; i, intestine; k, kidney; l, lung; li, liver; s, stomach; sc, spinal cord; sm, submaxillary gland; t, thymus.

endoderm cells [31,32]. To promote cellular differentiation, P19 cells were cultured as aggregates in the presence of medium or all-*trans*-retinoic acid (RA)- or dimethyl sulfoxide (DMSO)-supplemented medium to obtain endoderm-like cells (untreated), neuron-like cells, or cardiac/skeletal myocytes, respectively. A significantly higher activity of the *Mjd* gene promoter was observed in cardiac and skeletal myocytes transfected with constructs p-237MjdCAT and p-1173MjdCAT, which presented a 244.4- and a 231.5-fold increase in gene activity, respectively, over cells transfected with the empty pCAT3-Basic plasmid (Fig. 4B). Endoderm-like cells presented a 164.7- and 144.3-fold increase over the empty-vector-transfected cells, when transfected with constructs p-237MjdCAT and p-1173MjdCAT, respectively. In contrast, neuron-like cells transfected with the same constructs, p-237MjdCAT and p-1173MjdCAT, showed a 19.3- and a 23.0-fold increase, respectively, relative to cells transfected with the empty vector (Fig. 4B). These data indicate that at early stages of embryogenesis, the *Mjd* gene is preferentially activated in endodermal (DMSO-treated and untreated) and mesodermal (DMSO-treated) derivatives, including cardiac and skeletal muscle, and relatively less in neuronal precursors.

Mouse ataxin-3 expression in adult mouse

The expression pattern of mouse ataxin-3 was studied by immunoblotting analysis of several tissues from adult wild-type mice, using the anti-ataxin-3-specific antiserum that cross-reacted with endogenous mouse ataxin-3. Tissue samples from the spinal cord, brain stem, cerebellum, cerebral cortex, heart, skeletal muscle, testis, kidney, lung, spleen, pancreas, liver, and stomach all presented an immunoreactive band of 42 kDa that corresponded to full-length mouse ataxin-3 and another band of approximately 160 kDa, potentially corresponding to an SDS-resistant tetramer (Fig. 5).

Cardiac and skeletal muscle expressed an additional and more prominent lower molecular mass species of 38 kDa that is also present in human counterpart tissues [9]. This species and another of higher molecular mass were also present in testis. Skeletal muscle presented additionally another immunoreactive band of 40 kDa (Fig. 5). These species could either represent different splice variants of the mouse *Mjd* gene (potentially corresponding to human H2 cDNA variant described by Ichikawa and colleagues [7]) or be the result of proteolysis. Their conservation in mouse and human suggests that they could be of functional relevance.

To assess the regional and cellular distribution of mouse ataxin-3, we performed immunohistochemistry studies, using the anti-ataxin-3 antiserum, in peripheral tissues and organs and in the CNS of wild-type mice. Mouse ataxin-3 seemed to be ubiquitously distributed and to have a cytoplasmic localization, as evidenced in immunostained sections (Figs. 6, 7, and 8). The protein was highly expressed in skeletal, cardiac, and smooth muscle (Figs. 6A–6D). The flagellum of the spermatozoa stained intensely (Fig. 6K), and Leydig cells were also reactive to the antibody (Fig. 6H).

Anti-mouse ataxin-3 immunoreactivity was found ubiquitously in the CNS (Fig. 7A) and particularly localized in the cytoplasm of both neurons and glial cells. Marked labeling was found in the cytoplasm of neurons in the brain stem (Fig. 7H) and in the substantia nigra (Fig. 7I). In the substantia nigra, mouse ataxin-3 was expressed both in the pars compacta and in the pars reticulata. In the cerebellum, immunoreactivity was found in both the granular and the molecular layer (Fig. 7E); in the Purkinje cells, mouse ataxin-3 appeared to be located mainly in the cytoplasm, as suggested by the absence of nuclear staining (Fig. 7F). As shown in Fig. 7G, staining for mouse ataxin-3 was found in all layers of the cerebral cortex. Myelinated fibers of the white matter were also marked, although the staining was less pronounced. Likewise, in fiber areas, such as the corpus callosum and the anterior commissure, the staining was less intense. Immunolabeling was very intense in the ependymal cells, as observed in the lateral, third, and fourth ventricles (Fig. 7C); the cilia of these cells were also labeled (Fig. 7D).

Expression of mouse ataxin-3 during embryonic development

To determine the pattern of expression of mouse ataxin-3 during mouse embryonic development, we performed immunohistochemistry using anti-ataxin-3 antiserum in sagittal sections of embryos, at embryonic day (E) 11.5, E12.5, E13.5, E14.5, E15.5, and E16.5. Mouse ataxin-3 was continuously expressed in several tissues, including the CNS, from the earliest age analyzed (E11.5) and exhibited a ubiquitous distribution (Figs. 8A–8F). Ciliated epithelia, like the olfactory (Fig. 8I) and cochlear epithelia (Fig. 8H), were intensely stained.

Discussion

In this study, we determined the entire genomic structure of the mouse *Mjd* gene, characterized the functional promoter activity for the 5′ flanking region in transient transfection assays, and investigated the expression of the gene in mouse embryonic carcinoma P19 cells and its developmental regulation in mice. Our results showed that the mouse *Mjd* gene, a gene of 36 kb, has an organization very similar to that of human *MJD:* both the number and the sizes of exons and introns—11 exons and 10 introns—are identical [7]. The *Mjd* gene contains a CAG repeat localized in exon 10, as occurs in the human gene. The *Mjd* cDNA has a high sequence similarity to its rat and human counterparts. At the amino acid level, mouse ataxin-3 revealed 94 and 82–86% identity with rat and human proteins, respectively. The $(CAG)_n$ repeat in the mouse *Mjd* gene, as well as in the rat gene [29], is shorter than in its human counterpart, containing 6 triplet units compared to the range of 10–51 repeats in the normal human population [12,13]. Reduced

length of polyglutamine tracts and high conservation at the amino acid level have also been observed in mouse homologues of other genes involved in human polyglutamine disorders, such as SCA1 [33], SCA2 [34], SCA7 [35], and HD [36,37]. This suggests that the polyglutamine stretch may have no relevance for function in the wild-type protein and that the expansion of repeats may be characteristic of primates, since no natural models of expanded poly(Q) are known in rodents.

Analysis of the 1173-bp regulating region upstream of mouse *Mjd* revealed the presence of putative binding sites for the transcription factors Sp1, USF, Max, Arnt, E47 and MyoD, which were conserved in the 5′ flanking region of the human gene, and the presence of potential binding sites for GATA-4, Nkx-2.5, myogenin, MEF-2, c-Myb, AP-2α, RAR-γ/RXR-β, N-Oct-3, Sox-5, GR, AP1, and MAZ. Similar to the human *MJD* promoter gene, no TATA or CCAAT boxes were found on the 5′ flanking region of *Mjd*. This and the presence of both constitutive and tissue-specific transcription factor regulatory sites suggest that the *Mjd* promoter is unusual, since it presents characteristics of both housekeeping and regulated genes. Interestingly, the results of the functional studies of this TATA-less promoter region correlate very well with the predicted roles of these putative transcription factor binding regions. Analysis of the promoter activity, using a series of constructs containing different lengths of the 5′ upstream region of the *Mjd* gene and *CAT* as a reporter gene, showed minimal activity of the promoter for the −1173 bp fragment, whereas fragments −237 and −358 bp presented maximal activity. The progressive decrease in activity for fragments larger than −358 bp suggest the existence of repressor binding sites in these regions. Sequence analysis of segments −237 and −358 bp revealed the repeated presence of similar regulatory regions on both fragments, except for the presence on the −358 bp segment of a putative GR binding region at position −290 bp. The similarity of results for the two constructs may relate to the absence of glucocorticoid exposure in the P19 system used in this study. The −237 bp region, containing putative binding sites for several ubiquitous transcription factors, such as Sp1, USF, Max, and Arnt, that are conserved in the human promoter, seems to be sufficient to direct maximal transcription in the P19 cells.

Having identified the minimal promoter region and potential regulatory elements, we then studied the *Mjd* promoter activity, in both RA-induced (neuronal) and DMSO-induced (cardiac/skeletal myocytes) differentiated P19 cells [31,32]. Cells transfected with constructs p-237MjdCAT and p-1173MjdCAT exhibited an increase in promoter activity of the *Mjd* gene when treated with DMSO—there was a 1.5- and 1.6-fold higher activity, respectively, relative to untreated cells. This is in agreement with the presence on the promoter of several putative binding regions for muscle-specific transcription factors, including myogenin, MyoD/E47, MEF-2, GATA-4, and Nkx-2.5. Of these, the MyoD binding site is also present in the human promoter. We confirmed the binding of the transcription factor MyoD to the mouse *Mjd* promoter by gel shift assay. These results are confirmed by the immunoblotting results that showed a high expression of the *Mjd* gene product—mouse ataxin-3—in cardiac and skeletal muscle. These tissues expressed smaller isoforms of the protein, 38 and 40 kDa in size, which are conserved in humans [9], suggesting the functional relevance of these isoforms. The expression of mouse-ataxin-3 in cardiac, skeletal, and smooth muscle was also confirmed by immunohistochemistry, both in adult mouse and during development, showing a cytoplasmic localization.

Untreated preaggregated P19 cells that correspond to endoderm-like cells [38] presented a relatively high activity of both *Mjd* promoter regions (−237 and −1173 bp), suggesting that the *Mjd* gene could be of functional relevance from the first stages of cell differentiation.

Neuron-like cells presenting morphologic and metabolic characteristics of normal neurons were obtained by RA-induced P19 differentiation. Interestingly, transient transfection of these cells with constructs p-237MjdCAT and p-1173MjdCAT originated an activity 8.5- and 6.3-fold weaker, respectively, than the untreated cells. The weaker activity of the minimal promoter (−237 bp) could be explained by the presence of two conserved putative binding sites for Max, at positions −109 and −182 bp. The Max and Mad genes are known to be up-regulated during RA-induced differentiation [39], thus Max/Mad heterodimers could bind and act as repressors of transcription. Simultaneously, down-regulation of the activator gene c-Myc, which is later expressed at high level (at day 14 of differentiation) [39], could also contribute to the observed decrease in promoter activity. Alternatively, a decrease in transcription may occur through the AhR/Arnt pathway, potentially acting at the conserved −105 and −178 bp binding sites. In fact, aryl hydrocarbon receptor (AhR) has been shown to be down-regulated in RA-treated cells [40].

Despite the presence on the p-1173MjdCAT construct of several potential binding regions for AP-2α, N-Oct-3, and RAR-γ/RXR-β, which are activators for neuron-specific genes, CAT activity on RA-differentiated cells transfected with this construct was rather similar to that obtained for the minimal promoter construct. It is possible that the potential activation of transcription by these factors is not sufficient to overcome the transcription repression of *Mjd* by the Max/Mad pathway, at least at this stage (day 6) of RA-induced differentiation. This does not exclude that at later stages of embryonic development, which are not mimicked by P19 cells, these transcription factors could eventually become activated. The presence of additional neuronal-specific enhancers of transcription upstream of the −1173 bp promoter region of *Mjd* also cannot be excluded and could account for the high expression of mouse ataxin-3 observed in the CNS during both adult and embryonic stages of the mouse.

In the CNS of the adult mouse, mouse ataxin-3 was ubiquitously expressed and was localized in the cytoplasm of both neurons and glial cells. Relevant reactivity was found in the brain stem (mainly in neurons), in the substantia nigra, and in both the granular and the molecular layer of the cerebellum. However, a very intense expression was also observed in other types of cells of the CNS, which are not affected in MJD. We suggest that the pathogenic mechanism in MJD may be independent of the function of ataxin-3, being due not only to a prominent expression of the mutant protein in the affected regions but also to other factors that contribute to a selective neuronal loss.

The study of the expression pattern of mouse ataxin-3 during embryonic development revealed that it is expressed since the early stages and confirmed the ubiquitous expression observed in adult mice.

The intense immunoreactivity of mouse ataxin-3 in ependymal cells, in the flagellum of the spermatozoa, and in ciliated olfactory and cochlear epithelia suggests that this protein may have an important function in cell structure and/or motility. Additionally, the presence in the promoter region of conserved binding sites for muscle-specific transcription factors, and the high activity of the *Mjd* promoter in DMSO-treated cells, in conjunction with the very intense expression of mouse ataxin-3 in cardiac, skeletal, and smooth muscle, suggests that the function of *Mjd* may be relevant in these tissues. These results can also be related to the structural modeling of ataxin-3, which has a distant homology to adaptins [28]. Adaptins are functionally related to and involved in the cytoskeleton machinery, vesicular trafficking, and clathrin-dependent endo- and exocytosis [28]. Further studies are necessary to determine whether mouse ataxin-3 may be a cytoskeleton-associated protein that could be important for motility and for cellular transport.

In summary, our studies indicate that *MJD* is highly conserved between species, within coding and 5′ regulatory regions, and its regulated expression during development suggests that ataxin-3 may have an important biological function. Given this conservation, the study of mouse *Mjd* may provide fundamental insights into the function of human ataxin-3.

Materials and methods

Computational methods

We applied the BLAST program [41] to search for the homologue cDNA sequence in mouse under Accession No. AK008675. All protein sequences were taken from the TrEMBL database. The accession numbers of human variants ataxin-3-v1, ataxin-3-v2/v3 as denoted in [28], and ataxin-3-v4 corresponding to H2 in [7]; rat ataxin-3;and mouse ataxin-3 are Q96TC4, Q96TC3, Q96TC3, BAB18798, O35815, and Q9CVD2, respectively. Multiple sequence alignment was constructed by means of CLUSTAL W [42]. Comparison of *MJD* sequence to the homologous 5′ upstream region in mouse *Mjd* was performed to uncover evolutionarily conserved regions using TRES/TRANSFAC with a score of 95% [43]. Conserved regions in *Mjd* were then scanned for the presence of potential transcription factor binding regions using TESS [44].

Cloning of the full-length Mjd and MyoD cDNAs by RT-PCR

Total RNA was isolated from adult C57Bl/6 mouse brain and skeletal muscle, using Trizol reagent (Gibco BRL). Five micrograms of total RNA was used to perform reverse transcription using the SuperScript First-Strand Synthesis System for RT-PCR (Gibco BRL) with an oligo(dT) primer. To amplify the *Mjd* cDNA, PCR was carried out using the Expand High Fidelity System (Roche) with primers mmMJD1 and mmMJD2 (see below) using mouse brain total RNA as template. To amplify the *MyoD* cDNA, PCR was carried out using the same system with primers MyoD1 and MyoD2 (see below) using mouse skeletal muscle total RNA as template. The PCR conditions consisted of 1 cycle of 2 min at 94°C, followed by 32 cycles of 1 min at 94°C, 1 min at 62°C, and 1 min at 72°C, and ending with 5 min at 72°C. The PCR products corresponding to *Mjd* and to *MyoD* cDNAs were purified using GFX PCR DNA and the Gel Band Purification Kit (Amersham Pharmacia Biotech) and cloned into the pGEM-T Easy vector (Promega) (pMjd1) and into the pDONR207 vector, respectively, using the Gateway system (Invitrogen Life Technologies) (pDON207MyoD).

PCR

The primers used for RT-PCR were mmMJD1 (5′-GAGGGGCTGCTCCGCGCCGGGGCCGT), mmMJD2 (5′-TCTGCTTTCAAGTTGTCTTTAGCAG), MyoD1 (5′-GGGGACAAGTTTGTACAAAAAAGCAGGCTATATGGAGCTTCTATCGCCGCCACTCCG), and MyoD2 (5′-GGGGACCACTTTGTCCAAGAAAGCTGGGTCTCAAAGCACCTGATAAATCGCATTG). The probe used for screening the BAC library was amplified by PCR, using the *Mjd* cDNA (pMjd1) as template, with primers mmMJD1 and mmMJD3 (5′-GTAAACCAGTGTTCTTTATAATTGCA), and performed with the same cyclic parameters used for RT-PCR. PCRs for the construction of CAT reporter plasmids were all performed using the Expand High Fidelity System (Roche) and performed under the following conditions: 1 cycle of 5 min at 95°C, followed by 35 cycles of 1 min at 95°C, 1 min at 55°C, 1 min at 72°C, and ending with 5 min at 72°C. For the insertion of the restriction enzyme sites we used the reverse primer PMjd-1BglIIR (5′-GCACAGATCTGTTTATTTGTCTGGAG) in conjunction with one of the forward primers: PMjd-237KpnIF (5′-CGAGGGTACCACAGCAGGCGGCGCC), PMjd-358KpnIF (5′-GCACGGTACCAGAAGGTGGAGATGG), PMjd-559KpnIF (5′-GGCTGGTACCGTATAATATTA-

CAAAAG), PMjd-928KpnIF (5′-CGAGGGTACCCA-GGGTCCTCCTATGTAAC), or PMjd-1173KpnIF (5′-GGCTGGTACCCCAGTCCCTCATCAAAGT).

Isolation of a genomic BAC clone

The genomic BAC clone was obtained from Incyte Genomics, Inc. A BAC Mouse II library was screened by direct hybridization, using a probe of 400 bp, constructed by PCR, using primers mmMJD1 and mmMJD3. These primers were designed on the basis of the cloned *Mjd* cDNA sequence. The positive BAC clone was grown overnight, at 37°C, in 2XYT medium containing the appropriate antibiotic (25 μg/ml chloramphenicol). BAC DNA was isolated using the Qiagen Large-Construct Kit (Qiagen).

Cell culture and differentiation

The P19 clone was obtained from the American Type Collection. Cells were cultured (plating 10^6 cells in 75-cm^3 tissue culture flasks, every 2 days) in Dulbecco's modified Eagle's medium (DMEM), supplemented with 10% fetal bovine serum (FBS), in a 5% CO_2 humidified chamber at 37°C. To promote cellular differentiation, cells were cultured as aggregates, in bacterial petri dishes, in medium supplemented with 1 μM RA (Sigma) for neuronal differentiation or with 1% DMSO for cardiac/skeletal myocyte differentiation. Cells (1×10^5/ml culture) were plated into bacterial petri dishes (day 0) and incubated with medium (no treatment) or with RA- or DMSO-supplemented medium, for 2 days. After 2 days, floating aggregates were collected and washed with medium and replated into bacterial petri dishes for 1 additional day. At day 3, the aggregates were harvested; dissociated by treatment with 0.25% trypsin, 1 mM EDTA (Gibco BRL); and then plated in DMEM, 10% FBS in 60-mm diameter tissue-culture-grade dishes. At day 4, cells were transfected with constructs p-237MjdCAT and p-1173MjdCAT. Cell viability was assessed by trypan blue exclusion.

Construction of CAT reporter and MyoD-His tag expression plasmids

To obtain different lengths of the 5′ flanking region of *Mjd*, PCRs were performed using the BAC clone 27521 as the template. We used the primer PMjd-1BglIIR to insert the 3′ restriction enzyme site for *Bgl*II (at the position −1 bp) into all fragments, in conjunction with one of the primers PMjd-237KpnIF, PMjd-358KpnIF, PMjd-559KpnIF, PMjd-928KpnIF, or PMjd-1173KpnIF to insert the 5′ restriction enzyme site for *Kpn*I, at the respective lengths of the 5′ region −237, −358, −559, −928, or −1173 bp. These PCR products were digested with *Bgl*II and *Kpn*I and subcloned into *Bgl*II—*Kpn*I-digested pCAT3-Basic vector (Promega). The resultant constructs were p-237MjdCAT, p-358MjdCAT, p-559MjdCAT, p-928MjdCAT, and p-1173MjdCAT. The recombinant mouse MyoD-His tag protein expression plasmid (pDEST17MyoD) was obtained by recombination of the pDONR207MyoD with the pDEST17 vector using the Gateway system (Invitrogen Life Technologies). All constructs were confirmed by automatic sequencing.

Expression and purification of recombinant MyoD-His tag protein

The pDEST17MyoD construct was transformed in *Escherichia coli* BL21SI bacteria. Culture was grown to OD_{600} of 0.5 L of LBON medium plus ampicillin (100 μg/ml). The expression was induced by the addition of NaCl to a final concentration of 0.3 M and culture was grown for 30 min. Cells were harvested, resuspended in 15 ml of phosphate buffer 1×, imidazole 10 mM, lysozyme 66 μg/ml, Triton X-100 0.1%, Complete EDTA-free protease inhibitor cocktail tablet (Roche) and incubated on ice for 1 h. The lysate was sonicated on ice eight times for 30 s each time and then centrifuged for 15 min at 12,000 rpm at 4°C. The supernatant was collected and the recombinant protein was purified using the HisTrap Kit (Amersham Pharmacia Biotech) using the manufacturer's conditions.

Electrophoretic mobility-shift assay

The −928 bp fragment of the *Mjd* gene promoter, generated by *Kpn*I/*Bgl*II restriction of the p-928MjdCAT, was used for EMSA. For the competition assay, single-stranded sense and antisense MyoD oligonucleotides were synthesized based on both the sequence in the 5′ region of the *Mjd* gene and the binding matrix for MyoD with Accession No. M00184 (TRANSFAC database). The oligonucleotides MyoD-sense (5′-AGCAGCTGTC) and MyoD-antisense (5′-GACAGCTGCT) were annealed by incubation at 30°C for 1 min and by slow cooling to room temperature. DNA–protein binding assays were performed at room temperature for 30 min, always using the same amount of DNA (300 ng of the −928 bp fragment) and different quantities of recombinant mouse MyoD protein in a final volume of 40 μl of TE. In the competition assay, the double-stranded oligonucleotides (2 or 4 μg) were incubated with the recombinant protein for 30 min before the incubation with the DNA. The mixtures were loaded in a 1.5% agarose gel and electrophoresed at room temperature.

Cell transfection and CAT assay

To analyze activities of the CAT reporter plasmids in undifferentiated, untreated (day 3), RA-treated (day 3), and DMSO-treated (day 3) P19 cells, these were seeded at 2×10^5, 7.5×10^5, 7.5×10^5, and 3×10^6 cells, respectively, per 60-mm-diameter tissue-culture-grade dishes in DMEM, 10% FBS 24 h prior to transfection. Transient transfection was carried out in serum-free medium (Opti-MEM; Life Technologies), using 10 μl of Lipofectamine2000 Reagent

(Life Technologies), to introduce 1.5 μg of reporter construct and 0.5 μg of pSV-β-galactosidase control vector (Promega). After transfection for 5 h, medium was replaced with DMEM, 10% FBS. Cells were harvested 48 h after transfection and washed three times with phosphate-buffered saline (PBS), and then cell extracts were prepared in 1× reporter lysis buffer (Roche). Cell extracts were assayed for CAT activity, using the CAT ELISA kit (Roche). Measurements were performed in duplicate, averaged, and then normalized to the β-galactosidase activity, to correct for transfection efficiency, and to the total protein amount. β-Galactosidase activity was measured using the β-Galactosidase Enzyme Activity System (Promega), and the total protein amount was assessed using the Lowry Protein assay kit (Sigma).

Immunoblotting

Proteins were extracted from different tissues of adult C57Bl/6 mice, using standard methods [45]. Total protein quantification was assessed using the Lowry Protein assay kit (Sigma). Proteins of spinal cord, brain stem, cerebellum, cerebral cortex, heart, skeletal muscle, testis, kidney, lung, spleen, pancreas, liver, and stomach tissues (30 μg) were resolved on a 10% SDS–polyacrylamide gel and transferred onto nitrocellulose membrane (Amersham Biotechnologies). The anti-human ataxin-3-specific antiserum (kindly provided by Henry Paulson) was used (1:2000). For detection of the immunocomplexes formed, the secondary antibody peroxidase-conjugated goat anti-rabbit IgG (Stressgen) (1:4000) or goat anti-mouse IgG (Jackson Immunoresearch Laboratories) (1:1000) was used. Staining intensity was developed with the chemiluminescence system (Roche).

Immunohistochemistry

Adult male C57Bl/6 mice were perfused transcardially, under anesthesia, with fixative solution (4% paraformaldehyde, in 0.1 M phosphate buffer, pH 7.4), for 10 min. The encephalon and peripheral tissues (skeletal muscle, cardiac muscle, pancreas, spleen, liver, and testis) were postfixed for 2 h in the same fixative. Mouse embryos were isolated from pregnant C57Bl/6 female mice, at E11.5, E12.5, E13.5, E14.5, E15.5, and E16.5. The day of plug detection was considered to be E0.5 (embryonic day 0.5). Embryos were washed with ice-cold PBS and fixed in 10% buffered formalin, for at least 24 h, at 4°C. After fixation, the samples (adult tissues and organs and embryos) were paraffin embedded. Nominal 5-mm tissue sections were cut and mounted onto positively charged slides (X-Tra Slides), deparaffinized on xylene, and rehydrated by passages through graded ethanol series. In formalin-fixed material, heating was performed to allow antigen recovery. Nonspecific binding was blocked with normal goat serum (Vectastain Elite ABC kit; Vector Laboratories). Sections were incubated overnight in primary anti-ataxin-3 antiserum diluted (1:2000) in PBS. Antibody labeling was visualized using the secondary anti-rabbit antibody by the avidin–biotin conjugation method (Vectastain Elite ABC kit; Vector Laboratories) and 3,3-diaminobenzidine (Vector Laboratories). Sections were counterstained with hematoxylin. Dehydration of sections was assessed through graded ethanols and xylene. Slides were mounted with Histomount. Positive controls were processed in parallel. Sections were analyzed using an Olympus BX-50 microscope, equipped with a Camedia C-2000Z Olympus digital camera. High-quality (1600 × 1200 pixel) images were captured to a PC equipped with the Olympus DP-Soft 3.0 software. Brain sections were referenced to [46].

Acknowledgments

We thank Mark Tessaro, Laura Montermini, Margarida Duarte, João Sousa, and Teresa Summavielle for their cooperation in this study and Sandra Macedo Ribeiro for critical review of the manuscript. We also thank Henry Paulson for providing of the anti-human ataxin-3 antiserum. This work was supported by the FSE/FEDER and the Fundacão para a Ciência e Tecnologia (FCT) (Project POCTI/MGI 33759/99) and the Fundacão Luso-Americana para o Desenvolvimento (Proc. 3.L./A.II/P.582/99) and by a grant from the Canadian Institutes of Health Research (CIHR, Grant MOP44045) to M.M.S. M.M.S. is the recipient of a CIHR New Investigator award. M.C.C. is the recipient of a Ph.D. scholarship from FCT, (BD/9759/2003). Printing of color figures was supported by Bioportugal, Bonsai Technologies, and Vidrolab.

References

[1] R.L. Margolis, The spinocerebellar ataxias: order emerges from chaos, Curr. Neurol. Neurosci. Rep. 2 (2002) 447–456.
[2] P. Coutinho, C. Andrade, Autosomal dominant system degeneration in Portuguese families of the Azores Islands: a new genetic disorder involving cerebellar, pyramidal, extrapyramidal and spinal cord motor functions, Neurology 28 (1978) 703–709.
[3] R.N. Rosenberg, Machado–Joseph disease: an autosomal dominant motor system degeneration, Mov. Disord. 3 (1992) 193–203.
[4] A. Dürr, et al., Spinocerebellar ataxia 3 and Machado–Joseph disease: clinical, molecular, and neuropathological features, Ann. Neurol. 39 (1996) 490–499.
[5] Y. Takiyama, et al., The gene for the Machado–Joseph disease is mapped to human chromosome 14q, Nat. Genet. 4 (1993) 300–304.
[6] Y. Kawaguchi, et al., CAG expansions in a novel gene for Machado–Joseph disease at chromosome 14q32.1, Nat. Genet. 8 (1994) 221–228.
[7] Y. Ichikawa, et al., The genomic structure and expression of MJD, the Machado–Joseph disease gene, J. Hum. Genet. 46 (2001) 413–422.
[8] J. Goto, et al., Machado–Joseph disease gene products carrying different carboxyl termini, Neurosci. Res. 28 (1997) 373–377.
[9] H.L. Paulson, et al., Machado–Joseph disease gene product is a cytoplasmic protein widely expressed in brain, Ann. Neurol. 41 (1997) 453–462.

[10] Y. Trottier, et al., Heterogeneous intracellular localization and expression of ataxin-3, Neurobiol. Dis. 5 (1998) 335–347.
[11] A.I. Su, et al., Large-scale analysis of the human and mouse transcriptomes, Proc. Natl. Acad. Sci. USA 99 (2002) 4465–4470.
[12] C.J. Cummings, H.Y. Zoghbi, Fourteen and counting: unraveling trinucleotide repeat diseases, Hum. Mol. Genet. 9 (2000) 909–916.
[13] P. Maciel, et al., Improvement in the molecular diagnosis of Machado–Joseph disease, Arch. Neurol. 58 (2001) 1821–1827.
[14] T. Schmidt, et al., An isoform of ataxin-3 accumulates in the nucleus of neuronal cells in affected brain regions of SCA3 patients, Brain Pathol. 8 (1998) 669–679.
[15] B.O. Evert, et al., High level expression of expanded full-length ataxin-3 in vitro causes cell death and formation of intranuclear inclusions in neuronal cells, Hum. Mol. Genet. 8 (1999) 1169–1176.
[16] H. Ikeda, et al., Expanded polyglutamine in the Machado–Joseph disease protein induces cell death in vitro and in vivo, Nat. Genet. 13 (1996) 196–202.
[17] C.K. Cemal, et al., YAC transgenic mice carrying pathological alleles of the MJD1 locus exhibit a mild and slowly progressive cerebellar deficit, Hum. Mol. Genet. 11 (2002) 1075–1094.
[18] C.A. Ross, Polyglutamine pathogenesis: emergence of unifying mechanisms for Huntington's disease and related disorders, Neuron 35 (2002) 819–822.
[19] H.Y. Chan, J.M. Warrick, G.L. Gray-Board, H.L. Paulson, N.M. Bonini, Mechanisms of chaperone suppression of polyglutamine disease: selectivity, synergy and modulation of protein solubility in Drosophila, Hum. Mol. Genet. 9 (2000) 2811–2820.
[20] H.L. Paulson, N.M. Bonini, K.A. Roth, Polyglutamine disease and neuronal cell death, Proc. Natl. Acad. Sci. USA 97 (2000) 12957–12958.
[21] Y. Chai, S.L. Koppenhafer, S.J. Shoesmith, M.K. Perez, H.L. Paulson, Evidence for proteasome involvement in polyglutamine disease: localization to nuclear inclusions in SCA3/MJD and suppression of polyglutamine aggregation in vitro, Hum. Mol. Genet. 8 (1999) 673–682.
[22] T. Schmidt, et al., Protein surveillance machinery in brains with spinocerebellar ataxia type 3: redistribution and differential recruitment of 26S proteasome subunits and chaperones to neuronal intranuclear inclusions, Ann. Neurol. 51 (2002) 302–310.
[23] J.P. Taylor, J. Hardy, K.H. Fischbeck, Toxic proteins in neurodegenerative disease, Science 296 (2002) 1991–1995.
[24] A.E. Bevivino, P.J. Loll, An expanded glutamine repeat destabilizes native ataxin-3 structure and mediates formation of parallel β-fibrils, Proc. Natl. Acad. Sci. USA 98 (2001) 11955–11960.
[25] S. Chen, V. Berthelier, J.B. Hamilton, B. O'Nuallain, R. Wetzel, Amyloid-like features of polyglutamine aggregates and their assembly kinetics, Biochemistry 41 (2002) 7391–7399.
[26] G. Wang, N. Sawai, S. Kotliarova, I. Kanazawa, N. Nukina, Ataxin-3, the MJD1 product, interacts with two human homologs of yeast DNA repair protein RAD23, HHR23A and HHR23B, Hum. Mol. Genet. 9 (2000) 1795–1803.
[27] F. Li, T. Macfarlan, R.N. Pittman, D. Chakravarti, Ataxin-3 is a histone-binding protein with two independent transcriptional corepressor activities, J. Biol. Chem. 277 (2002) 45004–45012.
[28] M. Albrecht, et al., Structural modeling of ataxin-3 reveals distant homology to adaptins, Proteins 50 (2003) 355–370.
[29] I. Schmitt, T. Brattig, M. Gossen, O. Riess, Characterization of the rat spinocerebellar ataxia type 3 gene, Neurogenetics 1 (1997) 103–112.
[30] I. Linhartova, et al., Conserved domains and lack of evidence for polyglutamine length polymorphism in the chicken homolog of the Machado–Joseph disease gene product ataxin-3, Biochim. Biophys. Acta 1444 (1999) 299–305.
[31] M.W. McBurney, E.M. Jones-Villeneuve, M.K. Edwards, P.J. Anderson, Control of muscle and neuronal differentiation in a cultured embryonal carcinoma cell line, Nature 299 (1982) 165–167.
[32] E.M. Jones-Villeneuve, M.W. McBurney, K.A. Rogers, V.I. Kalnis, Retinoic acid induces embryonal carcinoma cells to differentiate into neurons and glial cells, J. Cell Biol. 94 (1982) 253–262.
[33] S. Banfi, et al., Cloning and developmental expression analysis of the murine homolog of the spinocerebellar ataxia type 1 gene (Sca1), Hum. Mol. Genet. 5 (1996) 33–40.
[34] T. Nechiporuk, et al., The mouse SCA2 gene: cDNA sequence, alternative splicing and protein expression, Hum. Mol. Genet. 7 (1998) 1301–1309.
[35] A.L. Strom, et al., Cloning and expression analysis of the murine homolog of the spinocerebellar ataxia type 7 (SCA7) gene, Gene 285 (2002) 91–99.
[36] B. Lin, et al., Sequence of the murine Huntington disease gene: evidence for conservation, alternative splicing and polymorphism in a triplet (CCG) repeat, Hum. Mol. Genet. 3 (1994) 85–92.
[37] G.T. Barnes, et al., Mouse Huntington's disease gene homolog (Hdh), Somatic Cell Mol. Genet. 20 (1994) 87–97.
[38] I.S. Skerjank, Cardiac and skeletal muscle development in P19 embryonal carcinoma cells, Trends Cardiovasc. Med. 9 (1999) 139–143.
[39] S.A. Sarkar, R.P. Sharma, Modulation of c-myc, max, and mad gene expression during neural differentiation of embryonic stem cells by all-trans-retinoic acid, Gene Exp. 10 (2002) 125–135.
[40] B.Y. Williams, S. Brommer, B.M. Czarnetzki, T. Rosenbach, The differentiation-related upregulation of aryl hydrocarbon receptor transcript levels is suppressed by retinoic acid, Biochem. Biophys. Res. Commun. 209 (1995) 706–711.
[41] S.F. Altschul, W. Gish, W. Miller, E.W. Myers, D.J. Lipman, Basic local alignment search tool, J. Mol. Biol. 215 (1990) 403–410.
[42] J.D. Thompson, D.G. Higgins, T.J. Gibson, CLUSTAL W: improving the sensitivity of progressive multiple sequence alignment through sequence weighting, position-specific gap penalties and weight matrix choice, Nucleic Acids Res. 22 (1994) 4673–4680.
[43] E. Wingender, et al., TRANSFAC: an integrated system for gene expression regulation, Nucleic Acids Res. 28 (2000) 316–319.
[44] J. Schug, G.C. Overton, TESS: Transcription Element Search Software on the WWW′, Technical Rep. CBIL-TR-1997-1001-v0.0, Computational Biology and Informatics Laboratory, School of Medicine, Univ. of Pennsylvania, Philadelphia, 1997.
[45] J. Sambrook, E.F. Fritsch, T. Maniatis, Molecular Cloning: A Laboratory Manual, Cold Spring Harbor Laboratory Press, Cold Spring Harbor, NY, 1989.
[46] G. Paxinos, K.B.J. Franklin, The Mouse Brain in Stereotaxic Coordinates, Academic Press, San Diego, 1997.

References

Accili D, Arden KC (2004) FoxOs at the crossroads of cellular metabolism, differentiation, and transformation. Cell 117:421-426

Adams JC, Seed B, Lawler J (1998) Muskelin, a novel intracellular mediator of cell adhesive and cytoskeletal responses to thrombospondin-1. Embo J 17:4964-4974

Albrecht M, Hoffmann D, Evert BO, Schmidt I, Wüllner U, Lengauer T (2003) Structural modeling of ataxin-3 reveals distant homology to adaptins. Proteins 50:355-370

Altschul SF, Gish W, Miller W, Myers EW, Lipman DJ (1990) Basic local alignment search tool. J Mol Biol 215:403-410

Amerik AY, Hochstrasser M (2004) Mechanism and function of deubiquitinating enzymes. Biochim Biophys Acta 1695:189-207

Amerik AY, Li SJ, Hochstrasser M (2000) Analysis of the deubiquitinating enzymes of the yeast Saccharomyces cerevisiae. Biol Chem 381:981-992

Antebi A (2007) Genetics of aging in Caenorhabditis elegans. PLoS Genet 3:1565-1571

Araujo JP, Klockgether T, Wüllner U, Evert BO (2007) Profiling of ataxin-3 interacting transcription factors. 2007 Neuroscience Meeting Planner San Diego, CA: Society for Neuroscience, 2007 Program No 487.7:X17

Attaix D, Ventadour S, Codran A, Bechet D, Taillandier D, Combaret L (2005) The ubiquitin-proteasome system and skeletal muscle wasting. Essays Biochem 41:173-186

Bai C, Sen P, Hofmann K, Ma L, Goebl M, Harper JW, Elledge SJ (1996) SKP1 connects cell cycle regulators to the ubiquitin proteolysis machinery through a novel motif, the F-box. Cell 86:263-274

Bajanca F, Luz M, Duxson MJ, Thorsteinsdottir S (2004) Integrins in the mouse myotome: developmental changes and differences between the epaxial and hypaxial lineage. Dev Dyn 231:402-415

Banfi S, Servadio A, Chung M, Capozzoli F, Duvick LA, Elde R, Zoghbi HY, Orr HT (1996) Cloning and developmental expression analysis of the murine homolog of the spinocerebellar ataxia type 1 gene (Sca1). Hum Mol Genet 5:33-40

Bao ZZ, Lakonishok M, Kaufman S, Horwitz AF (1993) Alpha 7 beta 1 integrin is a component of the myotendinous junction on skeletal muscle. J Cell Sci 106 (Pt 2):579-589

Barnes GT, Duyao MP, Ambrose CM, McNeil S, Persichetti F, Srinidhi J, Gusella JF, MacDonald ME (1994) Mouse Huntington's disease gene homolog (Hdh). Somat Cell Mol Genet 20:87-97

Barthel A, Schmoll D, Unterman TG (2005) FoxO proteins in insulin action and metabolism. Trends Endocrinol Metab 16:183-189

Bartoli M, Richard I (2005) Calpains in muscle wasting. Int J Biochem Cell Biol 37:2115-2133

Bastie CC, Nahle Z, McLoughlin T, Esser K, Zhang W, Unterman T, Abumrad NA (2005) FoxO1 stimulates fatty acid uptake and oxidation in muscle cells through CD36-dependent and -independent mechanisms. J Biol Chem 280:14222-14229

Bendixen C, Gangloff S, Rothstein R (1994) A yeast mating-selection scheme for detection of protein-protein interactions. Nucleic Acids Res 22:1778-1779

Berg JS, Powell BC, Cheney RE (2001) A millennial myosin census. Mol Biol Cell 12:780-794

Berke SJ, Paulson HL (2003) Protein aggregation and the ubiquitin proteasome pathway: gaining the UPPer hand on neurodegeneration. Curr Opin Genet Dev 13:253-261

Berke SJS, Chai Y, Marrs GL, Wen H, Paulson HL (2005) Defining the role of ubiquitin interacting motifs in the polyglutamine disease protein, ataxin-3. J Biol Chem 280:32026-32034

Berke SJS, Schmied FAF, Brunt ER, Ellerby LM, Paulson HL (2004) Caspase-mediated proteolysis of the polyglutamine disease protein ataxin-3. J Neurochem 89:908-918

Berkes CA, Tapscott SJ (2005) MyoD and the transcriptional control of myogenesis. Semin Cell Dev Biol 16:585-595

Berrier AL, Yamada KM (2007) Cell-matrix adhesion. J Cell Physiol 213:565-573

Biggs WH, 3rd, Cavenee WK, Arden KC (2001) Identification and characterization of members of the FKHR (FOX O) subclass of winged-helix transcription factors in the mouse. Mamm Genome 12:416-425

Biggs WH, 3rd, Meisenhelder J, Hunter T, Cavenee WK, Arden KC (1999) Protein kinase B/Akt-mediated phosphorylation promotes nuclear exclusion of the winged helix transcription factor FKHR1. Proc Natl Acad Sci U S A 96:7421-7426

Blaineau C, Tessier M, Dubessay P, Tasse L, Crobu L, Pages M, Bastien P (2007) A novel microtubule-depolymerizing kinesin involved in length control of a eukaryotic flagellum. Curr Biol 17:778-782

Boeddrich A, Gaumer S, Haacke A, Tzvetkov N, Albrecht M, Evert BO, Muller EC, Lurz R, Breuer P, Schugardt N, Plassmann S, Xu K, Warrick JM, Suopanki J, Wullner U, Frank R, Hartl UF, Bonini NM, Wanker EE (2006) An arginine/lysine-rich motif is crucial for VCP/p97-mediated modulation of ataxin-3 fibrillogenesis. Embo J 25:1547-1558

Bosch-Comas A, Lindsten K, Gonzalez-Duarte R, Masucci MG, Marfany G (2006) The ubiquitin-specific protease USP25 interacts with three sarcomeric proteins. Cell Mol Life Sci 63:723-734

Bose R, Molina H, Patterson AS, Bitok JK, Periaswamy B, Bader JS, Pandey A, Cole PA (2006) Phosphoproteomic analysis of Her2/neu signaling and inhibition. Proc Natl Acad Sci U S A 103:9773-9778

Bounpheng MA, Dimas JJ, Dodds SG, Christy BA (1999) Degradation of Id proteins by the ubiquitin-proteasome pathway. Faseb J 13:2257-2264

Boutet SC, Disatnik MH, Chan LS, Iori K, Rando TA (2007) Regulation of Pax3 by proteasomal degradation of monoubiquitinated protein in skeletal muscle progenitors. Cell 130:349-362

Braak H, de Vos RA, Bohl J, Del Tredici K (2006) Gastric alpha-synuclein immunoreactive inclusions in Meissner's and Auerbach's plexuses in cases staged for Parkinson's disease-related brain pathology. Neurosci Lett 396:67-72

Braun T, Rudnicki MA, Arnold HH, Jaenisch R (1992) Targeted inactivation of the muscle regulatory gene Myf-5 results in abnormal rib development and perinatal death. Cell 71:369-382

Breeden L, Nasmyth K (1985) Regulation of the yeast HO gene. Cold Spring Harb Symp Quant Biol 50:643-650

Brent R, Finley RL, Jr. (1997) Understanding gene and allele function with two-hybrid methods. Annu Rev Genet 31:663-704

Brummelkamp TR, Nijman SM, Dirac AM, Bernards R (2003) Loss of the cylindromatosis tumour suppressor inhibits apoptosis by activating NF-kappaB. Nature 424:797-801

Bruneel A, Labas V, Mailloux A, Sharma S, Royer N, Vinh J, Pernet P, Vaubourdolle M, Baudin B (2005) Proteomics of human umbilical vein endothelial cells applied to etoposide-induced apoptosis. Proteomics 5:3876-3884

Brunet A, Bonni A, Zigmond MJ, Lin MZ, Juo P, Hu LS, Anderson MJ, Arden KC, Blenis J, Greenberg ME (1999) Akt promotes cell survival by phosphorylating and inhibiting a Forkhead transcription factor. Cell 96:857-868

Brunet A, Park J, Tran H, Hu LS, Hemmings BA, Greenberg ME (2001) Protein kinase SGK mediates survival signals by phosphorylating the forkhead transcription factor FKHRL1 (FOXO3a). Mol Cell Biol 21:952-965

Brunet A, Sweeney LB, Sturgill JF, Chua KF, Greer PL, Lin Y, Tran H, Ross SE, Mostoslavsky R, Cohen HY, Hu LS, Cheng HL, Jedrychowski MP, Gygi SP, Sinclair DA, Alt FW, Greenberg ME (2004) Stress-dependent regulation of FOXO transcription factors by the SIRT1 deacetylase. Science 303:2011-2015

Brunner D, Nurse P (2000) CLIP170-like tip1p spatially organizes microtubular dynamics in fission yeast. Cell 102:695-704

Buckingham M, Bajard L, Chang T, Daubas P, Hadchouel J, Meilhac S, Montarras D, Rocancourt D, Relaix F (2003) The formation of skeletal muscle: from somite to limb. J Anat 202:59-68

Burnett BG, Li F, Pittman RN (2003) The polyglutamine neurodegenerative protein ataxin-3 binds polyubiquitylated proteins and has ubiquitin protease activity. Hum Mol Genet 12:3195-3205

Burnett BG, Pittman RN (2005) The polyglutamine neurodegenerative protein ataxin 3 regulates aggresome formation. Proceedings of the National Academy of Science USA 102:4330-4335

Burns KE, Baumgart S, Dorrestein PC, Zhai H, McLafferty FW, Begley TP (2005) Reconstitution of a new cysteine biosynthetic pathway in Mycobacterium tuberculosis. J Am Chem Soc 127:11602-11603

Cachaco AS, Pereira CS, Pardal RG, Bajanca F, Thorsteinsdottir S (2005) Integrin repertoire on myogenic cells changes during the course of primary myogenesis in the mouse. Dev Dyn 232:1069-1078

Cans C, Passer BJ, Shalak V, Nancy-Portebois V, Crible V, Amzallag N, Allanic D, Tufino R, Argentini M, Moras D, Fiucci G, Goud B, Mirande M, Amson R, Telerman A (2003) Translationally controlled tumor protein acts as a guanine nucleotide dissociation inhibitor on the translation elongation factor eEF1A. Proc Natl Acad Sci U S A 100:13892-13897

Cassimeris L, Spittle C (2001) Regulation of microtubule-associated proteins. Int Rev Cytol 210:163-226

Centner T, Yano J, Kimura E, McElhinny AS, Pelin K, Witt CC, Bang ML, Trombitas K, Granzier H, Gregorio CC, Sorimachi H, Labeit S (2001) Identification of muscle specific ring finger proteins as potential regulators of the titin kinase domain. J Mol Biol 306:717-726

Chai Y, Berke SS, Cohen RE, Paulson HL (2004) Poly-ubiquitin binding by the polyglutamine disease protein ataxin-3 links its normal function to protein surveillance pathways. J Biol Chem 279:3605-3611

Chai Y, Koppenhafer SL, Bonini NM, Paulson HL (1999a) Analysis of the role of heat shock protein (Hsp) molecular chaperones in polyglutamine disease. J Neurosci 19:10338-10347

Chai Y, Koppenhafer SL, Shoesmith SJ, Perez MK, Paulson HL (1999b) Evidence for proteasome involvement in polyglutamine disease: localization to nuclear inclusions in SCA3/MJD and suppression of polyglutamine aggregation in vitro. Hum Mol Genet 8:673-682

Chai Y, Wu L, Griffin JD, Paulson HL (2001) The role of protein composition in specifying nuclear inclusion formation in polyglutamine disease. J Biol Chem 276:44889-44897

Chandra S, Gallardo G, Fernandez-Chacon R, Schluter OM, Sudhof TC (2005) Alpha-synuclein cooperates with CSPalpha in preventing neurodegeneration. Cell 123:383-396

Chang BD, Watanabe K, Broude EV, Fang J, Poole JC, Kalinichenko TV, Roninson IB (2000) Effects of p21Waf1/Cip1/Sdi1 on cellular gene expression: implications for carcinogenesis, senescence, and age-related diseases. Proc Natl Acad Sci U S A 97:4291-4296

Chien CT, Bartel PL, Sternglanz R, Fields S (1991) The two-hybrid system: a method to identify and clone genes for proteins that interact with a protein of interest. Proc Natl Acad Sci U S A 88:9578-9582

Choi J, Park SY, Costantini F, Jho EH, Joo CK (2004) Adenomatous polyposis coli is down-regulated by the ubiquitin-proteasome pathway in a process facilitated by Axin. J Biol Chem 279:49188-49198

Chow MKM, Mackay JP, Whisstock JC, Scanlon MJ, Bottomley SP (2004) Structural and functional analysis of the josephin domain of the polyglutamine protein ataxin-3. Biochem Biophys Res Com 322:387-394

Colbert T, Hahn S (1992) A yeast TFIIB-related factor involved in RNA polymerase III transcription. Genes Dev 6:1940-1949

Coleman PD, Yao PJ (2003) Synaptic slaughter in Alzheimer's disease. Neurobiol Aging 24:1023-1027

Colland F, Jacq X, Trouplin V, Mougin C, Groizeleau C, Hamburger A, Meil A, Wojcik J, Legrain P, Gauthier JM (2004) Functional proteomics mapping of a human signaling pathway. Genome Res 14:1324-1332

Collo G, Starr L, Quaranta V (1993) A new isoform of the laminin receptor integrin alpha 7 beta 1 is developmentally regulated in skeletal muscle. J Biol Chem 268:19019-19024

Combaret L, Adegoke OA, Bedard N, Baracos V, Attaix D, Wing SS (2005) USP19 is a ubiquitin-specific protease regulated in rat skeletal muscle during catabolic states. Am J Physiol Endocrinol Metab 288:E693-700

Conforti L, Adalbert R, Coleman MP (2007) Neuronal death: where does the end begin? Trends in Neurosciences 30(4):159-66

Costa MC, Gomes-da-Silva J, Miranda CJ, Sequeiros J, Santos MM, Maciel P (2004) Genomic structure, promoter activity, and developmental expression of the mouse homologue of the Machado-Joseph disease (MJD) gene. Genomics 84:361-373

Costa MC, Sequeiros J, Maciel P (2002) Identification of three novel polymorphisms in the MJD1 gene and study of their frequency in the Portuguese population. J Hum Genet 47:205-207

Cote M, Payet MD, Gallo-Payet N (1997) Association of alpha S-subunit of the GS protein with microfilaments and microtubules: implication during adrenocorticotropin stimulation in rat adrenal glomerulosa cells. Endocrinology 138:69-78

Coutinho P (1992) Doença de Machado-Joseph: Tentativa de definição. Porto

Coutinho P, Andrade C (1978) Autosomal dominant system degeneration in Portuguese families of the Azores Islands: a new genetic disorder involving cerebellar, pyramidal, extrapyramidal and spinal cord motor functions. Neurology 28:703-709

Coutinho P, Sequeiros J (1981) [Clinical, genetic and pathological aspects of Machado-Joseph disease]. J Genet Hum 29:203-209

Crawford SE, Qi C, Misra P, Stellmach V, Rao MS, Engel JD, Zhu Y, Reddy JK (2002) Defects of the heart, eye, and megakaryocytes in peroxisome proliferator activator receptor-binding protein (PBP) null embryos implicate GATA family of transcription factors. J Biol Chem 277:3585-3592

Cregan SP, Dawson VL, Slack RS (2004) Role of AIF in caspase-dependent and caspase-independent cell death. Oncogene 23:2785-2796

Cukierman E, Pankov R, Stevens DR, Yamada KM (2001) Taking cell-matrix adhesions to the third dimension. Science 294:1708-1712

Cummings CJ, Zoghbi HY (2000) Fourteen and counting: unraveling trinucleotide repeat diseases. Hum Mol Genet 9:909-916

Cusick ME, Klitgord N, Vidal M, Hill DE (2005) Interactome: gateway into systems biology. Hum Mol Genet 14 Spec No. 2:R171-181

Dahlmann B (2007) Role of proteasomes in disease. BMC Biochem 8 Suppl 1:S3

Davies JE, Sarkar S, Rubinsztein DC (2007) The ubiquitin proteasome system in Huntington's disease and the spinocerebellar ataxias. BMC Biochem 8 Suppl 1:S2

Deane CM, Salwinski L, Xenarios I, Eisenberg D (2002) Protein interactions: two methods for assessment of the reliability of high throughput observations. Mol Cell Proteomics 1:349-356

Denti S, Sirri A, Cheli A, Rogge L, Innamorati G, Putignano S, Fabbri M, Pardi R, Bianchi E (2004) RanBPM is a phosphoprotein that associates with the plasma membrane and interacts with the integrin LFA-1. J Biol Chem 279:13027-13034

Deval C, Mordier S, Obled C, Bechet D, Combaret L, Attaix D, Ferrara M (2001) Identification of cathepsin L as a differentially expressed message associated with skeletal muscle wasting. Biochem J 360:143-150

Donaldson KM, Li W, Ching KA, Batalov S, Tsai CC, Joazeiro CA (2003a) Ubiquitin-mediated sequestration of normal cellular proteins into polyglutamine aggregates. Proc Natl Acad Sci U S A 100:8892-8897

Donaldson KM, Yin H, Gekakis N, Supek F, Joazeiro CA (2003b) Ubiquitin signals protein trafficking via interaction with a novel ubiquitin binding domain in the membrane fusion regulator, Vps9p. Curr Biol 13:258-262

Doss-Pepe EW, Stenroos ES, Johnson WG, Madura K (2003) Ataxin-3 interactions with Rad23 and valosin-containing protein and its associations with ubiquitin chains and the proteasome are consistent with a role in ubiquitin-mediated proteolysis. Mol Cellular Biol 23:6469-6483

Dragatsis I, Levine MS, Zeitlin S (2000) Inactivation of Hdh in the brain and testis results in progressive neurodegeneration and sterility in mice. Nat Genet 26:300-306

Du J, Wang X, Miereles C, Bailey JL, Debigare R, Zheng B, Price SR, Mitch WE (2004) Activation of caspase-3 is an initial step triggering accelerated muscle proteolysis in catabolic conditions. J Clin Invest 113:115-123

Duan L, Reddi AL, Ghosh A, Dimri M, Band H (2004) The Cbl family and other ubiquitin ligases: destructive forces in control of antigen receptor signaling. Immunity 21:7-17

Dubessay P, Blaineau C, Bastien P, Tasse L, Van Dijk J, Crobu L, Pages M (2006) Cell cycle-dependent expression regulation by the proteasome pathway and characterization of the nuclear targeting signal of a Leishmania major Kin-13 kinesin. Mol Microbiol 59:1162-1174

Dunah AW, Jeong H, Griffin A, Kim YM, Standaert DG, Hersch SM, Mouradian MM, Young AB, Tanese N, Krainc D (2002) Sp1 and TAFII130 transcriptional activity disrupted in early Huntington's disease. Science 296:2238-2243

Durfee T, Becherer K, Chen PL, Yeh SH, Yang Y, Kilburn AE, Lee WH, Elledge SJ (1993) The retinoblastoma protein associates with the protein phosphatase type 1 catalytic subunit. Genes Dev 7:555-569

Eisenmann KM, McCarthy JB, Simpson MA, Keely PJ, Guan JL, Tachibana K, Lim L, Manser E, Furcht LT, Iida J (1999) Melanoma chondroitin sulphate proteoglycan regulates cell spreading through Cdc42, Ack-1 and p130cas. Nat Cell Biol 1:507-513

Elsasser S, Finley D (2005) Delivery of ubiquitinated substrates to protein-unfolding machines. Nat Cell Biol 7:742-749

Emes RD, Ponting CP (2001) A new sequence motif linking lissencephaly, Treacher Collins and oral-facial-digital type 1 syndromes, microtubule dynamics and cell migration. Hum Mol Genet 10:2813-2820

Evert BO, Araujo J, Vieira-Saecker AM, de Vos RA, Harendza S, Klockgether T, Wullner U (2006) Ataxin-3 represses transcription via chromatin binding, interaction with histone deacetylase 3, and histone deacetylation. J Neurosci 26:11474-11486

Felton-Edkins ZA, Fairley JA, Graham EL, Johnston IM, White RJ, Scott PH (2003) The mitogen-activated protein (MAP) kinase ERK induces tRNA synthesis by phosphorylating TFIIIB. Embo J 22:2422-2432

Fernandez-Valle C, Tang Y, Ricard J, Rodenas-Ruano A, Taylor A, Hackler E, Biggerstaff J, Iacovelli J (2002) Paxillin binds schwannomin and regulates its density-dependent localization and effect on cell morphology. Nat Genet 31:354-362

Ferrante RJ, Kubilus JK, Lee J, Ryu H, Beesen A, Zucker B, Smith K, Kowall NW, Ratan RR, Luthi-Carter R, Hersch SM (2003) Histone deacetylase inhibition by sodium butyrate chemotherapy ameliorates the neurodegenerative phenotype in Huntington's disease mice. J Neurosci 23:9418-9427

Ferro A, Carvalho AL, Teixeira-Castro A, Almeida C, Tomé RL, Cortes L, Rodrigues A-J, Logarinho E, Sequeiros J, Macedo-Ribeiro S, Maciel P (2007) NEDD8: a new ataxin-3 interactor. Biochim Biophys Acta (BBA) - Mol Cell Res 1773:1619-1627

Fields S (2005) High-throughput two-hybrid analysis. The promise and the peril. Febs J 272:5391-5399

Fields S, Song O (1989) A novel genetic system to detect protein-protein interactions. Nature 340:245-246

Fujigasaki H, Uchihara T, Takahashi J, Matsushita H, Nakamura A, Koyano S, Iwabuchi K, Hirai S, Mizusawa H (2001) Preferential recruitment of ataxin-3 independent of expanded polyglutamine: an immunohistochemical study on Marinesco bodies. J Neurol Neurosurg Psych 71:518-520

Fukushi J, Makagiansar IT, Stallcup WB (2004) NG2 proteoglycan promotes endothelial cell motility and angiogenesis via engagement of galectin-3 and alpha3beta1 integrin. Mol Biol Cell 15:3580-3590

Furuyama T, Kitayama K, Yamashita H, Mori N (2003) Forkhead transcription factor FOXO1 (FKHR)-dependent induction of PDK4 gene expression in skeletal muscle during energy deprivation. Biochem J 375:365-371

Furuyama T, Nakazawa T, Nakano I, Mori N (2000) Identification of the differential distribution patterns of mRNAs and consensus binding sequences for mouse DAF-16 homologues. Biochem J 349:629-634

Furuyama T, Yamashita H, Kitayama K, Higami Y, Shimokawa I, Mori N (2002) Effects of aging and caloric restriction on the gene expression of Foxo1, 3, and 4 (FKHR, FKHRL1, and AFX) in the rat skeletal muscles. Microsc Res Tech 59:331-334

Gales L, Cortes L, Almeida C, Melo CV, Costa MC, Maciel P, Clarke DT, Damas AM, Macedo-Ribeiro S (2005) Towards a structural understanding of the fibrillization pathway in Machado-Joseph's disease: trapping early oligomers of non-expanded ataxin-3. J Mol Biol 353:642-654

Ganem NJ, Compton DA (2004) The KinI kinesin Kif2a is required for bipolar spindle assembly through a functional relationship with MCAK. J Cell Biol 166:473-478

Gaspar C, Lopes-Cendes I, Hayes S, Goto J, Arvidsson K, Dias A, Silveira I, et al. (2001) Ancestral origins of the Machado-Joseph disease mutation: a worldwide haplotype study. Am J Hum Genet 68:523-528

Gautel M, Mues A, Young P (1999) Control of sarcomeric assembly: the flow of information on titin. Rev Physiol Biochem Pharmacol 138:97-137

Geerts D, Fontao L, Nievers MG, Schaapveld RQ, Purkis PE, Wheeler GN, Lane EB, Leigh IM, Sonnenberg A (1999) Binding of integrin alpha6beta4 to plectin prevents plectin association with F-actin but does not interfere with intermediate filament binding. J Cell Biol 147:417-434

Gietz RD, Schiestl RH, Willems AR, Woods RA (1995) Studies on the transformation of intact yeast cells by the LiAc/SS-DNA/PEG procedure. Yeast 11:355-360

Giot L, Bader JS, Brouwer C, Chaudhuri A, Kuang B, Li Y, Hao YL, et al. (2003) A protein interaction map of Drosophila melanogaster. Science 302:1727-1736

Glickman MH, Ciechanover A (2002) The ubiquitin-proteasome proteolytic pathway: destruction for the sake of construction. Physiol Rev 82:373-428

Goehler H, Lalowski M, Stelzl U, Waelter S, Stroedicke M, Worm U, Droege A, Lindenberg KS, Knoblich M, Haenig C, Herbst M, Suopanki J, Scherzinger E, Abraham C, Bauer B, Hasenbank R, Fritzsche A, Ludewig AH, Bussow K, Coleman SH, Gutekunst CA, Landwehrmeyer BG, Lehrach H, Wanker EE (2004) A protein interaction network links GIT1, an enhancer of huntingtin aggregation, to Huntington's disease. Mol Cell 15:853-865

Goldberg AL (2003) Protein degradation and protection against misfolded or damaged proteins. Nature 426:895-899

Goldberg YP, Nicholson DW, Rasper DM, Kalchman MA, Koide HB, Graham RK, Bromm M, Kazemi-Esfarjani P, Thornberry NA, Vaillancourt JP, Hayden MR (1996) Cleavage of huntingtin by apopain, a proapoptotic cysteine protease, is modulated by the polyglutamine tract. Nat Genet 13:442-449

Gomez-Roman N, Grandori C, Eisenman RN, White RJ (2003) Direct activation of RNA polymerase III transcription by c-Myc. Nature 421:290-294

Gomis RR, Alarcon C, He W, Wang Q, Seoane J, Lash A, Massague J (2006) A FoxO-Smad synexpression group in human keratinocytes. Proc Natl Acad Sci U S A 103:12747-12752

Goodrich JS, Clouse KN, Schupbach T (2004) Hrb27C, Sqd and Otu cooperatively regulate gurken RNA localization and mediate nurse cell chromosome dispersion in Drosophila oogenesis. Development 131:1949-1958

Goti D, Katzen SM, Mez J, Kurtis J, Kiluk J, Ben-Haïem L, Jenkins NA, Copeland NG, Kakizuka A, Sharp AH, Ross CA, Mouton PR, Colomer V (2004) A mutant ataxin-3 putative-cleavage fragment in brains of Machado-Joseph disease patients and transgenic mice is cytotoxic above a critical concentration. J Neurosci 24:10266-10279

Goto J, Watanable M, Ichikawa Y, Yee S-B, Ihara N, Endo K, Igarashi S, Takiyama Y, Gaspar C, Maciel P, Tsuji S, Rouleau GA, Kanazawa I (1997) Machado-Joseph disease gene products carrying different carboxyl termini. Neurosci Res 28:373-377

Goto M, Eddy EM (2004) Speriolin is a novel spermatogenic cell-specific centrosomal protein associated with the seventh WD motif of Cdc20. J Biol Chem 279:42128-42138

Gousseva N, Baker RT (2003) Gene structure, alternate splicing, tissue distribution, cellular localization, and developmental expression pattern of mouse deubiquitinating enzyme isoforms Usp2-45 and Usp2-69. Gene Expr 11:163-179

Grewal SI, Moazed D (2003) Heterochromatin and epigenetic control of gene expression. Science 301:798-802

Groisman R, Polanowska J, Kuraoka I, Sawada J, Saijo M, Drapkin R, Kisselev AF, Tanaka K, Nakatani Y (2003) The ubiquitin ligase activity in the DDB2 and CSA complexes is differentially regulated by the COP9 signalosome in response to DNA damage. Cell 113:357-367

Gros J, Scaal M, Marcelle C (2004) A two-step mechanism for myotome formation in chick. Dev Cell 6:875-882

Guarente L, Kenyon C (2000) Genetic pathways that regulate ageing in model organisms. Nature 408:255-262

Guo D, Hu K, Lei Y, Wang Y, Ma T, He D (2004) Identification and characterization of a novel cytoplasm protein ICF45 that is involved in cell cycle regulation. J Biol Chem 279:53498-53505

Guo S, Rena G, Cichy S, He X, Cohen P, Unterman T (1999) Phosphorylation of serine 256 by protein kinase B disrupts transactivation by FKHR and mediates effects of insulin on insulin-like growth factor-binding protein-1 promoter activity through a conserved insulin response sequence. J Biol Chem 274:17184-17192

Haacke A, Hartl FU, Breuer P (2007) Calpain Inhibition Is Sufficient to Suppress Aggregation of Polyglutamine-expanded Ataxin-3. J Biol Chem 282:18851-18856

Harper JW, Adami GR, Wei N, Keyomarsi K, Elledge SJ (1993) The p21 Cdk-interacting protein Cip1 is a potent inhibitor of G1 cyclin-dependent kinases. Cell 75:805-816

Hatakeyama S, Nakayama KI (2003) U-box proteins as a new family of ubiquitin ligases. Biochem Biophys Res Commun 302:635-645

Hatakeyama S, Yada M, Matsumoto M, Ishida N, Nakayama KI (2001) U box proteins as a new family of ubiquitin-protein ligases. J Biol Chem 276:33111-33120

Hayashi YK, Chou FL, Engvall E, Ogawa M, Matsuda C, Hirabayashi S, Yokochi K, Ziober BL, Kramer RH, Kaufman SJ, Ozawa E, Goto Y, Nonaka I, Tsukahara T, Wang JZ, Hoffman EP, Arahata K (1998) Mutations in the integrin alpha7 gene cause congenital myopathy. Nat Genet 19:94-97

Heir R, Ablasou C, Dumontier E, Elliott M, Fagotto-Kaufmann C, Bedford FK (2006) The UBL domain of PLIC-1 regulates aggresome formation. EMBO Rep 7:1252-1258

Henning D, Valdez BC (2001) Expression of p40/Epstein-Barr virus nuclear antigen 1 binding protein 2. Biochem Biophys Res Commun 283:430-436

Henry KW, Wyce A, Lo WS, Duggan LJ, Emre NC, Kao CF, Pillus L, Shilatifard A, Osley MA, Berger SL (2003) Transcriptional activation via sequential histone H2B ubiquitylation and deubiquitylation, mediated by SAGA-associated Ubp8. Genes Dev 17:2648-2663

Hershko A (1983) Ubiquitin: roles in protein modification and breakdown. Cell 34:11-12

Higgins JJ, Nee LE, Vasconcelos O, Ide SE, Lavedan C, Goldfarb LG, Polymeropoulos MH (1996) Mutations in American families with spinocerebellar ataxia (SCA) type 3: SCA3 is allelic to Machado-Joseph disease. Neurology 46:208-213

Hirabayashi M, Inoue K, Tanaka K, Nakadate K, Ohsawa Y, Kamei Y, Popiel AH, Sinohara A, Iwamatsu A, Kimura Y, Uchiyama Y, Hori S, Kakizuka A (2001) VCP/p97 in abnormal protein aggregates, cytoplasmic vacuoles,. Cell Death Dif 8:977-984

Hirano T (2006) At the heart of the chromosome: SMC proteins in action. Nat Rev Mol Cell Biol 7:311-322

Hirsch HA, Jawdekar GW, Lee KA, Gu L, Henry RW (2004) Distinct mechanisms for repression of RNA polymerase III transcription by the retinoblastoma tumor suppressor protein. Mol Cell Biol 24:5989-5999

Hiyama H, Yokoi M, Masutani C, Sugasawa K, Maekawa T, Tanaka K, Hoeijmakers JH, Hanaoka F (1999) Interaction of hHR23 with S5a. The ubiquitin-like domain of hHR23 mediates interaction with S5a subunit of 26 S proteasome. J Biol Chem 274:28019-28025

Hockly E, Richon VM, Woodman B, Smith DL, Zhou X, Rosa E, Sathasivam K, Ghazi-Noori S, Mahal A, Lowden PA, Steffan JS, Marsh JL, Thompson LM, Lewis CM, Marks PA, Bates GP (2003) Suberoylanilide hydroxamic acid, a histone deacetylase inhibitor, ameliorates motor deficits in a mouse model of Huntington's disease. Proc Natl Acad Sci U S A 100:2041-2046

Hoekman MF, Jacobs FM, Smidt MP, Burbach JP (2006) Spatial and temporal expression of FoxO transcription factors in the developing and adult murine brain. Gene Expr Patterns 6:134-140

Hoffman M, Chiang HL (1996) Isolation of degradation-deficient mutants defective in the targeting of fructose-1,6-bisphosphatase into the vacuole for degradation in Saccharomyces cerevisiae. Genetics 143:1555-1566

Hoffner G, Kahlem P, Djian P (2002) Perinuclear localization of huntingtin as a consequence of its binding to microtubules through an interaction with b-tubulin: relevance to Huntington's disease. J Cell Sci 115:941-948

Holmberg CI, Staniszewski KE, Mensah KN, Matouscheck A, Morimoto RI (2004) Inefficient degradation of truncated polyglutamine proteins by the proteasome. EMBO J 23(21):4307-18

Hoppe T (2005) Multiubiquitylation by E4 enzymes: 'one size' doesn't fit all. Trends Biochem Sci 30:183-187

Hori T, Osaka F, Chiba T, Miyamoto C, Okabayashi K, Shimbara N, Kato S, Tanaka K (1999) Covalent modification of all members of human cullin family proteins by NEDD8. Oncogene 18:6829-6834

Howard J, Hyman AA (2003) Dynamics and mechanics of the microtubule plus end. Nature 422:753-758

Hribal ML, Nakae J, Kitamura T, Shutter JR, Accili D (2003) Regulation of insulin-like growth factor-dependent myoblast differentiation by Foxo forkhead transcription factors. J Cell Biol 162:535-541

Hsieh HC, Hsieh YH, Huang YH, Shen FC, Tsai HN, Tsai JH, Lai YT, Wang YT, Chuang WJ, Huang W (2005) HHR23A, a human homolog of Saccharomyces cerevisiae Rad23, regulates xeroderma pigmentosum C protein and is required for nucleotide excision repair. Biochem Biophys Res Commun 335:181-187

Huang H, Regan KM, Wang F, Wang D, Smith DI, van Deursen JM, Tindall DJ (2005) Skp2 inhibits FOXO1 in tumor suppression through ubiquitin-mediated degradation. Proc Natl Acad Sci U S A 102:1649-1654

Huang HJ, Norris JD, McDonnell DP (2002) Identification of a negative regulatory surface within estrogen receptor alpha provides evidence in support of a role for corepressors in regulating cellular responses to agonists and antagonists. Mol Endocrinol 16:1778-1792

Hunter AW, Caplow M, Coy DL, Hancock WO, Diez S, Wordeman L, Howard J (2003) The kinesin-related protein MCAK is a microtubule depolymerase that forms an ATP-hydrolyzing complex at microtubule ends. Mol Cell 11:445-457

Hwang JW, Min KW, Tamura TA, Yoon JB (2003) TIP120A associates with unneddylated cullin 1 and regulates its neddylation. FEBS Lett 541:102-108

Ichikawa Y, Goto J, Hattori M, Toyoda A, Ishii K, Jeong S-Y, Hashida H, Masuda N, Ogata K, Kasai F, M H, Maciel P, Rouleau GA, Sakaki Y, Kanazawa I (2001) The genomic structure and expression of MJD, the Machado-Joseph disease gene. J Hum Genet 46:413-422

Ideguchi H, Ueda A, Tanaka M, Yang J, Tsuji T, Ohno S, Hagiwara E, Aoki A, Ishigatsubo Y (2002) Structural and functional characterization of the USP11 deubiquitinating enzyme, which interacts with the RanGTP-associated protein RanBPM. Biochem J 367:87-95

Igarashi S, Takiyama Y, Cancel G, Rogaeva EA, Sasaki H, Wakisaka A, Zhou YX, et al. (1996) Intergenerational instability of the CAG repeat of the gene for Machado-Joseph disease (MJD1) is affected by the genotype of the normal chromosome: implications for the molecular mechanisms of the instability of the CAG repeat. Hum Mol Genet 5:923-932

Ikeda H, Yamaguchi M, Sugai S, Aze Y, Narumiya S, Kakizuka A (1996) Expanded polyglutamine in the Machado-Joseph disease protein induces cell death in vitro and in vivo. Nature Genetics 13:196-202

Ito T, Chiba T, Ozawa R, Yoshida M, Hattori M, Sakaki Y (2001) A comprehensive two-hybrid analysis to explore the yeast protein interactome. Proc Natl Acad Sci U S A 98:4569-4574

Jackson PK, Eldridge AG, Freed E, Furstenthal L, Hsu JY, Kaiser BK, Reimann JD (2000) The lore of the RINGs: substrate recognition and catalysis by ubiquitin ligases. Trends Cell Biol 10:429-439

Jacobsen JS, Wu CC, Redwine JM, Comery TA, Arias R, Bowlby M, Martone R, Morrison JH, Pangalos MN, Reinhart PH, Bloom FE (2006) Early-onset behavioral and synaptic deficits in a mouse model of Alzheimer's disease. Proc Natl Acad Sci U S A 103:5161-5166

Jana NR, Dikshit P, Goswami A, Kotliarova S, Murata S, Tanaka K, Nukina N (2005) Co-chaperone CHIP associates with expanded polyglutamine protein and promotes their degradation by proteasomes. J Biol Chem 280:11635-11640

Janiesch PC, Kim J, Mouysset J, Barikbin R, Lochmuller H, Cassata G, Krause S, Hoppe T (2007) The ubiquitin-selective chaperone CDC-48/p97 links myosin assembly to human myopathy. Nat Cell Biol 9:379-390

Job D, Valiron O, Oakley B (2003) Microtubule nucleation. Curr Opin Cell Biol 15:111-117

Jones-Villeneuve EM, McBurney MW, Rogers KA, Kalnins VI (1982) Retinoic acid induces embryonal carcinoma cells to differentiate into neurons and glial cells. J Cell Biol 94:253-262

Jones J, Wu K, Yang Y, Guerrero C, Nillegoda N, Pan ZQ, Huang L (2008) A Targeted Proteomic Analysis of the Ubiquitin-Like Modifier Nedd8 and Associated Proteins. J Proteome Res 7(3):1274-87

Kaabeche K, Guenou H, Bouvard D, Didelot N, Listrat A, Marie PJ (2005) Cbl-mediated ubiquitination of alpha5 integrin subunit mediates fibronectin-dependent osteoblast detachment and apoptosis induced by FGFR2 activation. J Cell Sci 118:1223-1232

Kahlem P, Terre C, Green H, Djian P (1996) Peptides containing glutamine repeats as substrates for transglutaminase-catalyzed cross-linking: relevance to diseases of the nervous system. Proc Natl Acad Sci U S A 93:14580-14585

Kaibuchi K, Kuroda S, Amano M (1999) Regulation of the cytoskeleton and cell adhesion by the Rho family GTPases in mammalian cells. Annu Rev Biochem 68:459-486

Kaltenbach LS, Romero E, Becklin RR, Chettier R, Bell R, Phansalkar A, Strand A, Torcassi C, Savage J, Hurlburt A, Cha GH, Ukani L, Chepanoske CL, Zhen Y, Sahasrabudhe S, Olson J, Kurschner C, Ellerby LM, Peltier JM, Botas J, Hughes RE (2007) Huntingtin interacting proteins are genetic modifiers of neurodegeneration. PLoS Genet 3:e82

Kamitani T, Kito K, Nguyen HP, Yeh ET (1997) Characterization of NEDD8, a developmentally down-regulated ubiquitin-like protein. J Biol Chem 272:28557-28562

Kamura T, Conrad MN, Yan Q, Conaway RC, Conaway JW (1999) The Rbx1 subunit of SCF and VHL E3 ubiquitin ligase activates Rub1 modification of cullins Cdc53 and Cul2. Genes Dev 13:2928-2933

Kaneko C, Hatakeyama S, Matsumoto M, Yada M, Nakayama K, Nakayama KI (2003) Characterization of the mouse gene for the U-box-type ubiquitin ligase UFD2a. Biochem Biophys Res Commun 300:297-304

Karpuj MV, Garren H, Slunt H, Price DL, Gusella J, Becher MW, Steinman L (1999) Transglutaminase aggregates huntingtin into nonamyloidogenic polymers, and its enzymatic activity increases in Huntington's disease brain nuclei. Proc Natl Acad Sci U S A 96:7388-7393

Kawaguchi Y, Okamoto T, Taniwaki M, Aizawa M, Inoue M, Katayama S, Kawakami H, Nakamura S, Nishimura M, Akiguchi I, Kimura J, Narumiya S, Kakizuka A (1994) CAG expansions in a novel gene for Machado-Joseph disease at chromosome 14q32.1. Nat Genet 8:221-228

Kawakami T, Chiba T, Suzuki T, Iwai K, Yamanaka K, Minato N, Suzuki H, Shimbara N, Hidaka Y, Osaka F, Omata M, Tanaka K (2001) NEDD8 recruits E2-ubiquitin to SCF E3 ligase. Embo J 20:4003-4012

Kee Y, Lyon N, Huibregtse JM (2005) The Rsp5 ubiquitin ligase is coupled to and antagonized by the Ubp2 deubiquitinating enzyme. Embo J 24:2414-2424

Keegan L, Gill G, Ptashne M (1986) Separation of DNA binding from the transcription-activating function of a eukaryotic regulatory protein. Science 231:699-704

Khan LA, Bauer PO, Miyazaki H, Lindenberg KS, Landwehrmeyer BG, Nukina N (2006) Expanded polyglutamines impair synaptic transmission and ubiquitin-proteasome system in Caenorhabditis elegans. J Neurochem 98:576-587

Kieran D, Hafezparast M, Bohnert S, Dick JR, Martin J, Schiavo G, Fisher EM, Greensmith L (2005) A mutation in dynein rescues axonal transport defects and extends the life span of ALS mice. J Cell Biol 169:561-567

Kim J, Hoppe T (2006) The ubiquitin proteasome system and muscle development. In: Mayer RJ CA, Rechsteiner M, (ed) Protein Degradation, Cell Biology of the Ubiquitin-Proteasome System. Vol 3. Wiley-VCH Verlag GmbH & Co. KGaA, Weinheim, pp 21-47

Kleijnen MF, Shih AH, Zhou P, Kumar S, Soccio RE, Kedersha NL, Gill G, Howley PM (2000) The hPLIC proteins may provide a link between the ubiquitination machinery and the proteasome. Mol Cell 6:409-419

Kline-Smith SL, Khodjakov A, Hergert P, Walczak CE (2004) Depletion of centromeric MCAK leads to chromosome congression and segregation defects due to improper kinetochore attachments. Mol Biol Cell 15:1146-1159

Kobayashi N, Yang J, Ueda A, Suzuki T, Tomaru K, Takeno M, Okuda K, Ishigatsubo Y (2007) RanBPM, Muskelin, p48EMLP, p44CTLH, and the armadillo-repeat proteins ARMC8alpha and ARMC8beta are components of the CTLH complex. Gene 396:236-247

Kobayashi T, Tanaka K, Inoue K, Kakizuka A (2002) Functional ATPase activity of p97/Valosin-containing protein (VCP) is required for the quality control of endoplasmic reticulum neuronally differentiated mammalian PC12 cells. J Biol Chem 277:47358-47365

Kobayashi Y, Kume A, Li M, Doyu M, Hata M, Ohtsuka K, Sobue G (2000) Chaperones Hsp70 and Hsp40 suppress aggregate formation and apoptosis in cultured neuronal cells expressing truncated androgen receptor protein with expanded polyglutamine tract. J Biol Chem 275:8772-8778

Kobayashi Y, Miwa S, Merry DE, Kume A, Mei L, Doyu M, Sobue G (1998) Caspase-3 cleaves the expanded androgen receptor protein of spinal and bulbar muscular atrophy in a polyglutamine repeat length-dependent manner. Biochem Biophys Res Commun 252:145-150

Koegl M, Hoppe T, Schlenker S, Ulrich HD, Mayer TU, Jentsch S (1999) A novel ubiquitination factor, E4, is involved in multiubiquitin chain assembly. Cell 96:635-644

Koppe RI, Hallauer PL, Karpati G, Hastings KE (1989) cDNA clone and expression analysis of rodent fast and slow skeletal muscle troponin I mRNAs. J Biol Chem 264:14327-14333

Kops GJ, de Ruiter ND, De Vries-Smits AM, Powell DR, Bos JL, Burgering BM (1999) Direct control of the Forkhead transcription factor AFX by protein kinase B. Nature 398:630-634

Kovalenko A, Chable-Bessia C, Cantarella G, Israel A, Wallach D, Courtois G (2003) The tumour suppressor CYLD negatively regulates NF-kappaB signalling by deubiquitination. Nature 424:801-805

Kudoh T, Ishidate T, Moriyama M, Toyoshima K, Akiyama T (1995) G1 phase arrest induced by Wilms tumor protein WT1 is abrogated by cyclin/CDK complexes. Proc Natl Acad Sci U S A 92:4517-4521

Kunst CB (2004) Complex genetics of amyotrophic lateral sclerosis. Am J Hum Genet 75:933-947

Kuzmichev A, Nishioka K, Erdjument-Bromage H, Tempst P, Reinberg D (2002) Histone methyltransferase activity associated with a human multiprotein complex containing the Enhancer of Zeste protein. Genes Dev 16:2893-2905

Lam YC, Bowman AB, Jafar-Nejad P, Lim J, Richman R, Fryer JD, Hyun ED, Duvick LA, Orr HT, Botas J, Zoghbi HY (2006) ATAXIN-1 interacts with the repressor Capicua in its native complex to cause SCA1 neuropathology. Cell 127:1335-1347

Lan W, Zhang X, Kline-Smith SL, Rosasco SE, Barrett-Wilt GA, Shabanowitz J, Hunt DF, Walczak CE, Stukenberg PT (2004) Aurora B phosphorylates centromeric MCAK and regulates its localization and microtubule depolymerization activity. Curr Biol 14:273-286

Landis MD, Seachrist DD, Montanez-Wiscovich ME, Danielpour D, Keri RA (2005) Gene expression profiling of cancer progression reveals intrinsic regulation of transforming growth factor-beta signaling in ErbB2/Neu-induced tumors from transgenic mice. Oncogene 24:5173-5190

Landsverk ML, Li S, Hutagalung AH, Najafov A, Hoppe T, Barral JM, Epstein HF (2007) The UNC-45 chaperone mediates sarcomere assembly through myosin degradation in Caenorhabditis elegans. J Cell Biol 177:205-210

Larminie CG, Cairns CA, Mital R, Martin K, Kouzarides T, Jackson SP, White RJ (1997) Mechanistic analysis of RNA polymerase III regulation by the retinoblastoma protein. Embo J 16:2061-2071

Le Sourd F, Boulben S, Le Bouffant R, Cormier P, Morales J, Belle R, Mulner-Lorillon O (2006) eEF1B: At the dawn of the 21st century. Biochim Biophys Acta 1759:13-31

Leavitt BR, van Raamsdonk JM, Shehadeh J, Fernandes H, Murphy Z, Graham RK, Wellington CL, Raymond LA, Hayden MR (2006) Wild-type huntingtin protects neurons from excitotoxicity. J Neurochem 96(4):1121-9

Lecker SH, Jagoe RT, Gilbert A, Gomes M, Baracos V, Bailey J, Price SR, Mitch WE, Goldberg AL (2004) Multiple types of skeletal muscle atrophy involve a common program of changes in gene expression. Faseb J 18:39-51

Lee HJ, Kim MS, Shin JM, Park TJ, Chung HM, Baek KH (2006) The expression patterns of deubiquitinating enzymes, USP22 and Usp22. Gene Expr Patterns 6:277-284

Lee RY, Hench J, Ruvkun G (2001) Regulation of C. elegans DAF-16 and its human ortholog FKHRL1 by the daf-2 insulin-like signaling pathway. Curr Biol 11:1950-1957

Lee SB, Huang K, Palmer R, Truong VB, Herzlinger D, Kolquist KA, Wong J, Paulding C, Yoon SK, Gerald W, Oliner JD, Haber DA (1999) The Wilms tumor suppressor WT1 encodes a transcriptional activator of amphiregulin. Cell 98:663-673

Leffers H, Nielsen MS, Andersen AH, Honore B, Madsen P, Vandekerckhove J, Celis JE (1993) Identification of two human Rho GDP dissociation inhibitor proteins whose overexpression leads to disruption of the actin cytoskeleton. Exp Cell Res 209:165-174

Leloup L, Daury L, Mazeres G, Cottin P, Brustis JJ (2007) Involvement of the ERK/MAP kinase signalling pathway in milli-calpain activation and myogenic cell migration. Int J Biochem Cell Biol 39:1177-1189

Li F, Macfarlan T, Pittman RN, Chakravarti D (2002) Ataxin-3 is a histone-binding protein with two independent transcriptional corepressor activities. J Biol Chem 277:45004-45012

Li HH, Kedar V, Zhang C, McDonough H, Arya R, Wang DZ, Patterson C (2004a) Atrogin-1/muscle atrophy F-box inhibits calcineurin-dependent cardiac hypertrophy by participating in an SCF ubiquitin ligase complex. J Clin Invest 114:1058-1071

Li L, Lu X, Peterson C, Legerski R (1997) XPC interacts with both HHR23B and HHR23A in vivo. Mutat Res 383:197-203

Li S, Armstrong CM, Bertin N, Ge H, Milstein S, Boxem M, Vidalain PO, et al. (2004b) A map of the interactome network of the metazoan C. elegans. Science 303:540-543

Li Z, Wang D, Messing EM, Wu G (2005) VHL protein-interacting deubiquitinating enzyme 2 deubiquitinates and stabilizes HIF-1alpha. EMBO Rep 6:373-378

Lim J, Crespo-Barreto J, Jafar-Nejad P, Bowman AB, Richman R, Hill DE, Orr HT, Zoghbi HY (2008) Opposing effects of polyglutamine expansion on native protein complexes contribute to SCA1. Nature 452(7188):713-8

Lima L, Coutinho P (1980) Clinical criteria for diagnosis of Machado-Joseph disease: report of a non-Azorena Portuguese family. Neurology 30:319-322

Lin B, Nasir J, MacDonald H, Hutchinson G, Graham RK, Rommens JM, Hayden MR (1994) Sequence of the murine Huntington disease gene: evidence for conservation, alternate splicing and polymorphism in a triplet (CCG) repeat [corrected]. Hum Mol Genet 3:85-92

Lin K, Dorman JB, Rodan A, Kenyon C (1997) daf-16: An HNF-3/forkhead family member that can function to double the life-span of Caenorhabditis elegans. Science 278:1319-1322

Lin K, Hsin H, Libina N, Kenyon C (2001) Regulation of the Caenorhabditis elegans longevity protein DAF-16 by insulin/IGF-1 and germline signaling. Nat Genet 28:139-145

Lindblad K, Lunkes A, Maciel P, Stevanin G, Zander C, Klockgether T, Ratzlaff T, Brice A, Rouleau GA, Hudson T, Auburger G, Schalling M (1996) Mutation detection in Machado-Joseph disease using repeat expansion detection. Mol Med 2:77-85

Lindon C, Albagli O, Domeyne P, Montarras D, Pinset C (2000) Constitutive instability of muscle regulatory factor Myf5 is distinct from its mitosis-specific disappearance, which requires a D-box-like motif overlapping the basic domain. Mol Cell Biol 20:8923-8932

Linhartová I, Repitz M, Dráber P, Nemec M, Wiche G, Propst F (1999) Conserved domains and lack of evidence for polyglutamine length polymorphism in the chicken homolog of the Machado-Joseph disease gene product ataxin-3. Biochimica et Biophysica Acta 1444:299-305

Lopes-Cendes I, Maciel P, Kish S, Gaspar C, Robitaille Y, Clark HB, Koeppen AH, Nance M, Schut L, Silveira I, Coutinho P, Sequeiros J, Rouleau GA (1996a) Somatic mosaicism in the central nervous system in spinocerebellar ataxia type 1 and Machado-Joseph disease. Ann Neurol 40:199-206

Lopes-Cendes I, Silveira I, Maciel P, Gaspar C, Radvany J, Chitayat D, Babul R, Stewart J, Dolliver M, Robitaille Y, Rouleau GA, Sequeiros J (1996b) Limits of clinical assessment in the accurate diagnosis of Machado-Joseph disease. Arch Neurol 53:1168-1174

Luo BH, Carman CV, Springer TA (2007) Structural basis of integrin regulation and signaling. Annu Rev Immunol 25:619-647

Ma J, Ptashne M (1988) Converting a eukaryotic transcriptional inhibitor into an activator. Cell 55:443-446

Maciel P, Costa MC, Ferro A, Rousseau M, Santos CS, Gaspar C, Barros J, Rouleau GA, Coutinho P, Sequeiros J (2001) Improvement in the molecular diagnosis of Machado-Joseph disease. Arch Neurol 58:1821-1827

Maciel P, Gaspar C, Guimarães L, Goto J, Lopes-Cendes I, Hayes S, Arvidsson K, Dias A, Sequeiros J, Sousa A, Rouleau GA (1999) Study of three intragenic polymorphisms in the Machado-Joseph disease gene (MJD1) in relation to genetic instability of the $(CAG)_n$ tract. Eur J Hum Genet 7:147-156

Maciel P, Gaspar C, DeStefano AL, Silveira I, Coutinho P, Radvany J, Dawson DM, Sudarsky L, Guimaraes J, Loureiro JE, et al. (1995) Correlation between CAG repeat length and clinical features in Machado-Joseph disease. Am J Hum Genet 57:54-61

Makarova O, Kamberov E, Margolis B (2000) Generation of deletion and point mutations with one primer in a single cloning step. Biotechniques 29:970-972

Maney T, Hunter AW, Wagenbach M, Wordeman L (1998) Mitotic centromere-associated kinesin is important for anaphase chromosome segregation. J Cell Biol 142:787-801

Mangiarini L, Sathasivam K, Seller M, Cozens B, Harper A, Hetherington C, Lawton M, Trottier Y, Lehrach H, Davies SW, Bates GP (1996) Exon 1 of the HD gene with an expanded CAG repeat is sufficient to cause a progressive neurological phenotype in transgenic mice. Cell 87:493-506

Mao Y, Senic-Matuglia F, Di Fiore PP, Polo S, Hodsdon ME, De Camilli P, (2005) Deubiquitinating function of ataxin-3: insights from the solution structure of the josephin domain. Proc Natl Acad Sci U S A 102:12700-12705

Mao Y, Schwarzbauer JE (2005) Fibronectin fibrillogenesis, a cell-mediated matrix assembly process. Matrix Biol 24:389-399

Margolis RL (2002) The spinocerebellar ataxias: order emerges from chaos. Curr Neurol Neurosci Rep 2:447-456

Martin LJ, Pan Y, Price AC, Sterling W, Copeland NG, Jenkins NA, Price DL, Lee MK (2006) Parkinson's disease alpha-synuclein transgenic mice develop neuronal mitochondrial degeneration and cell death. J Neurosci 26:41-50

Martin PT, Kaufman SJ, Kramer RH, Sanes JR (1996) Synaptic integrins in developing, adult, and mutant muscle: selective association of alpha1, alpha7A, and alpha7B integrins with the neuromuscular junction. Dev Biol 174:125-139

Martin TF (1998) Phosphoinositide lipids as signaling molecules: common themes for signal transduction, cytoskeletal regulation, and membrane trafficking. Annu Rev Cell Dev Biol 14:231-264

Maruyama H, Nakamura S, Matsuyama Z, Sakai T, Doyu M, Sobue G, Seto M, Tsujihata M, Oh-i T, Nishio T, et al. (1995) Molecular features of the CAG repeats and clinical manifestation of Machado-Joseph disease. Hum Mol Genet 4:807-812

Masino L, Musi V, Menon P, Fusi P, Kelly G, Frenkiel TA, Trottier Y, Pastore A (2003) Domain architecture of the polyglutamine protein ataxin-3: a globular domain followed by a flexible tail. FEBS Letters 549:21-25

Matsumoto M, Yada M, Hatakeyama S, Ishimoto H, Tanimura T, Tsuji S, Kakizuka A, Kitagawa M, Nakayama KI (2004) Molecular clearance of ataxin-3 is regulated by a mammalian E4. EMBO J 23:659-669

Matsuzaki H, Daitoku H, Hatta M, Tanaka K, Fukamizu A (2003) Insulin-induced phosphorylation of FKHR (Foxo1) targets to proteasomal degradation. Proc Natl Acad Sci U S A 100:11285-11290

Matsuzawa SI, Reed JC (2001) Siah-1, SIP, and Ebi collaborate in a novel pathway for beta-catenin degradation linked to p53 responses. Mol Cell 7:915-926

Mayer U (2003) Integrins: redundant or important players in skeletal muscle? J Biol Chem 278:14587-14590

Mayer U, Saher G, Fassler R, Bornemann A, Echtermeyer F, von der Mark H, Miosge N, Poschl E, von der Mark K (1997) Absence of integrin alpha 7 causes a novel form of muscular dystrophy. Nat Genet 17:318-323

McBurney MW, Jones-Villeneuve EM, Edwards MK, Anderson PJ (1982) Control of muscle and neuronal differentiation in a cultured embryonal carcinoma cell line. Nature 299:165-167

McCampbell A, Taylor JP, Taye AA, Robitschek J, Li M, Walcott J, Merry D, Chai Y, Paulson HL, Sobue G, Fischbeck KH (2000) CREB-binding protein sequestration by expanded polyglutamine. Hum Mol Genet 9:2197-2202

McElhinny AS, Kakinuma K, Sorimachi H, Labeit S, Gregorio CC (2002) Muscle-specific RING finger-1 interacts with titin to regulate sarcomeric M-line and thick filament structure and may have nuclear functions via its interaction with glucocorticoid modulatory element binding protein-1. J Cell Biol 157:125-136

McElhinny AS, Perry CN, Witt CC, Labeit S, Gregorio CC (2004) Muscle-specific RING finger-2 (MURF-2) is important for microtubule, intermediate filament and sarcomeric M-line maintenance in striated muscle development. J Cell Sci 117:3175-3188

McKenna NJ, O'Malley BW (2000) From ligand to response: generating diversity in nuclear receptor coregulator function. J Steroid Biochem Mol Biol 74:351-356

McKinsey TA, Zhang CL, Olson EN (2002) MEF2: a calcium-dependent regulator of cell division, differentiation and death. Trends Biochem Sci 27:40-47

Mielenz D, Hapke S, Poschl E, von Der Mark H, von Der Mark K (2001) The integrin alpha 7 cytoplasmic domain regulates cell migration, lamellipodia formation, and p130CAS/Crk coupling. J Biol Chem 276:13417-13426

Miller SL, Malotky E, O'Bryan JP (2004) Analysis of the role of ubiquitin-interacting motifs in ubiquitin binding and ubiquitylation. J Biol Chem 279:33528-33537

Miller SL, Scappini EL, O'Bryan J (2007) Ubiquitin-interacting motifs inhibit aggregation of polyQ-expanded huntingtin. J Biol Chem 282:10096-10103

Miller VM, Xia H, Marrs GL, Gouvion CM, Lee G, Davidson BL, Paulson HL (2003) Allele-specific silencing of dominant disease genes. Proc Natl Acad Sci U S A 100:7195-7200

Miranti CK, Brugge JS (2002) Sensing the environment: a historical perspective on integrin signal transduction. Nat Cell Biol 4:E83-90

Misaghi S, Galardy PJ, Meester WJ, Ovaa H, Ploegh HL, Gaudet R (2005) Structure of the ubiquitin hydrolase UCH-L3 complexed with a suicide substrate. J Biol Chem 280:1512-1520

Misra P, Qi C, Yu S, Shah SH, Cao WQ, Rao MS, Thimmapaya B, Zhu Y, Reddy JK (2002) Interaction of PIMT with transcriptional coactivators CBP, p300, and PBP differential role in transcriptional regulation. J Biol Chem 277:20011-20019

Molkentin JD, Black BL, Martin JF, Olson EN (1995) Cooperative activation of muscle gene expression by MEF2 and myogenic bHLH proteins. Cell 83:1125-1136

Molkentin JD, Olson EN (1996) Defining the regulatory networks for muscle development. Curr Opin Genet Dev 6:445-453

Morgan JE, Partridge TA (2003) Muscle satellite cells. Int J Biochem Cell Biol 35:1151-1156

Mori F, Nishie M, Piao YS, Kito K, Kamitani T, Takahashi H, Wakabayashi K (2005) Accumulation of NEDD8 in neuronal and glial inclusions of neurodegenerative disorders. Neuropathol Appl Neurobiol 31:53-61

Mori N (1997) Molecular genetic approaches to the genes of longevity, aging and neurodegeneration in mammals. Mech Ageing Dev 98:223-230

Motta MC, Divecha N, Lemieux M, Kamel C, Chen D, Gu W, Bultsma Y, McBurney M, Guarente L (2004) Mammalian SIRT1 represses forkhead transcription factors. Cell 116:551-563

Mount LE (1978) Heat transfer between animal and environment. Proc Nutr Soc 37:21-27

Mues A, van der Ven PF, Young P, Furst DO, Gautel M (1998) Two immunoglobulin-like domains of the Z-disc portion of titin interact in a conformation-dependent way with telethonin. FEBS Lett 428:111-114

Murakami K, Etlinger JD (1987) Degradation of proteins with blocked amino groups by cytoplasmic proteases. Biochem Biophys Res Commun 146:1249-1255

Murata T, Shimotohno K (2006) Ubiquitination and proteasome-dependent degradation of human eukaryotic translation initiation factor 4E. J Biol Chem 281:20788-20800

Nakamura M, Masuda H, Horii J, Kuma K, Yokoyama N, Ohba T, Nishitani H, Miyata T, Tanaka M, Nishimoto T (1998) When overexpressed, a novel centrosomal protein, RanBPM, causes ectopic microtubule nucleation similar to gamma-tubulin. J Cell Biol 143:1041-1052

Nakamura M, Zhou XZ, Lu KP (2001) Critical role for the EB1 and APC interaction in the regulation of microtubule polymerization. Curr Biol 11:1062-1067

Nakano KK, Dawson DM, Spence A (1972) Machado disease. A hereditary ataxia in Portuguese emigrants to Massachusetts. Neurology 22:49-55

Nechiporuk T, Huynh DP, Figueroa K, Sahba S, Nechiporuk A, Pulst SM (1998) The mouse SCA2 gene: cDNA sequence, alternative splicing and protein expression. Hum Mol Genet 7:1301-1309

Nicastro G, Menon RP, Masino L, Knowles PP, McDonald NQ, Pastore A (2005) The solution structure of the josephin domain of ataxin-3: structural determinants for molecular recognition. Proc Natl Acad Sci U S A 102:10493-40498

Nicolas E, Ait-Si-Ali S, Trouche D (2001) The histone deacetylase HDAC3 targets RbAp48 to the retinoblastoma protein. Nucleic Acids Res 29:3131-3136

Nicolas E, Morales V, Magnaghi-Jaulin L, Harel-Bellan A, Richard-Foy H, Trouche D (2000) RbAp48 belongs to the histone deacetylase complex that associates with the retinoblastoma protein. J Biol Chem 275:9797-9804

Niethammer P, Kronja I, Kandels-Lewis S, Rybina S, Bastiaens P, Karsenti E (2007) Discrete states of a protein interaction network govern interphase and mitotic microtubule dynamics. PLoS Biol 5:e29

Nigg EA (2001) Mitotic kinases as regulators of cell division and its checkpoints. Nat Rev Mol Cell Biol 2:21-32

Nijman SM, Luna-Vargas MP, Velds A, Brummelkamp TR, Dirac AM, Sixma TK, Bernards R (2005) A genomic and functional inventory of deubiquitinating enzymes. Cell 123:773-786

Noren NK, Pasquale EB (2004) Eph receptor-ephrin bidirectional signals that target Ras and Rho proteins. Cell Signal 16:655-666

Nury D, Doucet C, Coux O (2007) Roles and potential therapeutic targets of the ubiquitin proteasome system in muscle wasting. BMC Biochem 8 Suppl 1:S7

Obermann WM, Gautel M, Steiner F, van der Ven PF, Weber K, Furst DO (1996) The structure of the sarcomeric M band: localization of defined domains of myomesin, M-protein, and the 250-kD carboxy-terminal region of titin by immunoelectron microscopy. J Cell Biol 134:1441-1453

Ogg S, Paradis S, Gottlieb S, Patterson GI, Lee L, Tissenbaum HA, Ruvkun G (1997) The Fork head transcription factor DAF-16 transduces insulin-like metabolic and longevity signals in C. elegans. Nature 389:994-999

Ohta T, Michel JJ, Schottelius AJ, Xiong Y (1999) ROC1, a homolog of APC11, represents a family of cullin partners with an associated ubiquitin ligase activity. Mol Cell 3:535-541

Okazawa H (2003) Polyglutamine diseases: a transcription disorder? Cell Mol Life Sci 60:1427-1439

Onodera Y, Hashimoto S, Hashimoto A, Morishige M, Mazaki Y, Yamada A, Ogawa E, Adachi M, Sakurai T, Manabe T, Wada H, Matsuura N, Sabe H (2005) Expression of AMAP1, an ArfGAP, provides novel targets to inhibit breast cancer invasive activities. Embo J 24:963-973

Orr HT, Zoghbi HY (2007) Trinucleotide repeat disorders. Annu Rev Neurosci 30:575-621

Ozeki N, Lim M, Yao CC, Tolar M, Kramer RH (2006) alpha7 integrin expressing human fetal myogenic progenitors have stem cell-like properties and are capable of osteogenic differentiation. Exp Cell Res 312:4162-4180

Pan ZQ, Kentsis A, Dias DC, Yamoah K, Wu K (2004) Nedd8 on cullin: building an expressway to protein destruction. Oncogene 23:1985-1997

Park KC, Kim JH, Choi EJ, Min SW, Rhee S, Baek SH, Chung SS, Bang O, Park D, Chiba T, Tanaka K, Chung CH (2002) Antagonistic regulation of myogenesis by two deubiquitinating enzymes, UBP45 and UBP69. Proc Natl Acad Sci U S A 99:9733-9738

Parry G, Estelle M (2004) Regulation of cullin-based ubiquitin ligases by the Nedd8/RUB ubiquitin-like proteins. Semin Cell Dev Biol 15:221-229

Paulson H (2006) RNA interference as potential therapy for neurodegenerative disease: applications to inclusion-body myositis? Neurology 66:S114-117

Paulson HL (2007) Dominantly inherited ataxias: lessons learned from Machado-Joseph disease/spinocerebellar ataxia type 3. Semin Neurol 27:133-142

Paulson HL, Das SS, Crino PB, Perez MK, Patel SC, Gotsdiner D, Fischbeck KH, Pittman RN (1997a) Machado-Joseph disease gene product is a cytoplasmic protein widely expressed in brain. Ann Neurol 41:453-462

Paulson HL, Perez MK, Trottier Y, Trojanowski JQ, Subramony SH, Das SS, Vig P, Mandel J-L, Fischbeck KH, Pittman RN (1997b) Intranuclear inclusions of expanded polyglutamine protein in spinocerebellar ataxia type 3. Neuron 19:333-344

Paxinos G, Franklin KBJ (1997) The Mouse Brain in Stereotaxic Coordinates. Academic Press, San Diego

Peluso JJ, Pappalardo A, Fernandez G, Wu CA (2004) Involvement of an unnamed protein, RDA288, in the mechanism through which progesterone mediates its antiapoptotic action in spontaneously immortalized granulosa cells. Endocrinology 145:3014-3022

Perutz MF, Johnson T, Suzuki M, Finch JT (1994) Glutamine repeats as polar zippers: their possible role in inherited neurodegenerative diseases. Proc Natl Acad Sci U S A 91:5355-5358

Peters JM (2002) The anaphase-promoting complex: proteolysis in mitosis and beyond. Mol Cell 9:931-943

Peth A, Boettcher JP, Dubiel W (2007) Ubiquitin-dependent proteolysis of the microtubule end-binding protein 1, EB1, is controlled by the COP9 signalosome: possible consequences for microtubule filament stability. J Mol Biol 368:550-563

Petroski MD, Deshaies RJ (2005) Function and regulation of cullin-RING ubiquitin ligases. Nat Rev Mol Cell Biol 6:9-20

Pickart CM (2001) Mechanisms underlying ubiquitination. Annu Rev Biochem 70:503-533

Pizon V, Iakovenko A, Van Der Ven PF, Kelly R, Fatu C, Furst DO, Karsenti E, Gautel M (2002) Transient association of titin and myosin with microtubules in nascent myofibrils directed by the MURF2 RING-finger protein. J Cell Sci 115:4469-4482

Pollard TD (2007) Regulation of actin filament assembly by Arp2/3 complex and formins. Annu Rev Biophys Biomol Struct 36:451-477

Polymeropoulos MH, Higgins JJ, Golbe LI, Johnson WG, Ide SE, Di Iorio G, Sanges G, Stenroos ES, Pho LT, Schaffer AA, Lazzarini AM, Nussbaum RL, Duvoisin RC (1996) Mapping of a gene for Parkinson's disease to chromosome 4q21-q23. Science 274:1197-1199

Polymeropoulos MH, Lavedan C, Leroy E, Ide SE, Dehejia A, Dutra A, Pike B, Root H, Rubenstein J, Boyer R, Stenroos ES, Chandrasekharappa S, Athanassiadou A, Papapetropoulos T, Johnson WG, Lazzarini AM, Duvoisin RC, Di Iorio G, Golbe LI, Nussbaum RL (1997) Mutation in the alpha-synuclein gene identified in families with Parkinson's disease. Science 276:2045-2047

Price SR (2003) Increased transcription of ubiquitin-proteasome system components: molecular responses associated with muscle atrophy. Int J Biochem Cell Biol 35:617-628

Raasi S, Varadan R, Fushman D, Pickart CM (2005) Diverse polyubiquitin interaction properties of ubiquitin-associated domains. Nat Struct Mol Biol 12:708-714

Rain JC, Selig L, De Reuse H, Battaglia V, Reverdy C, Simon S, Lenzen G, Petel F, Wojcik J, Schachter V, Chemama Y, Labigne A, Legrain P (2001) The protein-protein interaction map of Helicobacter pylori. Nature 409:211-215

Reddy PH, Williams M, Charles V, Garrett L, Pike-Buchanan L, Whetsell WO, Jr., Miller G, Tagle DA (1998) Behavioural abnormalities and selective neuronal loss in HD transgenic mice expressing mutated full-length HD cDNA. Nat Genet 20:198-202

Regelmann J, Schule T, Josupeit FS, Horak J, Rose M, Entian KD, Thumm M, Wolf DH (2003) Catabolite degradation of fructose-1,6-bisphosphatase in the yeast Saccharomyces cerevisiae: a genome-wide screen identifies eight novel GID genes and indicates the existence of two degradation pathways. Mol Biol Cell 14:1652-1663

Reimers K, Antoine M, Zapatka M, Blecken V, Dickson C, Kiefer P (2001) NoBP, a nuclear fibroblast growth factor 3 binding protein, is cell cycle regulated and promotes cell growth. Mol Cell Biol 21:4996-5007

Rena G, Woods YL, Prescott AR, Peggie M, Unterman TG, Williams MR, Cohen P (2002) Two novel phosphorylation sites on FKHR that are critical for its nuclear exclusion. Embo J 21:2263-2271

Rodrigues AJ, Coppola G, Santos C, Costa MC, Ailion M, Sequeiros J, Geschwind DH, Maciel P (2007) Functional genomics and biochemical characterization of the C. elegans orthologue of the Machado-Joseph disease protein ataxin-3. Faseb J 21:1126-1136

Rolfs A, Koeppen AH, Bauer I, Bauer P, Buhlmann S, Topka H, Schols L, Riess O (2003) Clinical features and neuropathology of autosomal dominant spinocerebellar ataxia (SCA17). Ann Neurol 54:367-375

Romanul FC, Fowler HL, Radvany J, Feldman RG, Feingold M (1977) Azorean disease of the nervous system. N Engl J Med 296:1505-1508

Rosenberg RN (1992) Machado-Joseph disease: an autosomal dominant motor system degeneration. Mov Disord 7:193-203

Rosenberg RN, Nyhan WL, Bay C, Shore P (1976) Autosomal dominant striatonigral degeneration. A clinical, pathologic, and biochemical study of a new genetic disorder. Neurology 26:703-714

Ross CA (1995) When more is less: pathogenesis of glutamine repeat neurodegenerative diseases. Neuron 15:493-496

Rual JF, Venkatesan K, Hao T, Hirozane-Kishikawa T, Dricot A, Li N, Berriz GF, et al. (2005) Towards a proteome-scale map of the human protein-protein interaction network. Nature 437:1173-1178

Rüb U, Del Turco D, Del Tredici K, de Vos RAI, Brunt ER, Reifenberger G, Seifried C, Schultz C, Auburger G, Braak H (2003) Thalamic involvement in a spinocerebellar ataxia type 2 (SCA2) and a spinocerebellar ataxia type 3 (SCA3) patient, and its clinical relevance. Brain 126:2257-2272

Rüb U, Gierga K, Brunt ER, de Vos RAI, Bauer M, Schöls L, Bürk K, Auburger G, Bohl J, Schultz C, Vuksic M, Burbach GJ, Braak H, Deller T (2005) Spinocerebellar ataxias types 2 and 3: degeneration of the precerebellar nuclei isolates the three phylogenetically defined regions of the cerebellum. J Neural Transmis 112(11):1523-45

Rudnicki MA, Braun T, Hinuma S, Jaenisch R (1992) Inactivation of MyoD in mice leads to up-regulation of the myogenic HLH gene Myf-5 and results in apparently normal muscle development. Cell 71:383-390

Sabourin LA, Rudnicki MA (2000) The molecular regulation of myogenesis. Clin Genet 57:16-25

Sajadi A, Schneider BL, Aebischer P (2004) Wlds-mediated protection of dopaminergic fibers in an animal model of Parkinson disease. Curr Biol 14:326-330

Sambrook J, Fritsh EF, Maniatis T (1989) Molecular Cloning - a laboratory manual. Cold Spring Harbor Laboratory Press.

Samuels SE, Thompson JR, Christopherson RJ (1996) Skeletal and cardiac muscle protein turnover during short-term cold exposure and rewarming in young rats. Am J Physiol 270:R1231-1239

Sandri M, Sandri C, Gilbert A, Skurk C, Calabria E, Picard A, Walsh K, Schiaffino S, Lecker SH, Goldberg AL (2004) Foxo transcription factors induce the atrophy-related ubiquitin ligase atrogin-1 and cause skeletal muscle atrophy. Cell 117:399-412

Sanger JW, Ayoob JC, Chowrashi P, Zurawski D, Sanger JM (2000) Assembly of myofibrils in cardiac muscle cells. Adv Exp Med Biol 481:89-102; discussion 103-105

Santos C (2005) Genética molecular da doença de Machado-Joseph: modelos de estudo em C. elegans. Universidade do Porto, Porto

Sarkar SA, Sharma RP (2002) Modulation of c-myc, max, and mad gene expression during neural differentiation of embryonic stem cells by all-trans-retinoic acid. Gene Expr 10:125-135

Saudou F, Finkbeiner S, Devys D, Greenberg ME (1998) Huntingtin acts in the nucleus to induce apoptosis but death does not correlate with the formation of intranuclear inclusions. Cell 95:55-66

Scheel H, Tomiuk S, Hofmann K (2003) Elucidation of ataxin-3 and ataxin-7 function by integrative bioinformatics. Human Molecular Genetics 12:2845-2852

Scheffner M, Huibregtse JM, Vierstra RD, Howley PM (1993) The HPV-16 E6 and E6-AP complex functions as a ubiquitin-protein ligase in the ubiquitination of p53. Cell 75:495-505

Schmidtt I, Brattig T, Gossen M, Riess O (1997) Characterization of the rat spinocerebellar ataxia type 3 gene. Neurogenetics 1:103-112

Schmitt I, Linden M, Khazneh H, Evert BO, Breuer P, Klockgether T, Wuellner U (2007) Inactivation of the mouse Atxn3 (ataxin-3) gene increases protein ubiquitination. Biochem Biophys Res Commun 362:734-739

Schols L, Bauer P, Schmidt T, Schulte T, Riess O (2004) Autosomal dominant cerebellar ataxias: clinical features, genetics, and pathogenesis. Lancet Neurol 3:291-304

Schubert U, Anton LC, Gibbs J, Norbury CC, Yewdell JW, Bennink JR (2000) Rapid degradation of a large fraction of newly synthesized proteins by proteasomes. Nature 404:770-774

Schug J, Overton G (1997) TESS: Transcription Element Search Software on the WWW, Technical Rep. CBIL-TR-1997-1001-v0.0. Computational Biology and Informatics Laboratory, School of Medicine, Univ. Pennsylvania, Philadelphia

Sequeiros J, Coutinho P (1993) Epidemiology and clinical aspects of Machado-Joseph disease. Adv Neurol 61:139-153

Sequeiros J, Silveira I, Maciel P, Coutinho P, Manaia A, Gaspar C, Burlet P, Loureiro L, Guimaraes J, Tanaka H, et al. (1994) Genetic linkage studies of Machado-Joseph disease with chromosome 14q STRPs in 16 Portuguese-Azorean kindreds. Genomics 21:645-648

Shen L, Tang BS, Tang JG, Jiang H, Wang C, Fang HY (2006) [Screening for proteins interacting with ataxin-3, the gene product of SCA3/MJD]. Zhong Nan Da Xue Xue Bao Yi Xue Ban 31:40-44

Shiraishi S, Zhou C, Aoki T, Sato N, Chiba T, Tanaka K, Yoshida S, Nabeshima Y, Nabeshima YI, Tamura TA (2007) TBP-interacting Protein 120B (TIP120B)/Cullin-associated and Neddylation-dissociated 2 (CAND2) Inhibits SCF-dependent Ubiquitination of Myogenin and Accelerates Myogenic Differentiation. J Biol Chem 282:9017-9028

Skerjanc IS (1999) Cardiac and skeletal muscle development in P19 embryonal carcinoma cells. Trends Cardiovasc Med 9:139-143

Skowyra D, Craig KL, Tyers M, Elledge SJ, Harper JW (1997) F-box proteins are receptors that recruit phosphorylated substrates to the SCF ubiquitin-ligase complex. Cell 91:209-219

Solomon V, Goldberg AL (1996) Importance of the ATP-ubiquitin-proteasome pathway in the degradation of soluble and myofibrillar proteins in rabbit muscle extracts. J Biol Chem 271:26690-26697

Song WK, Wang W, Sato H, Bielser DA, Kaufman SJ (1993) Expression of alpha 7 integrin cytoplasmic domains during skeletal muscle development: alternate forms, conformational change, and homologies with serine/threonine kinases and tyrosine phosphatases. J Cell Sci 106 (Pt 4):1139-1152

Southgate RJ, Neill B, Prelovsek O, El-Osta A, Kamei Y, Miura S, Ezaki O, McLoughlin TJ, Zhang W, Unterman TG, Febbraio MA (2007) FOXO1 regulates the expression of 4E-BP1 and inhibits mTOR signaling in mammalian skeletal muscle. J Biol Chem 282:21176-21186

Sporle R (2001) Epaxial-adaxial-hypaxial regionalisation of the vertebrate somite: evidence for a somitic organiser and a mirror-image duplication. Dev Genes Evol 211:198-217

Spurny R, Abdoulrahman K, Janda L, Runzler D, Kohler G, Castanon MJ, Wiche G (2007) Oxidation and nitrosylation of cysteines proximal to the intermediate filament (IF)-binding site of plectin: effects on structure and vimentin binding and involvement in IF collapse. J Biol Chem 282:8175-8187

Steffan JS, Bodai L, Pallos J, Poelman M, McCampbell A, Apostol BL, Kazantsev A, Schmidt E, Zhu YZ, Greenwald M, Kurokawa R, Housman DE, Jackson GR, Marsh JL, Thompson LM (2001) Histone deacetylase inhibitors arrest polyglutamine-dependent neurodegeneration in Drosophila. Nature 413:739-743

Stegmeier F, Sowa ME, Nalepa G, Gygi SP, Harper JW, Elledge SJ (2007) The tumor suppressor CYLD regulates entry into mitosis. Proc Natl Acad Sci U S A 104:8869-8874

Stitt TN, Drujan D, Clarke BA, Panaro F, Timofeyva Y, Kline WO, Gonzalez M, Yancopoulos GD, Glass DJ (2004) The IGF-1/PI3K/Akt pathway prevents expression of muscle atrophy-induced ubiquitin ligases by inhibiting FOXO transcription factors. Mol Cell 14:395-403

Strand AD, Baquet ZC, Aragaki AK, Holmans P, Yang L, Cleren C, Beal MF, Jones L, Kooperberg C, Olson JM, Jones KR (2007) Expression profiling of Huntington's disease models suggests that brain-derived neurotrophic factor depletion plays a major role in striatal degeneration. J Neurosci 27:11758-11768

Strom AL, Jonasson J, Hart P, Brannstrom T, Forsgren L, Holmberg M (2002) Cloning and expression analysis of the murine homolog of the spinocerebellar ataxia type 7 (SCA7) gene. Gene 285:91-99

Struhl K (1998) Histone acetylation and transcriptional regulatory mechanisms. Genes Dev 12:599-606

Su AI, Cooke MP, Ching KA, Hakak Y, Walker JR, Wiltshire T, Orth AP, Vega RG, Sapinoso LM, Moqrich A, Patapoutian A, Hampton GM, Schultz PG, Hogenesch JB (2002) Large-scale analysis of the human and mouse transcriptomes. Proc Natl Acad Sci U S A 99:4465-4470

Sugasawa K, Ng JM, Masutani C, Maekawa T, Uchida A, van der Spek PJ, Eker AP, Rademakers S, Visser C, Aboussekhra A, Wood RD, Hanaoka F, Bootsma D, Hoeijmakers JH (1997) Two human homologs of Rad23 are functionally interchangeable in complex formation and stimulation of XPC repair activity. Mol Cell Biol 17:6924-6931

Sun J, Barbieri JT (2004) ExoS Rho GTPase-activating protein activity stimulates reorganization of the actin cytoskeleton through Rho GTPase guanine nucleotide disassociation inhibitor. J Biol Chem 279:42936-42944

Tait D, Riccio M, Sittler A, Scherzinger E, Santi S, Ognibene A, Maraldi NM, Lehrach H, Wanker EE (1998) Ataxin-3 is transported into the nucleus and associated with the nuclear matrix. Hum Mol Genet 7:991-997

Takahashi J, Tanaka J, Arai K, Funata N, Hattori T, Fukuda T, Fujigasaki H, Uchihara T (2001) Recruitment of nonexpanded polyglutamine proteins to intranuclear aggregates in neuronal intranuclear hyaline inclusion disease. J Neuropathol Exp Neurol 60:369-376

Takiyama Y, Nishizawa M, Tanaka H, Kawashima S, Sakamoto H, Karube Y, Shimazaki H, Soutome M, Endo K, Ohta S, et al. (1993) The gene for Machado-Joseph disease maps to human chromosome 14q. Nat Genet 4:300-304

Tapscott SJ (2005) The circuitry of a master switch: Myod and the regulation of skeletal muscle gene transcription. Development 132:2685-2695

Taverna D, Disatnik MH, Rayburn H, Bronson RT, Yang J, Rando TA, Hynes RO (1998) Dystrophic muscle in mice chimeric for expression of alpha5 integrin. J Cell Biol 143:849-859

Taylor JP, Taye AA, Campbell C, Kazemi-Esfarjani P, Fischbeck KH, Min KT (2003) Aberrant histone acetylation, altered transcription, and retinal degeneration in a Drosophila model of polyglutamine disease are rescued by CREB-binding protein. Genes Dev 17:1463-1468

Teixeira-Castro A (2007) In vivo dynamics of ataxin-3 aggregation in Caenorhabditis elegans neurons. University of Minho, Braga

Thomas PS, Jr., Fraley GS, Damian V, Woodke LB, Zapata F, Sopher BL, Plymate SR, La Spada AR (2006) Loss of endogenous androgen receptor protein accelerates motor neuron degeneration and accentuates androgen insensitivity in a mouse model of X-linked spinal and bulbar muscular atrophy. Hum Mol Genet 15:2225-2238

Thompson JD, Higgins DG, Gibson TJ (1994) CLUSTAL W: improving the sensitivity of progressive multiple sequence alignment through sequence weighting, position-specific gap penalties and weight matrix choice. Nucleic Acids Research 22:4673-4680

Tintignac LA, Lagirand J, Batonnet S, Sirri V, Leibovitch MP, Leibovitch SA (2005) Degradation of MyoD mediated by the SCF (MAFbx) ubiquitin ligase. J Biol Chem 280:2847-2856

Tirnauer JS, Grego S, Salmon ED, Mitchison TJ (2002) EB1-microtubule interactions in Xenopus egg extracts: role of EB1 in microtubule stabilization and mechanisms of targeting to microtubules. Mol Biol Cell 13:3614-3626

Todi SV, Laco MN, Winborn BJ, Travis SM, Wen HM, Paulson HL (2007) Cellular turnover of the polyglutamine disease protein ataxin-3 is regulated by its catalytic activity. J Biol Chem 282:29348-29358

Tomczak KK, Marinescu VD, Ramoni MF, Sanoudou D, Montanaro F, Han M, Kunkel LM, Kohane IS, Beggs AH (2004) Expression profiling and identification of novel genes involved in myogenic differentiation. Faseb J 18:403-405

Tournebize R, Popov A, Kinoshita K, Ashford AJ, Rybina S, Pozniakovsky A, Mayer TU, Walczak CE, Karsenti E, Hyman AA (2000) Control of microtubule dynamics by the antagonistic activities of XMAP215 and XKCM1 in Xenopus egg extracts. Nat Cell Biol 2:13-19

Tran H, Brunet A, Griffith EC, Greenberg ME (2003) The many forks in FOXO's road. Sci STKE 2003:RE5

Trinick J (1994) Titin and nebulin: protein rulers in muscle? Trends Biochem Sci 19:405-409

Trompouki E, Hatzivassiliou E, Tsichritzis T, Farmer H, Ashworth A, Mosialos G (2003) CYLD is a deubiquitinating enzyme that negatively regulates NF-kappaB activation by TNFR family members. Nature 424:793-796

Trottier Y, Cancel G, An-Gourfinkel I, Lutz Y, Weber C, Brice A, Hirsch E, Mandel J-L (1998) Heterogeneous intracellular localization and expression of ataxin-3. Neurobiol Dis 5:335-347

Tsai J, Grutzendler J, Duff K, Gan WB (2004) Fibrillar amyloid deposition leads to local synaptic abnormalities and breakage of neuronal branches. Nat Neurosci 7:1181-1183

Tsai YC, Fishman PS, Thakor NV, Oyler GA (2003) Parkin facilitates the elimination of expanded polyglutamine proteins and leads to preservation of proteasome function. J Biol Chem 278:22044-22055

Tzvetkov N, Breuer P (2007) Josephin domain-containing proteins from a variety of species are active de-ubiquitination enzymes. Biol Chem 388:973-978

Uetz P, Giot L, Cagney G, Mansfield TA, Judson RS, Knight JR, Lockshon D, Narayan V, Srinivasan M, Pochart P, Qureshi-Emili A, Li Y, Godwin B, Conover D, Kalbfleisch T, Vijayadamodar G, Yang M, Johnston M, Fields S, Rothberg JM (2000) A comprehensive analysis of protein-protein interactions in Saccharomyces cerevisiae. Nature 403:623-627

Vadlamudi RK, Wang RA, Mazumdar A, Kim Y, Shin J, Sahin A, Kumar R (2001) Molecular cloning and characterization of PELP1, a novel human coregulator of estrogen receptor alpha. J Biol Chem 276:38272-38279

Van Der Heide LP, Hoekman MF, Smidt MP (2004) The ins and outs of FoxO shuttling: mechanisms of FoxO translocation and transcriptional regulation. Biochem J 380:297-309

van der Heide LP, Smidt MP (2005) Regulation of FoxO activity by CBP/p300-mediated acetylation. Trends Biochem Sci 30:81-86

Vandekerckhove J, Bugaisky G, Buckingham M (1986) Simultaneous expression of skeletal muscle and heart actin proteins in various striated muscle tissues and cells. A quantitative determination of the two actin isoforms. J Biol Chem 261:1838-1843

Velling T, Collo G, Sorokin L, Durbeej M, Zhang H, Gullberg D (1996) Distinct alpha 7A beta 1 and alpha 7B beta 1 integrin expression patterns during mouse development: alpha 7A is restricted to skeletal muscle but alpha 7B is expressed in striated muscle, vasculature, and nervous system. Dev Dyn 207:355-371

Vo N, Goodman RH (2001) CREB-binding protein and p300 in transcriptional regulation. J Biol Chem 276:13505-13508

von Mikecz A (2006) The nuclear ubiquitin-proteasome system. J Cell Sci 119:1977-1984

Walhout AJ, Boulton SJ, Vidal M (2000) Yeast two-hybrid systems and protein interaction mapping projects for yeast and worm. Yeast 17:88-94

Walker RA, O'Brien ET, Pryer NK, Soboeiro MF, Voter WA, Erickson HP, Salmon ED (1988) Dynamic instability of individual microtubules analyzed by video light microscopy: rate constants and transition frequencies. J Cell Biol 107:1437-1448

Walters KJ, Goh AM, Wang Q, Wagner G, Howley PM (2004) Ubiquitin family proteins and their relationship to the proteasome: a structural perspective. Biochim Biophys Acta 1695:73-87

Wang G-H, Sawai N, Kotliarova S, Kanazawa I, Nukina N (2000) Ataxin-3, the MJD1 gene product, interacts with the two human homologs of yeast DNA repair protein RAD23, HHR23A and HHR23B. Human Molecular Genetics 9:1795-1803

Wang G, Ide K, Nukina N, Goto J, Ichikawa Y, Uchida K, Sakamoto T, Kanazawa I (1997) Machado-Joseph disease gene product identified in lymphocytes and brain. Biochem Biophys Res Commun 233:476-479

Wang H, Jia N, Fei E, Wang Z, Liu C, Zhang T, Fan J, Wu M, Chen L, Nukina N, Zhou J, Wang G (2007) p45, an ATPase subunit of the 19S proteasome, targets the polyglutamine disease protein ataxin-3 to the proteasome. J Neurochem 101(6):1651-61

Wang Q, Li L, Ye Y (2006) Regulation of retrotranslocation by p97-associated deubiquitinating enzyme ataxin-3. J Cell Biol 174:963-971

Wang Z, Roeder RG (1995) Structure and function of a human transcription factor TFIIIB subunit that is evolutionarily conserved and contains both TFIIB- and high-mobility-group protein 2-related domains. Proc Natl Acad Sci U S A 92:7026-7030

Wanner R, Brommer S, Czarnetzki BM, Rosenbach T (1995) The differentiation-related upregulation of aryl hydrocarbon receptor transcript levels is suppressed by retinoic acid. Biochem Biophys Res Commun 209:706-711

Warrick JM, Chan HY, Gray-Board GL, Chai Y, Paulson HL, Bonini NM (1999) Suppression of polyglutamine-mediated neurodegeneration in Drosophila by the molecular chaperone HSP70. Nat Genet 23:425-428

Warrick JM, Paulson HL, Gray-Board GL, Bui QT, Fischbeck KH, Pittman RN, Bonini NM (1998) Expanded polyglutamine protein forms nuclear inclusions and causes neural degeneration in Drosophila. Cell 93:939-949

Watanabe T, Hayashi K, Tanaka A, Furumoto T, Hanaoka F, Ohkuma Y (2003) The carboxy terminus of the small subunit of TFIIE regulates the transition from transcription initiation to elongation by RNA polymerase II. Mol Cell Biol 23:2914-2926

Webb DJ, Zhang H, Majumdar D, Horwitz AF (2007) alpha5 integrin signaling regulates the formation of spines and synapses in hippocampal neurons. J Biol Chem 282:6929-6935

Welchman RL, Gordon C, Mayer RJ (2005) Ubiquitin and ubiquitin-like proteins as multifunctional signals. Nat Rev Mol Cell Biol 6:599-609

Wellington CL, Ellerby LM, Hackam AS, Margolis RL, Trifiro MA, Singaraja R, McCutcheon K, Salvesen GS, Propp SS, Bromm M, Rowland KJ, Zhang T, Rasper D, Roy S, Thornberry N, Pinsky L, Kakizuka A,

Ross CA, Nicholson DW, Bredesen DE, Hayden MR (1998) Caspase cleavage of gene products associated with triplet expansion disorders generates truncated fragments containing the polyglutamine tract. J Biol Chem 273:9158-9167

Werner A, Willem M, Jones LL, Kreutzberg GW, Mayer U, Raivich G (2000) Impaired axonal regeneration in alpha7 integrin-deficient mice. J Neurosci 20:1822-1830

Willems AR, Schwab M, Tyers M (2004) A hitchhiker's guide to the cullin ubiquitin ligases: SCF and its kin. Biochim Biophys Acta 1695:133-170

Wilson CA, Cajulis EE, Green JL, Olsen TM, Chung YA, Damore MA, Dering J, Calzone FJ, Slamon DJ (2005) HER-2 overexpression differentially alters transforming growth factor-beta responses in luminal versus mesenchymal human breast cancer cells. Breast Cancer Res 7:R1058-1079

Wing SS (2005) Control of ubiquitination in skeletal muscle wasting. Int J Biochem Cell Biol 37:2075-2087

Wingender E, Chen X, Hehl R, Karas H, Liebich I, Matys V, Meinhardt T, Pruss M, Reuter I, Schacherer F (2000) TRANSFAC: an integrated system for gene expression regulation. Nucleic Acids Res 28:316-319

Wirth B (2000) An update of the mutation spectrum of the survival motor neuron gene (SMN1) in autosomal recessive spinal muscular atrophy (SMA). Hum Mutat 15:228-237

Witt SH, Granzier H, Witt CC, Labeit S (2005) MURF-1 and MURF-2 target a specific subset of myofibrillar proteins redundantly: towards understanding MURF-dependent muscle ubiquitination. J Mol Biol 350:713-722

Woelk T, Sigismund S, Penengo L, Polo S (2007) The ubiquitination code: a signalling problem. Cell Div 2:11

Woods BT, Schaumburg HH (1972) Nigro-spino-dentatal degeneration with nuclear ophthalmoplegia. A unique and partially treatable clinico-pathological entity. J Neurol Sci 17:149-166

Wordeman L (2005) Microtubule-depolymerizing kinesins. Curr Opin Cell Biol 17:82-88

Wordeman L, Mitchison TJ (1995) Identification and partial characterization of mitotic centromere-associated kinesin, a kinesin-related protein that associates with centromeres during mitosis. J Cell Biol 128:95-104

Wu G, Xu G, Schulman BA, Jeffrey PD, Harper JW, Pavletich NP (2003) Structure of a beta-TrCP1-Skp1-beta-catenin complex: destruction motif binding and lysine specificity of the SCF(beta-TrCP1) ubiquitin ligase. Mol Cell 11:1445-1456

Wu JT, Lin HC, Hu YC, Chien CT (2005) Neddylation and deneddylation regulate Cul1 and Cul3 protein accumulation. Nat Cell Biol 7:1014-1020

Wu K, Chen A, Pan ZQ (2000) Conjugation of Nedd8 to CUL1 enhances the ability of the ROC1-CUL1 complex to promote ubiquitin polymerization. J Biol Chem 275:32317-32324

Wu X, Yen L, Irwin L, Sweeney C, Carraway KL, 3rd (2004) Stabilization of the E3 ubiquitin ligase Nrdp1 by the deubiquitinating enzyme USP8. Mol Cell Biol 24:7748-7757

Xirodimas DP, Sundqvist A, Nakamura A, Shen L, Botting C, Hay RT (2008) Ribosomal proteins are targets for the NEDD8 pathway. EMBO Rep 9(3):280-6

Yaffe D, Saxel O (1977) Serial passaging and differentiation of myogenic cells isolated from dystrophic mouse muscle. Nature 270:725-727

Yamada M, Tan C-F, Inenaga C, Tsuji S, Takahashi H (2004) Sharing of polyglutamine localization by the neuronal nucleus and cytoplasm in CAG-repeat diseases. Neuropath Appl Neurobiol 30:665-675

Yamashita K, Shinohara M, Shinohara A (2004) Rad6-Bre1-mediated histone H2B ubiquitylation modulates the formation of double-strand breaks during meiosis. Proc Natl Acad Sci U S A 101:11380-11385

Yang F, Jiang Q, Zhao J, Ren Y, Sutton MD, Feng J (2005) Parkin stabilizes microtubules through strong binding mediated by three independent domains. J Biol Chem 280:17154-17162

Yang L, Li N, Wang C, Yu Y, Yuan L, Zhang M, Cao X (2004) Cyclin L2, a novel RNA polymerase II-associated cyclin, is involved in pre-mRNA splicing and induces apoptosis of human hepatocellular carcinoma cells. J Biol Chem 279:11639-11648

Yang W, Li C, Ward DM, Kaplan J, Mansour SL (2000) Defective organellar membrane protein trafficking in Ap3b1-deficient cells. J Cell Sci 113 (Pt 22):4077-4086

Yao CC, Breuss J, Pytela R, Kramer RH (1997) Functional expression of the alpha 7 integrin receptor in differentiated smooth muscle cells. J Cell Sci 110 (Pt 13):1477-1487

Yoon JW, Kita Y, Frank DJ, Majewski RR, Konicek BA, Nobrega MA, Jacob H, Walterhouse D, Iannaccone P (2002) Gene expression profiling leads to identification of GLI1-binding elements in target genes and a role for multiple downstream pathways in GLI1-induced cell transformation. J Biol Chem 277:5548-5555

Young P, Deveraux Q, Beal RE, Pickart CM, Rechsteiner M (1998) Characterization of two polyubiquitin binding sites in the 26 S protease subunit 5a. J Biol Chem 273:5461-5467

Zhang Q, Vo N, Goodman RH (2000) Histone binding protein RbAp48 interacts with a complex of CREB binding protein and phosphorylated CREB. Mol Cell Biol 20:4970-4978

Zhong W, Sternberg PW (2006) Genome-wide prediction of C. elegans genetic interactions. Science 311:1481-1484

Zhong X, Pittman RN (2006) Ataxin-3 binds VCP/p97 and regulates retrotranslocation of ERAD substrates. Hum Mol Genet 15:2409-2420

Ziober BL, Vu MP, Waleh N, Crawford J, Lin CS, Kramer RH (1993) Alternative extracellular and cytoplasmic domains of the integrin alpha 7 subunit are differentially expressed during development. J Biol Chem 268:26773-26783